AN ABSTRACT OF THE DISSERTATION OF

Aaron S. Tamashiro for the degree of Doctor of Philosophy in Nuclear Engineering presented on September 12, 2022.

Title: Measurement of ^{239}Pu, ^{237}Np, and ^{238}U Fission Product γ Rays

Abstract approved: _____

Camille J. Palmer

Fission product yields (FPYs) are used for a wide range of applications including nuclear fission theory, nuclear reactor design, reactor antineutrino anomaly, stellar nucleosynthesis, and nuclear forensics. These applications rely on FPYs that were last evaluated in 1993, which included measurements from all over the world up until 1993. In this work, the most recent measurement of ^{239}Pu FPY and ^{237}Np FPY using Godiva IV critical assembly is presented. Both measurements used the same experimental setup and same analysis codes. Discrepancies in γ-ray branching ratios were observed for both measurements and the data was limited to 45 minutes after irradiation. This led to the construction of the Lāpaki array in order to perform γ-γ coincidence measurements. An experiment to study ^{238}U short-lived FPY was conducted using the Lāpaki array with the Oregon State University (OSU) Training, Research, Isotopes General Atomics (TRIGA) reactor rabbit facility. This allows for ^{238}U fission product γ rays to be observed within seconds after irradiation. A new rabbit was designed and fabricated with high-purity polyethylene along with a new procedure was established to reduce as much background γ rays as possible when studying short-lived isotopes. A new digital data acquisition (DAQ) system from Mesytec was used for this experiment.

Measurement of ^{239}Pu, ^{237}Np, and ^{238}U Fission Product γ Rays

by

Aaron S. Tamashiro

A DISSERTATION

submitted to

Oregon State University

in partial fulfillment of
the requirements for the
degree of

Doctor of Philosophy

Presented September 12, 2022
Commencement June 2023

Doctor of Philosophy thesis of Aaron S. Tamashiro presented on September 12, 2022.

APPROVED:

Major Professor, representing Nuclear Engineering

Head of the School of Nuclear Science and Engineering

Dean of the Graduate School

I understand that my thesis will become part of the permanent collection of Oregon State University libraries. My signature below authorizes release of my thesis to any reader upon request.

Aaron S. Tamashiro, Author

ACKNOWLEDGEMENTS

I would like to express my gratitude to my advisor Dr. Camille J. Palmer for her limitless patience and invaluable feedback during my doctoral journey. I am truly grateful for the research team that you have put together and the support that we have for each other. My experimental setup wouldn't have been completed in a timely manner without the research team.

Thank you Dr. Jason T. Harke and the rest of the Millennium Falcon lab group at Lawrence Livermore National Laboratory for their support in this work. Thank you for all the opportunities from being an undergraduate summer intern in 2015 to me finishing my dissertation work in 2022. I really enjoyed my time in Livermore and I look forward to collaborating with you in the future.

Thank you to my committee members: Dr. Kenneth S. Krane, Dr. Steven R. Reese, Dr. Todd S. Palmer, and Dr. Walter D. Loveland. Thank you to Dr. Leah D. Minc for being my graduate committee representative at such a short notice. Thank you all for your guidance throughout my PhD journey.

Lastly, I would like to thank God for His guidance throughout my life. Thank you to my family and friends who have supported me in the ups and downs. Thank you to my wife Kaisha Rose Laconsay Tamashiro for being by my side and always supporting me. Thank you to my Pembroke Welsh Corgi named Katsu Tamashiro.

This work was funded by the Office of Defense Nuclear Nonproliferation Research and Development within the U.S. Department of Energy's National Nuclear Security Administration by Lawrence Livermore National Laboratory under Contract No DE-AC52-07NA27344. The U.S. Department of Energy's Nuclear Criticality Safety Programs National Criticality Experiments Research Center (NCERC), utilized in this work, is supported by the National Nuclear Security Administration's Office of the Chief of Defense Nuclear Safety, NA-511. This work was performed with the assistance of the Radiation Center at Oregon State University.

TABLE OF CONTENTS

LIST OF FIGURES

LIST OF TABLES

1 Introduction

Fission product yields (FPY) are relevant to nuclear fission theory, nuclear reactor design, reactor antineutrino anomaly, stellar nucleosynthesis, and nuclear forensics. Yet, the last fission product yields evaluation occurred in 1993 [38]. Since then, there have been significant improvements in detection capabilities and data processing. In collaboration with Lawrence Livermore National Laboratory (LLNL), this thesis seeks to improved fission product yields: (a) using the Godiva IV critical assembly and (b) apply state-of-the-art detectors and electronics with modifications to the existing rabbit system at the Oregon State University (OSU) Training, Research, Isotopes, General Atomics (TRIGA) reactor. The rabbit system will enable short exposure of samples and transportation to the detection setup, allowing γ rays to be observed 3 seconds to 1 hour after irradiation. A new rabbit (sample carrier) was designed and fabricated to reduce interfering γ rays from neutron activated impurities found in the current rabbit. A new detection setup was constructed with up to eight Compton suppressed large high-purity germanium (HPGe) detectors segmented for γ-γ and fission product yield measurements. Modern electronics recorded data in list mode, bringing flexibility in data analysis. Post processing software was developed using ROOT [39]; a data analysis framework designed for high energy particle physics.

1.1 Applications of FPY Data

Fission product yield data is utilized in a wide variety of nuclear application space including nuclear reactor design, reactor antineutrino signatures, stellar nucleosynthesis, and nuclear forensics. These are briefly discussed below.

1.1.1 Nuclear Reactor Design

Fission product yields are necessary in a wide variety of roles (listed below) for nuclear reactor design and operation [38].

- criticality and reactivity calculations
- fuel and reactor core management
- reactor safety
- determining safe operation limits in new plants
- nuclear materials transport

A well known code to simulate reactors is SCALE. SCALE was developed by Oak Ridge National Laboratory (ORNL) and used by the Nuclear Regulatory Commission (NRC) for various analyses [40]. These analyses fulfill some of the NRC duties which are "Transportation and storage licensing", "Reactor physics confirmatory analysis", and "severe accident and consequence analysis". Since fission product yields are embedded in the data set of SCALE, improvements in fission product yields will improve the NRC's analyses.

Another consideration for reactor design is fuel burnup. Burnup is a measure of the amount of energy extracted from a nuclear fuel and its depletion. As time goes on, burnup of a fuel element decreases due to the increase in neutron poisons and decrease in fissioning actinides. For nuclear fuel burnup calculations, the two highest priority in nuclear data needs are fast reactor fission product yields as a function of neutron energy and improved decay data for radionuclides used as burnup monitors [41]. This research will fulfill the mentioned nuclear data needs

for nuclear fuel burnup calculations.

Decay heat plays a role in fuel burnup, on-site storage, and off-site storage [42]. Decay heat is relevant from the moment of fission to a few days after in fuel burnup which determines the consequence of a loss of coolant accident (LOCA). On-site storage time in spent nuclear fuel pool must be consistent with decay heat calculations. Off-site storage decay heat will depend on the much longer-lived fission products. TRITON is a code part of SCALE that is used to calculate reactor decay heat [43]. Improvements to fission products in minutes, hours, days, etc. will improve decay heat calculations. Figure 1 shows the various heat contribution to decay heat after a reactor shutdown. Measured fission product yields may be used with TRITON to calculate reactor decay heat in reactor shutdown (including LOCA) scenarios.

1.1.2 Reactor Antineutrino Anomaly

There have been antineutrino detector measurements placed near nuclear reactors with a goal in detecting nuclear reactors from a distance. With available decay data, an antineutrino spectrum may be directly calculated to predict the antineutrino flux from a nearby reactor. The anomaly comes from the fact that there are differences in antineutrinos measured than predicted from a radioactive source (e.g. nuclear reactor) (see Figure 2) [44, 45]. One plausible explanation is that the lower counts in antineutrinos is due to the uncertainties in the decay data and fission product yields. With new measured fission product yields and decay data, a new antineutrino energy spectrum may be directly calculated and compared with previous measurements. There has been recent work in comparing measured and calculated antineutrino spectrum from fission product yield data.

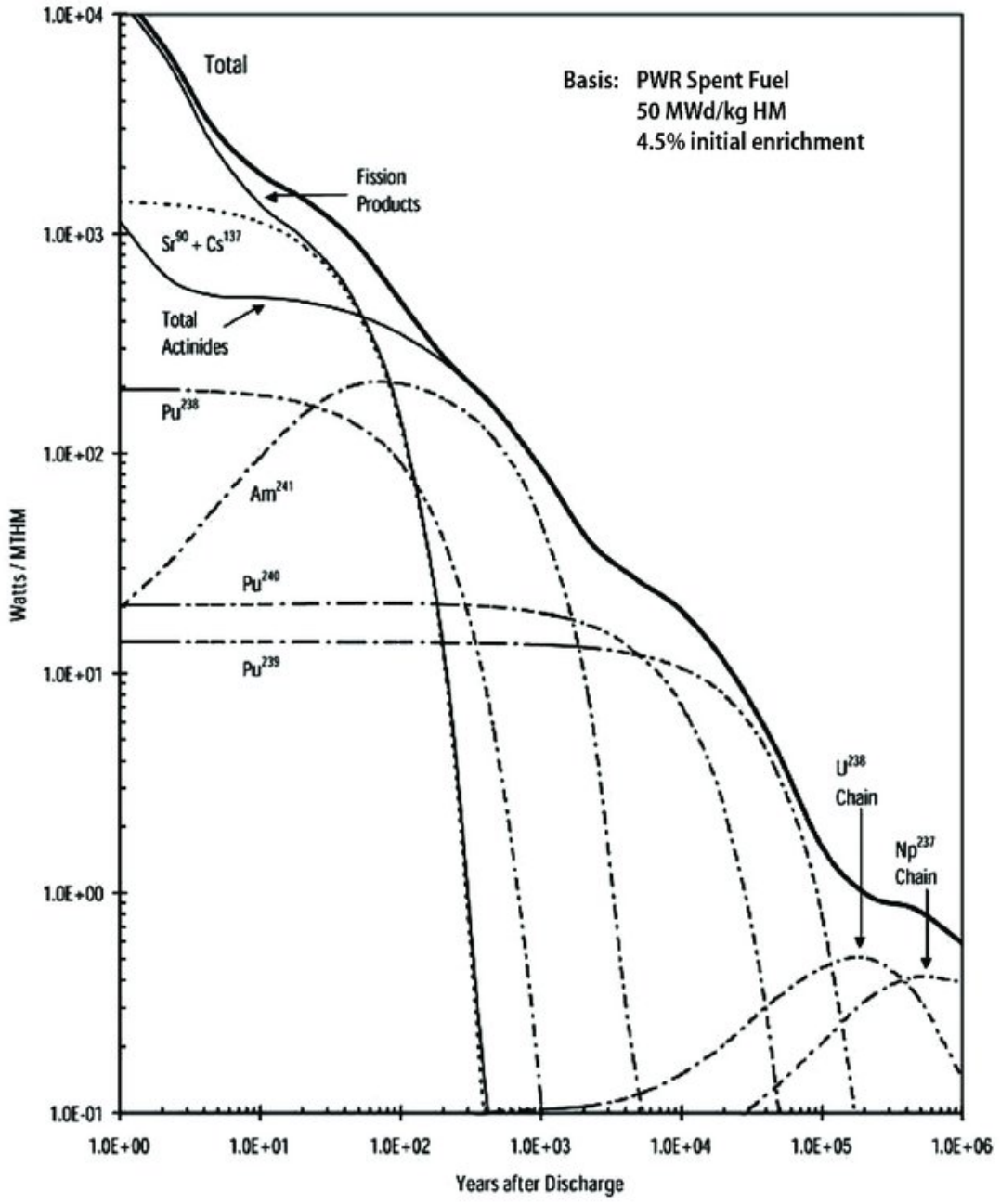

Figure 1: Contribution to heat generated after a reactor shutdown provided by [31].

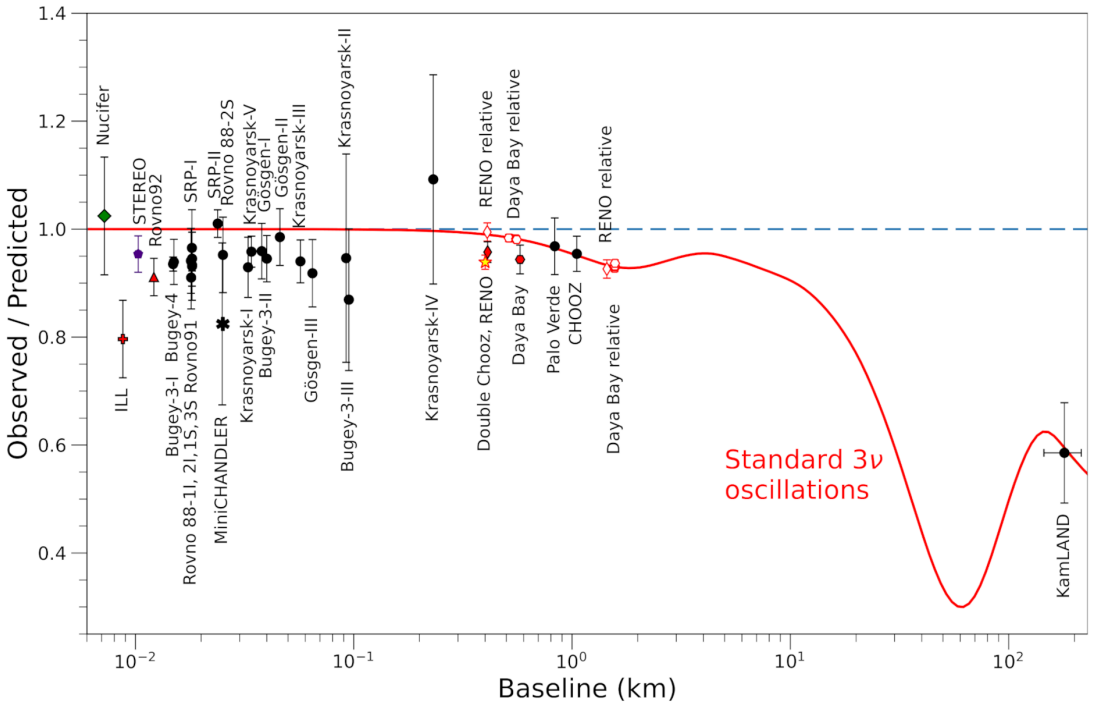

Figure 2: Ratios of measured and calculated neutrinos provided by [32]

1.1.3 Stellar Nucleosynthesis

The marriage between astrophysics and nuclear physics allowed for the explanation behind stellar nucleosynthesis. Figure 3 provides a nice summary of the different process that occurs in a star. The r-process is important for the involvement of fission product yields. As the daughters do not have enough time to β^- decay to stability, the r-process forces isotopes to keep getting heavier with more and more neutron capture until it meets its end with spontaneous or neutron induced fission.

The importance of nuclear decay data and fission product yields in the context of stellar nucleosynthesis are found in a 1983 technical report [46]. Measured fission product yields will contribute to the understanding of the r-process calcu-

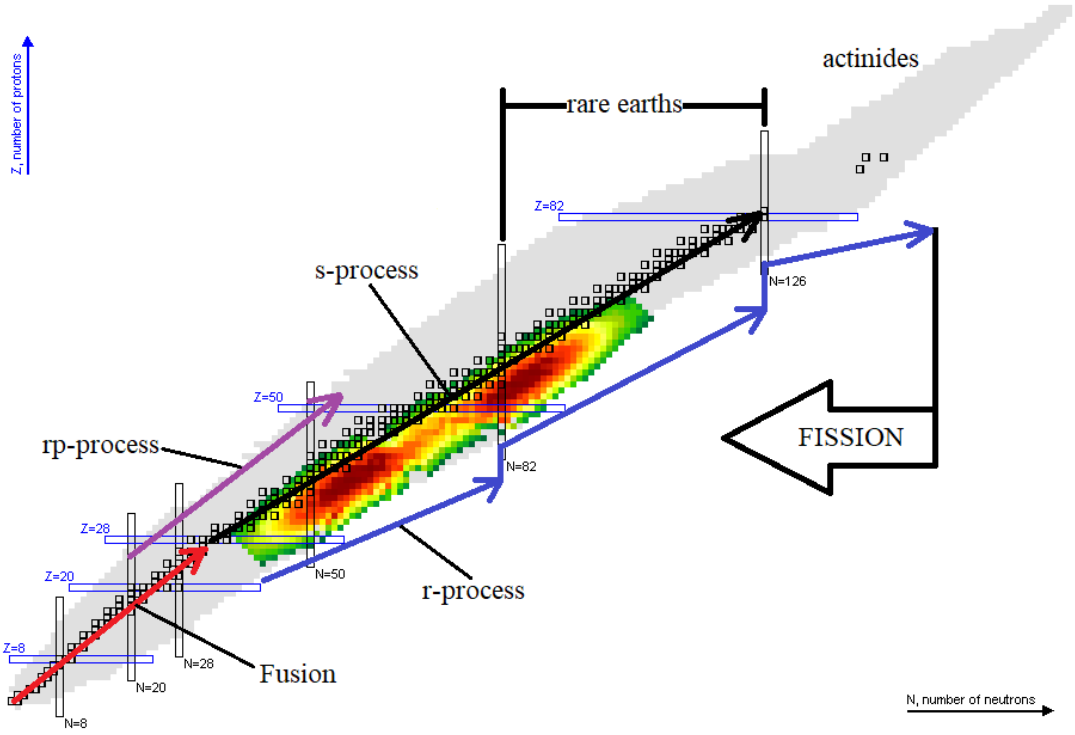

Figure 3: Visualization of nucleosynthesis on the chart of the nuclide with ^{235}U thermal fission product yields displayed in color.

lations and provide a constraint to theoretical mass and density of isotopes within a star.

1.1.4 Nuclear Forensics

Nuclear forensics and safeguards rely on fission product yield data to help determine and back track a nuclear material. Using ratio measurements and comparing different actinides assist in determining the compositions of special nuclear materials. A non-destructive method relies on γ decay data which includes the branching ratios. These branching ratios have applications to nuclear safeguards and specifically for ratio-based measurements of isotopics which provides Equation 1 and 2. [47]. Equation 1 is provided to calculate number of atoms N from measured counts C.

$$C = N \cdot \lambda \cdot E \cdot BR \tag{1}$$

λ is the decay constant for the nuclide, E is the detector efficiency, and BR is the γ-ray branching ratio. For ratio-based measurements, a ratio of counts between two isotopes is shown in Equation 2.

$$\frac{C_1}{C_2} = \frac{N_1}{N_2}\frac{\lambda_1}{\lambda_2}\frac{RE_1}{RE_2}\frac{BR_1}{BR_2} \tag{2}$$

RE is the relative efficiency at the γ-ray energies. If the two γ-rays are from the same isotope, then Equation 2 simplifies to Equation 3.

$$\frac{C_1}{C_2} = \frac{RE_1}{RE_2}\frac{BR_1}{BR_2} \tag{3}$$

Branching ratios have an important role in nuclear forensics and any improvements will improve their method in ratio-based measurements of isotopes.

1.2 Nuclear Fission Theory

Fission product yields that are not measured are estimated using theoretical models. When predicting fission product yields, both theoretical models and systematics are used [48]. Theoretical models describe "what is happening" in the nucleus while systematics is a function fit. A compiled summary of nuclear fission theory is found in [49]. While significant efforts has gone into understanding nuclear fission, but it remains an incomplete theory [50–52]. Systematic contributions describe the shape of fission product yield distribution. For example, five Gaussian functions have been used to represent the fission product yield distribution [53]. A representation of both fission models and systematics are plotted in Figure 4. Improving the overall models will improve the predictions of fission product yields for isotopes that are difficult to observe (very short half-life and very low yields).

1.3 Measuring Fission Product Yields

There are 3 main approaches to measure fission product yields. They consist of radiochemical methods, mass spectrometry, and γ-ray spectroscopy which are explained in the following sections.

1.3.1 Radiochemical Methods

Radiochemical techniques were the first methods to be used to analyze fission product yields [54]. This method used chemical separations to isolate certain isotopes of interests. For the discovery of fission, it was barium that was separated from a fissioned uranium [55]. In the case of cumulative yield determinations, it is the last or longest-lived member of the β decay chain that is isolated. In order to

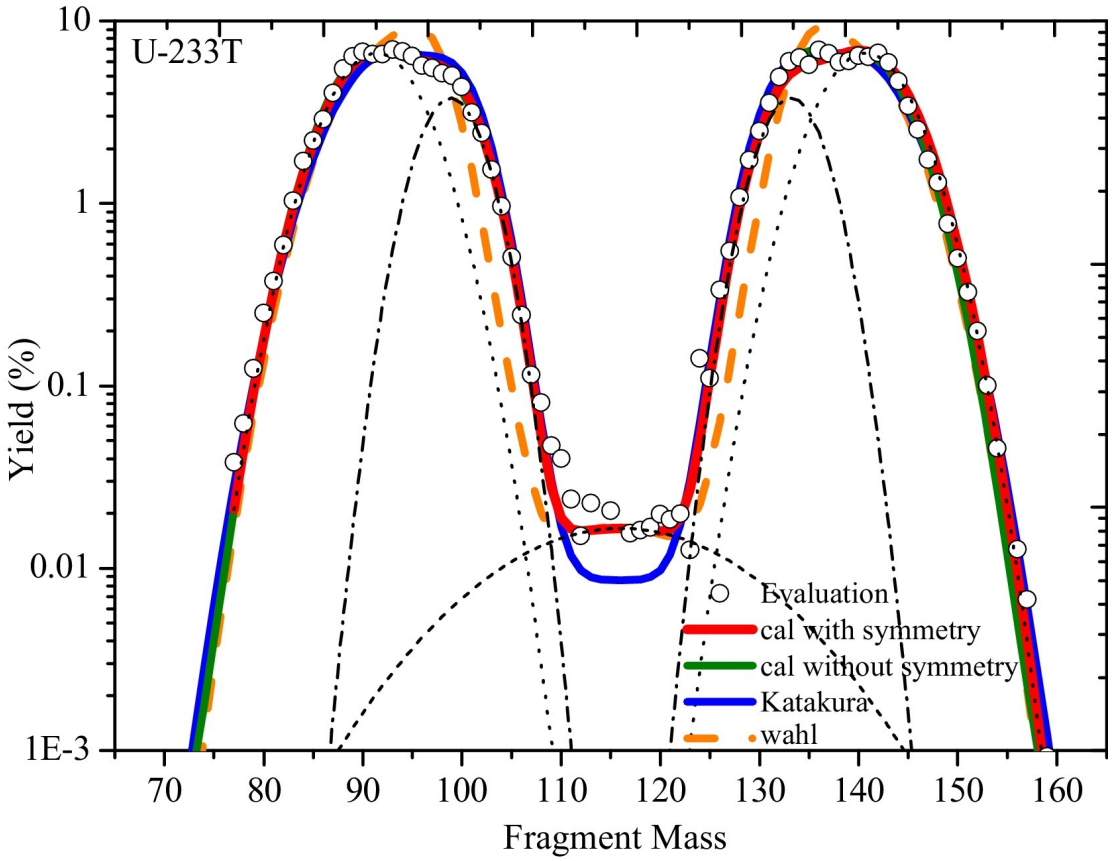

Figure 4: ^{233}U thermal fission product yields fitted using different functions provided by [33].

make these measurements, the experimentalist is required to wait for the parent to decay.

The main challenge for radiochemical methods is the amount of time needed for chemical separation. Performing chemical separation requires time after fission to isolate an isotope of interest. Very short-lived fission products will not be observed. Also, isolating an isotope can be challenging for fission products with multiple oxidation states. These require a complete oxidation/reduction cycle to fulfill a "complete chemical exchange". An example of this is the element iodine where natural iodine may precipitate in a solution, but radioactive iodate would remain aqueous [54].

For each isotope of interest, the isotope must be separated and isolated from the irradiated sample. In order to study all fission product yields, a very large sample is required. This would be challenging for a chemist to handle a large sample and chemically separate out the fission products. Although, a large sample makes it possible to analyze fission products with very low yields ($< 0.1\%$). In 1939, β-counting was the primary way of measuring activity. The absolute activity of the fission product of interest must be counted after being chemically isolated and dried. β-counting is non-selective implying all β particles will be detected. Therefore, chemical separation must be nearly perfect. Along with this strict requirement, there are other corrections necessary for the experiment. These include separation efficiency, detector efficiency, self attenuation, etc. There can be other isotopes present if the separation wasn't optimal. This would requires the use of a half-life analysis of the β^--decay to ensure the correct isotope is being measured. With the introduction of high resolution γ-ray spectroscopy, β

counting was phased out over γ-ray measurements [54].

1.3.2 Classical Mass Spectrometry

In 1940, A.O.C. Nier and colleagues established the role of mass spectrometry in nuclear science [56]. Mass spectrometry would be used following a chemical separation of an isotope of interest [54].

Classical mass spectrometry takes a sample of fission products and introduces it into an ion source at the entrance of the mass separator [57]. The sample is then heated, evaporated and then ionized and electrostatically accelerated. The accelerated samples are mangetically separated by their mass. One issue is that the results need to be normalized to a known amount of a relative isotope (close in mass). This implies that the normalization of the yields is the biggest source of uncertainty. Not to mention the uncertainties included with radiochemical separation. Overall, classical mass spectrometry would require more time to measure fission product yields.

1.3.3 γ-ray Spectroscopy

γ-ray spectroscopy is an accurate way to study a wide range of fission product yields for any actinide of interest [58]. In this approach, a target is irradiated and fission product yields are ready to be measured via γ-spectroscopy. An advantage of this approach is that the sample does not need to be chemically separated. The sample may be counted right after irradiation. The disadvantage of this technique is the dependence of nuclear decay data. The data analysis relies heavily on decay characteristics for each fission product. Low yield regions would not be observed. Also, short half-lives would cause the fission product to disappear rapidly. Even

if the γ-ray was analyzed, the short time of the analysis limits the statistical accuracy.

The key feature for γ-ray spectroscopy is to evaluate a wide range of fission product yields at short time scales after fission. This is attractive for evaluating any actinide of interest. Also, γ-ray spectroscopy requires a really small sample size compared to the previous two techniques discussed since it is a non-destructive technique. This is the method used in this research.

1.3.4 Comparison of the main experimental techniques

According to Table 1, γ-spectroscopy offers the least sources of uncertainty. The limitation of this technique is its reliance of nuclear decay data. For instance, fission product yields are proportionally related to γ-ray branching ratios.

	Radiochemistry			Mass	γ-Spectroscopy		
	Abs.	Rel.	R-value	Spectrometry	Abs.	Rel.	R-value
Number of Fissions	x	–	–	x	x	–	–
Standard Yield Normalization	–	x	x	x	–	x	x
Reference Yield Normalization	–	–	x	–	–	–	x
Processing Losses	x	x	x	x	–	–	–
Contamination	x	x	x	x	x	x	x
Decay Data	x	x	–	x	x	x	–
Neutron capture data	–	–	–	x	–	–	–
β Counting Corrections	x	x	x	–	–	–	–
γ Counting Corrections	x	x	x	–	x	x	x

Table 1: Possible sources of uncertainty for a fission product yield in [36]

1.4 Nuclear Decay Data

Nuclear decay data is the collection of information describing any isotope decay characteristics. These decay modes are α-decay, β-decay, γ-decay, etc. This research focuses on γ-decay data. The database to be used in the proposed research is the Evaluated Nuclear Structure Data File (ENSDF). Values are used for the fission product yield analysis. Figure 5 shows the most up to date evaluations for different decay chains. In past evaluations, the fission product yields are limited to isotopes with mass A = 66 – 172. Any improvements to nuclear decay data for any fission product will update evaluated values. The accepted technique in measuring γ-ray branching ratios of different decay modes is to perform γ-γ coincidence measurements.

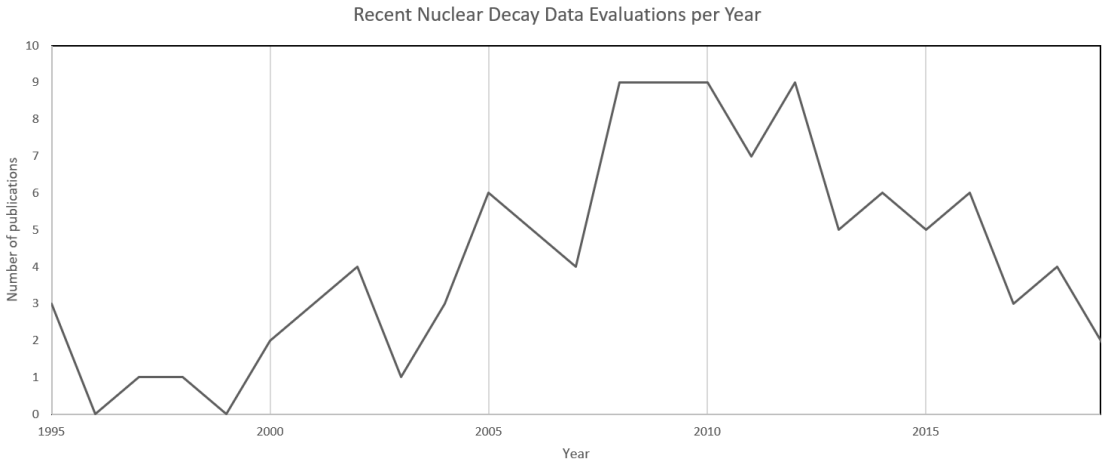

Figure 5: These are the evaluations per year for different mass decay chains for A = 66 – 172.

1.5 Past Fission Product Yield Experiments Using a Reactor Rabbit System

A rabbit is traditionally a pneumatically driven transport tube to transport samples into a reactor for irradiation. This is one of multiple ways to transport samples in a safe manner to create distance for people. Besides using a reactor or integral measurement, rabbit systems have been implemented with monoenergetic neutron experiments. Since the 1950s, there have been multiple fission product yield studies conducted using a rabbit system. The advent of HPGe γ-ray detectors led to high precision γ-ray spectroscopy and isotopic identification. A few past experiments are mentioned below.

In 1966, one of the earliest measurement was conducted at the Omega West Reactor (OWR) [59]. Which was located in Los Alamos National Laboratory (LANL). A nylon rabbit with a quartz tube to encapsulate the ^{235}U sample was transported into the thermal column of OWR. After 1 second of irradiation, the sample had a contact exposure rate that exceeds 5 rem/hour. The sample was counted in front of a sodium iodide (NaI) detector, which was standard at the time.

In 1975, ORNL conducted experiments at the Oak Ridge Research Reactor (ORR) [60]. Their rabbit system was utilized in the transport of a hydrocarbon rabbit encapsulating the fissile material into the reactor and to the detection setup. They had the capability to measure fission products from 2–2000 seconds (later improvements led to 2–14000 seconds [61]) after fission. The limitation in this experiment is the use of NaI detectors to conduct γ-spectroscopy. The advantage in using NaI is the efficiency in detecting γ-rays, but the energy resolution is

a lot broader (20-30x) compared to Ge detectors.

Recently in 2019, a proof of principle measurement was conducted at OSU by this research group [62]. Initially, a polyethylene rabbit encased a quartz tube that contained a ^{238}U sample. The sample was irradiated for 1 second and measured within 10 seconds from fission. A γ-ray from ^{28}Al produced a massive Compton spectrum that made observing any very short-lived fission product impossible. The solution was to use a neutron activation analysis (NAA) grade poly vial instead of a quartz tube. ^{28}Al is a product of ^{28}Si(n,p) reaction and silicon is present in quartz. The irradiation was repeated with the NAA poly vial with success. The γ spectra was measured using a HPGe detector.

1.6 Past Polyethylene Rabbits

In 1958, the Ford Nuclear Reactor group at University of Michigan used a nylon and Lustroid rabbit [63]. The nylon rabbit design were press fit and in some cases fell apart while in transit. The Lustroid rabbit design were two Lustroid tubes taped together. In 1959, the group started to use a polyethylene rabbit as their sample container [64]. These rabbits were redesigned with a screw cap. Their 1959 technical report investigates trace contaminants present in the polyethylene rabbit. Intramedic polyethylene tubing was irradiated for ten minutes with a one minute rest period before γ-ray measurement. From the γ spectra, there were Na, Cl, and Al present. At the time of the report, their post doctoral D. Kaiser determined there were 2E-7 g/g of aluminum to polyethylene. In 1960, a University of Michigan doctoral thesis by J.L. Brownlee describes the "bunny rabbit" facility and the new rabbit design for short-lived isotope measurements [65].

In 1962, a Naval Postgraduate School master's thesis by A.O. Paas describes an experiment where Hf was irradiated in the AGN-201 Reactor to measure it's short-lived isotopes [66]. The rabbit used was made out of balsa wood. The powdered form of Hf was contained in a gelatin medicinal capsule within the rabbit. The rabbit was transported from the reactor to directly in front of the detection system to measure 18.2 seconds half-life of ^{179m}Hf.

In 1965, General Atomic division of General Dynamics Corporation explored using the rabbit facility in reactor pulse mode instead of steady-state operations [67]. The sample was double encapsulated with an inner polyethylene vial and an outer "white" or "black" rabbit. The inner polyethylene vial was welded at the cap and body with a soldering iron. The "white" rabbit is designed to be "transparent" to neutrons, similar to the rabbit that University of Michigan used in 1959. The "black" rabbit is designed to shield thermal neutrons by including a ^{10}B lining attached with lacquer and 20 mm of Cd within that.

In 1967, the Analytical Chemistry Division of the National Bureau of Standards performed neutron activation analysis using polyethylene rabbits [68]. A special polyethylene rabbit was produced by Olympic Plastics (based in Los Angeles, CA). These were proven to be superior sample containers in terms of oxygen content in the polyethylene. The procedure for their measurements included 4 minutes of irradiation in the rabbit facility, then 2.5 minutes of decay time. This is required due to the presence of ^{28}Al and other impurities in the sample carrier.

In 1974, a technical report describes neutron activation techniques and the use of a rabbit facility for measuring trace metals in environmental samples [69]. Solid samples are heat sealed in polyethylene, polypropylene, or high purity quartz vials. Although, quartz contain more impurities than polyethylene or polypropylene.

Also in 1974, the Lewis Research Center describes their new instrumental

neutron activation analysis capability at the Plum Brook Reactor [70]. Initially, aluminum rabbits were used and measurements of short-lived isotopes would be lost in the first 5 minutes. It was shown that high density polyethylene were an acceptable rabbit material. Polyethylene rabbits were used for short-lived isotopes and aluminum rabbits were used for long-lived isotopes.

In 1980, an International Atomic Energy Agency (IAEA) technical report on elemental analysis of biological materials highlights trace contaminants in laboratory-ware materials [71]. High pressure polyethylene, or known as low density polyethylene, was identified to have trace impurities of Al, Ca, Cl, Co, Cr, Cu, Fe, Mg, Mn, Na, Pb, Sb, Si, Sr, and Zn. The amount of impurities were reported in nanograms per gram of polyethylene. The uncertainties were not listed in this report.

In 1983, an instrumental neutron activation analysis was performed on polyethylene to determine it's trace impurities [72]. It's stated that polyethylene is one of the preferred materials for sample containers used in neutron activation analysis. Even though polyethylene will break down faster in a radiation field compared to silica and aluminum. Therefore, polyethylene is used for a short irradiation time. There are two types of polyethylene mentioned in the paper. These are high density polyethylene (HDPE) and low density polyethylene (LDPE). HDPE will contain more impurities, because the process in making HDPE includes Ziegler catalysts and will introduce Al, Co, Cr, Ti, and Zn into the polyethylene. Bralen® LDPE (produced by Slovnaft in Bratislava, Czechoslovakia) was studied in this journal article. After irradiation, the radionuclides identified were ^{27}Al, ^{76}As, ^{198}Au, ^{82}Br, ^{38}Cl, ^{60}Co, ^{51}Cr, ^{64}Cu, ^{59}Fe, ^{197}Hg, ^{203}Hg, ^{42}K, ^{140}La, ^{56}Mn, ^{99}Mo, ^{99m}Tc, ^{24}Na, ^{122}Sb, ^{124}Sb, ^{46}Sc, ^{153}Sm, ^{52}V, and ^{65}Zn. The amount of impurities were reported in nanograms per gram of polyethylene. The uncertainties

were listed in this article. It was concluded that the availability of high purity polyethylene is important for determining very low levels of trace elements in neutron activation analysis.

In 2019, a proof of principle study was conducted at OSU TRIGA reactor rabbit facility [73]. This experiment was to show the feasibility in measuring fission product γ-rays within seconds of irradiation. Initially, a quartz vial was used to contain ^{238}U. A large dominant 1778 keV γ-ray and Compton continuum made it impossible to identify any of the short-lived fission product γ-rays. It was determined that the 1778 keV γ-ray originated from ^{28}Al which was produced by ^{28}Si(n,p)^{28}Al. A second test was performed by placing ^{238}U in a LAContainer NAA Polyvials™. Since the current rabbit at OSU had impurities,the vial containing irradiated ^{238}U was removed from the rabbit and placed in front of a high purity germanium (HPGe) detector. The LAContainer NAA Polyvials™ was very pure and allowed for short-lived fission product γ-rays to be measured within 7 seconds of irradiation. This prompted the design of a new high purity polyethylene rabbit to perform like LAContainer NAA Polyvials™ to study short-lived fission products within 3 seconds of irradiation.

1.7 Research Objectives

The objective of this research is to employ improved detection capabilities to reduce the known uncertainty in ^{239}Pu, ^{237}Np, and ^{238}U fission product yields. Specifically, this objective will be accomplished by the following:

1. Reduce uncertainty in fission product yields.
   (a) ^{239}Pu fission product yields were measured using the Godiva IV critical assembly within an hour of prompt irradiation.
   (b) ^{237}Np fission product yields were measured using the Godiva IV critical assembly within an hour of prompt irradiation.
2. Reduce uncertainty in fission product γ-ray branching ratios.
   (a) A new array was designed and constructed to measure ^{238}U fission product γ rays within seconds of irradiation.
   (b) An experimental campaign was performed at the OSU TRIGA Reactor, involving a modification to the existing rabbit system to allow for rapid delivery of irradiated samples to a new γ-ray counting setup.
   (c) A new high-efficiency and highly segmented gamma-ray counting station, consisting of seven Compton-suppressed HPGe Clover detectors was designed and constructed at the OSU TRIGA Reactor.
   (d) A new digital data acquisition system from Mesytec was put together for this measurement.
3. Reduce neutron activated impurities found in the rabbit carrier.
   (a) Samples of polyethylene were irradiated and neutron activated impurity masses were measured via γ-ray spectroscopy.

   (b) A new high-purity polyethylene rabbit was designed and fabricated for the use of rapid neutron activation analysis.

4. Software was developed to interpret the measured data from the experiment.

   (a) Codes are written in C/C++/ROOT to perform automatic peak searching and isotopic identification.

   (b) The activity of various isotopes, following irradiation, are used to determine their fission yield.

5. Results from this new measurement are compared to past evaluated fission product yield data to identify any discrepancies.

   (a) The expected significant reduction in the uncertainty in fission product yield for some isotopes are quantified.

The goal of the three mentioned experiments is to reduce the uncertainties of fission product yields. The two Godiva IV critical assembly measurements are in addition to other actinides previously measured and analyzed. The OSU TRIGA experiment will measure ^{238}U fission product yields within seconds of irradiation. This is much shorter compared to measurements at Godiva IV critical assembly (measure γ rays 45 minutes after irradiation).

1.8 Dissertation Overview

This dissertation is comprised of three independent journal manuscripts as Chapters 2 to 4 and concluding remarks as Chapter 5. Chapters 2 to 4 are submitted manuscripts.

- Chapter 2 is a manuscript presenting ^{239}Pu cumulative fission product yield results following a Godiva IV prompt burst irradiation. γ rays were measured and analyzed to fit the initial activity of each fission product. The initial activity was used to calculate the fission product yield.

- Chapter 3 is a manuscript similar to Chapter 2, but presenting ^{237}Np cumulative fission product yield results. Both Chapter 2 and Chapter 3 show similar variations in fission product yields for different γ ray analyzed. Both concluded that variation in fission product yield results may be caused by discrepancies in γ-ray branching ratios.

- Chapter 4 is a manuscript on a new detector array to measure short-lived fission product γ rays within seconds of irradiation using a rabbit system. A new high-purity polyethylene rabbit was designed and fabricated to lessen interfering γ rays produced from neutron activated impurities in polyethylene. The goal of the detector array is to perform γ-γ coincidence measurements for γ-ray branching ratios.

- Chapter 5 is concluding remarks and future work for fission product yield studies.

2 ^{239}Pu Fission Spectrum Cumulative Fission Product Yield Measurement Using Godiva IV Critical Assembly

A.S. Tamashiro[1], J.T. Harke[2], S.W. Padgett[2], G. Slavik[2], S. Burcher[2], N. Harward[2], N. Gharibyan[2], R.A. Henderson[2], L.R. Greenwood[3], B.D. Pierson[3], J.M. Goda[4], J.A. Bounds[4], D.K. Hayes[4], and C.J. Palmer[1]

Preprint submitted to Nuclear Data Sheets July 17, 2022

[1]School of Nuclear Science and Engineering, Oregon State University, Corvallis, OR 97331, USA

[2]Nuclear and Chemical Sciences Division, Lawrence Livermore National Laboratory, Livermore, CA 94550, USA

[3]Energy and Environment Directorate, Pacific Northwest National Laboratory, Richland, WA 99354, USA

[4]Advanced Nuclear Technology Group, Los Alamos National Laboratory, Los Alamos, NM 87545, USA

2.1 Abstract

Precise integral measurement of fast neutron-induced fission product yields for various actinides is of high interest for applied nuclear science. The goal of this effort is to improve uncertainties in fission product yield values of ^{239}Pu. Fission was induced in a pure ^{239}Pu ($> 99\%$) target using the Godiva IV critical assembly in burst mode. The irradiated sample was transferred to a high-resolution γ-ray detector within 45 minutes. γ-ray list mode data was collected from 45 minutes to 1 week after the irradiation. γ-ray spectroscopy was performed to analyze the time dependent γ-ray yields using an automated peak search algorithm to identify isotopes by their decay γ-ray energy and half-life. The initial activity for each isotope identified was used to calculate their fission product yield.

2.2 Introduction

The Short-Lived Fission Product Yield (SLFPY) project objective is to provide improved measurements of fission product yields for actinides. The measured fission product yields are needed for applied and fundamental nuclear science. Data exists for fission product yields on fissioning of ^{235}U [74], ^{238}U [75], and ^{239}Pu with fission spectrum neutrons.

Recently, the Godiva IV critical assembly was employed to perform a burst irradiation of a sample of ^{239}Pu with the goal of measuring fission product yields [76]. A γ spectroscopy-based data analysis procedure has been developed for the prediction of fission product yields that is independent of the actinide sample. Some representative results will be presented in this article.

2.3 Background

Fission product yields are used in the prediction of the behavior and performance of engineered systems involving nuclear fission. Measurements of fission product yields have been traditionally performed through radiochemistry, mass spectrometry, and γ-ray spectroscopy, often with mono-energetic neutrons.

To date, the most recent fission product yield evaluation was conducted in 1993 by England and Rider, almost 3 decades ago [77]. There were 1388 fission product yield values compiled for ^{239}Pu fast neutron-induced fission, 313 of which were measured using radiochemistry. The evaluation compiled publications from 1951 – 1982, making the most recent results four decades old. Although, ten of these publications were γ-ray spectroscopy without chemical separation [78–87], all of these measurements used fission spectrum neutrons and Ge(Li) detectors. In total, 84 fission product yield results for 40 isotopes via γ-ray spectroscopy without chemical separation were included in the England and Rider's evaluation. Table 2 lists these 40 isotopes along with their half-lives and reference fission product yields.

Table 2: List of isotopes in the England and Rider's evaluation that were measured using γ-ray spectroscopy without chemical separation.

Isotope	$\tau_{1/2}$	FPY_{ref} (%) [37]
^{87}Br	55.65 ± 0.13 s [2]	0.80200 ± 0.06416
^{85m}Kr	4.480 ± 0.008 h [1]	0.3929 ± 0.0055
^{87}Kr	76.3 ± 0.5 m [2]	1.0350 ± 0.0207
^{88}Kr	2.825 ± 0.019 h [3]	1.28500 ± 0.03599
^{91}Sr	9.65 ± 0.06 h [5]	2.51000 ± 0.07027
^{92}Sr	2.611 ± 0.017 h [6]	3.01200 ± 0.08433

^{95}Zr	64.032 ± 0.006 d [8]	4.76000 ± 0.02856
^{97}Zr	16.749 ± 0.008 h [9]	5.25600 ± 0.07358
^{95}Nb	34.991 ± 0.06 d [8]	4.7570 ± 0.0666
^{97}Nb	72.1 ± 0.7 m [9]	5.28700 ± 0.05287
^{97m}Nb	58.7 ± 1.8 s [9]	5.00100 ± 0.07001
^{99}Mo	65.924 ± 0.006 h [10]	6.23000 ± 0.04361
^{104}Tc	18.3 ± 0.3 m [88]	6.557 ± 0.098
^{103}Ru	39.249 ± 0.003 d [11]	6.81600 ± 0.09543
^{105}Ru	4.439 ± 0.011 h [12]	5.351 ± 0.214
^{106}Ru	371.8 ± 18 d [89]	4.35500 ± 0.06097
^{105}Rh	35.341 ± 0.019 h [12]	5.3510 ± 0.1498
^{129}Sb	4.366 ± 0.026 h [15]	1.3740 ± 0.1099
^{130m}Sb	6.3 ± 2 m [16]	1.2950 ± 0.8285
^{132}Te	3.204 ± 0.013 d [18]	5.1430 ± 0.1029
^{133m}Te	55.4 ± 0.4 m [19]	3.1400 ± 0.1884
^{134}Te	41.8 ± 0.8 m [20]	4.7630 ± 0.2858
^{131}I	8.0252 ± 0.0006 d [17]	3.87100 ± 0.03871
^{132}I	2.295 ± 0.013 h [18]	5.306 ± 3.396
^{133}I	20.83 ± 0.08 h [19]	6.896 ± 4.413
^{134}I	52.5 ± 0.2 m [20]	7.0960 ± 0.1987
^{135}I	6.58 ± 0.03 h [21]	6.0270 ± 0.2411
^{137}I	24.5 ± 0.2 s [90]	1.9880 ± 0.2187
^{133}Xe	5.2475 ± 0.0005 d [19]	6.958 ± 4.453
^{133m}Xe	2.198 ± 13 d [19]	0.11840 ± 0.07576
^{135}Xe	9.14 ± 2 h [21]	7.52800 ± 0.07528
^{135m}Xe	15.29 ± 0.05 m [21]	1.4820 ± 0.4741

^{136}Cs	13.01 ± 0.05 d [91]	6.18200 ± 0.03956
^{140}Ba	12.751 ± 0.004 d [24]	5.3000 ± 0.0371
^{140}La	1.67858 ± 0.00021 d [24]	5.300 ± 0.053
^{142}La	91.1 ± 0.5 m [26]	4.74200 ± 0.06639
^{141}Ce	32.511 ± 0.013 d [25]	5.1380 ± 0.1439
^{143}Ce	33.039 ± 0.006 h [27]	4.32800 ± 0.02164
^{144}Ce	284.91 ± 0.05 d [92]	3.69000 ± 0.02583
^{147}Nd	10.98 ± 0.01 d [93]	2.01000 ± 0.01407

2.4 Experiment

Godiva IV is a critical assembly composed of unreflected highly enriched uranium (HEU) metal fuel [94]. This device was intended to irradiate samples using prompt bursts of fast fission neutrons of around 24 μsec FWHM in duration with a peak neutron flux of around 4×10^{18} neutrons/cm^2/sec [94]. Large neutron fluxes allow shorter irradiation times, minimizing neutron absorption in the subsequent fission products, and assuring larger fission product generation rates.

2.4.1 Data Collection System

The data collection system consists of two Broad Energy Germanium (BEGe) detectors, each coupled to a Lynx data acquisition system. The BEGe detectors (Canberra, model BE6530) were 60% relative efficiency (3"x3" NaI detector at 1.33 MeV) and mounted in large cryostats filled with liquid nitrogen. The γ-rays detected by the BEGe spectrometers were stored in list mode format by the Lynx

systems (Canberra, Digital Signal Analyzer). Data from each detector were stored in a separate file with each γ-ray interaction recorded by a time stamp and energy. The timing between detectors was synchronized using a 5 MHz oscillator such that timing between the two detectors could be used as a filter for coincident events in the future. The live time and real time values for the data acquisition system were recorded approximately 30 times per second by the Lynx data acquisition system and recorded with the list mode data stream. The live time is the duration that the data acquisition was collecting data while the real time is the wall-clock time. For data rates of approximately 25 kHz or less the live time fraction of the data acquisition system was high enough to prevent instabilities or errors in data recording with the Lynx data acquisition system.

The two BEGe detectors (detectors are labelled as 8815 and 8816) were positioned a minimum of 114 cm from each wall in the counting location. The detector cold finger was mounted in a 32 L dewar placed on the concrete floor and the distance from the center of the face of the BEGe detector was approximately 70 cm from the floor. The two detectors were oriented 180° from each other with the source material placed equidistant between them (see Figure 24).

The front face of each detector were 9.0 cm from the plutonium sample location. Thin iron and Teflon™ absorber materials were placed in front of each detector. A 1/16" thick iron was placed directly in front of the detector face followed by a 1.5 cm thick Teflon™ absorber. The Teflon™ piece absorbed β-particles emitted by the decaying sample. β-particles striking the BEGe detector result in prompt summing that occurs when β-particles and γ-rays emitted by the decaying sample strike the active detector volume simultaneously. When this takes place, the interactions are recorded as a single event and the additional energy from the β-particles effectively pushes the γ-ray full energy out of the photopeak. The

impact of summing the γ rays and β particles ultimately reduces the γ photopeak efficiency and broadens the peak resolution. Hence, the placement of the Teflon™ absorber between the radioactive sample and the BEGe detector curtails this summation and improves the spectroscopic quality of the data. Radiation (Bremsstrahlung) produced in the Teflon™ disk from the β-particles losing energy prior to absorption. The iron also limits the detection of X-rays from the radioactive sample. Like β-particles, these X-rays will be detected by the active volume of the BEGe, causing summing and poorer quality spectra. From a characterization effort, a 1/16" thickness of iron was determined to reduce the detection of photons with energies less than 100 keV sufficiently to reduce summing effects in the BEGe detectors.

The sample and detector geometry were held in place rigidly by a printed plastic cylinder. The source position location was defined by a 0.5 cm open slit at the center of the plastic cylinder, which was designed such that the sample position was repeatable. Additional cardboard inserts were used to constrain the sample position and prevent movement. The space between the sample and the detectors were unobstructed except for the Teflon™ and iron disks. The printed plastic and cardboard inserts did not extend over the source region. The plastic cylinder had an open section across the top and marked at 0.5 cm intervals. This opening permitted the detector and absorber positions to be observed and measured. The plastic cylinder diameter nearly equaled the circumference of the BEGe detector face, thus allowing ease of movement and accurate alignment of the detectors.

The source position and sensitive detection areas were shielded from background radiation with Cu plates and Pb bricks. The Cu was a four-sided box of 3/8" thickness. Copper was used as graded shielding, absorbing X-rays produced as secondary radiation from source and background γ-rays striking the surround-

Figure 6: Counting setup.

ing Pb bricks. The Pb bricks were 2"x4"x8" in volume and covered the same surface area as the Cu plates.

2.4.2 System Calibrations

The BEGe detectors and shielding used for this measurement were exactly the same as those used for previous ^{235}U [74] and ^{238}U [75] fission product yield measurements [76]. Radioactive sources of ^{22}Na, ^{60}Co, ^{137}Cs, ^{133}Ba, and ^{54}Mn were placed in the source position and used to determine the energy calibration and detection efficiencies. The four ^{239}Pu samples have masses of 5.0 mg, 9.3 mg, 18.1 mg, and 19.2 mg. These are labeled as Pu1, Pu2, Pu3, and Pu4 respectively. The plutonium metal has an isotopic purity of 99.11% ^{239}Pu, 0.88% ^{240}Pu, 1.1E-3%

^{241}Pu, 5.0E-3% ^{242}Pu, and about 1.1E-2% ^{241}Am by mass, based on Thermal Ionization Mass Spectrometry (TIMS) measurements decayed to the irradiation date. These plutonium metal samples were counted for short periods (tens of minutes each) on 11/15/2018. A background measurement was performed overnight on 11/27/2018 for twelve hours.

2.4.3 Irradiation and Measurement

For the irradiation in the central volume of Godiva IV, the witness foils were wrapped together in aluminum foil. These witness foils consisted of small quantities of Cu (102.804 mg), Au (137.027 mg), Co (31.277 mg), Fe (113.533 mg) and Ti (58.601 mg). That packet was placed along with the quartz ampoules in the aluminum sample holder tube into the Godiva glory hole. Figure 26 shows the four samples prior to irradiation. Figure 8 shows the aluminum tube that holds the quartz vials and witness foil for placement inside of Godiva.

The four ^{239}Pu metal samples were inserted into Godiva on November 28, 2018 at 08:35 a.m. PDT and the burst occurred at 09:42:48 a.m. The radiation monitor (an RMS-III detector) primarily measures gamma dose and exceeded its measurement limit during the burst. 700 R/hr is the highest reading observed before it went over-limit. Two resistance temperature detectors (RTDs) in Godiva IV are used to measure the temperature in the safety block (closest to the center) and in a ring. The safety block's RTD measured the core to be 13°C and increased by 143°C during the burst. The dose rate from Godiva itself needed to decrease enough for personnel entry to be allowed to retrieve the samples. The samples weren't retrieved until 10:07:52 a.m. The witness foils and empty quartz ampule were set aside for subsequent packaging and shipment to Pacific Northwest National Laboratory (PNNL). The plutonium samples were packaged together for

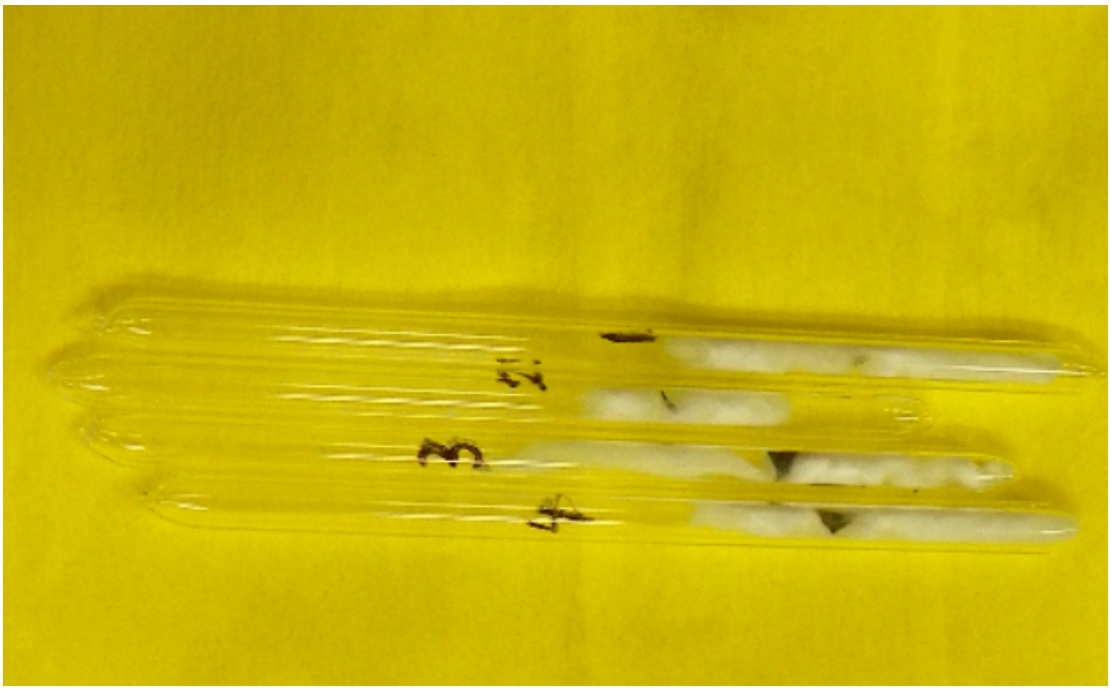

Figure 7: ^{239}Pu samples in quartz ampoules. The samples were packed with quartz wool to position the sample towards the center.

transport to the counting station at 10:18 a.m. Sample Pu2 was mounted on a sample holder and placed in the central location between the BEGe detectors. The detection rate was approximately 67 kHz at 10:22 a.m. Pu2 was quickly removed and replaced with Pu1. The detected rate on each detector was 37 kHz. This sample was kept in front of the detectors and counting began at 10:27:45 a.m. At 1:40:39 p.m. the data acquisition was stopped, data were saved, then Pu3 + Pu4 were mounted and placed in the central position. The second measurement started at 2:14:16 p.m. on November 28, 2018. The detected rate on each system was approximately 12 kHz. The measurement of Pu3 and Pu4 continued until 09:47 a.m. on December 10, 2018. From November 28, 2018 through December 10, 2018 there was no radioactive material activity in the area surrounding the counting system. The room was closed and not accessed except for occasional filling of liquid nitrogen. An unintentional high voltage shut off occurred for de-

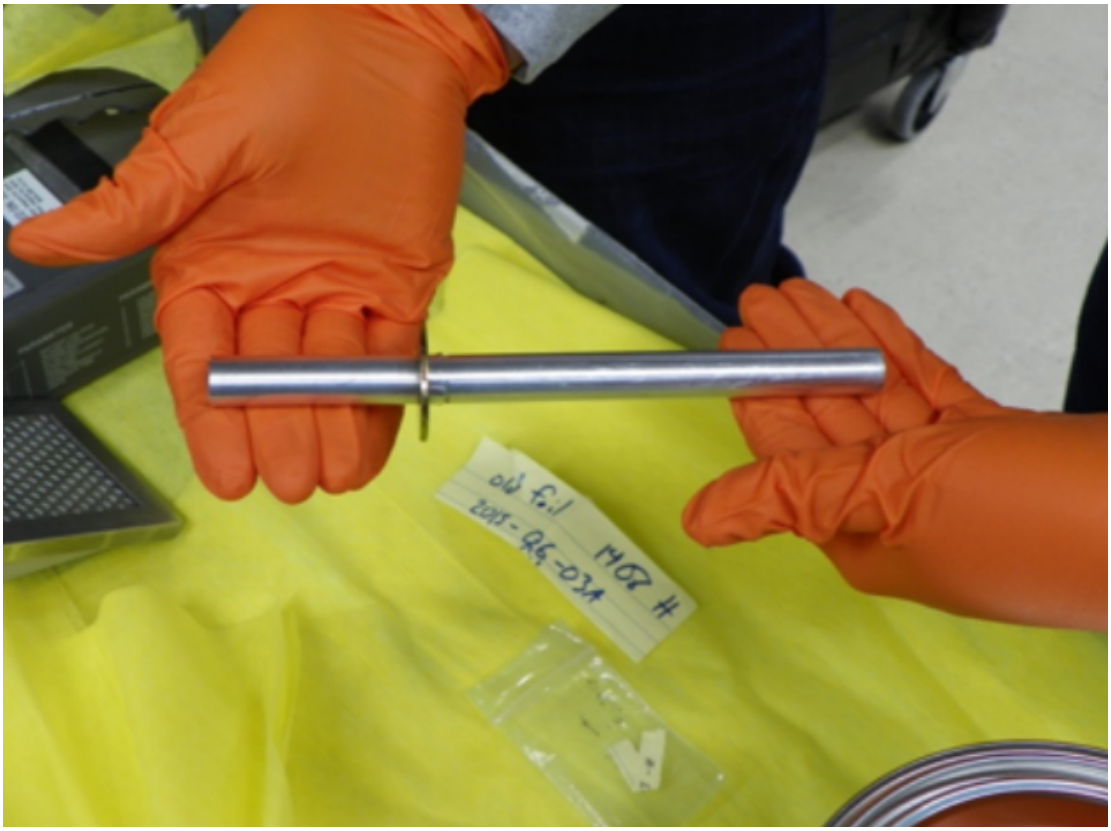

Figure 8: Metal tube containing the quartz vials with plutonium and fluence monitor package for insertion into Godiva.

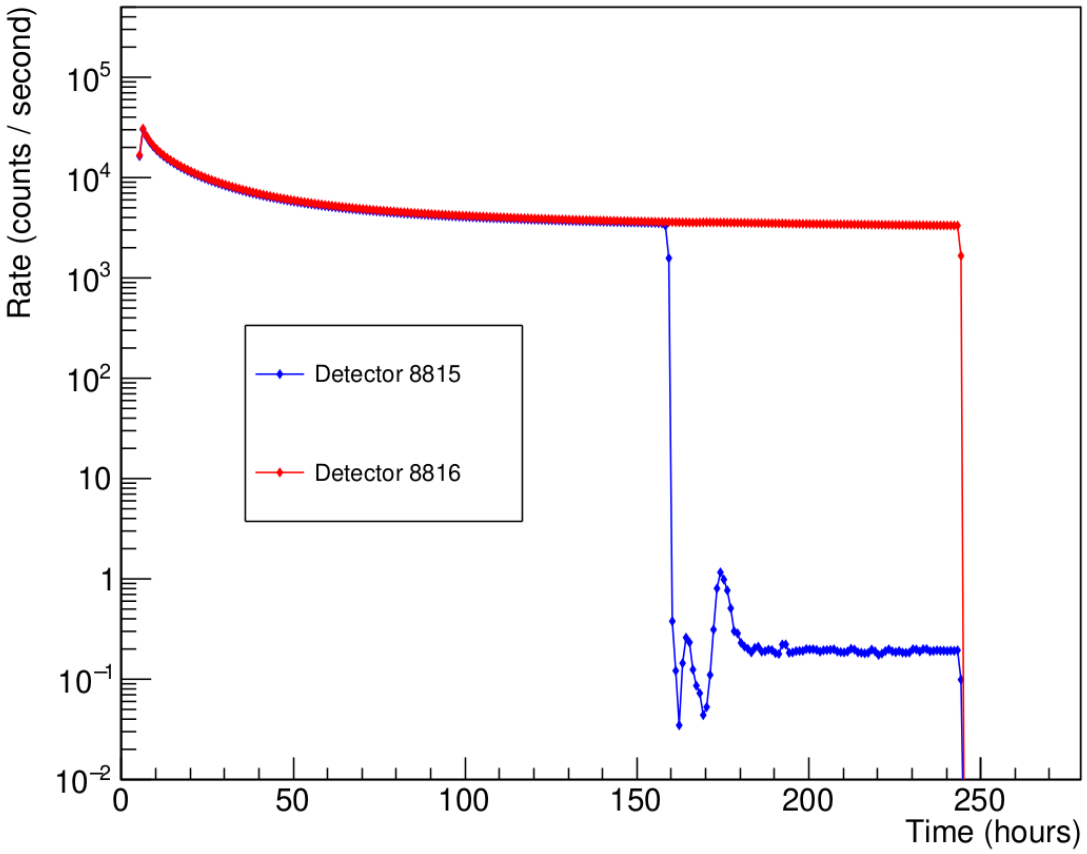

Figure 9: The decrease in counting rate observed for detector 8815 at around 160 hours is due to a bias shutdown.

tector number 8815 late on December 4, 2018, at approximately 155 hours into the data acquisition. Detector number 8816 continued counting until the end of the run on December 10, 2018. Figure 9 shows the large drop in count rate when the high voltage shut off occurred in detector 8815 but not in detector 8816.

2.4.4 Witness Foil Analysis

The witness foil pack was irradiated with the plutonium samples and analyzed at PNNL. Table 16 shows the measured specific activity for each activated metal. From this measurement, the neutron energy spectrum (see Figure 27) was calculated using the STAYSL PNNL code [95]. The STAYSL analysis estimated

Table 3: Witness foil reactions and measured sample activation values, corrected to the burst irradiation time.

Sample	Mass (mg)	Reaction	Isotope	Specific Activity (Bq/mg)
Cu	102.804	^{63}Cu(n,γ) ^{65}Cu(n,2n)	^{64}Cu	4.1E5 ± 1E4
		^{63}Cu(n,α)	^{60}Co	2.32 ± 0.07
Au	137.027	^{197}Au(n,γ)	^{198}Au	2.89E5 ± 6E3
		^{197}Au(n,2n)	^{196}Au	1.84 ± 0.04
Co	31.277	^{59}Co(n,γ)	^{60}Co	92 ± 2
		^{59}Co(n,p)	^{59}Fe	389 ± 8
		^{59}Co(n,2n)	^{58}Co	91 ± 2
Fe	113.533	^{58}Fe(n,γ)	^{59}Fe	4.2 ± 0.2
		^{54}Fe(n,p)	^{54}Mn	208 ± 4
		^{56}Fe(n,p)	^{56}Mn	1.36E5 ± 7E3
		^{54}Fe(n,α)	^{51}Cr	25 ± 2
Ti	58.601	^{46}Ti(n,p)	^{46}Sc	181 ± 4
		^{47}Ti(n,p)	^{47}Sc	6.5E3 ± 1E2
		^{48}Ti(n,p)	^{48}Sc	2.0E3 ± 1E2

1.28E12 ± 9E10 fissions per gram of the plutonium samples.

2.5 Data Analysis

The fission product yield, FPY_i, for isotope i can be calculated directly from the ratio of the number of decay events from isotope i to the total number of fission events in the irradiation experiment. The total number of fission events N_f is generated assuming a known reference fission product yield, FPY_{ref}:

$$N_f = \frac{A_{0,ref}\tau_{1/2,ref}}{\ln(2)FPY_{ref}\epsilon_{\gamma ref}I_{ref}R_{ref}}. \tag{4}$$

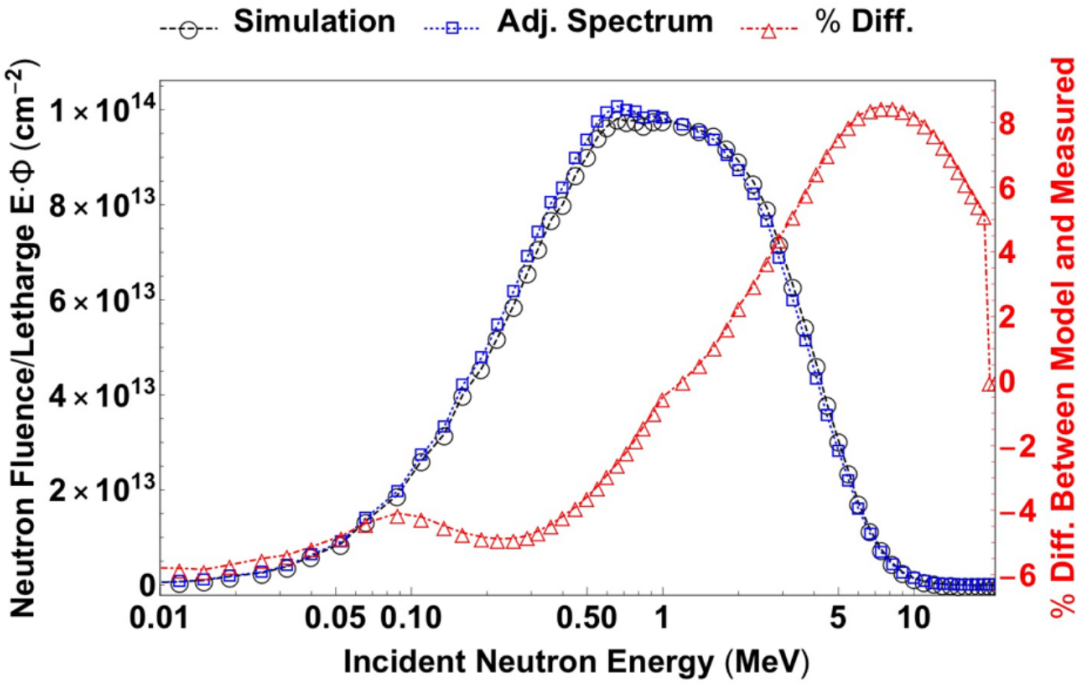

Figure 10: A plot of the MCNP simulated and adjusted neutron fluence spectrum for Godiva IV during the ^{239}Pu pulsed irradiation.

The measured fission yield for isotope i can then be written in terms of the reference isotope:

$$\frac{FPY_i}{FPY_{ref}} = \left(\frac{A_{0,i}}{A_{0,ref}}\right) \left[\frac{\tau_{1/2,i}/\epsilon_{\gamma,i} I_i R_i}{\tau_{1/2,ref}/\epsilon_{\gamma,ref} I_{ref} R_{ref}}\right]. \tag{5}$$

Here, A_0 is the initial activity of the induced radioactive fission product, $\tau_{1/2}$ is the half-life of the specific isotope, ϵ_γ is the absolute detector efficiency, I is the self attenuation of the γ ray through the target, and R is the branching ratio of the γ ray observed. The activities, half-life, and efficiencies are measured in the experiment, while the other parameters are from ENDF-VIII.0 [37]. The reference fission product used to estimate the total number of fission events is ^{99}Mo (^{99}Mo and ^{140}Ba are common standards for fission product yield measurements [96]).

2.5.1 Detector Efficiency – ϵ_γ

Table 4: Eckert & Ziegler calibration sources used for detector characterization.

Source	$\tau_{1/2}$	Activity (μCi)	Date
^{60}Co	1925.28 ± 0.14 d [97]	1.03 ± 0.03	11/15/2007
^{137}Cs	30.08 ± 0.09 y [90]	1.03 ± 0.03	11/15/2007
^{22}Na	2.6018 ± 0.0022 y [98]	1.06 ± 0.03	11/15/2007
^{54}Mn	312.20 ± 0.20 d [99]	1.02 ± 0.03	11/15/2007
^{133}Ba	10.551 ± 0.011 y [19]	1.03 ± 0.03	11/15/2007

Table 17 lists the calibration sources used. This data is used for energy calibration and detector efficiency fits. The equation used to fit the detector efficiency is the following:

$$\epsilon_\gamma = P_0 E^{-P_1} + P_2 - P_3 e^{-P_4 E} \tag{6}$$

where E is energy in MeV. The parameters 0–4 were extracted from the efficiency fit (see Table 29 and Figures 28 and 29). The uncertainty was calculated using the following ROOT generated covariance matrices:

	P_0	P_1	P_2	P_3	P_4
P_0	8.6E-9	-2.7E-6	-8.6E-9	-1.1E-6	-1.3E-6
P_1	-2.7E-6	8.5E-4	2.6E-6	3.6E-4	1.0E-4
P_2	-8.6E-9	2.6E-6	8.7E-9	1.1E-6	1.6E-6
P_3	-1.1E-6	3.6E-4	1.1E-6	1.7E-4	4.4E-4
P_4	-1.3E-6	1.0E-4	1.6E-6	4.4E-4	2.7E-2

$$\begin{array}{c} \\ P_0 \\ P_1 \\ P_2 \\ P_3 \\ P_4 \end{array} \begin{array}{c} \begin{array}{ccccc} P_0 & P_1 & P_2 & P_3 & P_4 \end{array} \\ \begin{bmatrix} \text{8.5E-9} & \text{-2.6E-6} & \text{-8.5E-9} & \text{-1.2E-6} & \text{-3.4E-6} \\ \text{-2.6E-6} & \text{8.E-4} & \text{2.6E-6} & \text{3.9E-4} & \text{8.1E-4} \\ \text{-8.5E-9} & \text{2.6E-6} & \text{8.7E-9} & \text{1.2E-6} & \text{3.7E-6} \\ \text{-1.2E-6} & \text{3.9E-4} & \text{1.2E-6} & \text{2.0E-4} & \text{8.1E-4} \\ \text{-3.4E-6} & \text{8.1E-4} & \text{3.7E-6} & \text{8.1E-4} & \text{2.7E-2} \end{bmatrix} \end{array}$$

for detector 8815 and 8816 respectively.

Table 5: Efficiency curve parameters.

P_i	Detector 8815	Detector 8816
[0]	$2.20 \times 10^{-3} \pm 9 \times 10^{-5}$	$2.26 \times 10^{-3} \pm 9 \times 10^{-5}$
[1]	1.15 ± 0.03	1.17 ± 0.03
[2]	$2.05 \times 10^{-3} \pm 9 \times 10^{-5}$	$2.27 \times 10^{-3} \pm 9 \times 10^{-5}$
[3]	0.27 ± 0.01	0.29 ± 0.01
[4]	27.6 ± 0.2	27.3 ± 0.2

2.5.2 Self-Attenuation – I

The self attenuation factor accounts for the γ rays attenuating effect through the ^{239}Pu samples, and is represented by the following:

$$I = \frac{I_{raw}}{C} = e^{-\frac{\mu}{\rho} x \rho} \tag{7}$$

where I_{raw} is the unnormalized self attenuation factor, C is the corrected counts without attenuation, μ/ρ is the mass attenuation for ^{239}Pu (provided by NIST XCOM [100]), x is the mean free path, and ρ is the density of ^{239}Pu (19.84 g/cm^3 [101]). Figures 30, 31, 32, and 33 are corrected counts of ^{239}Pu γ rays listed in Table 19 and fitted with Equation 14. The normalized counts resulted in Pu1 mass to be 4.5 ± 0.1 mg and 4.0 ± 0.1 mg for detectors 8815 and 8816

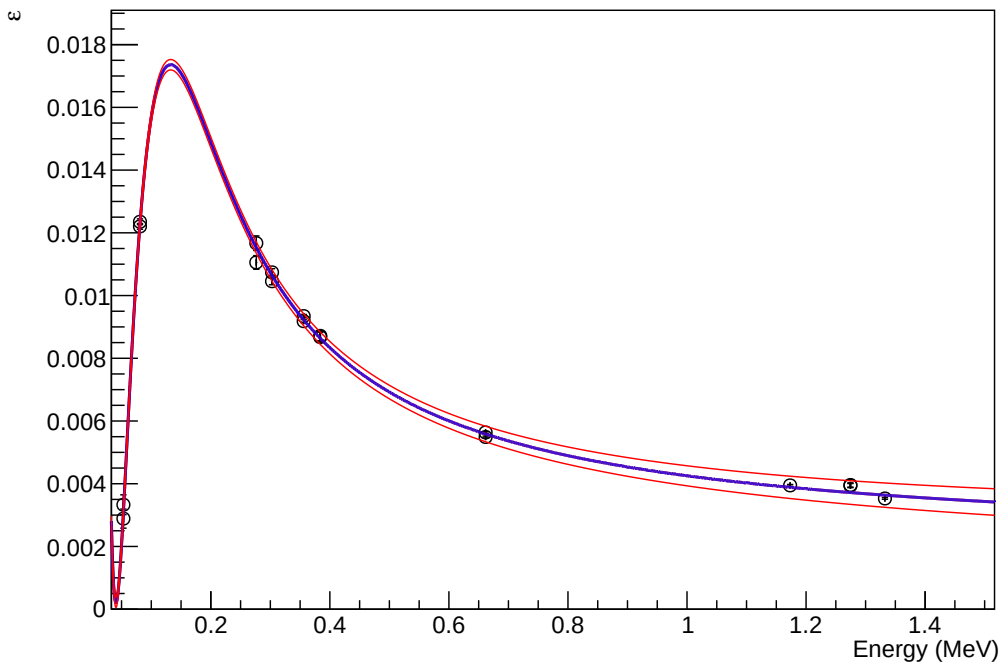

Figure 11: The detection efficiency of detector 8815 was measured for different calibration sources.

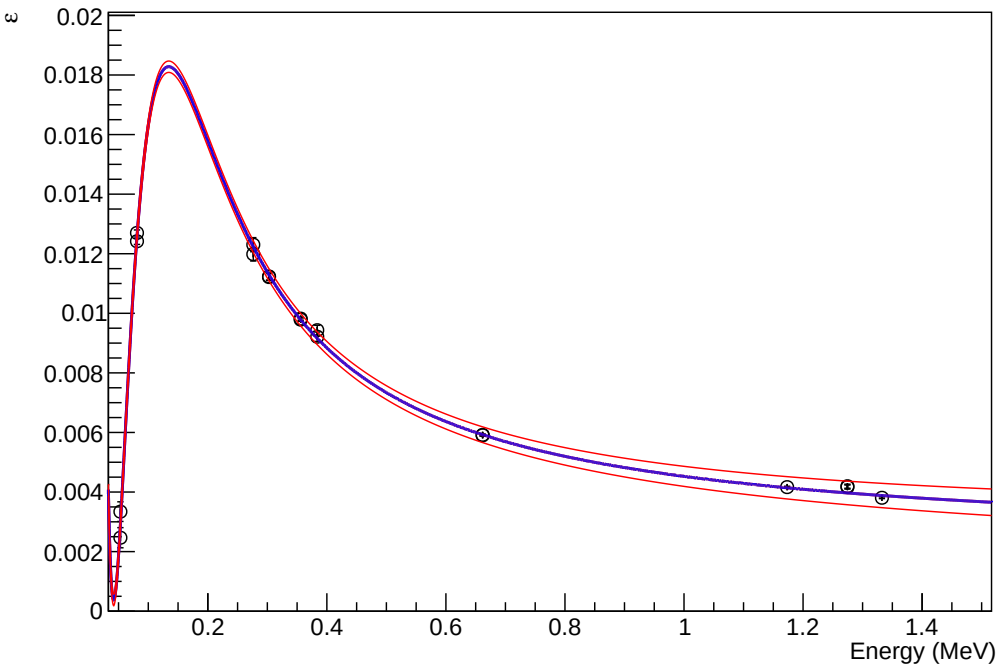

Figure 12: The detection efficiency of detector 8816 was measured for different calibration sources.

Table 6: ^{239}Pu γ-rays used to determine the self attenuation factor. All γ-rays were used for Pu3 + Pu4 while only two were used for Pu1.

E_γ (keV)	R_γ	Pu1?
38.7	$1.044 \times 10^{-4} \pm 0.013 \times 10^{-4}$	–
51.6	$2.722 \times 10^{-4} \pm 0.022 \times 10^{-4}$	✓
129.3	$6.31 \times 10^{-5} \pm 0.04 \times 10^{-5}$	–
171.4	$1.10 \times 10^{-6} \pm 0.02 \times 10^{-6}$	–
195.7	$1.07 \times 10^{-6} \pm 0.01 \times 10^{-6}$	–
203.6	$5.69 \times 10^{-6} \pm 0.03 \times 10^{-6}$	–
332.8	$4.94 \times 10^{-6} \pm 0.03 \times 10^{-6}$	–
336.1	$1.12 \times 10^{-6} \pm 0.02 \times 10^{-6}$	–
345.0	$5.56 \times 10^{-6} \pm 0.05 \times 10^{-6}$	–
375.1	$1.554 \times 10^{-5} \pm 0.009 \times 10^{-5}$	✓
380.2	$3.05 \times 10^{-6} \pm 0.06 \times 10^{-6}$	–
382.8	$2.59 \times 10^{-6} \pm 0.05 \times 10^{-6}$	–
413.7	$1.466 \times 10^{-5} \pm 0.011 \times 10^{-5}$	–
451.5	$1.894 \times 10^{-6} \pm 0.016 \times 10^{-6}$	–

respectively. The Pu1 mass was 5.0 mg. The Pu1 sample mass difference is caused by a position offset of the sample compared to the position of the calibration sources. The normalized counts resulted in large Pu3 + Pu4 mass to be 35.0 ± 0.1 mg and 35.3 ± 0.1 mg for detectors 8815 and 8816 respectively. The Pu3 and Pu4 masses were 18.1 mg and 19.2 mg respectively, which summed to 37.3 mg. The Pu3 + Pu4 mass difference is caused by a position offset of the sample compared to the position of the calibration sources.

2.5.3 Total Fission – N_f

The total number of fission events used in this analysis was calculated with Equation 11. The reference fission product is ^{99}Mo, specifically the 739.5 keV γ-ray from Pu3 + Pu4. Table 21 lists the parameters used to determine the total number of fission events. All fission product yield values in this paper will use the

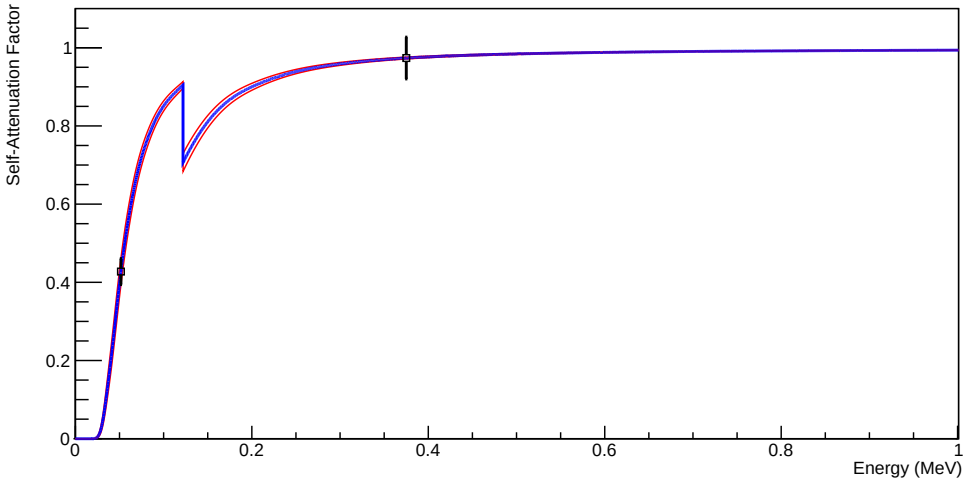

Figure 13: Pu1 self attenuation measured with detector 8815 where x = 3.8E-3 ± 4E-4 cm.

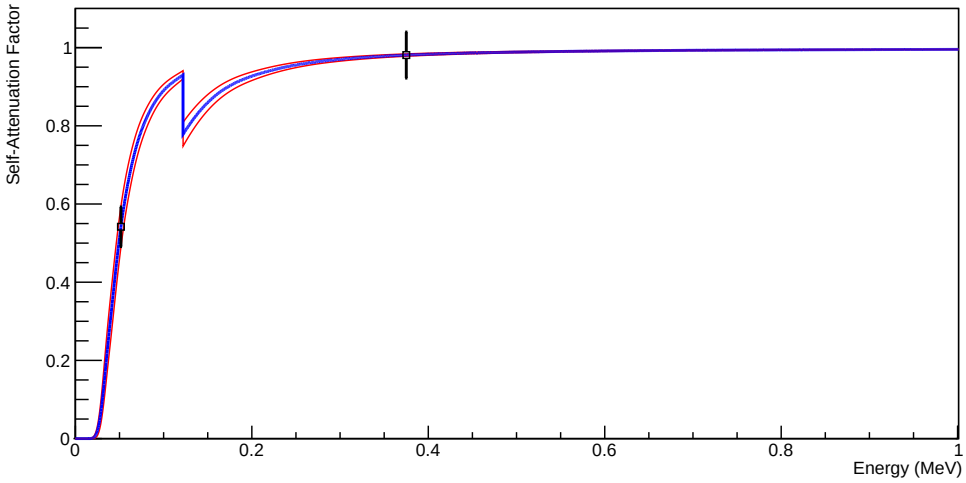

Figure 14: Pu1 self attenuation measured with detector 8816 where x = 2.8E-3 ± 4E-4 cm.

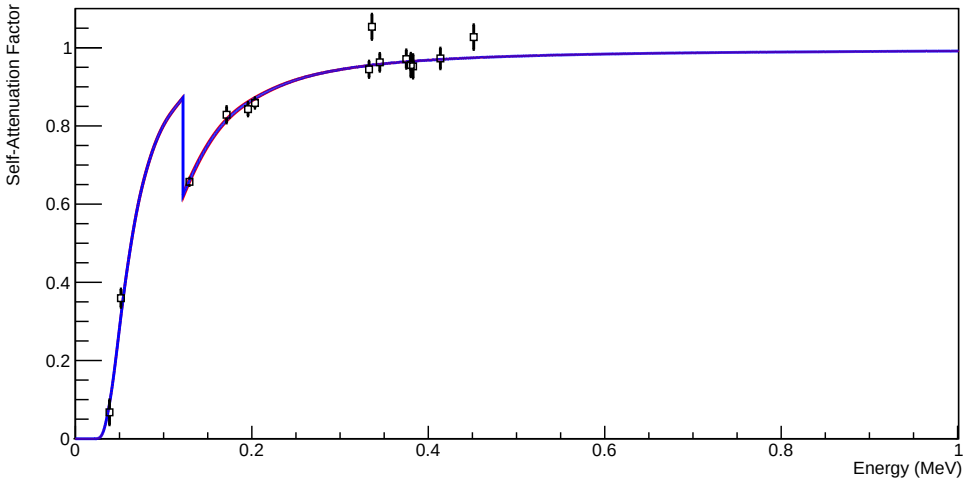

Figure 15: Pu3 + Pu4 self attenuation measured with detector 8815 where x = 5.2E-3 ± 2E-4 cm.

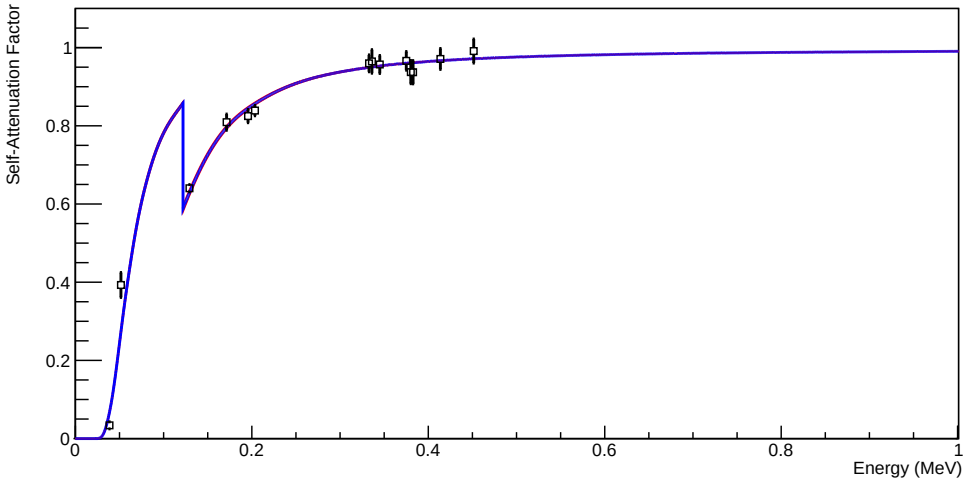

Figure 16: Pu3 + Pu4 self attenuation measured with detector 8816 where x = 5.8E-3 ± 2E-4 cm.

weighted mean of the total number of fission events between the two detectors. Pu1's total number of fission events is based on Pu3 + Pu4's result for ^{142}La 894.9

Table 7: Parameters used to determine Pu3 + Pu4's total number of fission events.

Parameter		
Isotope	^{99}Mo	
$\tau_{1/2}$ (hrs)	65.976 ± 0.024 [10]	
FPY (%)	6.23 ± 0.04 [37]	
E_γ (keV)	739.500 ± 0.017 [10]	
R_γ (%)	12.2 ± 0.2 [10]	
Detector	8815	8816
A_0 (Bq)	$4.735 \times 10^0 \pm 5 \times 10^{-3}$	$4.978 \times 10^0 \pm 6 \times 10^{-3}$
ϵ_γ	$5.2 \times 10^{-3} \pm 3 \times 10^{-4}$	$5.5 \times 10^{-3} \pm 3 \times 10^{-4}$
I_γ	$9.879 \times 10^{-1} \pm 4 \times 10^{-4}$	$9.865 \times 10^{-1} \pm 4 \times 10^{-4}$
N_f	$4.2 \times 10^{10} \pm 2 \times 10^9$	$4.1 \times 10^{10} \pm 2 \times 10^9$
$\overline{N_f}$	$4.1 \times 10^{10} \pm 2 \times 10^9$	

keV γ-ray.

Table 8: Parameters used to determine Pu1's total number of fission events.

Parameter		
Isotope	^{142}La	
$\tau_{1/2}$ (hrs)	1.518 ± 0.008 [26]	
FPY (%)	5.2 ± 0.3 (Pu3 + Pu4 result)	
E_γ (keV)	894.9 ± 0.4 [26]	
R_γ (%)	8.34 ± 0.17 [26]	
Detector	8815	8816
A_0 (Bq)	$1.263 \times 10^1 \pm 2 \times 10^{-2}$	$1.33 \times 10^1 \pm 1 \times 10^{-1}$
ϵ_γ	$4.6 \times 10^{-3} \pm 3 \times 10^{-4}$	$4.8 \times 10^{-3} \pm 3 \times 10^{-4}$
I_γ	$9.929 \times 10^{-1} \pm 7 \times 10^{-4}$	$9.949 \times 10^{-1} \pm 8 \times 10^{-4}$
N_f	$5.1 \times 10^9 \pm 4 \times 10^8$	$5.1 \times 10^9 \pm 4 \times 10^8$
$\overline{N_f}$	$5.1 \times 10^9 \pm 4 \times 10^8$	

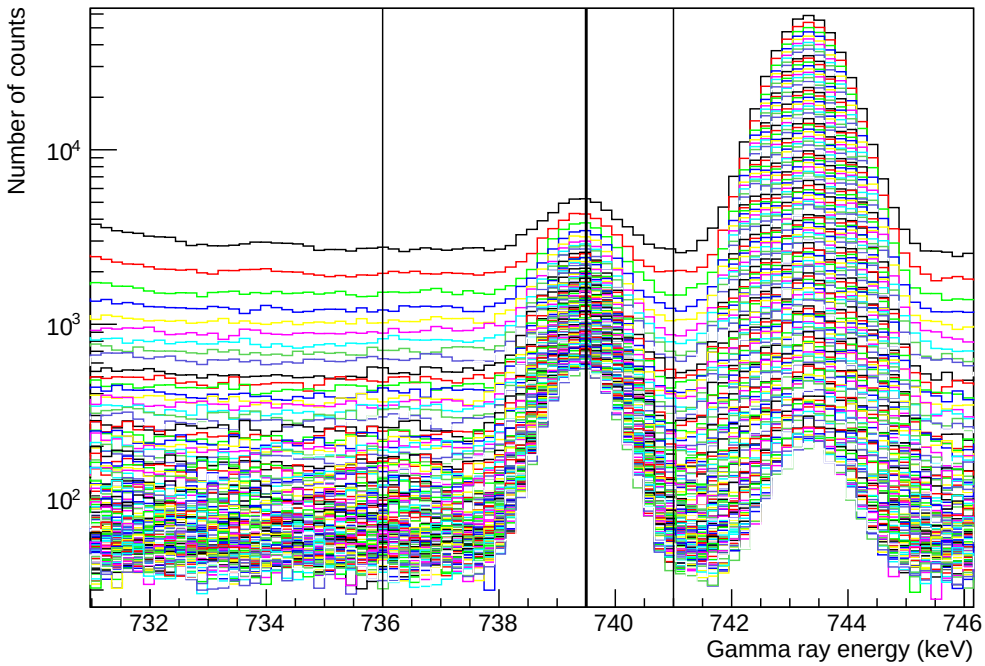

Figure 17: ^{99}Mo γ-ray cascade plot for the 739.5 keV γ ray. For more details, please refer to the text.

2.5.4 γ-Ray Analysis

The γ ray peaks are analyzed using a code written in ROOT [39]. By defining unique energy intervals for each peak, we isolate the peaks in the spectrum so they can be analyzed independently. These intervals are determined visually using cascade plots as illustrated in Figure 34 for the case of a γ-ray peak at 793.5 keV associated with the fission product ^{99}Mo. Each color represents a different time bin and as time progresses the overall counts decrease. In this example, the energy interval is set to [736 keV, 741 keV] to filter out the peak around 743 keV. The interval chosen attempts to include information of the background and photo-peak.

As the time binned data is acquired, the live and raw time are used for the dead time correction by multiplying the counts for an energy bin with the ratio of raw time divided by live time. The energy bin channel number is converted into energy deposited by multiplying by the ratio of total energy range to the total number of energy bins. In this case, the energy range is [0,2500 keV] and there are 16384 energy channel bins. The time binned data are histograms of counts vs. energy for each time bin. When the time and energy intervals are chosen, a Gaussian fit function with a linear background is used to fit the histogram for each time:

$$F(E) = N \exp\left[-\frac{(E-\mu)^2}{2\sigma^2} \right] + mE + y, \tag{8}$$

where N is the amplitude of the peak, μ is the energy of the peak, σ is the resolution of the detector, m is the slope of the background, y is the y-intercept of the background, and E is energy. This technique is used when there is a background continuum present [102]. Before the code fits every time slice, a master fit is produced to provide the centroid of the γ-ray peak [see Figure 35].

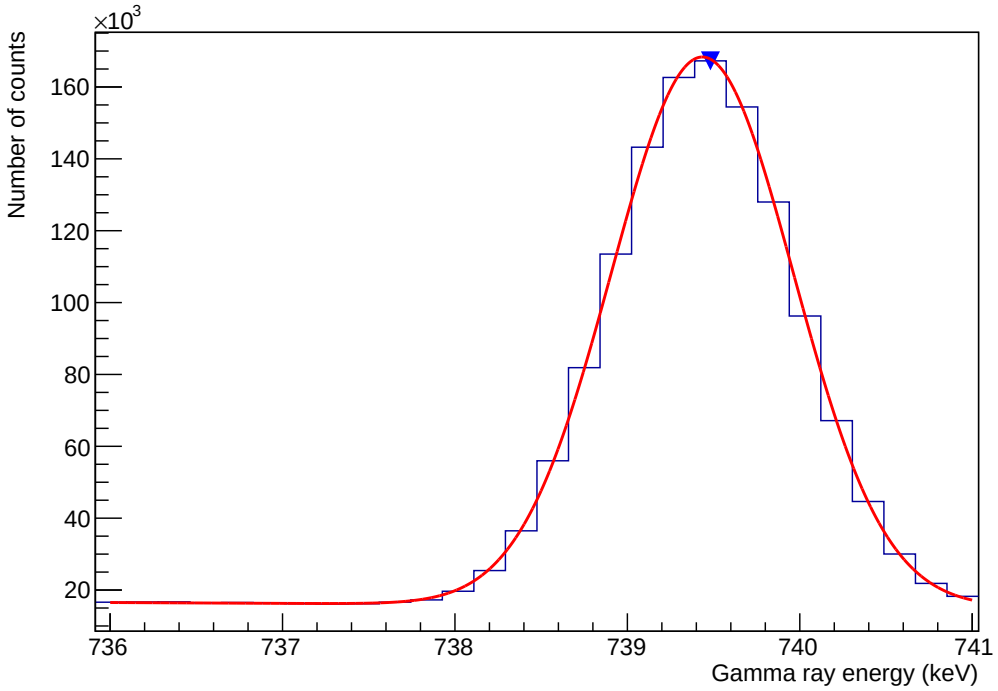

Figure 18: ^{99}Mo master sum plot fit for the 739.5 keV γ ray

The histogram for the master fit is the produced by summing the data over all the time bins in the chosen time interval for each channel.

The linear background is subtracted out and the integral S is the net counts in each respective time bin.

$$\begin{aligned} S &= \int \left(N \exp\left[-\frac{(E-\mu)^2}{2\sigma^2} \right] + mE + y \right) dx \\ &\quad - \int (mE + y)\, dx \\ &= \int \left(N \exp\left[-\frac{(E-\mu)^2}{2\sigma^2} \right] \right) dx. \end{aligned} \tag{9}$$

2.5.5 Decay Curve Fitting Routine – $\tau_{1/2}$, A_0

Net counts and half-life data are used to fit a decay curve that is extrapolated to time zero. The data for this curve consists of the counts integrated over each

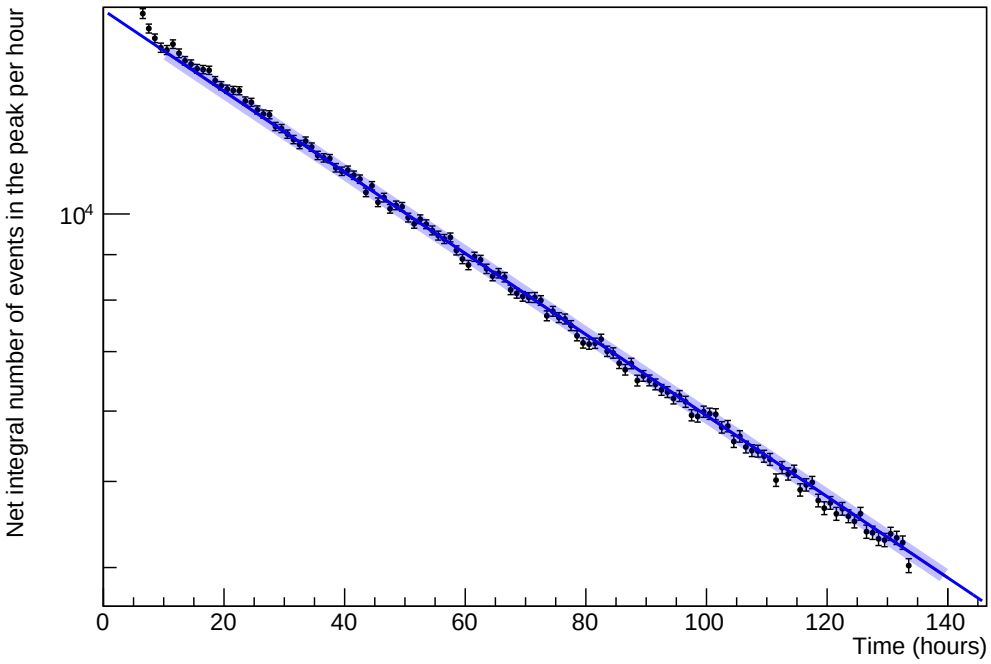

Figure 19: ^{99}Mo γ ray half-life plot for the 739.5 keV γ ray

peak (using the energy interval established previously) in each time bin . To secure a proper decay curve, the half life and time increments were fixed. The only parameter to change would be the initial count rate. Provided is the fit function:

$$N(t) = \left(\frac{A_0\tau_{1/2}}{\ln(2)}\right)\left(\exp\left(-\frac{\ln(2)}{\tau_{1/2}}t\right) - \exp\left(-\frac{\ln(2)}{\tau_{1/2}}(t+\Delta t)\right)\right), \tag{10}$$

where $N(t)$ is the counts of γ rays, A_0 is the initial count rate of γ rays, $\tau_{1/2}$ is half life, Δt is time step, and t is time. This equation is derived from the integral of the count rate over a time bin.

Figure 36 shows the number of events in the peak per hour bin, where the blue line is the fit function and the thicker line indicates the time interval used in the fitting. The black points are the net counts with error for each time bin.

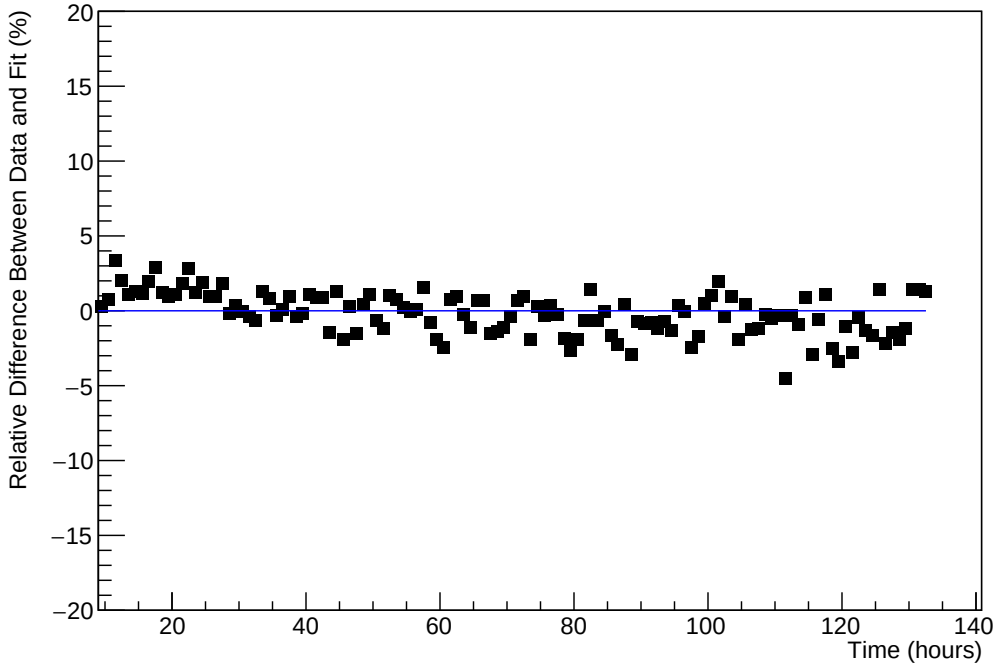

Figure 20: ^{99}Mo γ ray residual plot for the 739.5 keV γ ray

Figure 37 shows the residuals plot from the fitting in Figure 36. The residual plot is another criteria used to help determine an energy and time interval for the γ ray analysis. A time interval is iterated until residuals are less than a user-defined value of 20%. The goal is to include as much fitting points as possible, while minimizing the relative differences in the residual plot.

2.6 Results

For Pu3 + Pu4, 26 isotopes were analyzed using 80 γ-rays, resulting in 80 cumulative fission product yield results (see Table 22). For Pu1, 20 isotopes were analyzed using 43 γ-rays, resulting in 43 cumulative fission product yield results (see Table 23). 10 isotopes from Pu1 overlapped with results from Pu3 + Pu4. These were ^{88}Kr, ^{92}Sr, ^{105}Ru, ^{127}Sn, ^{132}Te, ^{133}I, ^{135}I, ^{141}La, ^{142}La, and ^{149}Nd. In

total, 36 different isotopes were analyzed from this experiment. Since only a single decay curve fit was used, all results are cumulative fission product yields.

Table 9: Pu3 + Pu4 cumulative fission product yield results from detectors 8815 and 8816. Values were combined by an uncertainty weighted mean. Reference values are from ENDF/B-VIII.0 [37]. ^{99}Mo reference fission product yield for 739.5 keV γ-ray was used to determine the total number of fission events.

Isotope	E_γ (keV)	FPY_{8815} (%)	ΔFPY_{8815} (%)	FPY_{8816} (%)	ΔFPY_{8816} (%)	$\overline{FPY}$ (%)	$\Delta\overline{FPY}$ (%)	FPY_{ref} (%)	ΔFPY_{ref} (%)
^{85m}Kr	151.195	0.615	0.051	0.614	0.051	0.615	0.036	0.393	0.006
^{87}Kr	402.587	1.197	0.105	1.182	0.104	1.189	0.074	1.035	0.021
^{88}Kr	196.301	1.586	0.118	1.575	0.117	1.580	0.083	1.285	0.036
^{88}Kr	1529.770	1.093	0.160	1.083	0.156	1.088	0.112	1.285	0.036
^{88}Kr	2029.840	1.003	0.188	0.996	0.182	0.999	0.131	1.285	0.036
^{88}Kr	2195.842	0.990	0.195	0.977	0.189	0.983	0.136	1.285	0.036
^{88}Kr	2392.110	0.995	0.210	0.991	0.205	0.993	0.147	1.285	0.036
^{91}Sr	652.900	2.915	0.241	2.963	0.245	2.939	0.172	2.510	0.070
^{91}Sr	749.800	2.651	0.221	2.678	0.223	2.664	0.157	2.510	0.070
^{91}Sr	1024.300	2.681	0.271	2.667	0.267	2.674	0.190	2.510	0.070
^{92}Sr	1383.930	2.461	0.344	2.464	0.341	2.463	0.242	3.012	0.084
^{93}Y	266.900	3.514	0.546	3.463	0.538	3.488	0.383	3.817	2.443
^{93}Y	1917.800	2.992	0.648	2.941	0.630	2.965	0.452	3.817	2.443

^{95}Zr	756.725	4.665	0.358	4.681	0.358	4.673	0.253	5.140	0.072
^{97}Zr	355.400	5.770	0.428	5.669	0.421	5.719	0.300	5.256	0.074
^{97}Zr	507.640	5.520	0.408	5.551	0.411	5.535	0.290	5.256	0.074
^{97}Zr	703.760	5.093	0.448	5.174	0.454	5.133	0.319	5.256	0.074
^{97}Zr	1147.970	5.976	0.671	6.060	0.674	6.018	0.476	5.256	0.074
^{97}Zr	1362.680	5.181	0.820	5.220	0.820	5.200	0.580	5.256	0.074
^{97}Zr	1750.240	4.178	0.758	4.232	0.760	4.205	0.537	5.256	0.074
^{99}Mo	181.068	5.741	0.347	5.827	0.352	5.783	0.247	6.230	0.044
^{99}Mo	739.500	6.230	0.484	6.230	0.483	6.230	0.342	6.230	0.044
^{99}Mo	777.921	6.261	0.502	6.440	0.515	6.348	0.359	6.230	0.044
^{103}Ru	497.085	6.836	0.444	6.886	0.449	6.861	0.316	6.816	0.095
^{105}Ru	469.370	5.700	0.400	5.725	0.403	5.712	0.284	5.351	0.214
^{105}Ru	499.300	6.958	1.072	7.004	1.080	6.981	0.761	5.351	0.214
^{105}Ru	724.300	5.455	0.412	5.425	0.409	5.440	0.290	5.351	0.214
^{105}Ru	969.440	5.681	0.558	5.676	0.554	5.678	0.393	5.351	0.214
^{105}Rh	319.231	5.718	0.384	5.697	0.383	5.708	0.271	5.351	0.150
^{127}Sn	583.300	0.929	0.205	0.754	0.179	0.830	0.135	0.353	0.226

^{127}Sn	1114.300	0.355	0.083	0.323	0.076	0.338	0.056	0.353	0.226
^{127}Sb	252.400	0.379	0.037	0.360	0.036	0.369	0.026	0.500	0.160
^{127}Sb	473.000	0.575	0.051	0.579	0.051	0.577	0.036	0.500	0.160
^{127}Sb	685.700	0.584	0.053	0.594	0.054	0.589	0.038	0.500	0.160
^{129}Sb	544.700	1.306	0.124	1.322	0.125	1.314	0.088	1.374	0.110
^{129}Sb	1030.100	1.370	0.168	1.375	0.168	1.373	0.119	1.374	0.110
^{131m}Te	793.750	1.167	0.096	1.175	0.097	1.171	0.068	0.730	0.328
^{131m}Te	852.210	1.168	0.103	1.159	0.101	1.163	0.072	0.730	0.328
^{131m}Te	1125.460	1.131	0.121	1.144	0.122	1.138	0.086	0.730	0.328
^{131m}Te	1206.600	1.125	0.127	1.108	0.124	1.116	0.088	0.730	0.328
^{131m}Te	1646.010	1.049	0.162	1.087	0.165	1.068	0.116	0.730	0.328
^{131m}Te	1887.700	1.064	0.182	1.045	0.176	1.054	0.126	0.730	0.328
^{132}Te	228.160	5.071	0.353	5.069	0.353	5.070	0.250	5.143	0.103
^{131}I	284.305	4.433	0.265	4.444	0.266	4.438	0.188	3.871	0.039
^{131}I	636.989	4.303	0.307	4.313	0.308	4.308	0.217	3.871	0.039
^{133}I	510.530	8.047	0.584	8.047	0.585	8.047	0.413	6.896	4.413
^{133}I	529.872	7.053	0.507	7.098	0.511	7.075	0.360	6.896	4.413

^{133}I	706.578	7.193	0.581	7.199	0.581	7.196	0.411	6.896	4.413
^{133}I	1298.223	7.235	0.881	7.280	0.877	7.258	0.622	6.896	4.413
^{135}I	220.502	6.380	0.430	6.039	0.407	6.200	0.296	6.027	0.241
^{135}I	288.451	5.616	0.385	5.525	0.379	5.570	0.270	6.027	0.241
^{135}I	417.633	6.462	0.446	6.507	0.450	6.484	0.317	6.027	0.241
^{135}I	546.557	6.774	0.500	6.805	0.503	6.790	0.354	6.027	0.241
^{135}I	836.804	5.937	0.527	5.988	0.529	5.962	0.373	6.027	0.241
^{135}I	1038.760	5.943	0.607	5.929	0.601	5.936	0.427	6.027	0.241
^{135}I	1131.511	5.818	0.632	5.829	0.628	5.824	0.445	6.027	0.241
^{135}I	1260.409	5.804	0.689	5.814	0.683	5.809	0.485	6.027	0.241
^{135}I	1457.560	5.569	0.750	5.532	0.736	5.550	0.526	6.027	0.241
^{135}I	1502.790	5.336	0.751	5.295	0.736	5.315	0.525	6.027	0.241
^{135}I	1566.410	5.168	0.752	5.110	0.734	5.138	0.525	6.027	0.241
^{135}I	1678.027	5.382	0.829	5.361	0.815	5.372	0.581	6.027	0.241
^{135}I	1706.459	5.261	0.828	5.239	0.814	5.250	0.580	6.027	0.241
^{135}I	1791.196	5.288	0.856	5.294	0.845	5.291	0.601	6.027	0.241
^{140}Ba	437.575	5.671	0.368	5.699	0.369	5.685	0.261	5.300	0.037

^{140}Ba	537.261	5.324	0.351	5.312	0.350	5.318	0.248	5.300	0.037
^{141}La	1354.520	5.152	0.669	5.249	0.674	5.200	0.475	5.138	0.308
^{142}La	641.285	5.311	0.378	5.355	0.381	5.333	0.268	4.742	0.066
^{142}La	894.900	5.217	0.462	5.120	0.451	5.167	0.323	4.742	0.066
^{142}La	1545.800	4.112	0.610	4.126	0.605	4.119	0.430	4.742	0.066
^{142}La	1901.300	3.913	0.664	3.890	0.650	3.901	0.464	4.742	0.066
^{142}La	2055.200	4.433	0.826	4.049	0.745	4.221	0.553	4.742	0.066
^{142}La	2397.800	3.393	0.703	3.339	0.680	3.365	0.489	4.742	0.066
^{143}Ce	293.266	4.203	0.247	4.215	0.248	4.209	0.175	4.328	0.022
^{143}Ce	350.619	4.372	0.266	4.397	0.268	4.384	0.189	4.328	0.022
^{143}Ce	664.571	5.014	0.363	4.934	0.357	4.973	0.254	4.328	0.022
^{143}Ce	880.460	4.677	0.403	4.746	0.407	4.711	0.286	4.328	0.022
^{149}Nd	155.873	1.277	0.105	1.344	0.106	1.310	0.074	1.239	0.025
^{151}Pm	167.750	0.757	0.067	0.771	0.069	0.764	0.048	0.783	0.011
^{151}Pm	177.160	1.004	0.093	0.963	0.090	0.983	0.065	0.783	0.011
^{151}Pm	340.080	0.759	0.054	0.745	0.053	0.752	0.038	0.783	0.011

Table 10: Pu1 cumulative fission product yield results from detectors 8815 and 8816. Values were combined by an uncertainty weighted mean. Reference values are from ENDF/B-VIII.0 [37]. Pu3 + Pu4's ^{142}La fission product yield result for 1.23 MeV γ-ray was used to determine the total number of fission events.

Isotope	E_γ (keV)	FPY_{8815} (%)	ΔFPY_{8815} (%)	FPY_{8816} (%)	ΔFPY_{8816} (%)	$\overline{FPY}$ (%)	$\Delta\overline{FPY}$ (%)	FPY_{ref} (%)	ΔFPY_{ref} (%)
^{88}Kr	1529.770	1.206	0.202	1.289	0.212	1.246	0.146	1.285	0.036
^{88}Kr	2195.842	1.101	0.235	1.091	0.229	1.096	0.164	1.285	0.036
^{88}Kr	2392.110	1.086	0.243	1.106	0.244	1.096	0.172	1.285	0.036
^{89}Rb	1248.140	1.578	0.236	2.133	0.318	1.776	0.190	1.717	0.069
^{92}Sr	1383.930	3.057	0.485	3.105	0.489	3.081	0.344	3.012	0.084
^{105}Ru	316.440	5.598	0.571	5.683	0.581	5.640	0.407	5.351	0.214
^{105}Ru	469.370	6.119	0.630	6.242	0.644	6.179	0.450	5.351	0.214
^{105}Ru	724.300	5.997	0.639	6.080	0.648	6.038	0.455	5.351	0.214
^{127}Sn	1095.600	0.441	0.132	0.338	0.102	0.376	0.081	0.353	0.226
^{127}Sn	1114.300	0.355	0.088	0.352	0.087	0.354	0.062	0.353	0.226
^{128}Sn	482.300	0.780	0.117	0.782	0.117	0.781	0.083	0.789	0.505
^{130}Sb	330.914	0.921	0.101	0.904	0.100	0.912	0.071	0.953	0.610
^{130}Sb	793.400	0.917	0.112	0.936	0.114	0.926	0.080	0.953	0.610

^{130}Sb	839.520	0.911	0.113	0.923	0.114	0.917	0.080	0.953	0.610
^{131}Sb	943.410	1.929	0.247	2.043	0.265	1.982	0.180	2.868	0.315
^{132}Te	228.160	5.562	0.573	5.677	0.587	5.618	0.410	5.143	0.103
^{133m}Te	863.955	3.990	0.565	3.946	0.558	3.968	0.397	3.140	0.188
^{133m}Te	912.671	4.637	0.660	4.715	0.671	4.675	0.471	3.140	0.188
^{133m}Te	1683.230	3.357	0.640	3.026	0.573	3.174	0.427	3.140	0.188
^{134}Te	201.235	3.629	0.384	3.666	0.389	3.647	0.273	4.763	0.286
^{134}Te	277.951	4.132	0.451	4.002	0.438	4.065	0.314	4.763	0.286
^{134}Te	460.997	3.251	0.388	3.485	0.419	3.359	0.285	4.763	0.286
^{133}I	529.872	7.039	0.731	7.132	0.743	7.085	0.521	6.896	4.413
^{135}I	1131.511	6.350	0.839	6.434	0.846	6.392	0.596	6.027	0.241
^{135}I	1260.409	6.151	0.864	6.184	0.863	6.168	0.611	6.027	0.241
^{138}Cs	871.800	8.228	0.957	8.240	0.958	8.234	0.677	5.937	0.475
^{138}Cs	1435.860	7.387	1.113	7.468	1.116	7.427	0.788	5.937	0.475
^{138}Cs	2218.000	6.518	1.353	6.589	1.350	6.553	0.956	5.937	0.475
^{139}Ba	165.857	6.369	0.610	6.119	0.591	6.240	0.424	5.600	0.112
^{141}Ba	190.328	4.639	0.551	4.029	0.481	4.293	0.362	5.068	0.304

^{141}La	1354.520	6.179	0.944	6.162	0.932	6.170	0.663	5.138	0.308
^{142}La	894.900	5.167	0.598	5.167	0.600	5.167	0.423	4.742	0.066
^{142}La	1043.700	5.114	0.959	5.447	0.696	5.332	0.563	4.742	0.066
^{142}La	1233.100	5.038	0.703	4.922	0.682	4.978	0.490	4.742	0.066
^{142}La	1545.800	4.361	0.725	4.434	0.731	4.397	0.515	4.742	0.066
^{142}La	1901.300	4.147	0.769	4.288	0.785	4.216	0.549	4.742	0.066
^{142}La	2187.200	4.987	1.032	4.766	0.973	4.870	0.708	4.742	0.066
^{142}La	2397.800	3.676	0.810	3.690	0.801	3.683	0.570	4.742	0.066
^{142}La	2542.700	3.141	0.723	3.239	0.734	3.189	0.515	4.742	0.066
^{146}Pr	453.880	4.510	0.520	4.665	0.540	4.585	0.375	2.455	0.025
^{149}Nd	114.314	1.598	0.196	1.735	0.214	1.661	0.144	1.239	0.025
^{149}Nd	155.873	1.323	0.152	1.150	0.135	1.226	0.101	1.239	0.025
^{149}Nd	270.166	1.278	0.138	1.383	0.150	1.326	0.101	1.239	0.025

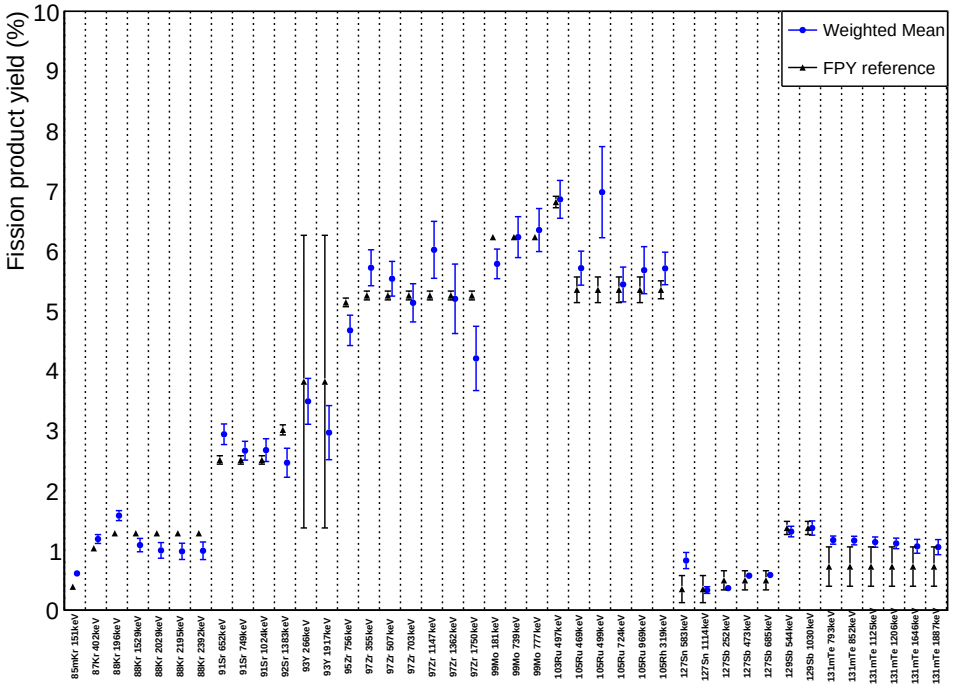

Figure 21: Pu3 + Pu4 weighted mean fission product yield results compared to evaluated England and Rider values. (part 1)

2.7 Fission Product Yield Analysis

This section describes how each γ-ray peak was fitted and the time chosen for the decay curve fit. The uncertainty budgets are tabulated in Section 2.8.

2.7.1 ^{85m}Kr ($\tau_{1/2} = 4.480 \pm 0.008$ h [1])

One γ-ray peak from Pu3 + Pu4 was analyzed. For the 151.2 keV γ ray, a multi-peak fit routine was used to account for an interfering γ ray at 149.5 keV. The decay curve fit was between 20 and 26 hours. The residual of the fit was within 5%.

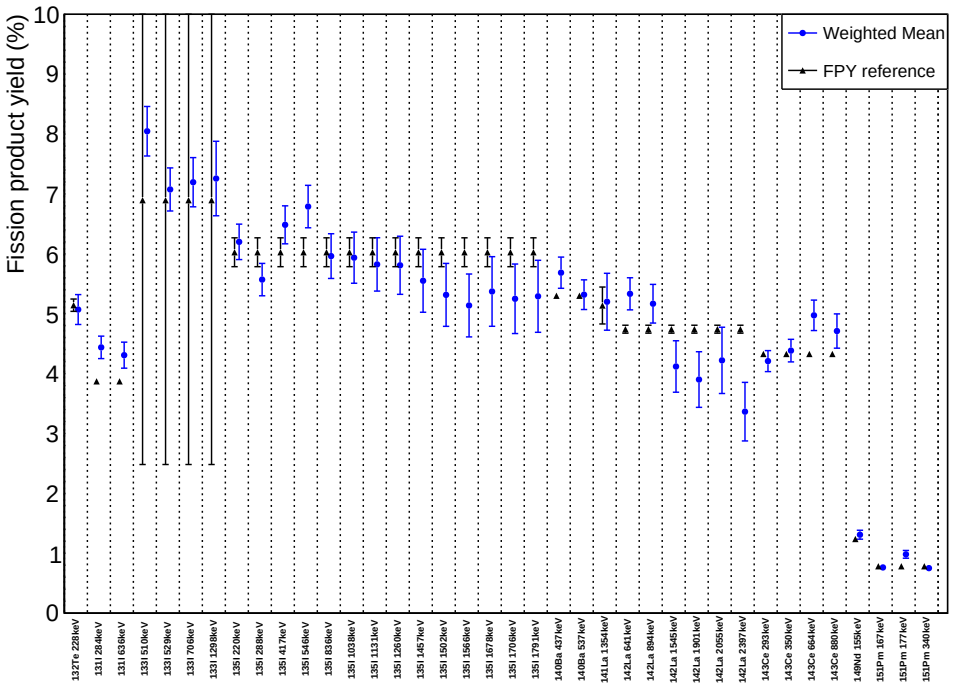

Figure 22: Pu3 + Pu4 weighted mean fission product yield results compared to evaluated England and Rider values. (part 2)

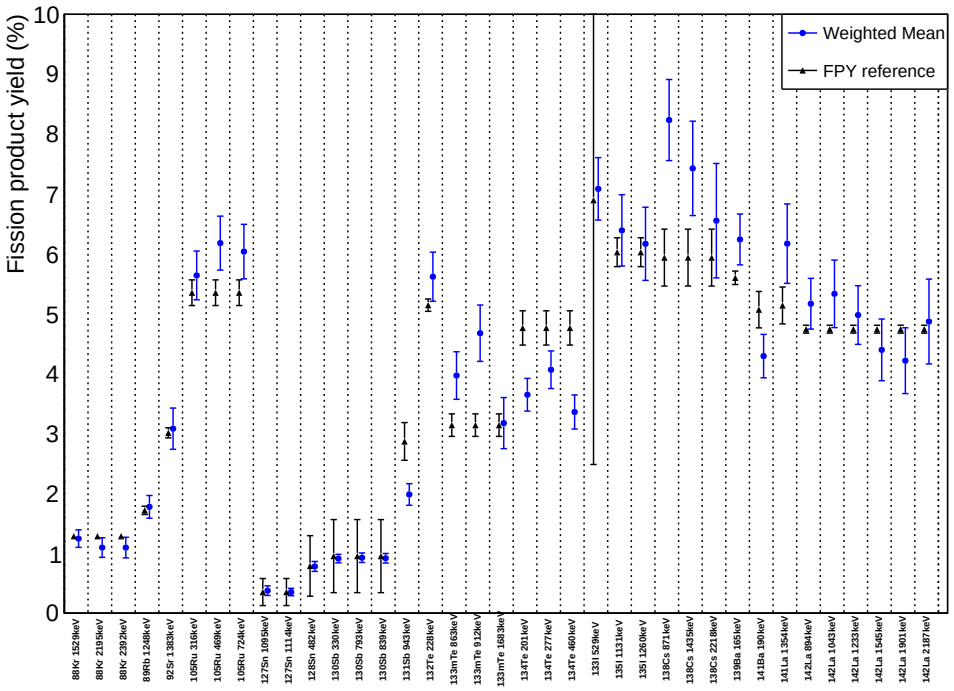

Figure 23: Pu1 weighted mean fission product yield results compared to evaluated England and Rider values.

2.7.2 ^{87}Kr ($\tau_{1/2} = 76.3 \pm 0.5$ **m** [**2**])

One γ-ray peak from Pu3 + Pu4 was analyzed. For the 402.6 keV γ ray, a multi-peak fit routine was used to account for an interfering γ ray at 400.6 keV. The decay curve fit was between 5 and 9 hours. The residual of the fit was within 10%.

2.7.3 ^{88}Kr ($\tau_{1/2} = 2.825 \pm 0.019$ **h** [**3**])

Five γ-ray peaks from Pu3 + Pu4 were analyzed. For the 196.3 keV γ ray, a single-peak fit routine was used. The decay curve fit was between 8 and 14 hours. The residual of the fit was within 10%. For the 1529.8 keV γ ray, a single-peak fit routine was used. The decay curve fit was between 5 and 15 hours. The residual of the fit was within 10%. For the 2029.8 keV γ ray, a single-peak fit routine was used. The decay curve fit was between 9 and 14 hours. The residual of the fit was within 10%. For the 2195.8 keV γ ray, a single-peak fit routine was used. The decay curve fit was between 6 and 15 hours. The residual of the fit was within 10%. For the 2392.1 keV γ ray, a single-peak fit routine was used. The decay curve fit was between 6 and 20 hours. The residual of the fit was within 10%.

Three γ-ray peaks from Pu1 were analyzed. For the 1529.8 keV γ ray, a single-peak fit routine was used. The decay curve fit was between 2.0 and 3.167 hours. The residual of the fit was within 10%. For the 2195.8 keV γ ray, a single-peak fit routine was used. The decay curve fit was between 2.5 and 3.167 hours. The residual of the fit was within 3%. For the 2392.1 keV γ ray, a single-peak fit routine was used. The decay curve fit was between 1.0 and 3.167 hours. The residual of the fit was within 7%.

2.7.4 ^{89}Rb ($\tau_{1/2} = 15.32 \pm 0.10$ **m** [**4**])

One γ-ray peak from Pu1 was analyzed. For the 1248.1 keV γ ray, a single-peak fit routine was used. The decay curve fit was between 1.0 and 1.334 hours. The residual of the fit was within 10%.

2.7.5 ^{91}Sr ($\tau_{1/2} = 9.65 \pm 0.06$ **h** [**5**])

Three γ-ray peaks from Pu3 + Pu4 were analyzed. For the 652.9 keV γ ray, a multi-peak fit routine was used to account for an interfering γ ray at 650.3 keV. The decay curve fit was between 5 and 9 hours. The residual of the fit was within 10%. For the 749.8 keV γ ray, a single-peak fit routine was used. The decay curve fit was between 6 and 20 hours. The residual of the fit was within 10%. For the 1024.3 keV γ ray, a single-peak fit routine was used. The decay curve fit was between 6 and 20 hours. The residual of the fit was within 10%.

2.7.6 ^{92}Sr ($\tau_{1/2} = 2.611 \pm 0.017$ **h** [**6**])

One γ-ray peak from Pu3 + Pu4 was analyzed. For the 1383.9 keV γ ray, a single-peak fit routine was used. The decay curve fit was between 12 and 30 hours. The residual of the fit was within 10%.

One γ-ray peak from Pu1 was analyzed. For the 1383.9 keV γ ray, a single-peak fit routine was used. The decay curve fit was between 0.834 and 3.167 hours. The residual of the fit was within 3%.

2.7.7 ^{93}Y ($\tau_{1/2} = 10.18 \pm 0.08$ **h** [**7**])

Two γ-ray peaks from Pu3 + Pu4 were analyzed. For the 266.9 keV γ ray, a single-peak fit routine was used. The decay curve fit was between 12 and 30

hours. The residual of the fit was within 5%. For the 1917.8 keV γ ray, a multi-peak fit routine was used to account for an interfering γ-ray at 1921.6 keV. The decay curve fit was between 14 and 30 hours. The residual of the fit was within 10%.

2.7.8 ^{95}Zr ($\tau_{1/2} = 64.032 \pm 0.006$ **d** [**8**])

One γ-ray peak from Pu3 + Pu4 was analyzed. For the 756.7 keV γ ray, a single-peak fit routine was used. The decay curve fit was between 60 and 150 hours. The residual of the fit was within 5%.

2.7.9 ^{97}Zr ($\tau_{1/2} = 16.749 \pm 0.008$ **h** [**9**])

Six γ-ray peaks from Pu3 + Pu4 were analyzed. For the 355.4 keV γ ray, a single-peak fit routine was used. The decay curve fit was between 6 and 40 hours. The residual of the fit was within 10%. For the 507.6 keV γ ray, a multi-peak fit routine was used to account for an interfering γ ray at 505.4 keV. The decay curve fit was between 6 and 50 hours. The residual of the fit was within 5%. For the 703.8 keV γ ray, a multi-peak fit routine was used to account for an interfering γ ray at 706.2 keV. The decay curve fit was between 25 and 45 hours. The residual of the fit was within 10%. For the 1148.0 keV γ ray, a single-peak fit routine was used. The decay curve fit was between 20 and 40 hours. The residual of the fit was within 10%. For the 1362.7 keV γ ray, a single-peak fit routine was used. The decay curve fit was between 13 and 70 hours. The residual of the fit was within 15%. For the 1750.2 keV γ ray, a single-peak fit routine was used. The decay curve fit was between 6 and 70 hours. The residual of the fit was within 15%.

2.7.10 ^{99}Mo ($\tau_{1/2} = 65.924 \pm 0.006$ h [10])

Three γ-ray peaks from Pu3 + Pu4 were analyzed. For the 181.1 keV γ ray, a multi-peak fit routine was used to account for an interfering γ ray at 179.3 keV. The decay curve fit was between 15 and 140 hours. The residual of the fit was within 5%. For the 739.5 keV γ ray, a single-peak fit routine was used. The decay curve fit was between 10 and 140 hours. The residual of the fit was within 5%. For the 777.9 keV γ ray, a single-peak fit routine was used. The decay curve fit was between 10 and 120 hours. The residual of the fit was within 10%.

2.7.11 ^{103}Ru ($\tau_{1/2} = 39.249 \pm 0.003$ d [11])

One γ-ray peak from Pu3 + Pu4 was analyzed. For the 497.1 keV γ ray, a single-peak fit routine was used. The decay curve fit was between 30 and 150 hours. The residual of the fit was within 3%.

2.7.12 ^{105}Ru ($\tau_{1/2} = 4.439 \pm 0.011$ h [12])

Five γ-ray peaks from Pu3 + Pu4 were analyzed. For the 316.4 keV γ ray, a multi-peak fit routine was used to account for an interfering γ ray at 313.9 keV and 319.0 keV. The decay curve fit was between 6 and 30 hours. The residual of the fit was within 5%. For the 469.4 keV γ ray, a single-peak fit routine was used. The decay curve fit was between 6 and 26 hours. The residual of the fit was within 3%. For the 499.3 keV γ ray, a multi-peak fit routine was used to account for an interfering γ ray at 496.9 keV. The decay curve fit was between 6 and 14 hours. The residual of the fit was within 5%. For the 724.3 keV γ ray, a single-peak fit routine was used. The decay curve fit was between 4 and 35 hours. The residual of the fit was within 10%. For the 969.4 keV γ ray, a multi-peak fit routine was used to account for an interfering γ ray at 966.7 keV and 972.4 keV. The decay

curve fit was between 7 and 14 hours. The residual of the fit was within 5%.

Three γ ray peaks from Pu1 were analyzed. For the 316.4 keV γ ray, a multi-peak fit routine was used to account for an interfering γ ray at 311.8 keV, 313.9 keV, and 319.0 keV. The decay curve fit was between 2.5 and 3.5 hours. The residual of the fit was within 5%. For the 469.4 keV γ ray, a single-peak fit routine was used. The decay curve fit was between 2.0 and 3.167 hours. The residual of the fit was within 5%. For the 724.3 keV γ ray, a single-peak fit routine was used. The decay curve fit was between 2.0 and 3.167 hours. The residual of the fit was within 3%.

2.7.13 ^{105}Rh ($\tau_{1/2} = 35.341 \pm 0.019$ h [12])

One γ-ray peak from Pu3 + Pu4 was analyzed. For the 319.2 keV γ ray, a single-peak fit routine was used. The decay curve fit was between 30 and 85 hours. The residual of the fit was within 3%.

2.7.14 ^{127}Sn ($\tau_{1/2} = 2.10 \pm 0.04$ h [13])

Two γ-ray peaks from Pu3 + Pu4 were analyzed. For the 583.3 keV γ ray, a single-peak fit routine was used. The decay curve fit was between 6 and 8 hours. The residual of the fit was within 10%. For the 1114.3 keV γ ray, a single-peak fit routine was used. The decay curve fit was between 5 and 9 hours. The residual of the fit was within 5%.

Two γ-ray peaks from Pu1 were analyzed. For the 1095.6 keV γ ray, a single-peak fit routine was used. The decay curve fit was between 1.7 and 3.5 hours. The residual of the fit was within 20%. For the 1114.3 keV γ ray, a single-peak fit routine was used. The decay curve fit was between 2.0 and 3.5 hours. The residual of the fit was within 15%.

2.7.15 ^{128}Sn ($\tau_{1/2} = 59.07 \pm 0.14$ **m** [**14**])

One γ-ray peak from Pu1 was analyzed. For the 482.3 keV γ ray, a single-peak fit routine was used. The decay curve fit was between 1.0 and 3.5 hours. The residual of the fit was within 10%.

2.7.16 ^{127}Sb ($\tau_{1/2} = 3.85 \pm 0.05$ **d** [**13**])

Three γ-ray peaks from Pu3 + Pu4 were analyzed. For the 252.4 keV γ ray, a multi-peak fit routine was used to account for an interfering γ ray at 255.1 keV. The decay curve fit was between 80 and 94 hours. The residual of the fit was within 20%. For the 473.0 keV γ ray, a single-peak fit routine was used. The decay curve fit was between 33 and 150 hours. The residual of the fit was within 15%. For the 685.7 keV γ ray, a single-peak fit routine was used. The decay curve fit was between 30 and 100 hours. The residual of the fit was within 6%.

2.7.17 ^{129}Sb ($\tau_{1/2} = 4.366 \pm 0.026$ **h** [**15**])

Two γ-ray peaks from Pu3 + Pu4 were analyzed. For the 544.7 keV γ ray, a single-peak fit routine was used. The decay curve fit was between 6 and 14 hours. The residual of the fit was within 5%. For the 1030.1 keV γ ray, a single-peak fit routine was used. The decay curve fit was between 5 and 24 hours. The residual of the fit was within 5%.

2.7.18 ^{130}Sb ($\tau_{1/2} = 39.5 \pm 0.8$ **m** [**16**])

Three γ-ray peaks from Pu1 were analyzed. For the 330.9 keV γ ray, a single-peak fit routine was used. The decay curve fit was between 1.2 and 3.2 hours. The residual of the fit was within 15%. For the 793.4 keV γ ray, a single-peak fit routine was used. The decay curve fit was between 1.5 and 3.5 hours. The residual

of the fit was within 15%. For the 839.5 keV γ ray, a multi-peak fit routine was used to account for an interfering γ ray at 834.7 keV and 836.8 keV. The decay curve fit was between 0.6 and 3.5 hours. The residual of the fit was within 7%.

2.7.19 ^{131}Sb ($\tau_{1/2} = 23.03 \pm 0.04$ **m** [**17**])

One γ-ray peak from Pu1 was analyzed. For the 943.4 keV γ ray, a multi-peak fit routine was used to account for an interfering γ ray at 936.3 keV. The decay curve fit was between 1.7 and 2.5 hours. The residual of the fit was within 10%.

2.7.20 ^{131m}Te ($\tau_{1/2} = 33.25 \pm 0.25$ **h** [**17**])

Six γ-rays from Pu3 + Pu4 were analyzed. For the 793.8 keV γ ray, a single-peak fit routine was used. The decay curve fit was between 15 and 100 hours. The residual of the fit was within 10%. For the 852.2 keV γ ray, a single-peak fit routine was used. The decay curve fit was between 40 and 100 hours. The residual of the fit was within 10%. For the 1125.5 keV γ ray, a single-peak fit routine was used. The decay curve fit was between 64 and 100 hours. The residual of the fit was within 15%. For the 1206.6 keV γ ray, a single-peak fit routine was used. The decay curve fit was between 6 and 100 hours. The residual of the fit was within 15%. For the 1646.0 keV γ ray, a single-peak fit routine was used. The decay curve fit was between 40 and 70 hours. The residual of the fit was within 20%. For the 1887.7 keV γ ray, a single-peak fit routine was used. The decay curve fit was between 13 and 80 hours. The residual of the fit was within 20%.

2.7.21 ^{132}Te ($\tau_{1/2} = 3.204 \pm 0.013$ **d** [**18**])

One γ-ray peak from Pu3 + Pu4 was analyzed. For the 228.2 keV γ ray, a single-peak fit routine was used. The decay curve fit was between 10 and 100 hours.

The residual of the fit was within 1%.

One γ-ray from Pu1 was analyzed. For the 228.2 keV γ ray, a single-peak fit routine was used. The decay curve fit was between 1.7 and 3.167 hours. The residual of the fit was within 5%.

2.7.22 ^{133m}Te ($\tau_{1/2} = 55.4 \pm 0.4$ m [19])

Three γ-ray peaks from Pu1 were analyzed. For the 864.0 keV γ ray, a multi-peak fit routine was used to account for an interfering γ ray at 861.6 keV. The decay curve fit was between 0.834 and 2.9 hours. The residual of the fit was within 10%. For the 912.7 keV γ ray, a multi-peak fit routine was used to account for an interfering γ ray at 914.7 keV. The decay curve fit was between 0.834 and 1.5 hours. The residual of the fit was within 1%. For the 1683.2 keV γ ray, a single-peak fit routine was used. The decay curve fit was between 1.0 and 2.0 hours. The residual of the fit was within 10%.

2.7.23 ^{134}Te ($\tau_{1/2} = 41.8 \pm 0.8$ m [20])

Three γ-ray peaks from Pu1 were analyzed. For the 201.2 keV γ ray, a multi-peak fit routine was used to account for an interfering γ ray at 203.5 keV. The decay curve fit was between 0.834 and 2.0 hours. The residual of the fit was within 5%. For the 278.0 keV γ ray, a single-peak fit routine was used. The decay curve fit was between 2.5 and 3.5 hours. The residual of the fit was within 5%. For the 461.0 keV γ ray, a multi-peak fit routine was used to account for an interfering γ ray at 458.9 keV and 462.6 keV. The decay curve fit was between 1.0 and 3.5 hours. The residual of the fit was within 20%.

2.7.24 ^{131}I ($\tau_{1/2} = 8.0252 \pm 0.0006$ **d** [**17**])

Two γ-ray peaks from Pu3 + Pu4 were analyzed. For the 966.4 keV γ ray, a multi-peak fit routine was used to account for an interfering γ ray at 285.6 keV. The decay curve fit was between 3 and 30 hours. The residual of the fit was within 15%. For the 637.0 keV γ ray, a single-peak fit routine was used. The decay curve fit was between 50 and 140 hours. The residual of the fit was within 10%.

2.7.25 ^{133}I ($\tau_{1/2} = 20.83 \pm 0.08$ **h** [**19**])

Four γ-ray peaks from Pu3 + Pu4 were analyzed. For the 510.5 keV γ ray, a multi-peak fit routine was used to account for an interfering γ ray at 505.7 keV and 507.9 keV. The decay curve fit was between 17 and 50 hours. The residual of the fit was within 10%. For the 529.9 keV γ ray, a single-peak fit routine was used. The decay curve fit was between 10 and 80 hours. The residual of the fit was within 1%. For the 706.6 keV γ ray, a multi-peak fit routine was used to account for an interfering γ ray at 703.4 keV. The decay curve fit was between 6 and 60 hours. The residual of the fit was within 15%. For the 1298.2 keV γ ray, a multi-peak fit routine was used to account for an interfering γ ray at 1295.2 keV. The decay curve fit was between 6 and 40 hours. The residual of the fit was within 10%.

One γ-ray peak from Pu1 was analyzed. For the 529.9 keV γ ray, a single-peak fit routine was used. The decay curve fit was between 1.7 and 3.167 hours. The residual of the fit was within 4%.

2.7.26 ^{135}I ($\tau_{1/2} = 6.58 \pm 0.03$ **h** [**21**])

Fourteen γ-ray peaks from Pu3 + Pu4 were analyzed. For the 220.5 keV γ ray, a multi-peak fit routine was used to account for an interfering γ ray at 218.7 keV.

The decay curve fit was between 6 and 25 hours. The residual of the fit was within 5%. For the 288.5 keV γ ray, a multi-peak fit routine was used to account for an interfering γ ray at 284.1 keV, 285.6 keV, and 293.0 keV. The decay curve fit was between 6 and 35 hours. The residual of the fit was within 10%. For the 417.6 keV γ ray, a single-peak fit routine was used. The decay curve fit was between 6 and 40 hours. The residual of the fit was within 15%. For the 546.6 keV γ ray, a multi-peak fit routine was used to account for an interfering γ ray at 544.4 keV. The decay curve fit was between 6 and 20 hours. The residual of the fit was within 2%. For the 836.8 keV γ ray, a single-peak fit routine was used. The decay curve fit was between 20 and 40 hours. The residual of the fit was within 10%. For the 1038.8 keV γ ray, a single-peak fit routine was used. The decay curve fit was between 6 and 50 hours. The residual of the fit was within 15%. For the 1131.5 keV γ ray, a single-peak fit routine was used. The decay curve fit was between 6 and 50 hours. The residual of the fit was within 10%. For the 1260.4 keV γ ray, a single-peak fit routine was used. The decay curve fit was between 6 and 50 hours. The residual of the fit was within 5%. For the 1457.6 keV γ ray, a single-peak fit routine was used. The decay curve fit was between 8 and 45 hours. The residual of the fit was within 15%. For the 1502.8 keV γ ray, a single-peak fit routine was used. The decay curve fit was between 6 and 40 hours. The residual of the fit was within 10%. For the 1566.4 keV γ ray, a single-peak fit routine was used. The decay curve fit was between 6 and 30 hours. The residual of the fit was within 10%. For the 1678.0 keV γ ray, a single-peak fit routine was used. The decay curve fit was between 6 and 50 hours. The residual of the fit was within 7%. For the 1706.5 keV γ ray, a single-peak fit routine was used. The decay curve fit was between 6 and 60 hours. The residual of the fit was within 15%. For the 1791.2 keV γ ray, a single-peak fit routine was used. The decay curve fit was between 6

and 70 hours. The residual of the fit was within 15%.

Two γ-ray peaks from Pu1 were analyzed. For the 1131.5 keV γ ray, a single-peak fit routine was used. The decay curve fit was between 1.5 and 3.167 hours. The residual of the fit was within 5%. For the 1260.4 keV γ ray, a single-peak fit routine was used. The decay curve fit was between 1.5 and 3.167 hours. The residual of the fit was within 5%.

2.7.27 ^{138}Cs ($\tau_{1/2} = 32.5 \pm 0.2$ **m** [**22**])

Three γ-ray peaks from Pu1 were analyzed. For the 871.8 keV γ ray, a single-peak fit routine was used. The decay curve fit was between 1.0 and 2.167 hours. The residual of the fit was within 5%. For the 1435.9 keV γ ray, a single-peak fit routine was used. The decay curve fit was between 1.0 and 2.334 hours. The residual of the fit was within 3%. For the 2218.0 keV γ ray, a single-peak fit routine was used. The decay curve fit was between 1.0 and 3.167 hours. The residual of the fit was within 10%.

2.7.28 ^{139}Ba ($\tau_{1/2} = 82.93 \pm 0.09$ **m** [**23**])

One γ-ray peak from Pu1 was analyzed. For the 165.9 keV γ ray, a multi-peak fit routine was used to account for an interfering γ ray at 168.8 keV. The decay curve fit was between 0.834 and 2.334 hours. The residual of the fit was within 5%.

2.7.29 ^{140}Ba ($\tau_{1/2} = 12.751 \pm 0.004$ **d** [**24**])

Two γ-ray peaks from Pu3 + Pu4 were analyzed. For the 437.6 keV γ ray, a multi-peak fit routine was used to account for an interfering γ ray at 440.3 keV. The decay curve fit was between 40 and 100 hours. The residual of the fit was

within 20%. For the 537.3 keV γ ray, a single-peak fit routine was used. The decay curve fit was between 20 and 150 hours. The residual of the fit was within 5%.

2.7.30 ^{141}Ba ($\tau_{1/2} = 18.27 \pm 0.07$ **m** [**25**])

One γ-ray peak from Pu1 was analyzed. For the 190.3 keV γ ray, a multi-peak fit routine was used to account for an interfering γ ray at 188.3 keV and 191.7 keV. The decay curve fit was between 1.0 and 3.0 hours. The residual of the fit was within 20%.

2.7.31 ^{141}La ($\tau_{1/2} = 3.92 \pm 0.03$ **h** [**25**])

One γ-ray peak from Pu3 + Pu4 was analyzed. For the 1354.5 keV γ ray, a single-peak fit routine was used. The decay curve fit was between 6 and 22 hours. The residual of the fit was within 15%.

2.7.32 ^{142}La ($\tau_{1/2} = 91.1 \pm 0.5$ **m** [**26**])

Six γ-ray peaks from Pu3 + Pu4 were analyzed. For the 641.3 keV γ ray, a single-peak fit routine was used. The decay curve fit was between 5 and 16 hours. The residual of the fit was within 10%. For the 894.9 keV γ ray, a multi-peak fit routine was used to account for an interfering γ ray at 897.9 keV. The decay curve fit was between 5 and 15 hours. The residual of the fit was within 20%. For the 1545.8 keV γ ray, a single-peak fit routine was used. The decay curve fit was between 5 and 10 hours. The residual of the fit was within 5%. For the 1901.3 keV γ ray, a single-peak fit routine was used. The decay curve fit was between 5 and 15 hours. The residual of the fit was within 5%. For the 2055.2 keV γ ray, a single-peak fit routine was used. The decay curve fit was between 5 and 13 hours.

The residual of the fit was within 10%. For the 2397.8 keV γ ray, a single-peak fit routine was used. The decay curve fit was between 5 and 16 hours. The residual of the fit was within 10%.

Eight γ-ray peaks from Pu1 were analyzed. For the 894.9 keV γ ray, a single-peak fit routine was used. The decay curve fit was between 2.0 and 3.5 hours. The residual of the fit was within 10%. For the 1043.7 keV γ ray, a single-peak fit routine was used. The decay curve fit was between 2.0 and 3.167 hours. The residual of the fit was within 10%. For the 1233.1 keV γ ray, a single-peak fit routine was used. The decay curve fit was between 1.0 and 3.167 hours. The residual of the fit was within 20%. For the 1545.8 keV γ ray, a single-peak fit routine was used. The decay curve fit was between 2.0 and 3.5 hours. The residual of the fit was within 15%. For the 1901.3 keV γ ray, a multi-peak fit routine was used to account for an interfering γ ray at 1897.8 keV. The decay curve fit was between 1.0 and 3.167 hours. The residual of the fit was within 20%. For the 2187.2 keV γ ray, a single-peak fit routine was used. The decay curve fit was between 1.0 and 2.0 hours. The residual of the fit was within 10%. For the 2397.8 keV γ ray, a multi-peak fit routine was used to account for an interfering γ ray at 2392.3 keV. The decay curve fit was between 1.0 and 3.167 hours. The residual of the fit was within 5%. For the 2542.7 keV γ ray, a single-peak fit routine was used. The decay curve fit was between 1.0 and 3.167 hours. The residual of the fit was within 10%.

2.7.33 ^{143}Ce ($\tau_{1/2} = 33.039 \pm 0.006$ h [27])

Four γ-ray peaks from Pu3 + Pu4 were analyzed. For the 293.3 keV γ ray, a single-peak fit routine was used. The decay curve fit was between 10 and 80 hours. The residual of the fit was within 2%. For the 350.6 keV γ ray, a multi-peak fit routine

was used to account for an interfering γ ray at 352.1 keV. The decay curve fit was between 35 and 60 hours. The residual of the fit was within 5%. For the 664.6 keV γ ray, a single-peak fit routine was used. The decay curve fit was between 20 and 90 hours. The residual of the fit was within 5%. For the 880.5 keV γ ray, a single-peak fit routine was used. The decay curve fit was between 20 and 100 hours. The residual of the fit was within 20%.

2.7.34 ^{146}Pr ($\tau_{1/2} = 24.09 \pm 0.10$ **m** [**28**])

One γ-ray peak from Pu1 was analyzed. For the 453.9 keV γ ray, a multi-peak fit routine was used to account for an interfering γ ray at 452.1 keV. The decay curve fit was between 2.3 and 3.167 hours. The residual of the fit was within 5%.

2.7.35 ^{149}Nd ($\tau_{1/2} = 1.728 \pm 0.001$ **h** [**29**])

One γ-ray peak from Pu3 + Pu4 was analyzed. For the 155.9 keV γ ray, a single-peak fit routine was used. The decay curve fit was between 6 and 13 hours. The residual of the fit was within 10%.

Three γ-ray peaks from Pu1 were analyzed. For the 114.3 keV γ ray, a multi-peak fit routine was used to account for an interfering γ ray at 111.3 keV, 116.0 keV, and 117.2 keV. The decay curve fit was between 2.0 and 3.5 hours. The residual of the fit was within 5%. For the 155.9 keV γ ray, a single-peak fit routine was used. The decay curve fit was between 1.5 and 2.3 hours. The residual of the fit was within 20%. For the 270.2 keV γ ray, a single-peak fit routine was used. The decay curve fit was between 1.5 and 2.5 hours. The residual of the fit was within 5%.

2.7.36 ^{151}Pm ($\tau_{1/2} = 28.40 \pm 0.04$ h [30])

Three γ-ray peaks from Pu3 + Pu4 were analyzed. For the 167.8 keV γ ray, a multi-peak fit routine was used to account for an interfering γ ray at 165.6 keV. The decay curve fit was between 16 and 30 hours. The residual of the fit was within 10%. For the 177.2 keV γ ray, a single-peak fit routine was used. The decay curve fit was between 20 and 50 hours. The residual of the fit was within 20%. For the 340.1 keV γ ray, a multi-peak fit routine was used to account for an interfering γ ray at 335.9 keV and 341.7 keV. The decay curve fit was between 12 and 100 hours. The residual of the fit was within 10%.

2.8 Fission Product Yield Parameter and Uncertainty Budget

Table 11: Values used to calculate Pu3 + Pu4 cumulative fission product yield results and uncertainties for detector 8815 where N_f = 4.2E10 ± 2E9.

Isotope	E_γ (keV)	A_0 (Bq)	ΔA_0 (Bq)	$\tau_{1/2}$ (hrs.)	$\Delta\tau_{1/2}$ (hrs.)	ϵ_γ	$\Delta\epsilon_\gamma$	I_γ	ΔI_γ	R_γ (%)	ΔR_γ (%)
^{85m}Kr	151.195	1.064E+02	8.542E-01	4.480	0.008	1.705E-02	1.673E-04	7.553E-01	7.161E-03	74.984	4.512
^{87}Kr	402.587	3.007E+02	2.492E+00	1.272	0.008	8.293E-03	1.981E-04	9.686E-01	1.043E-03	49.600	3.114
^{88}Kr	196.301	1.509E+02	6.736E-01	2.840	0.030	1.507E-02	1.707E-04	8.609E-01	4.355E-03	25.985	1.214
^{88}Kr	1529.770	1.142E+01	9.276E-02	2.840	0.030	3.404E-03	4.258E-04	9.941E-01	1.990E-04	10.934	0.534
^{88}Kr	2029.840	3.865E+00	1.067E-01	2.840	0.030	3.029E-03	5.119E-04	9.948E-01	1.745E-04	4.529	0.227
^{88}Kr	2195.842	1.080E+01	7.530E-02	2.840	0.030	2.945E-03	5.373E-04	9.950E-01	1.690E-04	13.183	0.618
^{88}Kr	2392.110	2.769E+01	1.099E-01	2.840	0.030	2.861E-03	5.652E-04	9.951E-01	1.634E-04	34.600	1.603
^{91}Sr	652.900	1.488E+01	3.750E-02	9.630	0.050	5.640E-03	2.462E-04	9.857E-01	4.799E-04	11.021	0.469
^{91}Sr	749.800	2.642E+01	3.753E-02	9.630	0.050	5.114E-03	2.665E-04	9.881E-01	3.995E-04	23.685	0.796
^{91}Sr	1024.300	3.110E+01	4.012E-02	9.630	0.050	4.193E-03	3.248E-04	9.917E-01	2.786E-04	33.500	1.100
^{92}Sr	1383.930	2.324E+02	7.662E-01	2.710	0.010	3.568E-03	3.979E-04	9.937E-01	2.125E-04	90.000	5.682
^{93}Y	266.900	2.236E+01	5.833E-02	10.180	0.080	1.188E-02	1.781E-04	9.287E-01	2.322E-03	7.320	1.054
^{93}Y	1917.800	1.121E+00	1.117E-02	10.180	0.080	3.095E-03	4.939E-04	9.947E-01	1.784E-04	1.545	0.208
^{95}Zr	756.725	6.649E-01	1.946E-03	1536.768	0.144	5.082E-03	2.680E-04	9.882E-01	3.951E-04	54.380	0.220
^{97}Zr	355.400	5.136E+00	2.277E-02	16.749	0.008	9.241E-03	1.905E-04	9.603E-01	1.314E-03	2.095	0.093

^{97}Zr	507.640	8.896E+00	2.203E-02	16.749	0.008	6.839E-03	2.171E-04	9.789E-01	7.039E-04	5.027	0.186
^{97}Zr	703.760	1.306E+00	1.829E-02	16.749	0.008	5.345E-03	2.568E-04	9.871E-01	4.331E-04	1.015	0.047
^{97}Zr	1147.970	2.921E+00	1.604E-02	16.749	0.008	3.931E-03	3.506E-04	9.926E-01	2.480E-04	2.616	0.102
^{97}Zr	1362.680	9.075E-01	6.460E-03	16.749	0.008	3.596E-03	3.938E-04	9.936E-01	2.149E-04	1.024	0.102
^{97}Zr	1750.240	6.955E-01	4.341E-03	16.749	0.008	3.210E-03	4.656E-04	9.945E-01	1.854E-04	1.089	0.102
^{99}Mo	181.068	5.666E+00	9.036E-03	65.976	0.024	1.582E-02	1.694E-04	8.358E-01	5.065E-03	6.142	0.124
^{99}Mo	739.500	4.735E+00	5.360E-03	65.976	0.024	5.163E-03	2.643E-04	9.879E-01	4.064E-04	12.260	0.218
^{99}Mo	777.921	1.615E+00	4.291E-03	65.976	0.024	4.987E-03	2.724E-04	9.886E-01	3.821E-04	4.303	0.080
^{103}Ru	497.085	3.604E+00	3.598E-03	941.928	0.072	6.956E-03	2.151E-04	9.782E-01	7.280E-04	91.000	1.221
^{105}Ru	469.370	1.285E+02	1.662E-01	4.440	0.020	7.289E-03	2.099E-04	9.760E-01	7.993E-04	17.548	0.552
^{105}Ru	499.300	1.733E+01	1.117E-01	4.440	0.020	6.931E-03	2.155E-04	9.784E-01	7.228E-04	2.034	0.285
^{105}Ru	724.300	2.411E+02	2.014E-01	4.440	0.020	5.238E-03	2.611E-04	9.876E-01	4.172E-04	47.300	0.500
^{105}Ru	969.440	9.276E+00	7.559E-02	4.440	0.020	4.333E-03	3.132E-04	9.912E-01	2.962E-04	2.105	0.074
^{105}Rh	319.231	2.392E+01	2.464E-02	35.360	0.060	1.016E-02	1.851E-04	9.507E-01	1.623E-03	19.100	0.630
^{127}Sn	583.300	6.829E+00	1.712E-01	2.100	0.040	6.135E-03	2.320E-04	9.831E-01	5.665E-04	3.192	0.662
^{127}Sn	1114.300	2.042E+01	3.292E-01	2.100	0.040	3.996E-03	3.436E-04	9.924E-01	2.553E-04	38.000	7.965
^{127}Sb	252.400	3.205E-01	1.291E-02	92.400	1.200	1.246E-02	1.764E-04	9.194E-01	2.609E-03	8.501	0.568
^{127}Sb	473.000	9.103E-01	4.039E-03	92.400	1.200	7.243E-03	2.106E-04	9.764E-01	7.892E-04	25.797	1.567
^{127}Sb	685.700	1.002E+00	3.509E-03	92.400	1.200	5.444E-03	2.530E-04	9.866E-01	4.484E-04	36.800	2.000
^{129}Sb	544.700	2.728E+01	1.363E-01	4.400	0.010	6.468E-03	2.243E-04	9.812E-01	6.295E-04	18.056	1.234
^{129}Sb	1030.100	1.313E+01	6.215E-02	4.400	0.010	4.179E-03	3.260E-04	9.918E-01	2.769E-04	12.687	0.975

^{131m}Te	793.750	1.832E+00	5.390E-03	33.250	0.250	4.920E-03	2.758E-04	9.889E-01	3.731E-04	13.370	0.297
^{131m}Te	852.210	2.656E+00	8.808E-03	33.250	0.250	4.696E-03	2.883E-04	9.898E-01	3.432E-04	20.279	0.567
^{131m}Te	1125.460	1.186E+00	9.809E-03	33.250	0.250	3.974E-03	3.459E-04	9.925E-01	2.528E-04	11.017	0.294
^{131m}Te	1206.600	9.703E-01	3.418E-03	33.250	0.250	3.827E-03	3.626E-04	9.930E-01	2.371E-04	9.411	0.221
^{131m}Te	1646.010	9.903E-02	3.051E-03	33.250	0.250	3.295E-03	4.471E-04	9.943E-01	1.910E-04	1.195	0.043
^{131m}Te	1887.700	1.038E-01	1.499E-03	33.250	0.250	3.114E-03	4.889E-04	9.947E-01	1.795E-04	1.307	0.044
^{132}Te	228.160	5.658E+01	1.857E-02	76.896	0.312	1.352E-02	1.738E-04	8.991E-01	3.230E-03	88.000	3.478
^{131}I	284.305	1.191E+00	1.256E-02	192.605	0.014	1.125E-02	1.803E-04	9.375E-01	2.043E-03	6.121	0.062
^{131}I	636.989	7.255E-01	2.616E-03	192.605	0.014	5.743E-03	2.429E-04	9.852E-01	4.972E-04	7.156	0.100
^{133}I	510.530	3.779E+00	1.695E-02	20.800	0.100	6.808E-03	2.177E-04	9.791E-01	6.975E-04	1.827	0.061
^{133}I	529.872	1.533E+02	5.132E-02	20.800	0.100	6.610E-03	2.214E-04	9.803E-01	6.574E-04	87.000	2.651
^{133}I	706.578	2.196E+00	9.572E-03	20.800	0.100	5.330E-03	2.574E-04	9.872E-01	4.308E-04	1.505	0.049
^{133}I	1298.223	2.398E+00	7.954E-03	20.800	0.100	3.684E-03	3.810E-04	9.934E-01	2.231E-04	2.349	0.075
^{135}I	220.502	1.687E+01	8.337E-02	6.570	0.020	1.388E-02	1.730E-04	8.912E-01	3.467E-03	1.751	0.062
^{135}I	288.451	2.217E+01	6.772E-02	6.570	0.020	1.111E-02	1.809E-04	9.394E-01	1.985E-03	3.100	0.113
^{135}I	417.633	2.172E+01	6.528E-02	6.570	0.020	8.037E-03	2.007E-04	9.706E-01	9.770E-04	3.530	0.114
^{135}I	546.557	3.741E+01	7.779E-02	6.570	0.020	6.451E-03	2.247E-04	9.813E-01	6.261E-04	7.146	0.240
^{135}I	836.804	2.279E+01	1.053E-01	6.570	0.020	4.752E-03	2.850E-04	9.896E-01	3.506E-04	6.687	0.227
^{135}I	1038.760	2.379E+01	4.577E-02	6.570	0.020	4.159E-03	3.278E-04	9.918E-01	2.744E-04	7.950	0.264
^{135}I	1131.511	6.309E+01	6.671E-02	6.570	0.020	3.962E-03	3.472E-04	9.925E-01	2.515E-04	22.587	0.723
^{135}I	1260.409	7.553E+01	6.376E-02	6.570	0.020	3.740E-03	3.735E-04	9.932E-01	2.285E-04	28.700	0.916

^{135}I	1457.560	2.038E+01	4.444E-02	6.570	0.020	3.481E-03	4.121E-04	9.939E-01	2.051E-04	8.667	0.278
^{135}I	1502.790	2.391E+00	1.807E-02	6.570	0.020	3.432E-03	4.207E-04	9.940E-01	2.012E-04	1.076	0.043
^{135}I	1566.410	2.728E+00	2.082E-02	6.570	0.020	3.368E-03	4.326E-04	9.942E-01	1.963E-04	1.292	0.050
^{135}I	1678.027	2.040E+01	3.902E-02	6.570	0.020	3.268E-03	4.528E-04	9.944E-01	1.891E-04	9.557	0.361
^{135}I	1706.459	8.503E+00	2.560E-02	6.570	0.020	3.244E-03	4.579E-04	9.944E-01	1.876E-04	4.104	0.172
^{135}I	1791.196	1.576E+01	3.316E-02	6.570	0.020	3.180E-03	4.726E-04	9.946E-01	1.835E-04	7.720	0.244
^{140}Ba	437.575	2.155E-01	3.785E-03	306.065	0.055	7.726E-03	2.042E-04	9.730E-01	9.002E-04	1.929	0.020
^{140}Ba	537.261	2.182E+00	3.404E-03	306.065	0.055	6.538E-03	2.228E-04	9.808E-01	6.432E-04	24.390	0.220
^{141}La	1354.520	6.194E+00	5.170E-02	3.920	0.030	3.606E-03	3.922E-04	9.936E-01	2.159E-04	1.640	0.070
^{142}La	641.285	7.489E+02	1.756E+00	1.518	0.008	5.715E-03	2.438E-04	9.853E-01	4.924E-04	47.400	0.500
^{142}La	894.900	1.036E+02	7.335E-01	1.518	0.008	4.552E-03	2.974E-04	9.904E-01	3.243E-04	8.342	0.167
^{142}La	1545.800	2.185E+01	4.813E-01	1.518	0.008	3.388E-03	4.288E-04	9.941E-01	1.978E-04	2.986	0.146
^{142}La	1901.300	4.570E+01	5.081E-01	1.518	0.008	3.105E-03	4.912E-04	9.947E-01	1.790E-04	7.157	0.161
^{142}La	2055.200	1.531E+01	2.770E-01	1.518	0.008	3.015E-03	5.159E-04	9.948E-01	1.736E-04	2.180	0.098
^{142}La	2397.800	6.768E+01	5.303E-01	1.518	0.008	2.859E-03	5.660E-04	9.952E-01	1.633E-04	13.272	0.317
^{143}Ce	293.266	4.500E+01	2.355E-02	33.039	0.006	1.095E-02	1.815E-04	9.414E-01	1.921E-03	42.800	0.420
^{143}Ce	350.619	3.075E+00	1.822E-02	33.039	0.006	9.351E-03	1.897E-04	9.592E-01	1.349E-03	3.231	0.040
^{143}Ce	664.571	3.803E+00	9.335E-03	33.039	0.006	5.568E-03	2.486E-04	9.860E-01	4.681E-04	5.692	0.068
^{143}Ce	880.460	5.330E-01	4.513E-03	33.039	0.006	4.599E-03	2.943E-04	9.902E-01	3.304E-04	1.031	0.013
^{149}Nd	155.873	4.582E+01	1.281E+00	1.728	0.001	1.690E-02	1.677E-04	7.714E-01	6.764E-03	5.931	0.309
^{151}Pm	167.750	2.356E+00	3.120E-02	28.400	0.040	1.643E-02	1.685E-04	8.061E-01	5.869E-03	8.325	0.560

^{151}Pm	177.160	1.436E+00	2.615E-02	28.400	0.040	1.600E-02	1.691E-04	8.280E-01	5.280E-03	3.825	0.272
^{151}Pm	340.080	4.432E+00	1.246E-02	28.400	0.040	9.606E-03	1.881E-04	9.567E-01	1.432E-03	22.500	0.900

Table 12: Values used to calculate Pu3 + Pu4 cumulative fission product yield results and uncertainties for detector 8816 where N_f = 4.1E10 ± 2E9.

	E_γ	A_0	ΔA_0	$\tau_{1/2}$	$\Delta\tau_{1/2}$					R_γ	ΔR_γ
Isotope	(keV)	(Bq)	(Bq)	(hrs.)	(hrs.)	ϵ_γ	$\Delta\epsilon_\gamma$	I_γ	ΔI_γ	(%)	(%)
^{85m}Kr	151.195	1.076E+02	1.065E+00	4.480	0.008	1.801E-02	1.914E-04	7.305E-01	6.322E-03	74.984	4.512
^{87}Kr	402.587	3.109E+02	3.305E+00	1.272	0.008	8.791E-03	2.157E-04	9.650E-01	9.486E-04	49.600	3.114
^{88}Kr	196.301	1.549E+02	7.111E-01	2.840	0.030	1.598E-02	1.933E-04	8.457E-01	3.905E-03	25.985	1.214
^{88}Kr	1529.770	1.201E+01	9.887E-02	2.840	0.030	3.643E-03	4.486E-04	9.934E-01	1.815E-04	10.934	0.534
^{88}Kr	2029.840	4.091E+00	6.931E-03	2.840	0.030	3.256E-03	5.408E-04	9.942E-01	1.591E-04	4.529	0.227
^{88}Kr	2195.842	1.137E+01	7.849E-02	2.840	0.030	3.170E-03	5.681E-04	9.944E-01	1.541E-04	13.183	0.618
^{88}Kr	2392.110	2.944E+01	1.135E-01	2.840	0.030	3.084E-03	5.982E-04	9.946E-01	1.491E-04	34.600	1.603
^{91}Sr	652.900	1.588E+01	3.936E-02	9.630	0.050	5.982E-03	2.616E-04	9.840E-01	4.373E-04	11.021	0.469
^{91}Sr	749.800	2.806E+01	3.936E-02	9.630	0.050	5.428E-03	2.820E-04	9.867E-01	3.642E-04	23.685	0.796
^{91}Sr	1024.300	3.264E+01	4.172E-02	9.630	0.050	4.464E-03	3.420E-04	9.907E-01	2.541E-04	33.500	1.100
^{92}Sr	1383.930	2.465E+02	7.968E-01	2.710	0.010	3.814E-03	4.190E-04	9.929E-01	1.938E-04	90.000	5.682
^{93}Y	266.900	2.300E+01	5.995E-02	10.180	0.080	1.261E-02	1.986E-04	9.205E-01	2.101E-03	7.320	1.054

^{93}Y	1917.800	1.173E+00	1.176E-02	10.180	0.080	3.324E-03	5.214E-04	9.941E-01	1.628E-04	1.545	0.208
^{95}Zr	756.725	7.014E-01	2.013E-03	1536.768	0.144	5.394E-03	2.835E-04	9.868E-01	3.601E-04	54.380	0.220
^{97}Zr	355.400	5.283E+00	2.416E-02	16.749	0.008	9.800E-03	2.089E-04	9.557E-01	1.194E-03	2.095	0.093
^{97}Zr	507.640	9.380E+00	2.372E-02	16.749	0.008	7.249E-03	2.333E-04	9.765E-01	6.408E-04	5.027	0.186
^{97}Zr	703.760	1.394E+00	1.885E-02	16.749	0.008	5.671E-03	2.722E-04	9.856E-01	3.947E-04	1.015	0.047
^{97}Zr	1147.970	3.129E+00	1.753E-02	16.749	0.008	4.190E-03	3.690E-04	9.918E-01	2.262E-04	2.616	0.102
^{97}Zr	1362.680	9.683E-01	6.592E-03	16.749	0.008	3.842E-03	4.146E-04	9.929E-01	1.960E-04	1.024	0.102
^{97}Zr	1750.240	7.489E-01	4.508E-03	16.749	0.008	3.443E-03	4.911E-04	9.938E-01	1.691E-04	1.089	0.102
^{99}Mo	181.068	5.917E+00	9.813E-03	65.976	0.024	1.676E-02	1.925E-04	8.182E-01	4.526E-03	6.142	0.124
^{99}Mo	739.500	4.978E+00	5.593E-03	65.976	0.024	5.479E-03	2.798E-04	9.865E-01	3.704E-04	12.260	0.218
^{99}Mo	777.921	1.747E+00	4.619E-03	65.976	0.024	5.295E-03	2.881E-04	9.873E-01	3.483E-04	4.303	0.080
^{103}Ru	497.085	3.807E+00	3.735E-03	941.928	0.072	7.372E-03	2.314E-04	9.757E-01	6.628E-04	91.000	1.221
^{105}Ru	469.370	1.353E+02	1.721E-01	4.440	0.020	7.725E-03	2.265E-04	9.732E-01	7.274E-04	17.548	0.552
^{105}Ru	499.300	1.830E+01	1.148E-01	4.440	0.020	7.346E-03	2.318E-04	9.758E-01	6.581E-04	2.034	0.285
^{105}Ru	724.300	2.520E+02	2.103E-01	4.440	0.020	5.558E-03	2.766E-04	9.861E-01	3.803E-04	47.300	0.500
^{105}Ru	969.440	9.770E+00	7.650E-02	4.440	0.020	4.610E-03	3.300E-04	9.902E-01	2.700E-04	2.105	0.074
^{105}Rh	319.231	2.493E+01	2.748E-02	35.360	0.060	1.078E-02	2.043E-04	9.450E-01	1.473E-03	19.100	0.630
^{127}Sn	583.300	5.819E+00	5.387E-01	2.100	0.040	6.504E-03	2.476E-04	9.811E-01	5.161E-04	3.192	0.662
^{127}Sn	1114.300	1.964E+01	3.311E-01	2.100	0.040	4.258E-03	3.617E-04	9.915E-01	2.328E-04	38.000	7.965
^{127}Sb	252.400	3.175E-01	1.375E-02	92.400	1.200	1.322E-02	1.973E-04	9.103E-01	2.358E-03	8.501	0.568
^{127}Sb	473.000	9.613E-01	4.366E-03	92.400	1.200	7.676E-03	2.272E-04	9.736E-01	7.183E-04	25.797	1.567

^{127}Sb	685.700	1.071E+00	3.691E-03	92.400	1.200	5.775E-03	2.684E-04	9.851E-01	4.086E-04	36.800	2.000
^{129}Sb	544.700	2.897E+01	1.408E-01	4.400	0.010	6.856E-03	2.402E-04	9.790E-01	5.733E-04	18.056	1.234
^{129}Sb	1030.100	1.391E+01	6.689E-02	4.400	0.010	4.449E-03	3.433E-04	9.908E-01	2.525E-04	12.687	0.975
^{131m}Te	793.750	1.940E+00	5.621E-03	33.250	0.250	5.225E-03	2.915E-04	9.876E-01	3.401E-04	13.370	0.297
^{131m}Te	852.210	2.773E+00	9.080E-03	33.250	0.250	4.990E-03	3.042E-04	9.886E-01	3.129E-04	20.279	0.567
^{131m}Te	1125.460	1.267E+00	9.469E-03	33.250	0.250	4.235E-03	3.641E-04	9.916E-01	2.305E-04	11.017	0.294
^{131m}Te	1206.600	1.010E+00	4.048E-03	33.250	0.250	4.082E-03	3.816E-04	9.921E-01	2.162E-04	9.411	0.221
^{131m}Te	1646.010	1.090E-01	3.056E-03	33.250	0.250	3.530E-03	4.713E-04	9.937E-01	1.742E-04	1.195	0.043
^{131m}Te	1887.700	1.086E-01	1.513E-03	33.250	0.250	3.344E-03	5.161E-04	9.940E-01	1.638E-04	1.307	0.044
^{132}Te	228.160	5.880E+01	1.928E-02	76.896	0.312	1.435E-02	1.954E-04	8.878E-01	2.912E-03	88.000	3.478
^{131}I	284.305	1.248E+00	1.318E-02	192.605	0.014	1.194E-02	2.004E-04	9.304E-01	1.850E-03	6.121	0.062
^{131}I	636.989	7.635E-01	2.758E-03	192.605	0.014	6.090E-03	2.584E-04	9.834E-01	4.530E-04	7.156	0.100
^{133}I	510.530	3.963E+00	1.750E-02	20.800	0.100	7.216E-03	2.338E-04	9.767E-01	6.351E-04	1.827	0.061
^{133}I	529.872	1.618E+02	5.369E-02	20.800	0.100	7.006E-03	2.374E-04	9.780E-01	5.987E-04	87.000	2.651
^{133}I	706.578	2.310E+00	1.028E-02	20.800	0.100	5.655E-03	2.728E-04	9.857E-01	3.926E-04	1.505	0.049
^{133}I	1298.223	2.553E+00	8.284E-03	20.800	0.100	3.933E-03	4.011E-04	9.926E-01	2.034E-04	2.349	0.075
^{135}I	220.502	1.658E+01	8.595E-02	6.570	0.020	1.473E-02	1.948E-04	8.791E-01	3.122E-03	1.751	0.062
^{135}I	288.451	2.279E+01	6.791E-02	6.570	0.020	1.179E-02	2.008E-04	9.324E-01	1.798E-03	3.100	0.113
^{135}I	417.633	2.292E+01	6.973E-02	6.570	0.020	8.519E-03	2.180E-04	9.672E-01	8.886E-04	3.530	0.114
^{135}I	546.557	3.942E+01	8.231E-02	6.570	0.020	6.838E-03	2.405E-04	9.791E-01	5.702E-04	7.146	0.240
^{135}I	836.804	2.419E+01	1.108E-01	6.570	0.020	5.048E-03	3.009E-04	9.883E-01	3.196E-04	6.687	0.227

^{135}I	1038.760	2.504E+01	4.750E-02	6.570	0.020	4.428E-03	3.452E-04	9.909E-01	2.502E-04	7.950	0.264
^{135}I	1131.511	6.676E+01	6.894E-02	6.570	0.020	4.223E-03	3.654E-04	9.916E-01	2.293E-04	22.587	0.723
^{135}I	1260.409	8.004E+01	7.624E-02	6.570	0.020	3.992E-03	3.931E-04	9.924E-01	2.084E-04	28.700	0.916
^{135}I	1457.560	2.147E+01	3.578E-02	6.570	0.020	3.723E-03	4.341E-04	9.932E-01	1.871E-04	8.667	0.278
^{135}I	1502.790	2.516E+00	1.904E-02	6.570	0.020	3.672E-03	4.432E-04	9.933E-01	1.835E-04	1.076	0.043
^{135}I	1566.410	2.864E+00	2.041E-02	6.570	0.020	3.605E-03	4.558E-04	9.935E-01	1.790E-04	1.292	0.050
^{135}I	1678.027	2.159E+01	4.127E-02	6.570	0.020	3.502E-03	4.775E-04	9.937E-01	1.725E-04	9.557	0.361
^{135}I	1706.459	8.998E+00	2.654E-02	6.570	0.020	3.478E-03	4.828E-04	9.938E-01	1.711E-04	4.104	0.172
^{135}I	1791.196	1.678E+01	3.442E-02	6.570	0.020	3.412E-03	4.986E-04	9.939E-01	1.674E-04	7.720	0.244
^{140}Ba	437.575	2.269E-01	3.847E-03	306.065	0.055	8.189E-03	2.212E-04	9.698E-01	8.190E-04	1.929	0.020
^{140}Ba	537.261	2.284E+00	3.615E-03	306.065	0.055	6.930E-03	2.388E-04	9.785E-01	5.857E-04	24.390	0.220
^{141}La	1354.520	6.682E+00	5.450E-02	3.920	0.030	3.853E-03	4.129E-04	9.928E-01	1.969E-04	1.640	0.070
^{142}La	641.285	7.929E+02	1.827E+00	1.518	0.008	6.060E-03	2.593E-04	9.836E-01	4.487E-04	47.400	0.500
^{142}La	894.900	1.071E+02	8.922E-01	1.518	0.008	4.839E-03	3.136E-04	9.892E-01	2.957E-04	8.342	0.167
^{142}La	1545.800	2.326E+01	5.103E-01	1.518	0.008	3.626E-03	4.518E-04	9.934E-01	1.804E-04	2.986	0.146
^{142}La	1901.300	4.837E+01	5.122E-01	1.518	0.008	3.335E-03	5.185E-04	9.941E-01	1.633E-04	7.157	0.161
^{142}La	2055.200	1.491E+01	3.210E-01	1.518	0.008	3.242E-03	5.451E-04	9.942E-01	1.584E-04	2.180	0.098
^{142}La	2397.800	7.118E+01	5.434E-01	1.518	0.008	3.081E-03	5.991E-04	9.946E-01	1.490E-04	13.272	0.317
^{143}Ce	293.266	4.716E+01	2.461E-02	33.039	0.006	1.162E-02	2.013E-04	9.347E-01	1.741E-03	42.800	0.420
^{143}Ce	350.619	3.238E+00	1.970E-02	33.039	0.006	9.917E-03	2.082E-04	9.545E-01	1.225E-03	3.231	0.040
^{143}Ce	664.571	3.932E+00	8.602E-03	33.039	0.006	5.906E-03	2.641E-04	9.844E-01	4.266E-04	5.692	0.068

^{143}Ce	880.460	5.696E-01	5.025E-03	33.039	0.006	4.888E-03	3.104E-04	9.890E-01	3.013E-04	1.031	0.013
^{149}Nd	155.873	4.902E+01	7.134E-01	1.728	0.001	1.786E-02	1.916E-04	7.480E-01	5.986E-03	5.931	0.309
^{151}Pm	167.750	2.457E+00	3.422E-02	28.400	0.040	1.739E-02	1.920E-04	7.858E-01	5.222E-03	8.325	0.560
^{151}Pm	177.160	1.417E+00	2.902E-02	28.400	0.040	1.695E-02	1.923E-04	8.096E-01	4.713E-03	3.825	0.272
^{151}Pm	340.080	4.555E+00	1.332E-02	28.400	0.040	1.019E-02	2.069E-04	9.516E-01	1.300E-03	22.500	0.900

Table 13: Values used to calculate Pu1 cumulative fission product yield results and uncertainties for detector 8815 where N_f = 5.1E9 ± 4E8.

Isotope	E_γ (keV)	A_0 (Bq)	ΔA_0 (Bq)	$\tau_{1/2}$ (hrs.)	$\Delta\tau_{1/2}$ (hrs.)	ϵ_γ	$\Delta\epsilon_\gamma$	I_γ	ΔI_γ	R_γ (%)	ΔR_γ (%)
^{88}Kr	1529.770	1.549E+00	5.176E-02	2.840	0.030	3.404E-03	4.258E-04	9.957E-01	4.048E-04	10.934	0.534
^{88}Kr	2195.842	1.476E+00	4.834E-02	2.840	0.030	2.945E-03	5.373E-04	9.963E-01	3.436E-04	13.183	0.618
^{88}Kr	2392.110	3.711E+00	3.126E-02	2.840	0.030	2.861E-03	5.652E-04	9.964E-01	3.323E-04	34.600	1.603
^{89}Rb	1248.140	1.059E+02	2.678E+00	0.252	0.002	3.759E-03	3.710E-04	9.950E-01	4.686E-04	45.917	2.620
^{92}Sr	1383.930	3.549E+01	9.245E-02	2.710	0.010	3.568E-03	3.979E-04	9.954E-01	4.323E-04	90.000	5.682
^{105}Ru	316.440	1.360E+01	1.103E-01	4.440	0.020	1.024E-02	1.847E-04	9.630E-01	3.402E-03	11.116	0.396
^{105}Ru	469.370	1.704E+01	1.075E-01	4.440	0.020	7.289E-03	2.099E-04	9.824E-01	1.634E-03	17.548	0.552
^{105}Ru	724.300	3.264E+01	1.237E-01	4.440	0.020	5.238E-03	2.611E-04	9.909E-01	8.501E-04	47.300	0.500
^{127}Sn	1095.600	1.606E+00	5.879E-02	2.100	0.040	4.034E-03	3.397E-04	9.943E-01	5.283E-04	19.380	5.214
^{127}Sn	1114.300	2.511E+00	5.825E-02	2.100	0.040	3.996E-03	3.436E-04	9.944E-01	5.194E-04	38.000	7.965
^{128}Sn	482.300	3.225E+01	1.878E-01	0.984	0.002	7.129E-03	2.123E-04	9.832E-01	1.562E-03	59.000	6.686
^{130}Sb	330.914	1.021E+02	5.369E-01	0.658	0.013	9.840E-03	1.868E-04	9.662E-01	3.108E-03	78.000	4.000
^{130}Sb	793.400	6.696E+01	4.788E-01	0.658	0.013	4.922E-03	2.757E-04	9.918E-01	7.604E-04	100.000	5.000
^{130}Sb	839.520	6.414E+01	2.814E-01	0.658	0.013	4.742E-03	2.856E-04	9.924E-01	7.113E-04	100.000	5.000
^{131}Sb	943.410	1.019E+02	1.219E+00	0.384	0.001	4.405E-03	3.077E-04	9.933E-01	6.216E-04	47.100	2.400
^{132}Te	228.160	7.835E+00	7.953E-02	76.896	0.312	1.352E-02	1.738E-04	9.250E-01	6.749E-03	88.000	3.478
^{133m}Te	863.955	2.927E+01	1.711E-01	0.923	0.007	4.655E-03	2.908E-04	9.926E-01	6.878E-04	14.887	1.274

^{133m}Te	912.671	9.662E+01	3.743E-01	0.923	0.007	4.496E-03	3.011E-04	9.931E-01	6.455E-04	43.767	3.666
^{133m}Te	1683.230	4.590E+00	1.134E-01	0.923	0.007	3.263E-03	4.538E-04	9.959E-01	3.841E-04	3.945	0.344
^{134}Te	201.235	6.059E+01	5.051E-01	0.697	0.013	1.482E-02	1.712E-04	9.013E-01	8.768E-03	8.850	0.380
^{134}Te	277.951	1.353E+02	1.331E+00	0.697	0.013	1.147E-02	1.795E-04	9.516E-01	4.420E-03	21.240	1.056
^{134}Te	460.997	3.246E+01	1.683E-01	0.697	0.013	7.398E-03	2.084E-04	9.819E-01	1.684E-03	9.735	0.646
^{133}I	529.872	1.888E+01	7.742E-02	20.800	0.100	6.610E-03	2.214E-04	9.856E-01	1.342E-03	87.000	2.651
^{135}I	1131.511	8.467E+00	5.377E-02	6.570	0.020	3.962E-03	3.472E-04	9.945E-01	5.117E-04	22.587	0.723
^{135}I	1260.409	9.842E+00	5.036E-02	6.570	0.020	3.740E-03	3.735E-04	9.950E-01	4.648E-04	28.700	0.916
^{138}Cs	871.800	3.415E+01	4.093E-01	0.557	0.003	4.628E-03	2.924E-04	9.927E-01	6.806E-04	5.112	0.131
^{138}Cs	1435.860	3.475E+02	7.682E-01	0.557	0.003	3.506E-03	4.080E-04	9.955E-01	4.214E-04	76.300	1.555
^{138}Cs	2218.000	5.113E+01	2.833E-01	0.557	0.003	2.935E-03	5.405E-04	9.963E-01	3.422E-04	15.184	0.311
^{139}Ba	165.857	1.510E+02	3.285E-01	1.384	0.005	1.651E-02	1.683E-04	8.501E-01	1.293E-02	23.760	0.250
^{141}Ba	190.328	9.439E+02	3.913E+00	0.304	0.001	1.536E-02	1.702E-04	8.892E-01	9.777E-03	46.000	3.302
^{141}La	1354.520	9.131E-01	2.754E-02	3.920	0.030	3.606E-03	3.922E-04	9.953E-01	4.392E-04	1.640	0.070
^{142}La	894.900	1.263E+01	1.774E-02	1.518	0.008	4.552E-03	2.974E-04	9.929E-01	6.602E-04	8.342	0.167
^{142}La	1043.700	3.694E+00	5.191E-01	1.518	0.008	4.148E-03	3.289E-04	9.940E-01	5.557E-04	2.702	0.055
^{142}La	1233.100	2.331E+00	5.523E-02	1.518	0.008	3.783E-03	3.680E-04	9.949E-01	4.734E-04	1.896	0.051
^{142}La	1545.800	2.848E+00	6.516E-02	1.518	0.008	3.388E-03	4.288E-04	9.957E-01	4.023E-04	2.986	0.146
^{142}La	1901.300	5.952E+00	5.528E-02	1.518	0.008	3.105E-03	4.912E-04	9.961E-01	3.641E-04	7.157	0.161
^{142}La	2187.200	3.512E+00	5.863E-02	1.518	0.008	2.949E-03	5.360E-04	9.963E-01	3.442E-04	3.697	0.103
^{142}La	2397.800	9.012E+00	5.769E-02	1.518	0.008	2.859E-03	5.660E-04	9.964E-01	3.321E-04	13.272	0.317

^{142}La	2542.700	5.696E+00	4.711E-02	1.518	0.008	2.806E-03	5.852E-04	9.965E-01	3.259E-04	10.001	0.259
^{146}Pr	453.880	3.888E+02	6.910E+00	0.403	0.003	7.494E-03	2.071E-04	9.814E-01	1.729E-03	48.000	2.830
^{149}Nd	114.314	2.621E+01	2.087E-01	1.728	0.001	1.691E-02	1.655E-04	8.882E-01	9.864E-03	19.166	1.492
^{149}Nd	155.873	6.242E+00	2.247E-01	1.728	0.001	1.690E-02	1.677E-04	8.268E-01	1.472E-02	5.931	0.309
^{149}Nd	270.166	8.706E+00	1.947E-01	1.728	0.001	1.176E-02	1.785E-04	9.486E-01	4.688E-03	10.723	0.503

Table 14: Values used to calculate Pu1 cumulative fission product yield results and uncertainties for detector 8816 where N_f = 5.1E9 ± 4E8.

Isotope	E_γ (keV)	A_0 (Bq)	ΔA_0 (Bq)	$\tau_{1/2}$ (hrs.)	$\Delta\tau_{1/2}$ (hrs.)	ϵ_γ	$\Delta\epsilon_\gamma$	I_γ	ΔI_γ	R_γ (%)	ΔR_γ (%)
^{88}Kr	1529.770	1.755E+00	4.393E-02	2.840	0.030	3.643E-03	4.486E-04	9.969E-01	4.884E-04	10.934	0.534
^{88}Kr	2195.842	1.558E+00	4.339E-02	2.840	0.030	3.170E-03	5.681E-04	9.973E-01	4.145E-04	13.183	0.618
^{88}Kr	2392.110	4.034E+00	3.223E-02	2.840	0.030	3.084E-03	5.982E-04	9.974E-01	4.009E-04	34.600	1.603
^{89}Rb	1248.140	1.512E+02	3.976E+00	0.252	0.002	4.012E-03	3.905E-04	9.964E-01	5.655E-04	45.917	2.620
^{92}Sr	1383.930	3.817E+01	9.560E-02	2.710	0.010	3.814E-03	4.190E-04	9.967E-01	5.217E-04	90.000	5.682
^{105}Ru	316.440	1.464E+01	1.169E-01	4.440	0.020	1.086E-02	2.039E-04	9.732E-01	4.143E-03	11.116	0.396
^{105}Ru	469.370	1.832E+01	1.120E-01	4.440	0.020	7.725E-03	2.265E-04	9.873E-01	1.978E-03	17.548	0.552
^{105}Ru	724.300	3.482E+01	1.286E-01	4.440	0.020	5.558E-03	2.766E-04	9.934E-01	1.027E-03	47.300	0.500
^{127}Sn	1095.600	1.298E+00	6.107E-02	2.100	0.040	4.298E-03	3.576E-04	9.959E-01	6.376E-04	19.380	5.214

^{127}Sn	1114.300	2.633E+00	5.754E-02	2.100	0.040	4.258E-03	3.617E-04	9.960E-01	6.269E-04	38.000	7.965
^{128}Sn	482.300	3.406E+01	2.084E-01	0.984	0.002	7.555E-03	2.288E-04	9.878E-01	1.891E-03	59.000	6.686
^{130}Sb	330.914	1.062E+02	6.319E-01	0.658	0.013	1.044E-02	2.057E-04	9.755E-01	3.781E-03	78.000	4.000
^{130}Sb	793.400	7.198E+01	5.677E-01	0.658	0.013	5.226E-03	2.914E-04	9.941E-01	9.184E-04	100.000	5.000
^{130}Sb	839.520	6.844E+01	2.857E-01	0.658	0.013	5.038E-03	3.015E-04	9.945E-01	8.590E-04	100.000	5.000
^{131}Sb	943.410	1.138E+02	2.924E+00	0.384	0.001	4.685E-03	3.242E-04	9.952E-01	7.505E-04	47.100	2.400
^{132}Te	228.160	8.583E+00	8.618E-02	76.896	0.312	1.435E-02	1.954E-04	9.453E-01	8.312E-03	88.000	3.478
^{133m}Te	863.955	3.049E+01	1.736E-01	0.923	0.007	4.946E-03	3.068E-04	9.947E-01	8.306E-04	14.887	1.274
^{133m}Te	912.671	1.035E+02	3.943E-01	0.923	0.007	4.780E-03	3.175E-04	9.950E-01	7.794E-04	43.767	3.666
^{133m}Te	1683.230	4.392E+00	1.169E-01	0.923	0.007	3.498E-03	4.784E-04	9.970E-01	4.634E-04	3.945	0.344
^{134}Te	201.235	6.611E+01	5.505E-01	0.697	0.013	1.572E-02	1.936E-04	9.278E-01	1.088E-02	8.850	0.380
^{134}Te	277.951	1.395E+02	1.399E+00	0.697	0.013	1.218E-02	1.997E-04	9.649E-01	5.400E-03	21.240	1.056
^{134}Te	460.997	3.667E+01	3.987E-01	0.697	0.013	7.841E-03	2.251E-04	9.869E-01	2.039E-03	9.735	0.646
^{133}I	529.872	2.014E+01	8.025E-02	20.800	0.100	7.006E-03	2.374E-04	9.896E-01	1.624E-03	87.000	2.651
^{135}I	1131.511	9.059E+00	5.847E-02	6.570	0.020	4.223E-03	3.654E-04	9.960E-01	6.176E-04	22.587	0.723
^{135}I	1260.409	1.046E+01	5.473E-02	6.570	0.020	3.992E-03	3.931E-04	9.964E-01	5.609E-04	28.700	0.916
^{138}Cs	871.800	3.603E+01	4.362E-01	0.557	0.003	4.918E-03	3.085E-04	9.947E-01	8.218E-04	5.112	0.131
^{138}Cs	1435.860	3.722E+02	7.954E-01	0.557	0.003	3.748E-03	4.297E-04	9.967E-01	5.085E-04	76.300	1.555
^{138}Cs	2218.000	5.510E+01	3.002E-01	0.557	0.003	3.159E-03	5.716E-04	9.974E-01	4.128E-04	15.184	0.311
^{139}Ba	165.857	1.590E+02	3.592E-01	1.384	0.005	1.747E-02	1.919E-04	8.894E-01	1.630E-02	23.760	0.250
^{141}Ba	190.328	8.884E+02	3.893E+00	0.304	0.001	1.629E-02	1.930E-04	9.188E-01	1.217E-02	46.000	3.302

^{141}La	1354.520	9.638E-01	2.674E-02	3.920	0.030	3.853E-03	4.129E-04	9.966E-01	5.300E-04	1.640	0.070
^{142}La	894.900	1.331E+01	1.329E-01	1.518	0.008	4.839E-03	3.136E-04	9.949E-01	7.972E-04	8.342	0.167
^{142}La	1043.700	4.151E+00	1.312E-01	1.518	0.008	4.416E-03	3.463E-04	9.957E-01	6.708E-04	2.702	0.055
^{142}La	1233.100	2.407E+00	5.556E-02	1.518	0.008	4.036E-03	3.873E-04	9.963E-01	5.713E-04	1.896	0.051
^{142}La	1545.800	3.070E+00	6.943E-02	1.518	0.008	3.626E-03	4.518E-04	9.969E-01	4.853E-04	2.986	0.146
^{142}La	1901.300	6.546E+00	5.795E-02	1.518	0.008	3.335E-03	5.185E-04	9.972E-01	4.392E-04	7.157	0.161
^{142}La	2187.200	3.577E+00	6.074E-02	1.518	0.008	3.174E-03	5.667E-04	9.973E-01	4.152E-04	3.697	0.103
^{142}La	2397.800	9.656E+00	6.009E-02	1.518	0.008	3.081E-03	5.991E-04	9.974E-01	4.006E-04	13.272	0.317
^{142}La	2542.700	6.275E+00	4.838E-02	1.518	0.008	3.028E-03	6.198E-04	9.975E-01	3.931E-04	10.001	0.259
^{146}Pr	453.880	4.239E+02	7.507E+00	0.403	0.003	7.942E-03	2.239E-04	9.865E-01	2.094E-03	48.000	2.830
^{149}Nd	114.314	3.045E+01	2.535E-01	1.728	0.001	1.770E-02	1.909E-04	9.180E-01	1.229E-02	19.166	1.492
^{149}Nd	155.873	5.987E+00	2.464E-01	1.728	0.001	1.786E-02	1.916E-04	8.718E-01	1.871E-02	5.931	0.309
^{149}Nd	270.166	1.004E+01	2.256E-01	1.728	0.001	1.248E-02	1.989E-04	9.626E-01	5.733E-03	10.723	0.503

2.9 Conclusion

The experimental setup and procedure is the same as the previous measurement for ^{235}U and ^{238}U fission spectrum cumulative fission product yields [103]. The data analysis described can be implemented for any actinide to study fission product γ rays. In this work, 123 γ rays were analyzed for 36 isotopes.

For the case of ^{142}La, the evaluators mainly based the decay scheme from a 1982 measurement [26]. In 1982, a γ-γ coincidence measurement was performed on ^{142}La using Cs fission products of ^{235}U [104]. A shield comprised of 1 mm of Cu, 1 mm of Pb, and 4 mm of B_4C was placed in front of the detectors and an efficiency calibration was performed using ^{152}Eu (with γ-ray branching ratios from 1979 [105]). Without accounting for the attenuation through the detector front shield, there should be an energy where the ^{142}La fission product yields are lower at higher γ-ray energies and higher at lower γ-ray energies. This energy would be between 1233–1545 keV (based on Figure 39 and 40). It is possible that the ^{152}Eu 1408 keV γ ray was used to determine the efficiency of the detectors for the 1982 ^{142}La γ-γ measurement.

There are more fission product yield results that exhibit variation for different γ ray analyzed. The variation in fission product yield results may be caused by discrepancies in γ-ray branching ratios.

2.10 Future Work

^{237}Np and ^{233}U are the next actinides to have their fission product yields measured using Godiva IV critical assembly. A new experimental setup, called the Lāpaki γ-γ array, was designed and constructed to measure short-lived fission product yield and γ-ray branching ratios [106]. An experiment at Oregon State University will

use Lāpaki to measure ^{238}U short-lived fission product yields and fission product γ rays.

Acknowledgements

This work was funded by the Office of Defense Nuclear Nonproliferation Research and Development within the U.S. Department of Energy's National Nuclear Security Administration by Lawrence Livermore National Laboratory under Contract No DE-AC52-07NA27344. The U.S. Department of Energy's Nuclear Criticality Safety Programs National Criticality Experiments Research Center (NCERC), utilized in this work, is supported by the National Nuclear Security Administration's Office of the Chief of Defense Nuclear Safety, NA-511. The authors would like to acknowledge the radiochemistry teams at LLNL (Lawrence Livermore) and PNNL (Pacific Northwest) for their efforts in characterizing and preparing the ^{239}Pu target material used for this experiment. Special thanks is given to Kevin Roberts of LLNL and Leah Arrigo of PNNL.

3 ^{237}Np Fission Spectrum Cumulative Fission Product Yield Measurement Using Godiva IV Critical Assembly

A.S. Tamashiro[1], J.T. Harke[2], S. Burcher[2], S.W. Padgett[2], P. Zhao[2], B.D. Pierson[3], N. Gharibyan[2], J.M. Goda[4], L.R. Greenwood[3], D.K. Hayes[4], J. Hutchinson[4], N. Harward[2], K. Roberts[2], G. Slavik[2], P. Yap-Chiongco[2], J. Walker[4], and C.J. Palmer[1]

Preprint submitted to Nuclear Data Sheets July 29, 2022

[1]School of Nuclear Science and Engineering, Oregon State University, Corvallis, OR 97331, USA

[2]Nuclear and Chemical Sciences Division, Lawrence Livermore National Laboratory, Livermore, CA 94550, USA

[3]Energy and Environment Directorate, Pacific Northwest National Laboratory, Richland, WA 99354, USA

[4]Advanced Nuclear Technology Group, Los Alamos National Laboratory, Los Alamos, NM 87545, USA

3.1 Abstract

Precise integral measurement of fast neutron-induced fission product yields for various actinides is of high interest for applied nuclear science. The goal of this effort is to improve uncertainties in fission product yield values of ^{237}Np. Fission was induced in a $NpO_2(NO_3)$ target using the Godiva IV critical assembly in burst mode. The irradiated sample was transferred to a high-resolution γ-ray detection setup within 50 minutes. γ-ray list mode data was collected from 50 minutes to 1 week after the irradiation. γ-ray spectroscopy was performed to analyze the time dependent γ-ray yields using an automated peak search algorithm to identify isotopes by their decay γ-ray energy and half-life. The initial activity for each isotope identified was used to calculate their fission product yield.

3.2 Introduction

The Short-Lived Fission Product Yield (SLFPY) project objective is to provide improved measurements of fission product yields for actinides. The measured fission product yields are needed for various areas of applied and fundamental nuclear science. Data exists for fission product yields on fissioning of ^{235}U [74], ^{238}U [75], and ^{239}Pu [107] with fission spectrum neutrons.

Recently, the Godiva IV critical assembly was utilized to perform a prompt burst irradiation of a sample of ^{237}Np with the goal of measuring fission product yields [76]. A γ spectroscopy-based data analysis procedure has been developed for the prediction of fission product yields that is independent of the actinide sample [103]. These results are part of a series of measurements performed by this research team where ^{235}U, ^{238}U, ^{239}Pu, ^{237}Np, and ^{233}U fission product yields have all been measured using an identical experimental setup and analysis. Some

representative results will be presented in this article.

3.3 Background

Fission product yields are used in the prediction of the behavior and performance of engineered systems involving nuclear fission. Measurements of fission product yields have been traditionally performed through radiochemistry, mass spectrometry, and γ-ray spectroscopy, often with mono-energetic neutrons.

To date, the most recent fission product yield evaluation was conducted in 1993 by England and Rider, almost 3 decades ago [77]. There were 653 fission product yield values compiled for ^{237}Np fast neutron-induced fission, 172 of which were measured using radiochemistry. The evaluation compiled publications from 1956 – 1987, making the most recent results three and a half decades old. Although, six of these publications were γ-ray spectroscopy without chemical separation [108–113]. All of these measurements used Ge(Li) or HPGe detectors. One measurement used ^{252}Cf spontaneous fission neutrons, one measurement used a thermal reactor with a 2 mm Cd shield around the sample, and the rest used fission spectrum neutrons. ^{241}Pu fission product yield values from 1987 [112] were included in the ^{237}Np fission product yield evaluation. In total, 43 fission product yield results for 29 isotopes via γ-ray spectroscopy without chemical separation were included in the England and Rider's evaluation. Table 15 lists these 29 isotopes along with their half-lives and reference fission product yields.

Table 15: List of isotopes in the England and Rider's evaluation that were measured using γ-ray spectroscopy without chemical separation. Majority of these evaluated ^{237}Np fission product yield values included ^{241}Pu fission product yields (indicated by a checkmark).

Isotope	$\tau_{1/2}$	FPY_{ref} (%) [37]	^{241}Pu [112]
^{85m}Kr	4.480 ± 0.008 h [1]	0.935 ± 0.037	–
^{87}Kr	76.3 ± 0.5 m [2]	1.741 ± 0.049	–
^{87}Br	55.65 ± 0.13 s [2]	1.474 ± 0.162	–
^{88}Kr	2.825 ± 0.019 h [3]	2.096 ± 0.126	–
^{91}Sr	9.65 ± 0.06 h [5]	3.925 ± 0.157	–
^{92}Y	3.54 ± 0.01 h [6]	4.385 ± 0.123	✓
^{92}Sr	2.611 ± 0.017 h [6]	4.371 ± 0.175	–
^{95}Zr	64.032 ± 0.006 d [8]	5.669 ± 0.134	✓
^{97}Zr	16.749 ± 0.008 h [9]	6.111 ± 0.171	✓
^{103}Ru	39.249 ± 0.003 d [11]	5.558 ± 0.156	✓
^{105}Ru	4.439 ± 0.011 h [12]	3.103 ± 0.186	✓
^{130}Sb	39.5 ± 0.8 m [16]	1.169 ± 0.748	✓
^{131}I	8.0252 ± 0.0006 d [17]	3.600 ± 0.072	✓
^{131}Te	25.0 ± 0.1 m [18]	3.031 ± 0.182	✓
^{132}Te	3.204 ± 0.013 d [18]	4.751 ± 0.190	✓
^{133}I	20.83 ± 0.08 h [19]	6.460 ± 4.135	✓
^{133m}Te	55.4 ± 0.4 m [19]	3.587 ± 0.287	✓
^{134}I	52.5 ± 0.2 m [20]	6.953 ± 0.195	✓
^{134}Te	41.8 ± 0.8 m [20]	4.415 ± 0.177	✓
^{135}Xe	9.14 ± 2 h [21]	7.255 ± 0.203	✓
^{135}I	6.58 ± 0.03 h [21]	6.708 ± 0.188	✓
^{137}I	24.5 ± 0.2 s [90]	2.450 ± 0.392	–

^{138}Cs	32.5 ± 0.2 m [22]	6.002 ± 0.240	✓
^{138}Xe	14.14 ± 0.07 m [22]	5.247 ± 0.420	–
^{139}Ba	82.93 ± 0.09 m [23]	5.634 ± 0.225	✓
^{140}La	1.67858 ± 0.00021 d [24]	5.494 ± 0.077	✓
^{140}Ba	12.751 ± 0.004 d [24]	5.488 ± 0.110	✓
^{142}La	91.1 ± 0.5 m [26]	4.794 ± 0.134	✓
^{143}Ce	33.039 ± 0.006 h [27]	4.650 ± 0.186	✓

3.4 Experiment

Godiva IV is a critical assembly composed of unreflected highly enriched uranium (HEU) metal fuel [94]. This device was intended to irradiate samples using prompt bursts of fast fission neutrons of around 24 μsec FWHM in duration with a peak neutron flux of around 4×10^{18} neutrons/cm^2/sec [94]. Large neutron fluxes allow shorter irradiation times, minimizing neutron absorption in the subsequent fission products, and assuring larger fission product generation rates. Section **??** is reproduced from Reference [107] and is included here for completeness.

3.4.1 Data Collection System

The setup consisted of two Broad-Energy Germanium (BEGe) detectors (Canberra, model BE6530), each coupled to a Lynx data acquisition system. The detectors (labelled as 8815 and 8816) were mounted on 30L liquid nitrogen dewars. The detectors are 180° from each other placed equidistant between them (see Figure 24). The detection volume is surrounded by a lead and copper to reduce background γ rays. A 1/16" thick iron followed by a 1.5 cm Teflon™ disks were

Figure 24: Counting setup.

placed in front of the detectors. This is to shield the detectors from β-particles and Bremmstrahlung X-rays.

The γ-rays detected by the BEGe spectrometers were stored in list mode format by the Lynx systems (Canberra, Digital Signal Analyzer). Data from each detector were stored in a separate file with each γ-ray interaction recorded by a time stamp and channel number. The timing between detectors was synchronized using a 5 MHz oscillator. such that timing between the two detectors could be used as a filter for coincident events in the future. For data rates of approximately 25 kHz or less the live time fraction of the data acquisition system was high enough to prevent instabilities or errors in data recording with the Lynx data acquisition system.

3.4.2 System Calibrations

The BEGe detectors and shielding used for this measurement were exactly the same as those used for previous ^{235}U [74], ^{238}U [75], and ^{239}Pu [107] fission product yield measurements [76]. Radioactive sources of ^{22}Na, ^{60}Co, ^{137}Cs, ^{133}Ba, and ^{152}Eu were placed in the source position and used to determine the energy calibration and detection efficiencies. The neptunium samples were made from a solution of $NpO_2(NO_3)$ (see Figure 25) and dried in quartz ampoules (see Figure 26). The quartz ampoules were flame sealed and leak checked to ensure no fission product gasses escaped during the measurement. The four ^{237}Np samples were counted for short periods (tens of minutes each) on 1/22/2020. From the γ spectra, the masses were determined to be 5.8 mg, 10.7 mg, 20.0 mg, and 42.89 mg for Np1, Np2, Np3, and Np4 respectively. A background measurement was performed for two hours.

3.4.3 Irradiation and Measurement

For the irradiation in the central volume of Godiva IV, the witness foils were wrapped together in aluminum foil. These witness foils consisted of small quantities of Cu (100.225 mg), Au (106.210 mg), Co (28.635 mg), Fe (108.108 mg), Ti (81.958 mg), Ni (31.678 mg), and Al (33.368 mg). That packet was placed along with the quartz ampoules in a aluminum sample holder tube into the Godiva glory hole. Figure 26 shows the four samples prior to irradiation.

The four ^{237}Np samples were inserted into Godiva on January 22, 2020 at 10:21 a.m. PST and the burst occurred at 10:57:54 a.m. The radiation monitor (an RMS-III detector) primarily measures gamma dose and exceeded its measurement limit during the burst. 700 R/hr is the highest reading observed before it went over-limit. Two resistance temperature detectors (RTDs) in Godiva IV are

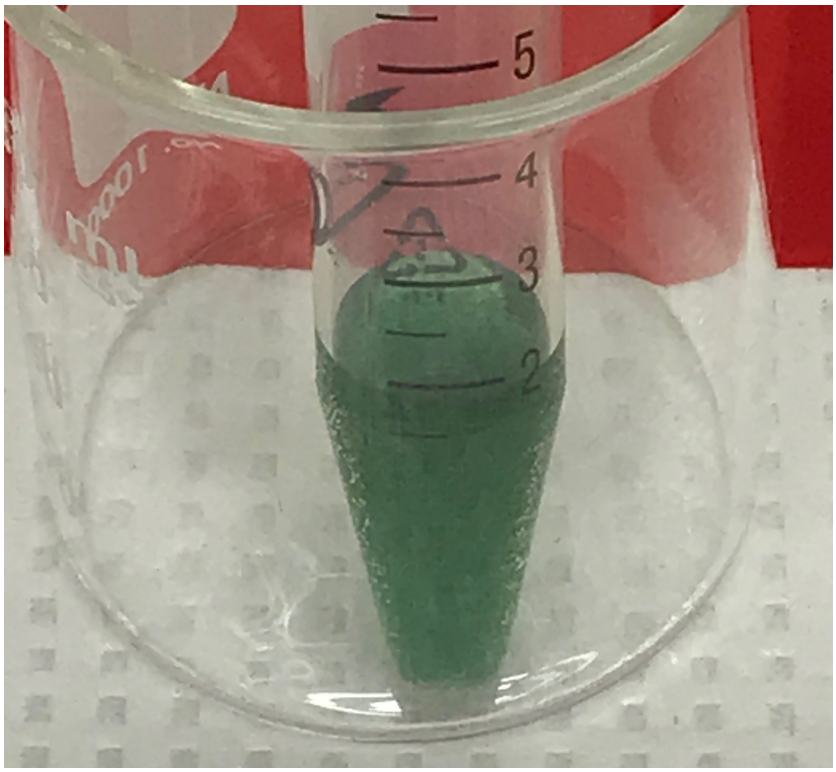

Figure 25: Solution of neptunium(V) as NpO_2NO_3.

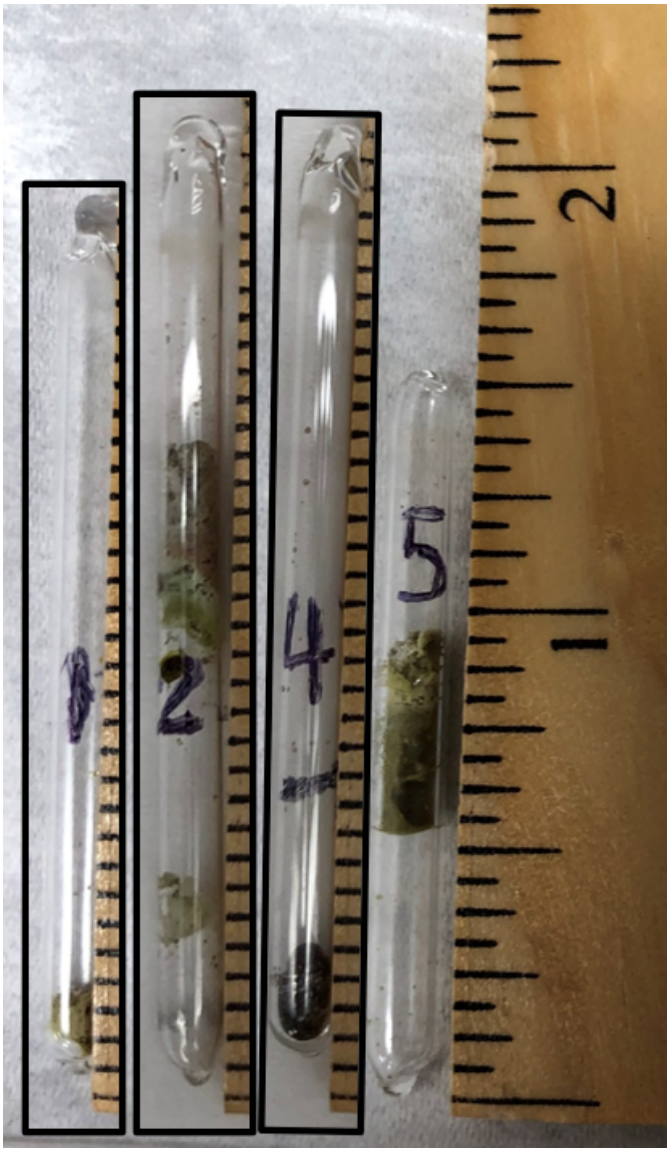

Figure 26: The $NpO_2(NO_3)/HNO_3$ solutions were delivered into the quartz tubes, then dried under house nitrogen steam and the quartz tubes were flame sealed. The ampoules were labeled 1, 2, 4, and 5, which are samples Np1, Np2, Np3, and Np4 respectively.

used to measure the temperature in the safety block (closest to the center) and in a ring. The safety block's RTD measured the core to be 13.7°C and increased by 137.4°C during the burst. The dose rate from Godiva itself needed to decrease enough for personnel entry to be allowed to retrieve the samples. The samples weren't retrieved until 11:40 a.m. The witness foils and empty quartz ampule were set aside for subsequent packaging and shipment to Pacific Northwest National Laboratory (PNNL). The neptunium samples were packaged together for transport to the counting station at 11:45 a.m. Sample Np2 was mounted on a sample holder and placed in the central location between the BEGe detectors. The detection rate was approximately 30 kHz at 11:48:31 a.m. At 3:05:09 p.m. the data acquisition was stopped, data were saved, then Np1 + Np3 were mounted and placed in the central position. The second measurement started at 3:31:20 p.m. on January 22, 2020. The detected rate on each system was approximately 20 kHz. The measurement of Np1 and Np3 continued until 09:46 a.m. on January 30, 2020. The room was closed and not accessed except for occasional filling of liquid nitrogen.

3.4.4 Witness Foil Analysis

The witness foil pack was irradiated with the neptunium samples and analyzed at PNNL. Table 16 shows the measured reaction rate for each activated metal. From this measurement, the neutron energy spectrum (see Figure 27) was calculated using the STAYSL PNNL code [95]. The STAYSL analysis estimated 7.3E11 ± 3E10 fission events per gram of the plutonium samples.

Table 16: Witness foil reactions and measured sample activation values, corrected to the burst irradiation time.

Sample	Mass (mg)	Reaction	Isotope	Reaction Rate [$\sigma\phi$] ($s^{-1}atom^{-1}$)
Cu	100.225	^{63}Cu(n,γ)	^{64}Cu	3.6E-12 ± 1E-13
		^{63}Cu(n,α)	^{60}Co	8.4E-14 ± 3E-15
Au	106.210	^{197}Au(n,γ)	^{198}Au	3.56E-11 ± 7E-13
		^{197}Au(n,2n)	^{196}Au	5.6E-13 ± 1E-14
Co	28.635	^{59}Co(n,γ)	^{60}Co	2.10E-12 ± 4E-14
Fe	108.108	^{58}Fe(n,γ)	^{59}Fe	7.3E-13 ± 4E-14
		^{54}Fe(n,p)	^{54}Mn	1.24E-11 ± 2E-13
		^{56}Fe(n,p)	^{56}Mn	1.70E-13 ± 3E-15
		^{54}Fe(n,α)	^{51}Cr	1.19E-13 ± 9E-15
Ti	81.958	^{46}Ti(n,p)	^{46}Sc	1.75E-12 ± 4E-14
		^{47}Ti(n,p)	^{47}Sc	2.98E-12 ± 6E-14
		^{48}Ti(n,p)	^{48}Sc	4.9E-14 ± 1E-15
Ni	31.678	^{58}Ni(n,p)	^{58}Co	1.58E-11 ± 3E-13
		^{60}Ni(n,p)	^{60}Co	1E-13 ± 1E-14
Al	33.368	^{27}Al(n,α)	^{24}Na	3.36E-13 ± 7E-15

3.5 Data Analysis

This section is reproduced from Reference [107] and is included here for completeness. The fission product yield, FPY_i, for isotope i can be calculated directly from the ratio of the number of decay events from isotope i to the total number of fission events in the irradiation experiment. The total number of fission events N_f is generated assuming a known reference fission product yield, FPY_{ref}:

$$N_f = \frac{A_{0,ref}\tau_{1/2,ref}}{\ln(2)FPY_{ref}\epsilon_{\gamma ref}I_{ref}R_{ref}}. \tag{11}$$

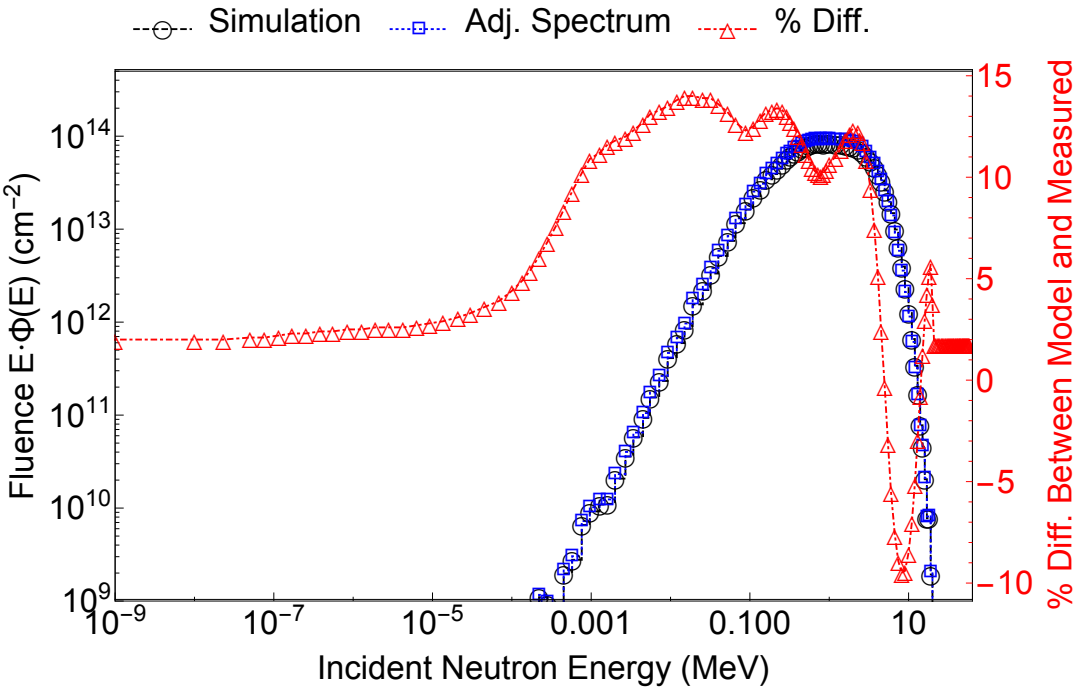

Figure 27: A plot of the MCNP simulated and adjusted neutron fluence spectrum for Godiva IV during the ^{237}Np pulsed irradiation.

The measured fission yield for isotope i can then be written in terms of the reference isotope:

$$\frac{FPY_i}{FPY_{ref}} = \left(\frac{A_{0,i}}{A_{0,ref}}\right)\left[\frac{\tau_{1/2,i}/\epsilon_{\gamma,i}I_iR_i}{\tau_{1/2,ref}/\epsilon_{\gamma,ref}I_{ref}R_{ref}}\right]. \tag{12}$$

Where should be used, A_0 is the initial activity of the induced radioactive fission product, $\tau_{1/2}$ is the half-life of the specific isotope, ϵ_γ is the absolute detector efficiency, I is the self attenuation of the γ ray through the target, and R is the branching ratio of the γ ray observed. The activities, half-life, and efficiencies are measured in the experiment, while the other parameters are from ENDF-VIII.0 [37]. The reference fission product used to estimate the total number of fission events is ^{140}Ba (^{99}Mo and ^{140}Ba are common standards for fission product yield measurements [96]).

3.5.1 Detector Efficiency – ϵ_γ

Table 17: Eckert & Ziegler calibration sources used for detector characterization.

Source	$\tau_{1/2}$	Activity (kBq)	Date
^{60}Co	1925.28 ± 0.14 d [97]	44 ± 1	8/1/2019
^{137}Cs	30.08 ± 0.09 y [90]	41 ± 4	8/1/2019
^{22}Na	2.6018 ± 0.0022 y [98]	42 ± 1	8/1/2019
^{133}Ba	312.20 ± 0.20 d [99]	42 ± 1	8/1/2019
^{152}Eu	10.551 ± 0.011 y [19]	44 ± 1	8/1/2019

Table 17 lists the calibration sources used. This data is used for energy calibration and detector efficiency fits. The equation used to fit the detector efficiency is the following:

$$\epsilon_\gamma = P_0 E^{-P_1} + P_2 - P_3 e^{-P_4 E} \tag{13}$$

where E is energy in MeV. The parameters 0–4 were extracted from the efficiency fit (see Table 29 and Figures 28 and 29). The uncertainty was calculated using the following ROOT generated covariance matrices:

$$\begin{array}{c} \\ P_0 \\ P_1 \\ P_2 \\ P_3 \\ P_4 \end{array} \begin{array}{c} \begin{array}{ccccc} P_0 & P_1 & P_2 & P_3 & P_4 \end{array} \\ \begin{bmatrix} \text{1.4E-9} & \text{-3.8E-7} & \text{-1.4E-9} & \text{-1.3E-7} & \text{-1.6E-6} \\ \text{-3.8E-7} & \text{1.1E-4} & \text{3.6E-7} & \text{3.6E-5} & \text{3.5E-4} \\ \text{-1.4E-9} & \text{3.6E-7} & \text{1.4E-9} & \text{1.2E-7} & \text{1.6E-6} \\ \text{-1.3E-7} & \text{3.6E-5} & \text{1.2E-7} & \text{1.3E-5} & \text{1.3E-4} \\ \text{-1.6E-6} & \text{3.5E-4} & \text{1.6E-6} & \text{1.3E-4} & \text{5.6E-3} \end{bmatrix} \end{array}$$

$$
\begin{array}{c} \\ P_0 \\ P_1 \\ P_2 \\ P_3 \\ P_4 \end{array}
\begin{array}{c}
\begin{array}{ccccc} P_0 & P_1 & P_2 & P_3 & P_4 \end{array} \\
\left[\begin{array}{ccccc}
\text{1.0E-9} & \text{-3.3E-7} & \text{-1.0E-9} & \text{-9.5E-8} & \text{-1.7E-6} \\
\text{-3.3E-7} & \text{1.1E-4} & \text{3.1E-7} & \text{3.3E-5} & \text{4.5E-4} \\
\text{-1.0E-9} & \text{3.1E-7} & \text{1.0E-9} & \text{8.9E-8} & \text{1.6E-6} \\
\text{-9.5E-8} & \text{3.3E-5} & \text{8.9E-8} & \text{1.0E-5} & \text{1.4E-4} \\
\text{-1.7E-6} & \text{4.5E-4} & \text{1.6E-6} & \text{1.4E-4} & \text{6.6E-3}
\end{array}\right]
\end{array}
$$

for detector 8815 and 8816 respectively.

Table 18: Efficiency curve parameters.

P_i	Detector 8815	Detector 8816
[0]	$2.18 \times 10^{-3} \pm 4 \times 10^{-5}$	$1.80 \times 10^{-3} \pm 3 \times 10^{-5}$
[1]	1.08 ± 0.01	1.09 ± 0.01
[2]	$1.41 \times 10^{-3} \pm 4 \times 10^{-5}$	$1.23 \times 10^{-3} \pm 3 \times 10^{-5}$
[3]	0.210 ± 0.004	0.178 ± 0.003
[4]	26.63 ± 0.07	26.44 ± 0.08

3.5.2 Self-Attenuation – I

The self attenuation factor accounts for the γ rays attenuating effect through the ^{237}Np samples, and is represented by the following:

$$I = \frac{I_{raw}}{C} = e^{-\frac{\mu}{\rho} x \rho} \tag{14}$$

where I_{raw} is the unnormalized self attenuation factor, C is the corrected counts without attenuation, μ/ρ is the mass attenuation for ^{237}Np (provided by NIST XCOM [100]), x is the mean free path, and ρ is the density of ^{237}Np (20.25 g/cm^3 [101]). Figures 30, 31, 32, and 33 are corrected counts of ^{237}Np γ rays listed in Table 19 and fitted with Equation 14. The normalized counts resulted in Np2 mass to be 12.0 ± 0.6 mg and 11.9 ± 0.6 mg for detectors 8815 and 8816

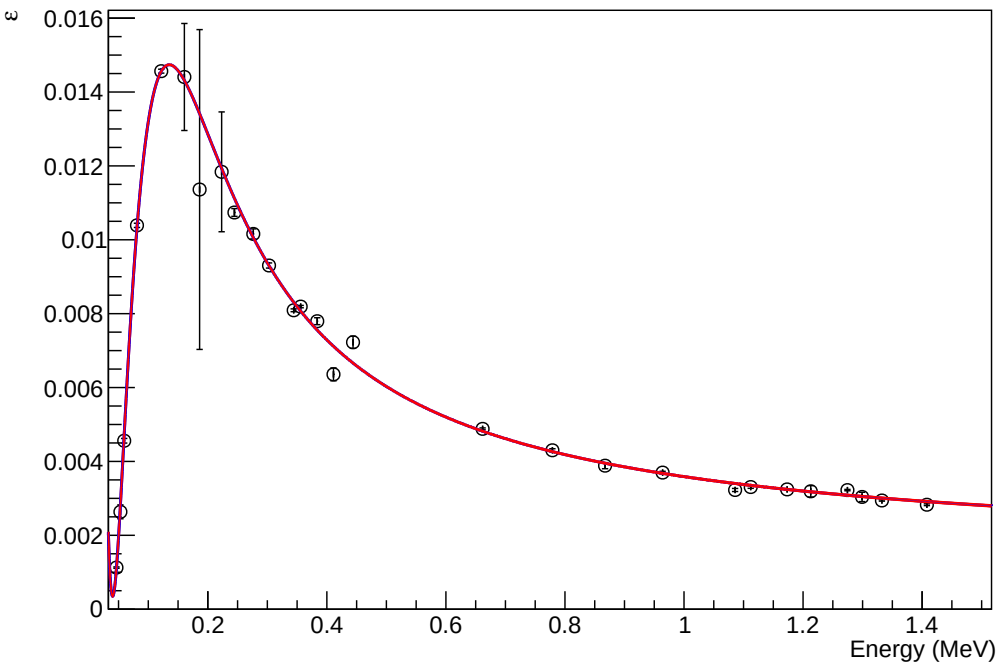

Figure 28: The detection efficiency of detector 8815 was measured for different calibration sources.

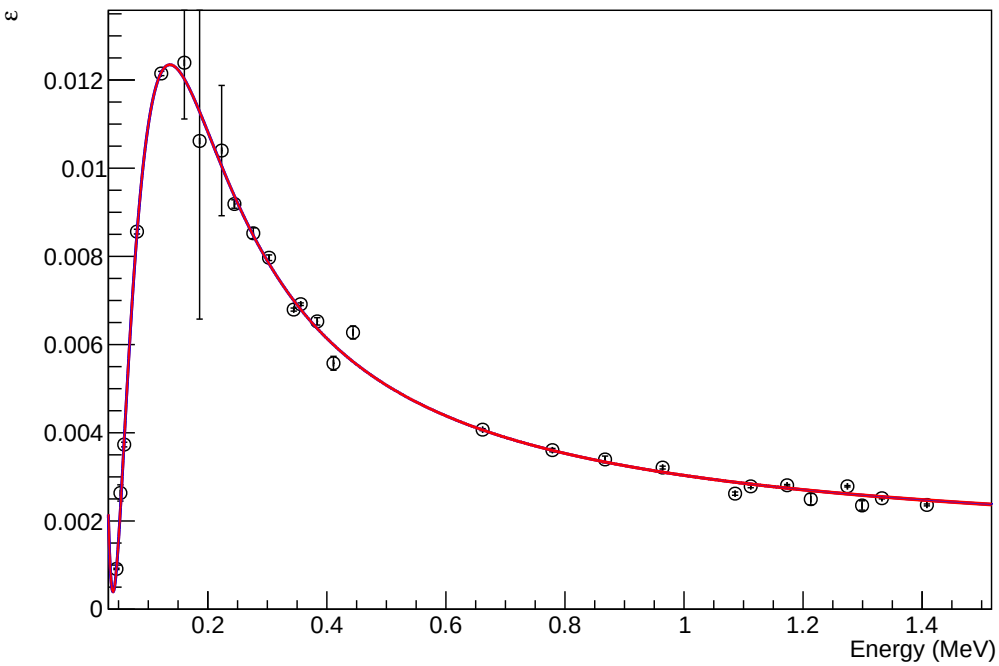

Figure 29: The detection efficiency of detector 8816 was measured for different calibration sources.

Table 19: ^{237}Np γ-rays used to determine the self attenuation factor.

E_γ (keV)	R_γ	Np1+Np3	Np2
117.7	$1.70 \times 10^{-3} \pm 0.04 \times 10^{-3}$	–	✓
134.3	$7.2 \times 10^{-4} \pm 0.3 \times 10^{-4}$	✓	✓
143.2	$4.16 \times 10^{-3} \pm 0.11 \times 10^{-3}$	–	✓
151.4	$2.44 \times 10^{-3} \pm 0.03 \times 10^{-3}$	✓	–
194.7	$1.82 \times 10^{-3} \pm 0.05 \times 10^{-3}$	✓	–
212.3	$1.52 \times 10^{-3} \pm 0.03 \times 10^{-3}$	✓	–
214.0	$3.57 \times 10^{-4} \pm 0.03 \times 10^{-4}$	✓	–

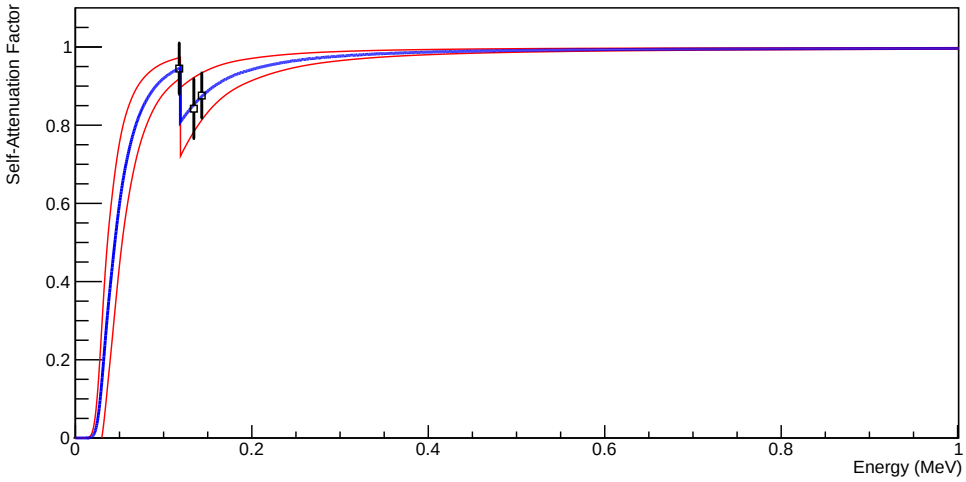

Figure 30: Np2 self attenuation measured with detector 8815 where x = 2E-3 ± 1E-3 cm.

respectively. The gravimetrically measured Np2 mass was 10.7 mg. The Np2 sample mass difference is caused by a position offset of the sample compared to the position of the calibration sources. The normalized counts resulted in large Np1 + Np3 mass to be 25.9 ± 0.7 mg and 26.1 ± 0.7 mg for detectors 8815 and 8816 respectively. The gravimetrically measured Np1 and Np3 masses were 5.8 mg and 20.0 mg respectively, which summed to 25.8 mg. The Np1 + Np3 mass difference is caused by a position offset of the sample compared to the position of the calibration sources.

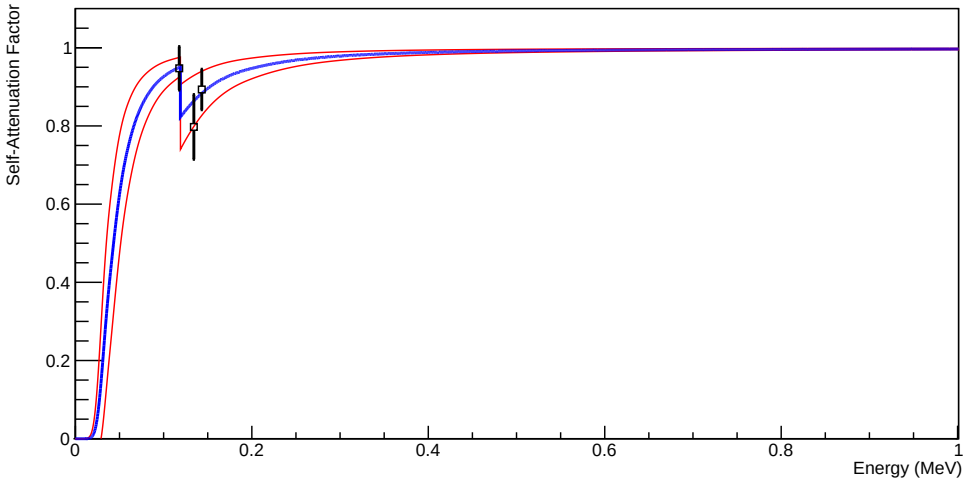

Figure 31: Np2 self attenuation measured with detector 8816 where 2E-3 ± 1E-3 cm.

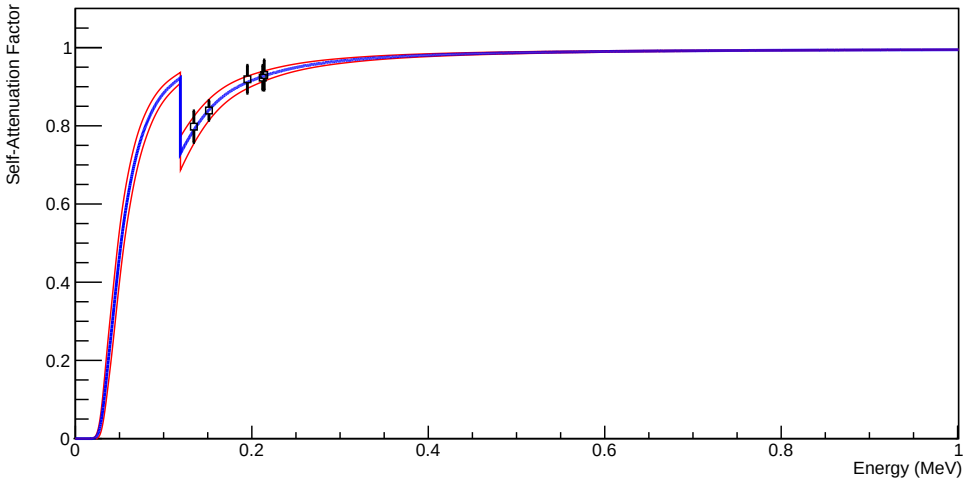

Figure 32: Np1 + Np3 self attenuation measured with detector 8815 where x = 3.4E-3 ± 6E-4 cm.

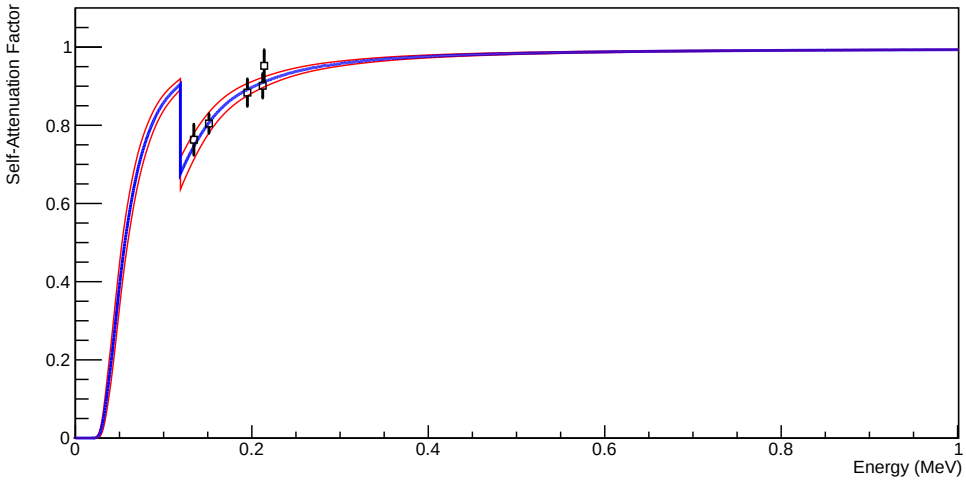

Figure 33: Np1 + Np3 self attenuation measured with detector 8816 where x = 4.2E-3 ± 6E-4 cm.

3.5.3 Total Fission – N_f

The total number of fission events used in this analysis was calculated with Equation 11. The reference fission product is ^{140}Ba, specifically the 537.3 keV γ-ray from Np1 + Np3. Table 21 lists the parameters used to determine the total number of fission events. All fission product yield values in this paper will use the weighted mean of the total number of fission events between the two detectors. Np2's total number of fission events is based on Np1 + Np3's result for ^{142}La 894.9 keV γ-ray.

3.5.4 γ-Ray Analysis

The γ ray peaks are analyzed using a code written in ROOT [39]. By defining unique energy intervals for each peak, we isolate the peaks in the spectrum so they can be analyzed independently. These intervals are determined visually using cascade plots as illustrated in Figure 34 for the case of a γ-ray peak at 537.3 keV associated with the fission product ^{140}Ba. Each color represents a different

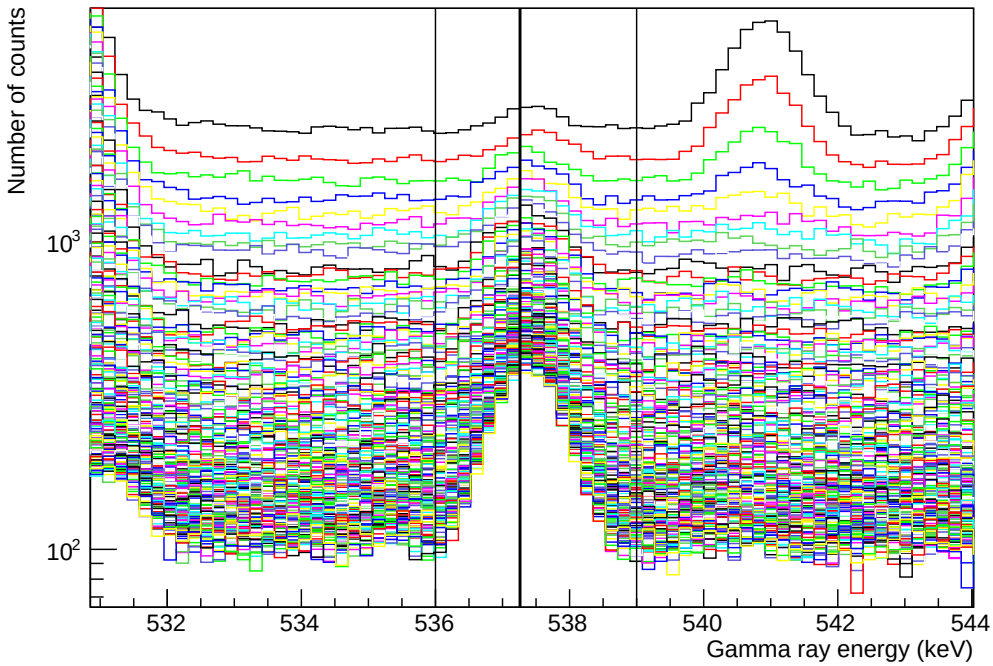

Figure 34: ^{140}Ba γ-ray cascade plot for the 537.3 keV γ ray. For more details, please refer to the text.

Table 20: Parameters used to determine Np1 + Np3's total number of fission events.

Parameter		
Isotope	^{140}Ba	
$\tau_{1/2}$ (d)	12.751 ± 0.004 [24]	
FPY (%)	5.488 ± 0.110 [37]	
E_γ (keV)	537.261 ± 0.009 [24]	
R_γ (%)	24.39 ± 0.22 [24]	
Detector	8815	8816
A_0 (Bq)	$8.53 \times 10^{-1} \pm 2 \times 10^{-3}$	$7.20 \times 10^{-1} \pm 2 \times 10^{-3}$
ϵ_γ	$5.68 \times 10^{-3} \pm 1 \times 10^{-5}$	$4.79 \times 10^{-3} \pm 1 \times 10^{-5}$
I_γ	$9.88 \times 10^{-1} \pm 2 \times 10^{-3}$	$9.86 \times 10^{-1} \pm 2 \times 10^{-3}$
N_f	$1.81 \times 10^{10} \pm 4 \times 10^{8}$	$1.81 \times 10^{10} \pm 4 \times 10^{8}$
$\overline{N_f}$	$1.81 \times 10^{10} \pm 4 \times 10^{8}$	

Table 21: Parameters used to determine Np2's total number of fission events.

Parameter		
Isotope	^{142}La	
$\tau_{1/2}$ (hrs)	1.518 ± 0.008 [26]	
FPY (%)	5.5 ± 0.2 (large sample result)	
E_γ (keV)	894.9 ± 0.4 [26]	
R_γ (%)	8.34 ± 0.17 [26]	
Detector	8815	8816
A_0 (Bq)	$1.62 \times 10^{1} \pm 1 \times 10^{-1}$	$1.41 \times 10^{1} \pm 1 \times 10^{-1}$
ϵ_γ	$3.87 \times 10^{-3} \pm 2 \times 10^{-5}$	$3.27 \times 10^{-3} \pm 2 \times 10^{-5}$
I_γ	$9.96 \times 10^{-1} \pm 2 \times 10^{-3}$	$9.96 \times 10^{-1} \pm 2 \times 10^{-3}$
N_f	$7.2 \times 10^{9} \pm 3 \times 10^{8}$	$7.5 \times 10^{9} \pm 3 \times 10^{8}$
$\overline{N_f}$	$7.3 \times 10^{9} \pm 3 \times 10^{8}$	

time bin and as time progresses the overall counts decrease. In this example, the energy interval is set to [536 keV, 539 keV]. The interval chosen attempts to include information of the background and photo-peak.

As the time binned data is acquired, the live and raw time are used for the

dead time correction by multiplying the counts for an energy bin with the ratio of raw time divided by live time. The energy bin channel number is converted into energy deposited by multiplying by the ratio of total energy range to the total number of energy bins. In this case, the energy range is [0,2600 keV] and there are 16384 energy channel bins. The time binned data are histograms of counts vs. energy for each time bin. When the time and energy intervals are chosen, a Gaussian fit function with a linear background is used to fit the histogram for each time:

$$F(E) = N \exp\left[- \frac{(E-\mu)^2}{2\sigma^2} \right] + mE + y, \tag{15}$$

where N is the amplitude of the peak, μ is the energy of the peak, σ is the resolution of the detector, m is the slope of the background, y is the y-intercept of the background, and E is energy. This technique is used when there is a background continuum present [102]. Before the code fits every time slice, a master fit is produced to provide the centroid of the γ-ray peak [see Figure 35]. The histogram for the master fit is the produced by summing the data over all the time bins in the chosen time interval for each channel.

The linear background is subtracted out and the integral S is the net counts in each respective time bin.

$$\begin{aligned} S &= \int \left(N \exp\left[- \frac{(E-\mu)^2}{2\sigma^2} \right] + mE + y \right) dx \\ &\quad - \int (mE + y)\, dx \\ &= \int \left(N \exp\left[- \frac{(E-\mu)^2}{2\sigma^2} \right] \right) dx. \end{aligned} \tag{16}$$

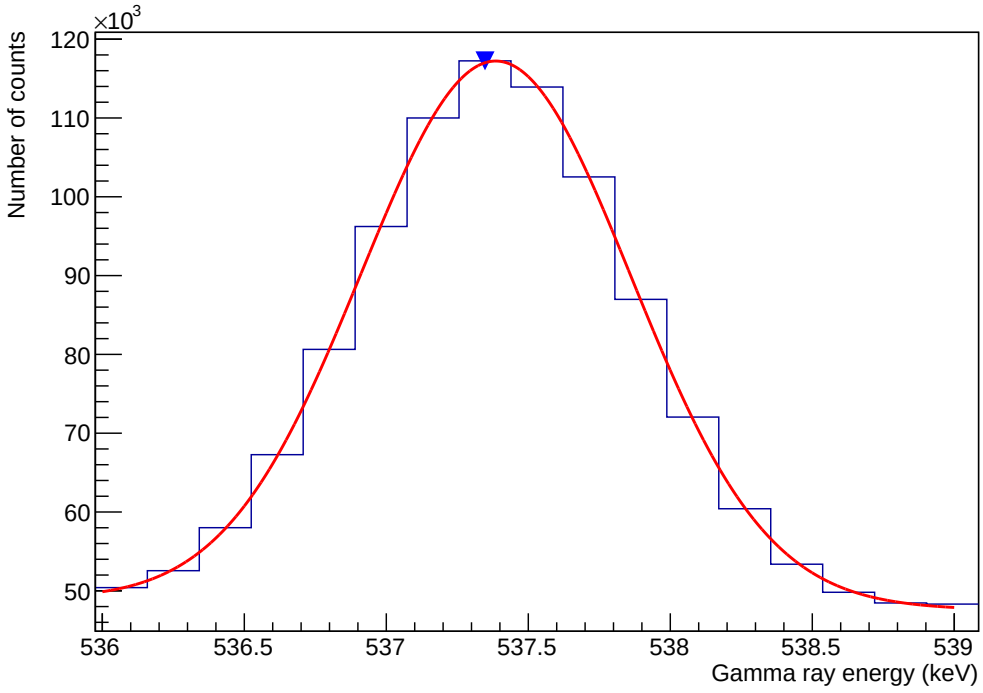

Figure 35: ^{140}Ba master sum plot fit for the 537.3 keV γ ray

3.5.5 Decay Curve Fitting Routine – $\tau_{1/2}$, A_0

Net counts and half-life data are used to fit a decay curve that is extrapolated to time zero. The data for this curve consists of the counts integrated over each peak (using the energy interval established previously) in each time bin . To secure a proper decay curve, the half life and time increments were fixed. The only parameter to change would be the initial count rate. Provided is the fit function:

$$N(t) = \left(\frac{A_0\tau_{1/2}}{\ln(2)}\right)\left(\exp\left(-\frac{\ln(2)}{\tau_{1/2}}t\right) - \exp\left(-\frac{\ln(2)}{\tau_{1/2}}(t+\Delta t)\right)\right), \tag{17}$$

where $N(t)$ is the counts of γ rays, A_0 is the initial count rate of γ rays, $\tau_{1/2}$ is half life, Δt is time step, and t is time. This equation is derived from the integral

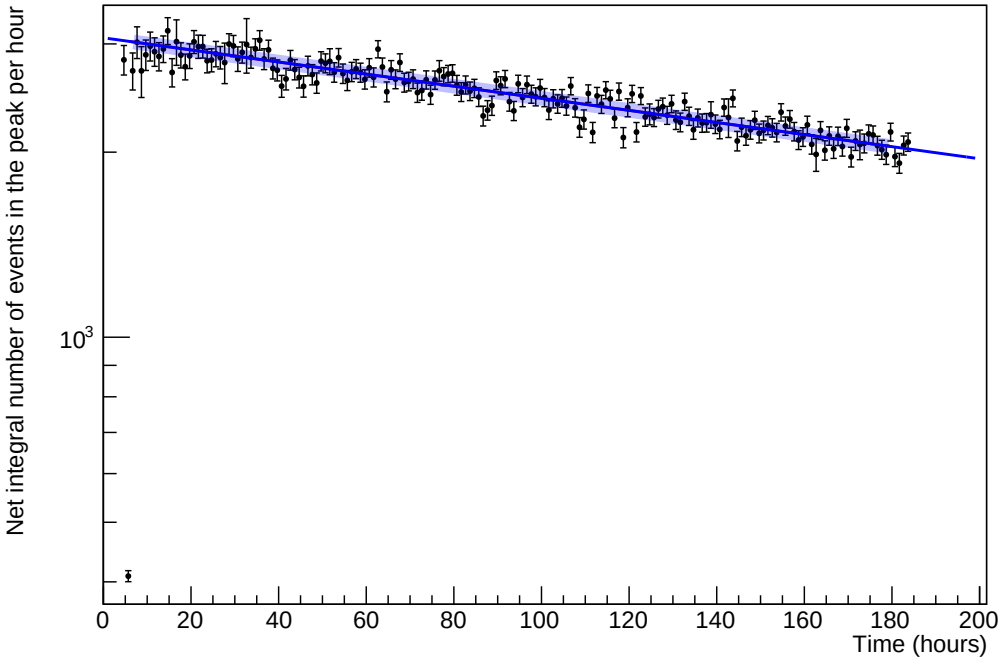

Figure 36: ^{140}Ba γ-ray half-life plot for the 537.3 keV γ ray

of the count rate over a time bin.

Figure 36 shows the number of events in the peak per hour bin, where the blue line is the fit function and the thicker line indicates the time interval used in the fitting. The black points are the net counts with error for each time bin.

Figure 37 shows the residuals plot from the fitting in Figure 36. The residual plot is another criteria used to help determine an energy and time interval for the γ ray analysis. A time interval is iterated until residuals are less than a user-defined value of 20%. The goal is to include as much fitting points as possible, while minimizing the relative differences in the residual plot.

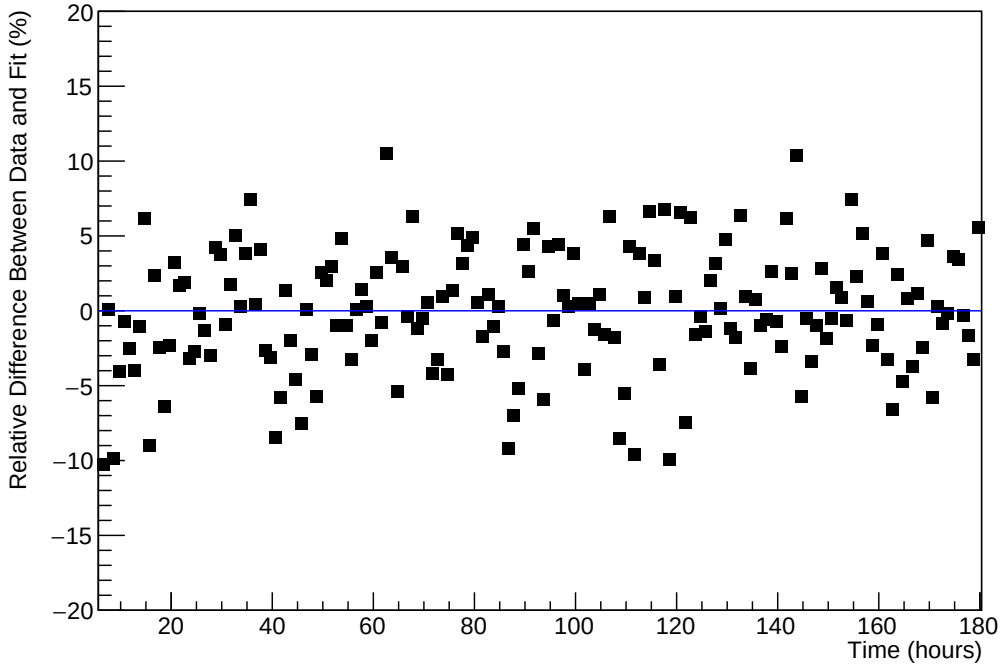

Figure 37: ^{140}Ba γ-ray residual plot for the 537.3 keV γ ray

3.6 Results

For Np1 + Np3, 20 isotopes were analyzed using 64 γ-rays, resulting in 64 cumulative fission product yield results (see Table 22). For Np2, 17 isotopes were analyzed using 37 γ-rays, resulting in 37 cumulative fission product yield results (see Table 23). 10 isotopes from Np2 overlapped with results from Np1 + Np3. These were ^{88}Kr, ^{91}Sr, ^{92}Sr, ^{93}Y, ^{105}Ru, ^{127}Sn, ^{131}I, ^{135}I, ^{142}La, and ^{143}Ce. In total, 27 different isotopes were analyzed from this experiment. Since only a single decay curve fit was used, all results are cumulative fission product yields.

Table 22: Np1 + Np3 cumulative fission product yield results from detectors 8815 and 8816. Values were combined by an uncertainty weighted mean. Reference values are from ENDF/B-VIII.0 [37]. ^{99}Mo reference fission product yield for 739.5 keV γ-ray was used to determine the total number of fission events.

Isotope	E_γ (keV)	FPY_{8815} (%)	ΔFPY_{8815} (%)	FPY_{8816} (%)	ΔFPY_{8816} (%)	$\overline{FPY}$ (%)	$\Delta\overline{FPY}$ (%)	FPY_{ref} (%)	ΔFPY_{ref} (%)
^{88}Kr	834.830	1.973	0.110	1.949	0.109	1.961	0.077	2.096	0.126
^{88}Kr	1518.390	1.723	0.124	1.879	0.134	1.794	0.091	2.096	0.126
^{88}Kr	1529.770	1.804	0.104	1.755	0.102	1.779	0.073	2.096	0.126
^{88}Kr	2029.840	1.762	0.109	1.739	0.110	1.751	0.077	2.096	0.126
^{88}Kr	2195.842	1.660	0.094	1.661	0.096	1.661	0.067	2.096	0.126
^{88}Kr	2392.110	1.646	0.093	1.635	0.094	1.640	0.066	2.096	0.126
^{91}Sr	749.800	3.970	0.167	3.958	0.167	3.964	0.118	3.925	0.157
^{92}Sr	1383.930	3.554	0.246	3.491	0.242	3.522	0.172	4.371	0.175
^{93}Y	266.900	4.728	0.693	4.737	0.695	4.732	0.491	5.116	3.275
^{93}Y	947.100	4.885	0.710	5.071	0.736	4.975	0.511	5.116	3.275
^{93}Y	1917.800	4.124	0.569	4.223	0.584	4.172	0.408	5.116	3.275
^{95}Zr	756.725	5.495	0.138	5.592	0.142	5.542	0.099	5.669	0.113
^{97}Zr	254.170	7.191	0.564	8.029	0.657	7.546	0.428	6.111	0.171

^{97}Zr	355.400	6.530	0.342	6.283	0.331	6.402	0.238	6.111	0.171
^{97}Zr	507.640	5.838	0.261	5.775	0.258	5.806	0.184	6.111	0.171
^{97}Zr	602.370	6.849	0.413	6.062	0.372	6.414	0.276	6.111	0.171
^{97}Zr	703.760	5.496	0.347	5.466	0.355	5.481	0.248	6.111	0.171
^{97}Zr	1147.970	6.411	0.300	6.310	0.296	6.360	0.211	6.111	0.171
^{97}Zr	1362.680	5.829	0.641	5.775	0.655	5.803	0.458	6.111	0.171
^{97}Zr	1750.240	5.134	0.503	4.962	0.489	5.046	0.351	6.111	0.171
^{99}Mo	739.500	6.625	0.203	6.507	0.200	6.565	0.142	6.118	0.245
^{99}Mo	777.921	6.385	0.202	6.459	0.207	6.421	0.145	6.118	0.245
^{103}Ru	497.085	5.866	0.166	5.723	0.162	5.793	0.116	5.558	0.156
^{105}Ru	469.370	3.241	0.131	3.270	0.132	3.256	0.093	3.103	0.186
^{105}Ru	499.300	3.788	0.544	3.550	0.511	3.662	0.373	3.103	0.186
^{105}Ru	676.360	3.482	0.143	3.408	0.140	3.444	0.100	3.103	0.186
^{105}Ru	724.300	3.367	0.092	3.326	0.092	3.346	0.065	3.103	0.186
^{127}Sn	1114.300	0.221	0.048	0.224	0.048	0.223	0.034	0.258	0.082
^{129}Sb	544.700	1.168	0.087	1.149	0.086	1.158	0.061	1.759	0.405
^{129}Sb	633.700	0.730	0.092	0.714	0.095	0.722	0.066	1.759	0.405

^{129}Sb	812.800	1.476	0.078	1.454	0.077	1.465	0.055	1.759	0.405
^{131m}Te	793.750	1.040	0.037	1.087	0.038	1.063	0.026	0.683	0.075
^{131m}Te	852.210	0.800	0.031	0.786	0.031	0.793	0.022	0.683	0.075
^{131m}Te	1125.460	0.819	0.037	0.793	0.037	0.806	0.026	0.683	0.075
^{131m}Te	1206.600	0.792	0.030	0.775	0.030	0.784	0.021	0.683	0.075
^{131}I	364.489	3.934	0.105	3.904	0.105	3.919	0.074	3.600	0.072
^{131}I	636.989	4.124	0.121	4.173	0.123	4.148	0.086	3.600	0.072
^{133}I	529.872	6.790	0.269	6.799	0.269	6.794	0.190	6.460	4.135
^{133}I	1298.223	7.376	0.311	7.263	0.309	7.319	0.219	6.460	4.135
^{135}I	220.502	7.472	0.337	7.135	0.340	7.305	0.239	6.708	0.188
^{135}I	836.804	6.670	0.283	6.594	0.280	6.632	0.199	6.708	0.188
^{135}I	1038.760	6.617	0.277	6.565	0.276	6.591	0.196	6.708	0.188
^{135}I	1131.511	6.594	0.270	6.564	0.270	6.579	0.191	6.708	0.188
^{135}I	1260.409	6.580	0.270	6.538	0.270	6.559	0.191	6.708	0.188
^{135}I	1457.560	6.309	0.263	6.328	0.266	6.319	0.187	6.708	0.188
^{135}I	1502.790	6.074	0.301	6.129	0.308	6.101	0.215	6.708	0.188
^{135}I	1566.410	5.870	0.285	5.638	0.278	5.751	0.199	6.708	0.188

^{135}I	1678.027	6.222	0.290	6.108	0.288	6.165	0.204	6.708	0.188
^{135}I	1706.459	6.127	0.307	5.970	0.303	6.047	0.216	6.708	0.188
^{140}Ba	537.261	5.488	0.145	5.488	0.146	5.488	0.103	5.488	0.110
^{141}La	1354.520	5.914	0.311	5.777	0.307	5.845	0.218	5.341	0.427
^{142}La	641.285	5.619	0.156	5.678	0.158	5.648	0.111	4.794	0.134
^{142}La	894.900	5.570	0.207	5.473	0.204	5.521	0.146	4.794	0.134
^{142}La	1043.700	5.552	0.316	5.402	0.391	5.493	0.246	4.794	0.134
^{142}La	1545.800	4.443	0.315	4.070	0.269	4.227	0.205	4.794	0.134
^{142}La	1901.300	4.105	0.166	4.099	0.172	4.102	0.120	4.794	0.134
^{142}La	2397.800	3.899	0.157	3.725	0.158	3.813	0.112	4.794	0.134
^{142}La	2542.700	3.184	0.139	3.383	0.154	3.274	0.103	4.794	0.134
^{143}Ce	293.266	4.420	0.121	4.341	0.119	4.380	0.085	4.650	0.186
^{143}Ce	350.619	5.256	0.156	5.234	0.157	5.245	0.111	4.650	0.186
^{143}Ce	490.368	4.507	0.140	4.526	0.143	4.516	0.100	4.650	0.186
^{143}Ce	721.929	4.993	0.141	4.963	0.141	4.978	0.100	4.650	0.186
^{143}Ce	880.460	4.313	0.187	4.235	0.190	4.275	0.133	4.650	0.186
^{151}Pm	717.720	0.689	0.056	0.411	0.030	0.474	0.026	0.727	0.029

Table 23: Np2 detectors 8815 and 8816. Values were combined by an uncertainty weighted mean. Reference values are from ENDF/B-VIII.0 [37]. Np1 + Np3's ^{142}La fission product yield result for 894.9 keV γ-ray was used to determine the total number of fission events.

Isotope	E_γ (keV)	FPY_{8815} (%)	ΔFPY_{8815} (%)	FPY_{8816} (%)	ΔFPY_{8816} (%)	$\overline{FPY}$ (%)	$\Delta\overline{FPY}$ (%)	FPY_{ref} (%)	ΔFPY_{ref} (%)
^{88}Kr	196.301	2.320	0.161	2.216	0.152	2.265	0.111	2.096	0.126
^{88}Kr	2195.842	1.832	0.120	1.675	0.111	1.748	0.081	2.096	0.126
^{88}Kr	2392.110	1.772	0.113	1.702	0.111	1.736	0.079	2.096	0.126
^{91}Sr	749.800	4.086	0.214	4.126	0.217	4.106	0.152	3.925	0.157
^{92}Sr	1383.930	4.545	0.340	4.357	0.327	4.447	0.236	3.012	0.084
^{93}Y	266.900	6.597	1.000	6.288	0.954	6.435	0.690	4.371	0.175
^{105}Ru	316.440	3.138	0.174	3.006	0.167	3.070	0.121	3.103	0.186
^{105}Ru	393.360	3.546	0.174	3.464	0.176	3.506	0.124	3.103	0.186
^{105}Ru	469.370	3.615	0.183	3.483	0.178	3.548	0.128	3.103	0.186
^{105}Rh	319.231	2.955	0.186	2.532	0.173	2.728	0.127	3.104	0.087

^{127}Sn	1095.600	0.251	0.074	0.234	0.069	0.242	0.051	0.258	0.082
^{127}Sn	1114.300	0.321	0.069	0.288	0.062	0.303	0.046	0.258	0.082
^{128}Sn	482.300	0.624	0.075	0.606	0.073	0.615	0.052	0.635	0.406
^{130}Sb	330.914	0.889	0.061	0.889	0.061	0.889	0.043	1.169	0.748
^{130}Sb	793.400	0.974	0.065	0.973	0.065	0.973	0.046	1.169	0.748
^{132}Te	228.160	5.745	0.346	4.963	0.296	5.293	0.225	4.751	0.190
^{133m}Te	863.955	3.661	0.347	3.677	0.349	3.669	0.246	3.587	0.287
^{133m}Te	912.671	4.509	0.419	4.430	0.412	4.469	0.294	3.587	0.287
^{133m}Te	1683.230	3.852	0.376	3.524	0.346	3.675	0.255	3.587	0.287
^{134}Te	201.235	4.646	0.316	4.479	0.301	4.559	0.218	4.415	0.177
^{134}Te	712.970	4.869	0.661	8.888	1.212	5.791	0.580	4.415	0.177
^{131}I	364.489	3.534	0.177	3.396	0.181	3.467	0.127	3.600	0.072
^{135}I	220.502	8.088	0.509	8.400	0.533	8.237	0.368	6.708	0.188
^{135}I	288.451	7.635	0.437	6.670	0.382	7.088	0.287	6.708	0.188
^{135}I	1131.511	7.045	0.360	6.926	0.356	6.985	0.253	6.708	0.188
^{135}I	1260.409	6.886	0.352	6.691	0.345	6.787	0.246	6.708	0.188
^{139}Ba	165.857	7.427	0.460	7.038	0.419	7.214	0.310	5.634	0.225

^{142}La	641.285	5.795	0.237	5.622	0.231	5.707	0.166	4.794	0.134
^{142}La	894.900	5.510	0.249	5.510	0.250	5.510	0.176	4.794	0.134
^{142}La	1043.700	6.209	0.308	5.737	0.292	5.961	0.212	4.794	0.134
^{142}La	1233.100	5.302	0.274	5.624	0.293	5.452	0.200	4.794	0.134
^{142}La	1901.300	4.746	0.226	4.449	0.216	4.591	0.156	4.794	0.134
^{142}La	2055.200	4.860	0.307	4.215	0.274	4.500	0.204	4.794	0.134
^{142}La	2100.400	3.745	0.414	3.472	0.384	3.598	0.282	4.794	0.134
^{142}La	2187.200	5.222	0.269	5.049	2.438	5.220	0.267	4.794	0.134
^{142}La	2542.700	3.600	0.184	3.433	0.180	3.515	0.129	4.794	0.134
^{143}Ce	293.266	4.558	0.196	4.341	0.188	4.445	0.136	4.650	0.186

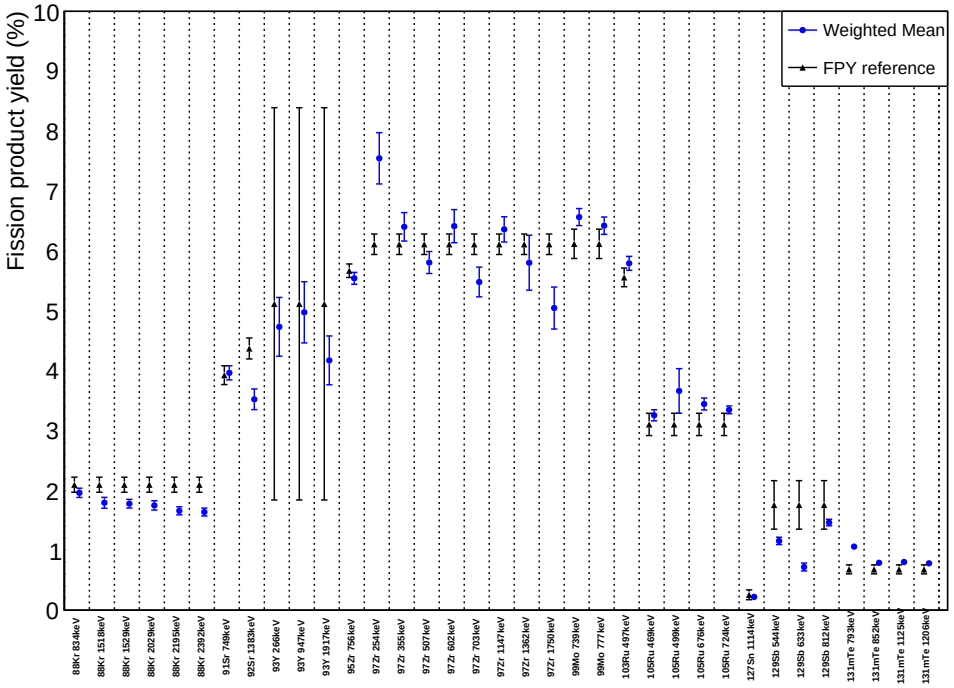

Figure 38: Np1 + Np3 weighted mean fission product yield results compared to evaluated England and Rider values. (part 1)

3.7 Fission Product Yield Analysis

This section describes how each γ-ray peak was fitted and the time chosen for the decay curve fit. The uncertainty budgets are tabulated in The uncertainty budgets are tabulated in Section 3.8.

3.7.1 ^{88}Kr ($\tau_{1/2} = 2.825 \pm 0.019$ h [3])

Six γ-ray peaks from Np1 + Np3 were analyzed. For the 834.8 keV γ ray, a multi-peak fit routine was used to account for an interfering γ ray at 836.9 keV. The decay curve fit was between 6 and 20 hours. The residual of the fit was within 10%. For the 1518.4 keV γ ray, a multi-peak fit routine was used to account for an interfering γ ray at 1515.6 keV. The decay curve fit was between 6 and 20 hours.

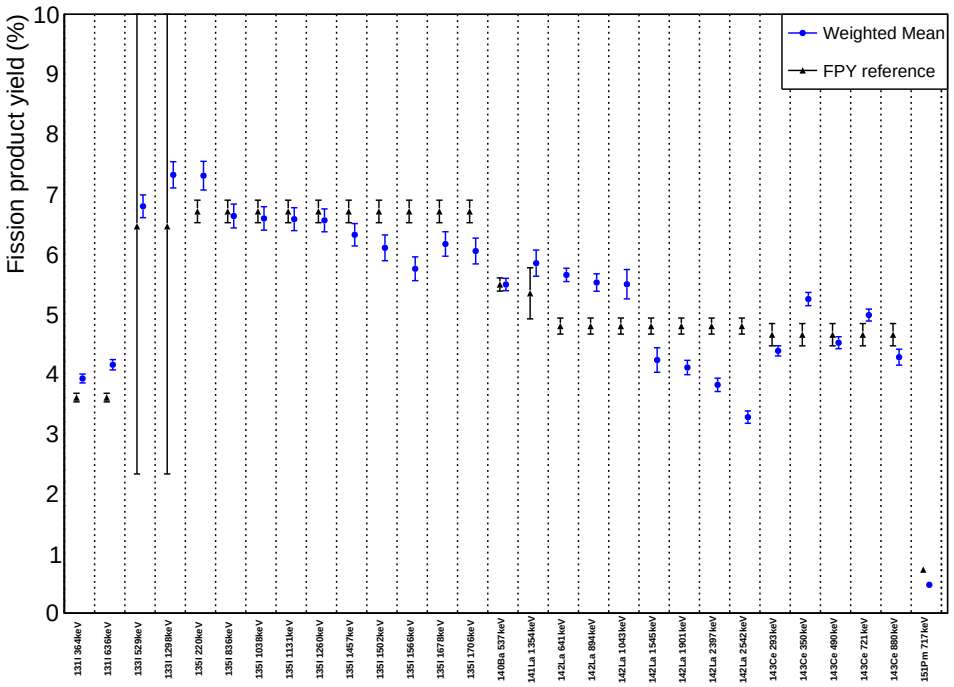

Figure 39: Np1 + Np3 weighted mean fission product yield results compared to evaluated England and Rider values. (part 2)

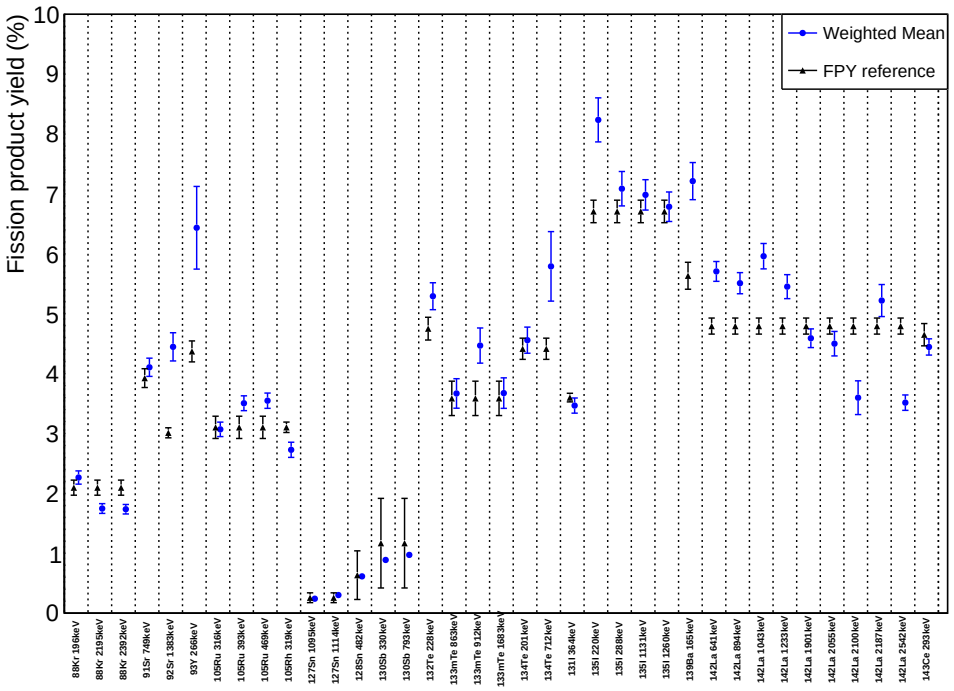

Figure 40: Np2 weighted mean fission product yield results compared to evaluated England and Rider values.

The residual of the fit was within 20%. For the 1529.8 keV γ ray, a single-peak fit routine was used. The decay curve fit was between 6 and 20 hours. The residual of the fit was within 15%. For the 2029.8 keV γ ray, a single-peak fit routine was used. The decay curve fit was between 6 and 20 hours. The residual of the fit was within 20%. For the 2195.8 keV γ ray, a single-peak fit routine was used. The decay curve fit was between 6 and 20 hours. The residual of the fit was within 10%. For the 2392.1 keV γ ray, a single-peak fit routine was used. The decay curve fit was between 6 and 20 hours. The residual of the fit was within 10%.

Three γ-ray peaks from Np2 were analyzed. For the 196.3 keV γ ray, a multi-peak fit routine was used to account for an interfering γ ray at 195.1 keV. The decay curve fit was between 1.8 and 3.8 hours. The residual of the fit was within 5%. For the 2195.8 keV γ ray, a single-peak fit routine was used. The decay curve fit was between 2.1 and 3.8 hours. The residual of the fit was within 15%. For the 2392.1 keV γ ray, a single-peak fit routine was used. The decay curve fit was between 1.0 and 3.8 hours. The residual of the fit was within 10%.

3.7.2 ^{91}Sr ($\tau_{1/2} = 9.65 \pm 0.06$ h [5])

One γ-ray peaks from Np1 + Np3 was analyzed. For the 749.8 keV γ ray, a single-peak fit routine was used. The decay curve fit was between 6 and 55 hours. The residual of the fit was within 15%.

One γ-ray peaks from Np2 was analyzed. For the 749.8 keV γ ray, a single-peak fit routine was used. The decay curve fit was between 1.3 and 3.8 hours. The residual of the fit was within 7%.

3.7.3 ^{92}Sr ($\tau_{1/2} = 2.611 \pm 0.017$ **h** [6])

One γ-ray peak from Np1 + Np3 was analyzed. For the 1383.9 keV γ ray, a single-peak fit routine was used. The decay curve fit was between 17 and 30 hours. The residual of the fit was within 20%.

One γ-ray peak from Np2 was analyzed. For the 1383.9 keV γ ray, a single-peak fit routine was used. The decay curve fit was between 1.0 and 4.0 hours. The residual of the fit was within 5%.

3.7.4 ^{93}Y ($\tau_{1/2} = 10.18 \pm 0.08$ **h** [7])

Three γ-ray peaks from Np1 + Np3 were analyzed. For the 266.9 keV γ ray, a single-peak fit routine was used. The decay curve fit was between 8 and 32 hours. The residual of the fit was within 15%. For the 947.1 keV γ ray, a single-peak fit routine was used. The decay curve fit was between 8 and 30 hours. The residual of the fit was within 15%. For the 1917.8 keV γ ray, a multi-peak fit routine was used to account for an interfering γ-ray at 1921.4 keV. The decay curve fit was between 6 and 30 hours. The residual of the fit was within 15%.

One γ-ray peaks from Np2 was analyzed. For the 266.9 keV γ ray, a single-peak fit routine was used. The decay curve fit was between 2.8 and 3.8 hours. The residual of the fit was within 10%.

3.7.5 ^{95}Zr ($\tau_{1/2} = 64.032 \pm 0.006$ **d** [8])

One γ-ray peak from Np1 + Np3 was analyzed. For the 756.7 keV γ ray, a multi-peak fit routine was used to account for an interfering γ-ray at 753.8 keV. The decay curve fit was between 6 and 120 hours. The residual of the fit was within 20%.

3.7.6 ^{97}Zr ($\tau_{1/2} = 16.749 \pm 0.008$ h [9])

Eight γ-ray peaks from Np1 + Np3 were analyzed. For the 254.2 keV γ ray, a single-peak fit routine was used. The decay curve fit was between 9 and 20 hours. The residual of the fit was within 15%. For the 355.4 keV γ ray, a single-peak fit routine was used. The decay curve fit was between 6 and 20 hours. The residual of the fit was within 15%. For the 507.6 keV γ ray, a multi-peak fit routine was used to account for an interfering γ ray at 506.1 and 510.6 keV. The decay curve fit was between 6 and 70 hours. The residual of the fit was within 15%. For the 602.4 keV γ ray, a multi-peak fit routine was used to account for an interfering γ ray at 599.9, 605.0, and 607.1 keV. The decay curve fit was between 6 and 31 hours. The residual of the fit was within 15%. For the 703.8 keV γ ray, a multi-peak fit routine was used to account for an interfering γ ray at 706.8 keV. The decay curve fit was between 20 and 30 hours. The residual of the fit was within 15%. For the 1148.0 keV γ ray, a multi-peak fit routine was used to account for an interfering γ ray at 1142.2 and 1143.9 keV. The decay curve fit was between 6 and 48 hours. The residual of the fit was within 15%. For the 1362.7 keV γ ray, a single-peak fit routine was used. The decay curve fit was between 40 and 50 hours. The residual of the fit was within 20%. For the 1750.2 keV γ ray, a single-peak fit routine was used. The decay curve fit was between 6 and 50 hours. The residual of the fit was within 15%.

3.7.7 ^{99}Mo ($\tau_{1/2} = 65.924 \pm 0.006$ h [10])

Two γ-ray peaks from Np1 + Np3 were analyzed. For the 739.5 keV γ ray, a single-peak fit routine was used. The decay curve fit was between 20 and 180 hours. The residual of the fit was within 15%. For the 777.9 keV γ ray, a single-peak fit routine was used. The decay curve fit was between 30 and 170 hours.

The residual of the fit was within 20%.

3.7.8 ^{103}Ru ($\tau_{1/2} = 39.249 \pm 0.003$ **d** [**11**])

One γ-ray peak from Np1 + Np3 was analyzed. For the 497.1 keV γ ray, a single-peak fit routine was used. The decay curve fit was between 30 and 180 hours. The residual of the fit was within 10%.

3.7.9 ^{105}Ru ($\tau_{1/2} = 4.439 \pm 0.011$ **h** [**12**])

Four γ-ray peaks from Np1 + Np3 were analyzed. For the 469.4 keV γ ray, a single-peak fit routine was used. The decay curve fit was between 6 and 20 hours. The residual of the fit was within 5%. For the 499.3 keV γ ray, a multi-peak fit routine was used to account for an interfering γ ray at 497.0 keV. The decay curve fit was between 6 and 21 hours. The residual of the fit was within 10%. For the 676.4 keV γ ray, a single-peak fit routine was used. The decay curve fit was between 6 and 20 hours. The residual of the fit was within 5%. For the 724.3 keV γ ray, a multi-peak fit routine was used to account for an interfering γ ray at 721.7 and 727.4 keV. The decay curve fit was between 6 and 19 hours. The residual of the fit was within 3%.

Three γ ray peaks from Np2 were analyzed. For the 316.4 keV γ ray, a single-peak fit routine was used. The decay curve fit was between 2.5 and 3.8 hours. The residual of the fit was within 10%. For the 393.4 keV γ ray, a single-peak fit routine was used. The decay curve fit was between 1.8 and 3.8 hours. The residual of the fit was within 15%. For the 469.4 keV γ ray, a multi-peak fit routine was used to account for an interfering γ ray at 471.8 keV. The decay curve fit was between 1.5 and 3.2 hours. The residual of the fit was within 5%.

3.7.10 ^{105}Rh ($\tau_{1/2} = 35.341 \pm 0.019$ h [12])

One γ-ray peak from Np2 was analyzed. For the 319.2 keV γ ray, a single-peak fit routine was used. The decay curve fit was between 2.5 and 3.8 hours. The residual of the fit was within 20%.

3.7.11 ^{127}Sn ($\tau_{1/2} = 2.10 \pm 0.04$ h [13])

One γ-ray peak from Np1 + Np3 was analyzed. For the 1114.3 keV γ ray, a single-peak fit routine was used. The decay curve fit was between 6 and 10 hours. The residual of the fit was within 5%.

Two γ-ray peaks from Np2 were analyzed. For the 1095.6 keV γ ray, a single-peak fit routine was used. The decay curve fit was between 1.1 and 1.8 hours. The residual of the fit was within 20%. For the 1114.3 keV γ ray, a single-peak fit routine was used. The decay curve fit was between 0.8 and 3.8 hours. The residual of the fit was within 20%.

3.7.12 ^{128}Sn ($\tau_{1/2} = 9.05 \pm 0.04$ h [14])

One γ-ray peak from Np2 was analyzed. For the 482.3 keV γ ray, a single-peak fit routine was used. The decay curve fit was between 1.0 and 3.8 hours. The residual of the fit was within 5%.

3.7.13 ^{129}Sb ($\tau_{1/2} = 4.366 \pm 0.026$ h [15])

Three γ-ray peaks from Np1 + Np3 was analyzed. For the 544.7 keV γ ray, a single-peak fit routine was used. The decay curve fit was between 4 and 8 hours. The residual of the fit was within 2%. For the 633.7 keV γ ray, a single-peak fit routine was used. The decay curve fit was between 4 and 10 hours. The residual of the fit was within 20%. For the 812.8 keV γ-ray, a multi-peak fit routine was

used to account for an interfering γ-ray at 809.6 keV. The decay curve fit was between 4 and 10 hours. The residual of the fit was within 1%.

3.7.14 ^{130}Sb ($\tau_{1/2} = 39.5 \pm 0.8$ **m** [16])

Two γ-ray peaks from Np2 were analyzed. 1 For the 330.9 keV γ ray, a single-peak fit routine was used. The decay curve fit was between 0.8 and 1.5 hours. The residual of the fit was within 5%. For the 793.4 keV γ ray, a single-peak fit routine was used. The decay curve fit was between 0.8 and 1.2 hours. The residual of the fit was within 5%.

3.7.15 ^{131m}Te ($\tau_{1/2} = 33.25 \pm 0.25$ **h** [17])

Four γ-rays from Np1 + Np3 were analyzed. For the 793.8 keV γ ray, a single-peak fit routine was used. The decay curve fit was between 10 and 80 hours. The residual of the fit was within 20%. For the 852.2 keV γ ray, a single-peak fit routine was used. The decay curve fit was between 20 and 60 hours. The residual of the fit was within 20%. For the 1125.5 keV γ ray, a single-peak fit routine was used. The decay curve fit was between 60 and 80 hours. The residual of the fit was within 20%. For the 1206.6 keV γ ray, a single-peak fit routine was used. The decay curve fit was between 20 and 60 hours. The residual of the fit was within 20%.

3.7.16 ^{132}Te ($\tau_{1/2} = 3.204 \pm 0.013$ **d** [18])

One γ-ray from Np2 was analyzed. For the 228.2 keV γ ray, a single-peak fit routine was used. The decay curve fit was between 1.0 and 3.8 hours. The residual of the fit was within 20%.

3.7.17 ^{133m}Te ($\tau_{1/2} = 55.4 \pm 0.4$ **m** [19])

Three γ-ray peaks from Np2 were analyzed. For the 864.0 keV γ ray, a multi-peak fit routine was used to account for an interfering γ ray at 861.7 keV. The decay curve fit was between 0.8 and 1.3 hours. The residual of the fit was within 2%. For the 912.7 keV γ ray, a multi-peak fit routine was used to account for an interfering γ ray at 914.7 keV. The decay curve fit was between 0.8 and 1.5 hours. The residual of the fit was within 2%. For the 1683.2 keV γ ray, a single-peak fit routine was used. The decay curve fit was between 1.0 and 3.8 hours. The residual of the fit was within 15%.

3.7.18 ^{134}Te ($\tau_{1/2} = 41.8 \pm 0.8$ **m** [20])

Two γ-ray peaks from Np2 were analyzed. For the 201.2 keV γ ray, a single-peak fit routine was used. The decay curve fit was between 0.8 and 2.0 hours. The residual of the fit was within 5%. For the 713.0 keV γ ray, a single-peak fit routine was used. The decay curve fit was between 0.8 and 2.0 hours. The residual of the fit was within 15%.

3.7.19 ^{131}I ($\tau_{1/2} = 8.0252 \pm 0.0006$ **d** [17])

Two γ-ray peaks from Np1 + Np3 were analyzed. For the 364.5 keV γ ray, a single-peak fit routine was used. The decay curve fit was between 120 and 180 hours. The residual of the fit was within 5%. For the 364.5 keV γ ray, a single-peak fit routine was used. The decay curve fit was between 60 and 180 hours. The residual of the fit was within 20%.

One γ-ray peak from Np2 was analyzed. For the 364.5 keV γ ray, a multi-peak fit routine was used to account for an interfering γ ray at 362.5 keV. The decay curve fit was between 1.8 and 3.8 hours. The residual of the fit was within 15%.

3.7.20 ^{133}I ($\tau_{1/2} = 20.83 \pm 0.08$ h [19])

Two γ-ray peaks from Np1 + Np3 were analyzed. For the 529.9 keV γ ray, a multi-peak fit routine was used to account for an interfering γ ray at 526.5 keV. The decay curve fit was between 6 and 130 hours. The residual of the fit was within 3%. For the 1298.2 keV γ ray, a multi-peak fit routine was used to account for an interfering γ ray at 1295.8 keV. The decay curve fit was between 20 and 40 hours. The residual of the fit was within 10%.

3.7.21 ^{135}I ($\tau_{1/2} = 6.58 \pm 0.03$ h [21])

Ten γ-ray peaks from Np1 + Np3 were analyzed. For the 220.5 keV γ ray, a multi-peak fit routine was used to account for an interfering γ ray at 222.8 keV. The decay curve fit was between 6 and 20 hours. The residual of the fit was within 15%. For the 836.8 keV γ ray, a multi-peak fit routine was used to account for an interfering γ ray at 834.9 keV. The decay curve fit was between 6 and 30 hours. The residual of the fit was within 5%. For the 1038.8 keV γ ray, a single-peak fit routine was used. The decay curve fit was between 6 and 50 hours. The residual of the fit was within 10%. For the 1131.5 keV γ ray, a single-peak fit routine was used. The decay curve fit was between 6 and 50 hours. The residual of the fit was within 10%. For the 1260.4 keV γ ray, a single-peak fit routine was used. The decay curve fit was between 6 and 60 hours. The residual of the fit was within 10%. For the 1457.6 keV γ ray, a multi-peak fit routine was used to account for an interfering γ ray at 1460.8 keV. The decay curve fit was between 8 and 50 hours. The residual of the fit was within 5%. For the 1502.8 keV γ ray, a single-peak fit routine was used. The decay curve fit was between 6 and 30 hours. The residual of the fit was within 20%. For the 1566.4 keV γ ray, a single-peak fit routine was used. The decay curve fit was between 6 and 40 hours. The residual of the fit was

within 20%. For the 1678.0 keV γ ray, a single-peak fit routine was used. The decay curve fit was between 6 and 40 hours. The residual of the fit was within 7%. For the 1706.5 keV γ ray, a single-peak fit routine was used. The decay curve fit was between 6 and 50 hours. The residual of the fit was within 20%.

Four γ-ray peaks from Np2 were analyzed. For the 220.5 keV γ ray, a single-peak fit routine was used. The decay curve fit was between 1.0 and 3.8 hours. The residual of the fit was within 20%. For the 288.5 keV γ ray, a single-peak fit routine was used. The decay curve fit was between 1.5 and 3.8 hours. The residual of the fit was within 20%. For the 1131.5 keV γ ray, a single-peak fit routine was used. The decay curve fit was between 1.0 and 2.8 hours. The residual of the fit was within 5%. For the 1260.4 keV γ ray, a single-peak fit routine was used. The decay curve fit was between 1.0 and 2.8 hours. The residual of the fit was within 5%.

3.7.22 ^{139}Ba ($\tau_{1/2} = 82.93 \pm 0.09$ **m** [**23**])

One γ-ray peak from Np2 was analyzed. For the 165.9 keV γ ray, a multi-peak fit routine was used to account for an interfering γ ray at 168.8 keV. The decay curve fit was between 0.8 and 4.0 hours. The residual of the fit was within 5%.

3.7.23 ^{140}Ba ($\tau_{1/2} = 12.751 \pm 0.004$ **d** [**24**])

One γ-ray peaks from Np1 + Np3 was analyzed. For the 537.3 keV γ ray, a single-peak fit routine was used. The decay curve fit was between 6 and 180 hours. The residual of the fit was within 15%.

3.7.24 ^{141}La ($\tau_{1/2} = 3.92 \pm 0.03$ h [25])

One γ-ray peak from Np1 + Np3 was analyzed. For the 1354.5 keV γ ray, a single-peak fit routine was used. The decay curve fit was between 6 and 20 hours. The residual of the fit was within 10%.

3.7.25 ^{142}La ($\tau_{1/2} = 91.1 \pm 0.5$ m [26])

Seven γ-ray peaks from Np1 + Np3 were analyzed. For the 641.3 keV γ ray, a single-peak fit routine was used. The decay curve fit was between 6 and 10 hours. The residual of the fit was within 5%. For the 894.9 keV γ ray, a multi-peak fit routine was used to account for an interfering γ ray at 898.1 keV. The decay curve fit was between 6 and 10 hours. The residual of the fit was within 20%. For the 1043.7 keV γ ray, a single-peak fit routine was used. The decay curve fit was between 6 and 11 hours. The residual of the fit was within 20%. For the 1545.8 keV γ ray, a multi-peak fit routine was used to account for an interfering γ ray at 1543.9 keV. The decay curve fit was between 6 and 12 hours. The residual of the fit was within 20%. For the 1901.3 keV γ ray, a single-peak fit routine was used. The decay curve fit was between 6 and 10 hours. The residual of the fit was within 7%. For the 2397.8 keV γ ray, a multi-peak fit routine was used to account for an interfering γ ray at 2392.6 keV. The decay curve fit was between 6 and 10 hours. The residual of the fit was within 10%. For the 1901.3 keV γ ray, a single-peak fit routine was used. The decay curve fit was between 6 and 16 hours. The residual of the fit was within 20%.

Nine γ-ray peaks from Pu1 were analyzed. For the 641.3 keV γ ray, a single-peak fit routine was used. The decay curve fit was between 2.0 and 3.8 hours. The residual of the fit was within 3%. For the 849.9 keV γ ray, a multi-peak fit routine was used to account for an interfering γ ray at 898.0 keV. The decay curve fit was

between 1.8 and 3.2 hours. The residual of the fit was within 3%. For the 1043.7 keV γ ray, a multi-peak fit routine was used to account for an interfering γ ray at 1052.5 keV. The decay curve fit was between 1.5 and 2.3 hours. The residual of the fit was within 10%. For the 1233.1 keV γ ray, a single-peak fit routine was used. The decay curve fit was between 0.8 and 3.8 hours. The residual of the fit was within 20%. For the 1901.3 keV γ ray, a multi-peak fit routine was used to account for an interfering γ ray at 1898.0 keV. The decay curve fit was between 0.8 and 3.8 hours. The residual of the fit was within 10%. For the 2055.2 keV γ ray, a single-peak fit routine was used. The decay curve fit was between 1.0 and 3.8 hours. The residual of the fit was within 20%. For the 2100.4 keV γ ray, a single-peak fit routine was used. The decay curve fit was between 1.8 and 3.5 hours. The residual of the fit was within 15%. For the 2187.2 keV γ ray, a single-peak fit routine was used. The decay curve fit was between 1.0 and 4.0 hours. The residual of the fit was within 15%. For the 2542.7 keV γ ray, a single-peak fit routine was used. The decay curve fit was between 0.8 and 4.0 hours. The residual of the fit was within 10%.

3.7.26 ^{143}Ce ($\tau_{1/2} = 33.039 \pm 0.006$ **h** [**27**])

Five γ-ray peaks from Np1 + Np3 were analyzed. For the 293.3 keV γ ray, a single-peak fit routine was used. The decay curve fit was between 6 and 120 hours. The residual of the fit was within 5%. For the 350.6 keV γ ray, a multi-peak fit routine was used to account for an interfering γ ray at 351.7 keV. The decay curve fit was between 10 and 40 hours. The residual of the fit was within 15%. For the 490.4 keV γ-ray, a multi-peak fit routine was used to account for an interfering γ-ray at 492.7 keV. The decay curve fit was between 13 and 60 hours. The residual of the fit was within 15%. For the 721.9 keV γ-ray, a multi-peak fit

routine was used to ccount for an interfering γ-ray at 724.2 and 727.3 keV. The decay curve fit was between 6 and 47 hours. The residual of the fit was within 15%. For the 880.5 keV γ-ray, a multi-peak fit routine was used to account for an interfering γ-ray at 882.8 keV. The decay curve fit was between 35 and 60 hours. The residual of the fit was within 15%.

One γ-ray peak from Np2 was analyzed. For the 293.3 keV γ ray, a single-peak fit routine was used. The decay curve fit was between 1.3 and 3.8 hours. The residual of the fit was within 10%.

3.7.27 ^{151}Pm ($\tau_{1/2} = 28.40 \pm 0.04$ h [30])

One γ-ray peak from Np1 + Np3 was analyzed. For the 717.7 keV γ ray, a multi-peak fit routine was used to account for an interfering γ ray at 713.1 and 715.6 keV. The decay curve fit was between 6 and 50 hours. The residual of the fit was within 20%.

3.8 Fission Product Yield Parameter and Uncertainty Budget

Table 24: Values used to calculate Np1 + Np3 cumulative fission product yield results and uncertainties for detector 8815 where N_f = 1.81E10 ± 4E8.

Isotope	E_γ (keV)	A_0 (Bq)	ΔA_0 (Bq)	$\tau_{1/2}$ (hrs.)	$\Delta\tau_{1/2}$ (hrs.)	ϵ_γ	$\Delta\epsilon_\gamma$	I_γ	ΔI_γ	R_γ (%)	ΔR_γ (%)
^{88}Kr	834.830	1.263E+01	1.311E-01	2.840	0.030	4.060E-03	1.746E-05	9.935E-01	1.203E-03	12.975	0.616
^{88}Kr	1518.390	1.264E+00	4.949E-02	2.840	0.030	2.796E-03	2.692E-05	9.962E-01	7.049E-04	2.152	0.114
^{88}Kr	1529.770	6.697E+00	6.707E-02	2.840	0.030	2.785E-03	2.709E-05	9.962E-01	7.019E-04	10.934	0.534
^{88}Kr	2029.840	2.358E+00	4.818E-02	2.840	0.030	2.422E-03	3.412E-05	9.966E-01	6.229E-04	4.529	0.227
^{88}Kr	2195.842	6.243E+00	5.616E-02	2.840	0.030	2.340E-03	3.639E-05	9.967E-01	6.089E-04	13.183	0.618
^{88}Kr	2392.110	1.568E+01	8.015E-02	2.840	0.030	2.257E-03	3.901E-05	9.968E-01	5.962E-04	34.600	1.603
^{91}Sr	749.800	1.478E+01	3.047E-02	9.630	0.050	4.387E-03	1.641E-05	9.926E-01	1.360E-03	23.685	0.796
^{92}Sr	1383.930	1.202E+02	1.245E+00	2.710	0.010	2.942E-03	2.501E-05	9.960E-01	7.467E-04	90.000	5.682
^{93}Y	266.900	1.170E+01	7.161E-02	10.180	0.080	1.036E-02	1.242E-05	9.561E-01	7.965E-03	7.320	1.054
^{93}Y	947.100	1.291E+00	1.590E-02	10.180	0.080	3.721E-03	1.892E-05	9.943E-01	1.047E-03	2.093	0.298
^{93}Y	1917.800	5.390E-01	5.369E-03	10.180	0.080	2.486E-03	3.257E-05	9.966E-01	6.344E-04	1.545	0.208
^{95}Zr	756.725	2.923E-01	2.347E-04	1536.768	0.144	4.357E-03	1.649E-05	9.927E-01	1.346E-03	54.380	0.220
^{97}Zr	254.170	1.753E+00	6.024E-02	16.749	0.008	1.079E-02	1.239E-05	9.510E-01	8.860E-03	1.145	0.075
^{97}Zr	355.400	2.238E+00	2.667E-02	16.749	0.008	8.081E-03	1.279E-05	9.758E-01	4.435E-03	2.095	0.093
^{97}Zr	507.640	3.579E+00	1.318E-02	16.749	0.008	5.953E-03	1.386E-05	9.872E-01	2.362E-03	5.027	0.186

^{97}Zr	602.370	1.005E+00	8.214E-03	16.749	0.008	5.184E-03	1.476E-05	9.901E-01	1.820E-03	1.378	0.075
^{97}Zr	703.760	5.280E-01	1.850E-02	16.749	0.008	4.599E-03	1.587E-05	9.920E-01	1.470E-03	1.015	0.047
^{97}Zr	1147.970	1.138E+00	6.094E-03	16.749	0.008	3.286E-03	2.167E-05	9.953E-01	8.634E-04	2.616	0.102
^{97}Zr	1362.680	3.661E-01	1.425E-02	16.749	0.008	2.968E-03	2.470E-05	9.959E-01	7.546E-04	1.024	0.102
^{97}Zr	1750.240	3.004E-01	2.998E-03	16.749	0.008	2.598E-03	3.022E-05	9.965E-01	6.567E-04	1.089	0.102
^{99}Mo	739.500	1.882E+00	4.057E-03	65.976	0.024	4.432E-03	1.628E-05	9.925E-01	1.383E-03	12.260	0.218
^{99}Mo	777.921	6.137E-01	3.873E-03	65.976	0.024	4.271E-03	1.675E-05	9.930E-01	1.303E-03	4.303	0.080
^{103}Ru	497.085	1.177E+00	2.089E-03	941.928	0.072	6.058E-03	1.377E-05	9.867E-01	2.443E-03	91.000	1.221
^{105}Ru	469.370	2.788E+01	9.404E-02	4.440	0.020	6.356E-03	1.355E-05	9.854E-01	2.683E-03	17.548	0.552
^{105}Ru	499.300	3.592E+00	6.760E-02	4.440	0.020	6.036E-03	1.379E-05	9.868E-01	2.426E-03	2.034	0.285
^{105}Ru	676.360	2.005E+01	8.273E-02	4.440	0.020	4.739E-03	1.556E-05	9.916E-01	1.548E-03	15.656	0.501
^{105}Ru	724.300	5.567E+01	1.048E-01	4.440	0.020	4.501E-03	1.611E-05	9.923E-01	1.418E-03	47.300	0.500
^{127}Sn	1114.300	4.636E+00	1.758E-01	2.100	0.040	3.348E-03	2.120E-05	9.952E-01	8.872E-04	38.000	7.965
^{129}Sb	544.700	9.250E+00	1.397E-01	4.400	0.010	5.619E-03	1.420E-05	9.885E-01	2.115E-03	18.056	1.234
^{129}Sb	633.700	7.892E-01	6.555E-02	4.400	0.010	4.982E-03	1.509E-05	9.908E-01	1.693E-03	2.771	0.252
^{129}Sb	812.800	2.075E+01	9.428E-02	4.400	0.010	4.138E-03	1.718E-05	9.933E-01	1.240E-03	43.300	2.000
^{131m}Te	793.750	6.075E-01	4.873E-03	33.250	0.250	4.209E-03	1.694E-05	9.931E-01	1.274E-03	13.370	0.297
^{131m}Te	852.210	6.738E-01	5.489E-03	33.250	0.250	4.001E-03	1.768E-05	9.936E-01	1.176E-03	20.279	0.567
^{131m}Te	1125.460	3.122E-01	7.909E-03	33.250	0.250	3.327E-03	2.135E-05	9.953E-01	8.790E-04	11.017	0.294
^{131m}Te	1206.600	2.473E-01	2.898E-03	33.250	0.250	3.188E-03	2.249E-05	9.955E-01	8.273E-04	9.411	0.221
^{131}I	364.489	4.467E+00	8.331E-03	192.605	0.014	7.904E-03	1.284E-05	9.770E-01	4.223E-03	81.500	0.759

^{131}I	636.989	2.618E-01	1.774E-03	192.605	0.014	4.962E-03	1.513E-05	9.909E-01	1.681E-03	7.156	0.100
^{133}I	529.872	5.604E+01	2.792E-02	20.800	0.100	5.747E-03	1.406E-05	9.880E-01	2.208E-03	87.000	2.651
^{133}I	1298.223	8.799E-01	7.186E-03	20.800	0.100	3.052E-03	2.379E-05	9.958E-01	7.812E-04	2.349	0.075
^{135}I	220.502	7.767E+00	8.428E-03	6.570	0.020	1.204E-02	1.232E-05	9.322E-01	1.215E-02	1.751	0.062
^{135}I	836.804	9.499E+00	3.678E-02	6.570	0.020	4.053E-03	1.748E-05	9.935E-01	1.200E-03	6.687	0.227
^{135}I	1038.760	9.692E+00	2.914E-02	6.570	0.020	3.501E-03	2.015E-05	9.949E-01	9.502E-04	7.950	0.264
^{135}I	1131.511	2.600E+01	4.533E-02	6.570	0.020	3.316E-03	2.144E-05	9.953E-01	8.747E-04	22.587	0.723
^{135}I	1260.409	3.089E+01	4.524E-02	6.570	0.020	3.106E-03	2.325E-05	9.957E-01	7.990E-04	28.700	0.916
^{135}I	1457.560	8.237E+00	2.460E-02	6.570	0.020	2.859E-03	2.606E-05	9.961E-01	7.222E-04	8.667	0.278
^{135}I	1502.790	9.683E-01	1.222E-02	6.570	0.020	2.812E-03	2.670E-05	9.962E-01	7.092E-04	1.076	0.043
^{135}I	1566.410	1.099E+00	1.304E-02	6.570	0.020	2.750E-03	2.761E-05	9.963E-01	6.928E-04	1.292	0.050
^{135}I	1678.027	8.317E+00	2.424E-02	6.570	0.020	2.654E-03	2.919E-05	9.964E-01	6.691E-04	9.557	0.361
^{135}I	1706.459	3.487E+00	1.653E-02	6.570	0.020	2.631E-03	2.960E-05	9.964E-01	6.640E-04	4.104	0.172
^{140}Ba	537.261	8.535E-01	2.377E-03	306.065	0.055	5.682E-03	1.413E-05	9.883E-01	2.161E-03	24.390	0.220
^{141}La	1354.520	2.550E+00	3.689E-02	3.920	0.030	2.979E-03	2.459E-05	9.959E-01	7.577E-04	1.640	0.070
^{142}La	641.285	2.983E+02	1.295E+00	1.518	0.008	4.937E-03	1.517E-05	9.910E-01	1.665E-03	47.400	0.500
^{142}La	894.900	4.090E+01	7.471E-01	1.518	0.008	3.868E-03	1.823E-05	9.940E-01	1.114E-03	8.342	0.167
^{142}La	1043.700	1.193E+01	5.542E-01	1.518	0.008	3.490E-03	2.022E-05	9.949E-01	9.456E-04	2.702	0.055
^{142}La	1545.800	8.380E+00	3.674E-01	1.518	0.008	2.769E-03	2.731E-05	9.962E-01	6.979E-04	2.986	0.146
^{142}La	1901.300	1.673E+01	3.047E-01	1.518	0.008	2.497E-03	3.234E-05	9.966E-01	6.362E-04	7.157	0.161
^{142}La	2397.800	2.663E+01	2.997E-01	1.518	0.008	2.255E-03	3.909E-05	9.968E-01	5.958E-04	13.272	0.317

^{142}La	2542.700	1.601E+01	2.623E-01	1.518	0.008	2.203E-03	4.098E-05	9.968E-01	5.888E-04	10.001	0.259
^{143}Ce	293.266	1.834E+01	2.435E-02	33.039	0.006	9.562E-03	1.251E-05	9.641E-01	6.545E-03	42.800	0.420
^{143}Ce	350.619	1.425E+00	1.395E-02	33.039	0.006	8.178E-03	1.276E-05	9.751E-01	4.555E-03	3.231	0.040
^{143}Ce	490.368	6.191E-01	7.989E-03	33.039	0.006	6.127E-03	1.372E-05	9.865E-01	2.497E-03	2.161	0.029
^{143}Ce	721.929	1.268E+00	7.065E-03	33.039	0.006	4.512E-03	1.608E-05	9.923E-01	1.424E-03	5.393	0.066
^{143}Ce	880.460	1.818E-01	6.035E-03	33.039	0.006	3.911E-03	1.804E-05	9.939E-01	1.134E-03	1.031	0.013
^{151}Pm	717.720	1.536E-01	5.473E-03	28.400	0.040	4.531E-03	1.603E-05	9.922E-01	1.434E-03	4.050	0.277

Table 25: Values used to calculate Np1 + Np3 cumulative fission product yield results and uncertainties for detector 8816 where N_f = 1.81E10 ± 4E8.

	E_γ	A_0	ΔA_0	$\tau_{1/2}$	$\Delta\tau_{1/2}$					R_γ	ΔR_γ
Isotope	(keV)	(Bq)	(Bq)	(hrs.)	(hrs.)	ϵ_γ	$\Delta\epsilon_\gamma$	I_γ	ΔI_γ	(%)	(%)
^{88}Kr	834.830	1.057E+01	1.244E-01	2.840	0.030	3.428E-03	1.620E-05	9.920E-01	1.223E-03	12.975	0.616
^{88}Kr	1518.390	1.173E+00	4.500E-02	2.840	0.030	2.373E-03	2.671E-05	9.953E-01	7.169E-04	2.152	0.114
^{88}Kr	1529.770	5.547E+00	6.071E-02	2.840	0.030	2.364E-03	2.689E-05	9.953E-01	7.139E-04	10.934	0.534
^{88}Kr	2029.840	1.988E+00	4.337E-02	2.840	0.030	2.062E-03	3.430E-05	9.958E-01	6.336E-04	4.529	0.227
^{88}Kr	2195.842	5.344E+00	5.146E-02	2.840	0.030	1.994E-03	3.665E-05	9.959E-01	6.193E-04	13.183	0.618
^{88}Kr	2392.110	1.333E+01	7.364E-02	2.840	0.030	1.926E-03	3.936E-05	9.960E-01	6.064E-04	34.600	1.603
^{91}Sr	749.800	1.246E+01	2.793E-02	9.630	0.050	3.702E-03	1.495E-05	9.909E-01	1.382E-03	23.685	0.796

^{92}Sr	1383.930	1.004E+02	9.906E-01	2.710	0.010	2.495E-03	2.465E-05	9.950E-01	7.593E-04	90.000	5.682
^{93}Y	266.900	9.815E+00	6.893E-02	10.180	0.080	8.729E-03	9.694E-06	9.460E-01	8.022E-03	7.320	1.054
^{93}Y	947.100	1.136E+00	1.095E-02	10.180	0.080	3.145E-03	1.789E-05	9.930E-01	1.065E-03	2.093	0.298
^{93}Y	1917.800	4.712E-01	4.785E-03	10.180	0.080	2.116E-03	3.268E-05	9.958E-01	6.452E-04	1.545	0.208
^{95}Zr	756.725	2.517E-01	4.872E-04	1536.768	0.144	3.677E-03	1.505E-05	9.910E-01	1.368E-03	54.380	0.220
^{97}Zr	254.170	1.636E+00	6.779E-02	16.749	0.008	9.088E-03	9.640E-06	9.398E-01	8.912E-03	1.145	0.075
^{97}Zr	355.400	1.811E+00	2.410E-02	16.749	0.008	6.809E-03	1.025E-05	9.701E-01	4.489E-03	2.095	0.093
^{97}Zr	507.640	2.986E+00	1.236E-02	16.749	0.008	5.017E-03	1.175E-05	9.842E-01	2.397E-03	5.027	0.186
^{97}Zr	602.370	7.514E-01	1.016E-02	16.749	0.008	4.371E-03	1.292E-05	9.878E-01	1.849E-03	1.378	0.075
^{97}Zr	703.760	4.440E-01	1.689E-02	16.749	0.008	3.879E-03	1.430E-05	9.902E-01	1.494E-03	1.015	0.047
^{97}Zr	1147.970	9.511E-01	4.511E-03	16.749	0.008	2.782E-03	2.099E-05	9.942E-01	8.779E-04	2.616	0.102
^{97}Zr	1362.680	3.085E-01	1.457E-02	16.749	0.008	2.517E-03	2.432E-05	9.950E-01	7.673E-04	1.024	0.102
^{97}Zr	1750.240	2.476E-01	2.837E-03	16.749	0.008	2.209E-03	3.021E-05	9.956E-01	6.679E-04	1.089	0.102
^{99}Mo	739.500	1.563E+00	3.738E-03	65.976	0.024	3.740E-03	1.480E-05	9.908E-01	1.405E-03	12.260	0.218
^{99}Mo	777.921	5.252E-01	3.959E-03	65.976	0.024	3.604E-03	1.536E-05	9.913E-01	1.325E-03	4.303	0.080
^{103}Ru	497.085	9.687E-01	2.084E-03	941.928	0.072	5.105E-03	1.163E-05	9.836E-01	2.479E-03	91.000	1.221
^{105}Ru	469.370	2.372E+01	8.729E-02	4.440	0.020	5.355E-03	1.133E-05	9.820E-01	2.721E-03	17.548	0.552
^{105}Ru	499.300	2.840E+00	6.124E-02	4.440	0.020	5.086E-03	1.166E-05	9.837E-01	2.462E-03	2.034	0.285
^{105}Ru	676.360	1.659E+01	8.070E-02	4.440	0.020	3.997E-03	1.391E-05	9.896E-01	1.573E-03	15.656	0.501
^{105}Ru	724.300	4.651E+01	9.646E-02	4.440	0.020	3.797E-03	1.459E-05	9.905E-01	1.441E-03	47.300	0.500
^{127}Sn	1114.300	3.990E+00	1.573E-01	2.100	0.040	2.833E-03	2.047E-05	9.941E-01	9.020E-04	38.000	7.965

^{129}Sb	544.700	7.681E+00	1.453E-01	4.400	0.010	4.736E-03	1.219E-05	9.858E-01	2.147E-03	18.056	1.234
^{129}Sb	633.700	6.516E-01	6.097E-02	4.400	0.010	4.201E-03	1.333E-05	9.887E-01	1.719E-03	2.771	0.252
^{129}Sb	812.800	1.729E+01	9.418E-02	4.400	0.010	3.493E-03	1.587E-05	9.917E-01	1.260E-03	43.300	2.000
^{131m}Te	793.750	5.375E-01	4.723E-03	33.250	0.250	3.553E-03	1.559E-05	9.915E-01	1.295E-03	13.370	0.297
^{131m}Te	852.210	5.605E-01	5.071E-03	33.250	0.250	3.379E-03	1.646E-05	9.921E-01	1.195E-03	20.279	0.567
^{131m}Te	1125.460	2.565E-01	7.054E-03	33.250	0.250	2.816E-03	2.065E-05	9.941E-01	8.938E-04	11.017	0.294
^{131m}Te	1206.600	2.056E-01	2.781E-03	33.250	0.250	2.699E-03	2.190E-05	9.945E-01	8.413E-04	9.411	0.221
^{131}I	364.489	3.730E+00	7.684E-03	192.605	0.014	6.660E-03	1.033E-05	9.716E-01	4.275E-03	81.500	0.759
^{131}I	636.989	2.239E-01	1.606E-03	192.605	0.014	4.185E-03	1.338E-05	9.888E-01	1.707E-03	7.156	0.100
^{133}I	529.872	4.735E+01	2.095E-02	20.800	0.100	4.844E-03	1.201E-05	9.852E-01	2.241E-03	87.000	2.651
^{133}I	1298.223	7.364E-01	6.736E-03	20.800	0.100	2.586E-03	2.333E-05	9.948E-01	7.944E-04	2.349	0.075
^{135}I	220.502	6.167E+00	9.218E-02	6.570	0.020	1.014E-02	9.521E-06	9.168E-01	1.216E-02	1.751	0.062
^{135}I	836.804	7.951E+00	3.422E-02	6.570	0.020	3.422E-03	1.623E-05	9.920E-01	1.220E-03	6.687	0.227
^{135}I	1038.760	8.156E+00	2.681E-02	6.570	0.020	2.961E-03	1.930E-05	9.937E-01	9.660E-04	7.950	0.264
^{135}I	1131.511	2.197E+01	4.428E-02	6.570	0.020	2.806E-03	2.074E-05	9.942E-01	8.894E-04	22.587	0.723
^{135}I	1260.409	2.608E+01	4.164E-02	6.570	0.020	2.631E-03	2.274E-05	9.947E-01	8.125E-04	28.700	0.916
^{135}I	1457.560	7.031E+00	2.289E-02	6.570	0.020	2.425E-03	2.578E-05	9.952E-01	7.345E-04	8.667	0.278
^{135}I	1502.790	8.317E-01	1.129E-02	6.570	0.020	2.386E-03	2.648E-05	9.953E-01	7.212E-04	1.076	0.043
^{135}I	1566.410	8.992E-01	1.183E-02	6.570	0.020	2.335E-03	2.744E-05	9.954E-01	7.046E-04	1.292	0.050
^{135}I	1678.027	6.960E+00	2.208E-02	6.570	0.020	2.255E-03	2.913E-05	9.955E-01	6.805E-04	9.557	0.361
^{135}I	1706.459	2.897E+00	1.509E-02	6.570	0.020	2.236E-03	2.956E-05	9.956E-01	6.753E-04	4.104	0.172

^{140}Ba	537.261	7.203E-01	2.216E-03	306.065	0.055	4.789E-03	1.210E-05	9.855E-01	2.193E-03	24.390	0.220
^{141}La	1354.520	2.119E+00	3.349E-02	3.920	0.030	2.525E-03	2.420E-05	9.949E-01	7.705E-04	1.640	0.070
^{142}La	641.285	2.547E+02	1.205E+00	1.518	0.008	4.163E-03	1.344E-05	9.889E-01	1.691E-03	47.400	0.500
^{142}La	894.900	3.404E+01	6.226E-01	1.518	0.008	3.267E-03	1.710E-05	9.926E-01	1.132E-03	8.342	0.167
^{142}La	1043.700	9.841E+00	6.332E-01	1.518	0.008	2.952E-03	1.938E-05	9.937E-01	9.614E-04	2.702	0.055
^{142}La	1545.800	6.538E+00	2.279E-01	1.518	0.008	2.351E-03	2.713E-05	9.953E-01	7.097E-04	2.986	0.146
^{142}La	1901.300	1.426E+01	2.837E-01	1.518	0.008	2.124E-03	3.244E-05	9.958E-01	6.471E-04	7.157	0.161
^{142}La	2397.800	2.178E+01	2.963E-01	1.518	0.008	1.924E-03	3.943E-05	9.960E-01	6.061E-04	13.272	0.317
^{142}La	2542.700	1.457E+01	2.439E-01	1.518	0.008	1.881E-03	4.138E-05	9.961E-01	5.989E-04	10.001	0.259
^{143}Ce	293.266	1.511E+01	2.287E-02	33.039	0.006	8.056E-03	9.833E-06	9.557E-01	6.605E-03	42.800	0.420
^{143}Ce	350.619	1.193E+00	1.321E-02	33.039	0.006	6.890E-03	1.022E-05	9.693E-01	4.609E-03	3.231	0.040
^{143}Ce	490.368	5.244E-01	7.564E-03	33.039	0.006	5.163E-03	1.156E-05	9.833E-01	2.534E-03	2.161	0.029
^{143}Ce	721.929	1.066E+00	6.782E-03	33.039	0.006	3.807E-03	1.455E-05	9.905E-01	1.447E-03	5.393	0.066
^{143}Ce	880.460	1.512E-01	5.270E-03	33.039	0.006	3.304E-03	1.688E-05	9.924E-01	1.153E-03	1.031	0.013
^{151}Pm	717.720	7.747E-02	5.300E-04	28.400	0.040	3.823E-03	1.449E-05	9.904E-01	1.457E-03	4.050	0.277

Table 26: Values used to calculate Np2 cumulative fission product yield results and uncertainties for detector 8815 where N_f = 7.2E9 ± 3E8.

Isotope	E_γ (keV)	A_0 (Bq)	ΔA_0 (Bq)	$\tau_{1/2}$ (hrs.)	$\Delta\tau_{1/2}$ (hrs.)	ϵ_γ	$\Delta\epsilon_\gamma$	I_γ	ΔI_γ	R_γ (%)	ΔR_γ (%)
^{88}Kr	196.301	3.606E+01	1.952E-01	2.840	0.030	1.301E-02	1.230E-05	9.402E-01	2.957E-02	25.985	1.214
^{88}Kr	2195.842	2.757E+00	3.841E-02	2.840	0.030	2.340E-03	3.639E-05	9.978E-01	1.128E-03	13.183	0.618
^{88}Kr	2392.110	6.751E+00	3.809E-02	2.840	0.030	2.257E-03	3.901E-05	9.978E-01	1.104E-03	34.600	1.603
^{91}Sr	749.800	6.092E+00	4.353E-02	9.630	0.050	4.387E-03	1.641E-05	9.950E-01	2.523E-03	23.685	0.796
^{92}Sr	1383.930	6.150E+01	1.087E-01	2.710	0.010	2.942E-03	2.501E-05	9.973E-01	1.383E-03	90.000	5.682
^{93}Y	266.900	6.622E+00	1.397E-01	10.180	0.080	1.036E-02	1.242E-05	9.702E-01	1.496E-02	7.320	1.054
^{105}Ru	316.440	9.559E+00	1.174E-01	4.440	0.020	8.949E-03	1.260E-05	9.792E-01	1.048E-02	11.116	0.396
^{105}Ru	393.360	3.054E+00	7.190E-02	4.440	0.020	7.395E-03	1.301E-05	9.865E-01	6.819E-03	3.775	0.062
^{105}Ru	469.370	1.249E+01	6.129E-03	4.440	0.020	6.356E-03	1.355E-05	9.902E-01	4.988E-03	17.548	0.552
^{105}Rh	319.231	1.928E+00	6.810E-02	35.360	0.060	8.880E-03	1.261E-05	9.796E-01	1.029E-02	19.100	0.630
^{127}Sn	1095.600	1.084E+00	1.264E-01	2.100	0.040	3.384E-03	2.094E-05	9.967E-01	1.671E-03	19.380	5.214
^{127}Sn	1114.300	2.693E+00	4.246E-02	2.100	0.040	3.348E-03	2.120E-05	9.968E-01	1.644E-03	38.000	7.965
^{128}Sn	482.300	3.196E+01	2.079E-01	0.984	0.002	6.212E-03	1.365E-05	9.906E-01	4.769E-03	59.000	6.686
^{130}Sb	330.914	1.236E+02	6.617E-01	0.658	0.013	8.605E-03	1.266E-05	9.811E-01	9.554E-03	78.000	4.000
^{130}Sb	793.400	8.612E+01	6.387E-01	0.658	0.013	4.210E-03	1.694E-05	9.954E-01	2.364E-03	100.000	5.000
^{132}Te	228.160	1.026E+01	7.194E-02	76.896	0.312	1.174E-02	1.234E-05	9.573E-01	2.129E-02	88.000	3.478
^{133m}Te	863.955	3.236E+01	2.970E-01	0.923	0.007	3.963E-03	1.783E-05	9.958E-01	2.147E-03	14.887	1.274

^{133m}Te	912.671	1.128E+02	3.949E-01	0.923	0.007	3.816E-03	1.846E-05	9.960E-01	2.021E-03	43.767	3.666
^{133m}Te	1683.230	6.043E+00	9.466E-02	0.923	0.007	2.650E-03	2.927E-05	9.976E-01	1.238E-03	3.945	0.344
^{134}Te	201.235	9.900E+01	5.924E-01	0.697	0.013	1.281E-02	1.230E-05	9.433E-01	2.807E-02	8.850	0.380
^{134}Te	712.970	2.074E+01	2.773E-01	0.697	0.013	4.554E-03	1.597E-05	9.947E-01	2.683E-03	4.720	0.604
^{131}I	364.489	1.616E+00	4.710E-02	192.605	0.014	7.904E-03	1.284E-05	9.844E-01	7.874E-03	81.500	0.759
^{135}I	220.502	3.437E+00	8.403E-02	6.570	0.020	1.204E-02	1.232E-05	9.538E-01	2.300E-02	1.751	0.062
^{135}I	288.451	4.730E+00	7.465E-02	6.570	0.020	9.699E-03	1.249E-05	9.748E-01	1.268E-02	3.100	0.113
^{135}I	1131.511	1.112E+01	5.921E-02	6.570	0.020	3.316E-03	2.144E-05	9.968E-01	1.621E-03	22.587	0.723
^{135}I	1260.409	1.294E+01	5.724E-02	6.570	0.020	3.106E-03	2.325E-05	9.971E-01	1.481E-03	28.700	0.916
^{139}Ba	165.857	2.286E+02	3.432E-01	1.384	0.005	1.415E-02	1.229E-05	9.120E-01	4.280E-02	23.760	0.250
^{142}La	641.285	1.233E+02	2.921E-01	1.518	0.008	4.937E-03	1.517E-05	9.939E-01	3.090E-03	47.400	0.500
^{142}La	894.900	1.620E+01	1.358E-01	1.518	0.008	3.868E-03	1.823E-05	9.959E-01	2.065E-03	8.342	0.167
^{142}La	1043.700	5.338E+00	1.150E-01	1.518	0.008	3.490E-03	2.022E-05	9.966E-01	1.753E-03	2.702	0.055
^{142}La	1233.100	2.885E+00	5.457E-02	1.518	0.008	3.146E-03	2.286E-05	9.970E-01	1.506E-03	1.896	0.051
^{142}La	1901.300	7.739E+00	5.439E-02	1.518	0.008	2.497E-03	3.234E-05	9.977E-01	1.179E-03	7.157	0.161
^{142}La	2055.200	2.329E+00	3.588E-02	1.518	0.008	2.409E-03	3.447E-05	9.977E-01	1.150E-03	2.180	0.098
^{142}La	2100.400	8.505E-01	3.969E-02	1.518	0.008	2.386E-03	3.509E-05	9.978E-01	1.142E-03	1.043	0.095
^{142}La	2187.200	4.130E+00	4.100E-02	1.518	0.008	2.344E-03	3.627E-05	9.978E-01	1.129E-03	3.697	0.103
^{142}La	2542.700	7.242E+00	4.622E-02	1.518	0.008	2.203E-03	4.098E-05	9.979E-01	1.091E-03	10.001	0.259
^{143}Ce	293.266	7.650E+00	6.745E-02	33.039	0.006	9.562E-03	1.251E-05	9.757E-01	1.226E-02	42.800	0.420

Table 27: Values used to calculate Np2 cumulative fission product yield results and uncertainties for detector 8816 where N_f = 7.5E9 ± 3E8.

Isotope	E_γ (keV)	A_0 (Bq)	ΔA_0 (Bq)	$\tau_{1/2}$ (hrs.)	$\Delta\tau_{1/2}$ (hrs.)	ϵ_γ	$\Delta\epsilon_\gamma$	I_γ	ΔI_γ	R_γ (%)	ΔR_γ (%)
^{88}Kr	196.301	3.012E+01	1.955E-01	2.840	0.030	1.095E-02	9.464E-06	9.450E-01	2.756E-02	25.985	1.214
^{88}Kr	2195.842	2.221E+00	3.456E-02	2.840	0.030	1.994E-03	3.665E-05	9.980E-01	1.046E-03	13.183	0.618
^{88}Kr	2392.110	5.722E+00	3.478E-02	2.840	0.030	1.926E-03	3.936E-05	9.980E-01	1.024E-03	34.600	1.603
^{91}Sr	749.800	5.369E+00	3.957E-02	9.630	0.050	3.702E-03	1.495E-05	9.954E-01	2.341E-03	23.685	0.796
^{92}Sr	1383.930	5.170E+01	1.008E-01	2.710	0.010	2.495E-03	2.465E-05	9.975E-01	1.283E-03	90.000	5.682
^{93}Y	266.900	5.512E+00	1.214E-01	10.180	0.080	8.729E-03	9.694E-06	9.726E-01	1.390E-02	7.320	1.054
^{105}Ru	316.440	7.993E+00	1.103E-01	4.440	0.020	7.540E-03	9.977E-06	9.809E-01	9.731E-03	11.116	0.396
^{105}Ru	393.360	2.602E+00	7.033E-02	4.440	0.020	6.231E-03	1.057E-05	9.876E-01	6.330E-03	3.775	0.062
^{105}Ru	469.370	1.049E+01	8.082E-02	4.440	0.020	5.355E-03	1.133E-05	9.910E-01	4.628E-03	17.548	0.552
^{105}Rh	319.231	1.442E+00	6.351E-02	35.360	0.060	7.482E-03	9.995E-06	9.813E-01	9.555E-03	19.100	0.630
^{127}Sn	1095.600	8.852E-01	1.027E-01	2.100	0.040	2.863E-03	2.018E-05	9.970E-01	1.549E-03	19.380	5.214
^{127}Sn	1114.300	2.114E+00	3.938E-02	2.100	0.040	2.833E-03	2.047E-05	9.970E-01	1.525E-03	38.000	7.965
^{128}Sn	482.300	2.709E+01	1.925E-01	0.984	0.002	5.235E-03	1.147E-05	9.914E-01	4.425E-03	59.000	6.686
^{130}Sb	330.914	1.077E+02	6.291E-01	0.658	0.013	7.250E-03	1.007E-05	9.826E-01	8.873E-03	78.000	4.000
^{130}Sb	793.400	7.510E+01	5.919E-01	0.658	0.013	3.554E-03	1.559E-05	9.957E-01	2.192E-03	100.000	5.000
^{132}Te	228.160	7.747E+00	3.151E-02	76.896	0.312	9.887E-03	9.544E-06	9.608E-01	1.981E-02	88.000	3.478
^{133m}Te	863.955	2.839E+01	2.770E-01	0.923	0.007	3.347E-03	1.664E-05	9.961E-01	1.991E-03	14.887	1.274

^{133m}Te	912.671	9.688E+01	3.654E-01	0.923	0.007	3.224E-03	1.737E-05	9.964E-01	1.874E-03	43.767	3.666
^{133m}Te	1683.230	4.858E+00	8.299E-02	0.923	0.007	2.251E-03	2.921E-05	9.978E-01	1.148E-03	3.945	0.344
^{134}Te	201.235	8.346E+01	5.499E-01	0.697	0.013	1.078E-02	9.472E-06	9.478E-01	2.616E-02	8.850	0.380
^{134}Te	712.970	3.304E+01	5.903E-01	0.697	0.013	3.842E-03	1.443E-05	9.952E-01	2.489E-03	4.720	0.604
^{131}I	364.489	1.355E+00	4.624E-02	192.605	0.014	6.660E-03	1.033E-05	9.857E-01	7.310E-03	81.500	0.759
^{135}I	220.502	3.120E+00	8.437E-02	6.570	0.020	1.014E-02	9.521E-06	9.575E-01	2.141E-02	1.751	0.062
^{135}I	288.451	3.607E+00	5.867E-02	6.570	0.020	8.172E-03	9.807E-06	9.769E-01	1.178E-02	3.100	0.113
^{135}I	1131.511	9.566E+00	5.450E-02	6.570	0.020	2.806E-03	2.074E-05	9.971E-01	1.503E-03	22.587	0.723
^{135}I	1260.409	1.101E+01	5.218E-02	6.570	0.020	2.631E-03	2.274E-05	9.973E-01	1.373E-03	28.700	0.916
^{139}Ba	165.857	1.896E+02	3.222E-01	1.384	0.005	1.189E-02	9.428E-06	9.190E-01	3.999E-02	23.760	0.250
^{142}La	641.285	1.043E+02	2.763E-01	1.518	0.008	4.163E-03	1.344E-05	9.944E-01	2.866E-03	47.400	0.500
^{142}La	894.900	1.415E+01	1.255E-01	1.518	0.008	3.267E-03	1.710E-05	9.963E-01	1.915E-03	8.342	0.167
^{142}La	1043.700	4.315E+00	1.042E-01	1.518	0.008	2.952E-03	1.938E-05	9.968E-01	1.626E-03	2.702	0.055
^{142}La	1233.100	2.680E+00	5.151E-02	1.518	0.008	2.665E-03	2.232E-05	9.973E-01	1.397E-03	1.896	0.051
^{142}La	1901.300	6.384E+00	5.026E-02	1.518	0.008	2.124E-03	3.244E-05	9.979E-01	1.093E-03	7.157	0.161
^{142}La	2055.200	1.779E+00	3.359E-02	1.518	0.008	2.051E-03	3.466E-05	9.979E-01	1.066E-03	2.180	0.098
^{142}La	2100.400	6.945E-01	3.185E-02	1.518	0.008	2.032E-03	3.530E-05	9.979E-01	1.059E-03	1.043	0.095
^{142}La	2187.200	3.519E+00	1.690E+00	1.518	0.008	1.997E-03	3.653E-05	9.980E-01	1.047E-03	3.697	0.103
^{142}La	2542.700	6.097E+00	4.276E-02	1.518	0.008	1.881E-03	4.138E-05	9.980E-01	1.011E-03	10.001	0.259
^{143}Ce	293.266	6.360E+00	6.912E-02	33.039	0.006	8.056E-03	9.833E-06	9.776E-01	1.139E-02	42.800	0.420

3.9 Conclusion

The experimental setup and procedure is the same as the previous measurement for ^{235}U , ^{238}U, and ^{239}Pu fission spectrum cumulative fission product yields [103, 107]. The data analysis described can be implemented for any actinide to study fission product γ rays. In this work, 101 γ rays were analyzed for 36 isotopes.

The variations in fission product yield results have been observed in past results [103, 107]. For the case of ^{142}La, the evaluators mainly based the decay scheme from a 1982 measurement [26]. In 1982, a γ-γ coincidence measurement was performed on ^{142}La using Cs fission products of ^{235}U [104]. A shield comprised of 1 mm of Cu, 1 mm of Pb, and 4 mm of B_4C was placed in front of the detectors and an efficiency calibration was performed using ^{152}Eu (with γ-ray branching ratios from 1979 [105]). The attenuation through the detector front shields were not included in the analysis and would cause γ-ray branching ratios to be lower at higher γ-ray energies and vice versa [107].

Similarly to the ^{239}Pu FPY measurement, there are more fission product yield results that exhibit variation for different γ ray analyzed [107]. The similar variation in fission product yield results for different actinides analyzed using the same experimental setup may be caused by discrepancies in γ-ray branching ratios.

3.10 Future Work

^{233}U is the next actinides to have their fission product yields measured using Godiva IV critical assembly. A new experimental setup, called the Lāpaki γ-γ array, was designed and constructed to measure short-lived fission product yield γ-ray branching ratios [106]. An experiment at Oregon State University will use Lāpaki to measure ^{238}U short-lived fission product yields and fission product γ

rays.

Acknowledgements

This work was funded by the Office of Defense Nuclear Nonproliferation Research and Development within the U.S. Department of Energy's National Nuclear Security Administration by Lawrence Livermore National Laboratory under Contract No DE-AC52-07NA27344. The U.S. Department of Energy's Nuclear Criticality Safety Programs National Criticality Experiments Research Center (NCERC), utilized in this work, is supported by the National Nuclear Security Administration's Office of the Chief of Defense Nuclear Safety, NA-511.

4 The Lāpaki γ-γ Array

A.S. Tamashiro[1], J.T. Harke[2], J.G. Duarte[2], Y. Mishnayot[2], S. Burcher[2], N. Harward[2], K. Roberts[2], S. Menn[3], T.M. Story[3], S. Reese[1], S. Smith[3], L.D. Minc[4], W. Loveland[5], V.L. Adriatico[1], BA. Konstanczer[1], S.L. Weidenbenner[1], N. Wiltbank[1], M. Branco-Katcher[1], C. Kulah[3], R. Schickler[3], and C.J. Palmer[1]

Preprint submitted to Nuclear Instruments and Methods in Physics Research Section A June 16, 2022

[1]School of Nuclear Science and Engineering, Oregon State University, Corvallis, OR 97331, USA

[2]Nuclear and Chemical Sciences Division, Lawrence Livermore National Laboratory, Livermore, CA 94550, USA

[3]Radiation Center, Oregon State University, Corvallis, OR 97331, USA

[4]School of Language, Culture, and Society, Oregon State University, Corvallis, OR 97331, USA

[5]Department of Chemistry, Oregon State University, Corvallis, OR 97331, USA

4.1 Abstract

The Lāpaki γ-γ array is a new detection setup to measure nuclear structure for short-lived fission products, fission product yields for various actinides, and neutron activation analysis. The array is designed to be used with a pneumatic transfer tube or rabbit system. Various calibration sources were used to determine the γ-ray detection efficiency of the array. The current rabbit carrier contained trace impurities, which led to a neutron activation analysis study of various polyethylene samples to design a new rabbit. These samples were irradiated using the Oregon State University Training, Research, Isotopes, General Atomics reactor rabbit facility. The impurities identified in the study were ^{27}Al, ^{48}Ca, ^{37}Cl, ^{63}Cu, ^{65}Cu, ^{127}I, ^{26}Mg, ^{55}Mn, ^{30}Si, and ^{50}Ti. Activated impurities with short half-lives like ^{28}Al require a decay time after irradiation. A purer polyethylene allows for measurements of short-lived isotopes immediately after irradiation. The polyethylene sample with the least amount of impurities by mass was used to make a new high-purity polyethylene rabbit.

4.2 Introduction

The Short-Lived Fission Product Yield (SLFPY) project objective is to provide improved measurements of fission product yields for actinides. The measured fission product yields are needed for applied and fundamental nuclear science. Data exists for fission product yields from the fission of ^{235}U, ^{238}U, ^{239}Pu, ^{237}Np, and ^{233}U using the Godiva-IV critical assembly. The resulting fission product γ-rays were recorded from 45 minutes to 10 days. To fill the shorter time scales than Godiva-IV is capable of, a pneumatic transfer tube is used to rapidly transport a rabbit (sample carrier) from irradiation to directly in front of a detection system.

Lāpaki (rabbit in Hawaiian [114]) is a new γ-ray detector array based on the STARLiTeR array [115] and Hyperion [116]. Lāpaki is comprised of up to eight Compton-suppressed, clover detectors for γ-γ coincidence measurements. The detector array is coupled with a pneumatic transfer tube to make rabbit irradiated with measurement within 3 seconds after irradiation. The existing polyethylene rabbit carrier contains impurities that would undergo neutron activation and require a decay time and preclude short-lived results. A new high-purity polyethylene rabbit was designed and fabricated to perform short-lived isotope measurements.

4.3 High-purity germanium detector array

The array employs up to eight cryogenically cooled clover detectors to be used as γ-ray spectrometers. A clover detector is comprised of four high-purity germanium (HPGe) crystals adjacent to each other in a four leaf configuration [117]. Each clover is inserted into a Compton suppression shield incorporating sixteen optically-isolated bismuth germanate oxide (BGO) crystal paired with photomultiplier (PMT) tubes. The clover crystals are surrounded by the BGO crystals. A Hevimet tungsten collimator is placed in front of the BGO detectors to shield γ rays from the sample and only measure γ rays scattered from the clover detectors.

The geometry of Lāpaki is based on the design of Hyperion, such that the BGO detector optimizes the solid angle of the clover detectors on a plane, which is 0.2 steradian per detector [116]. The BGO/clover pairs are placed 45° relative to each other (see Figure 41, 42, and 43).

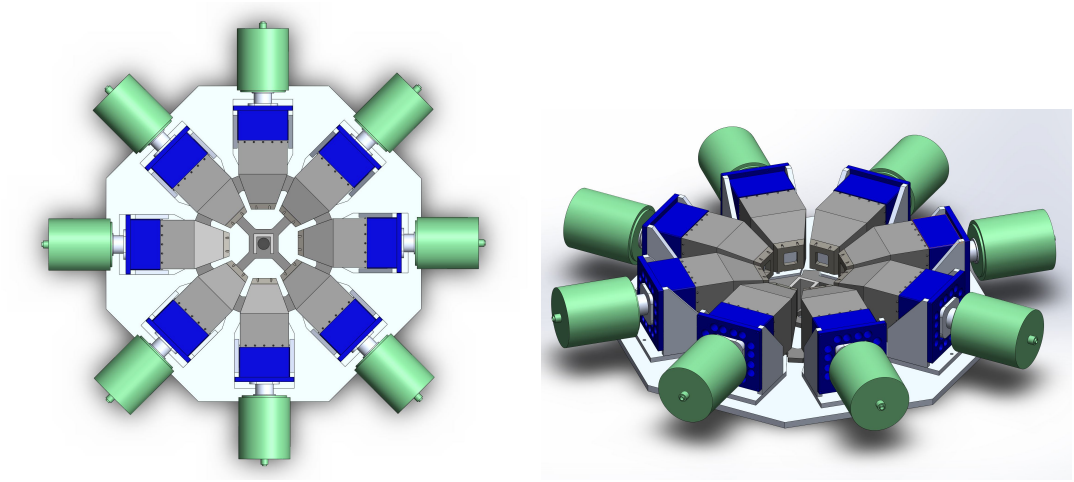

(a) Top view (b) Isometric view

Figure 41: Computer-aided design (CAD) drawings of the Lāpaki array. The length of the array is approximately eight feet.

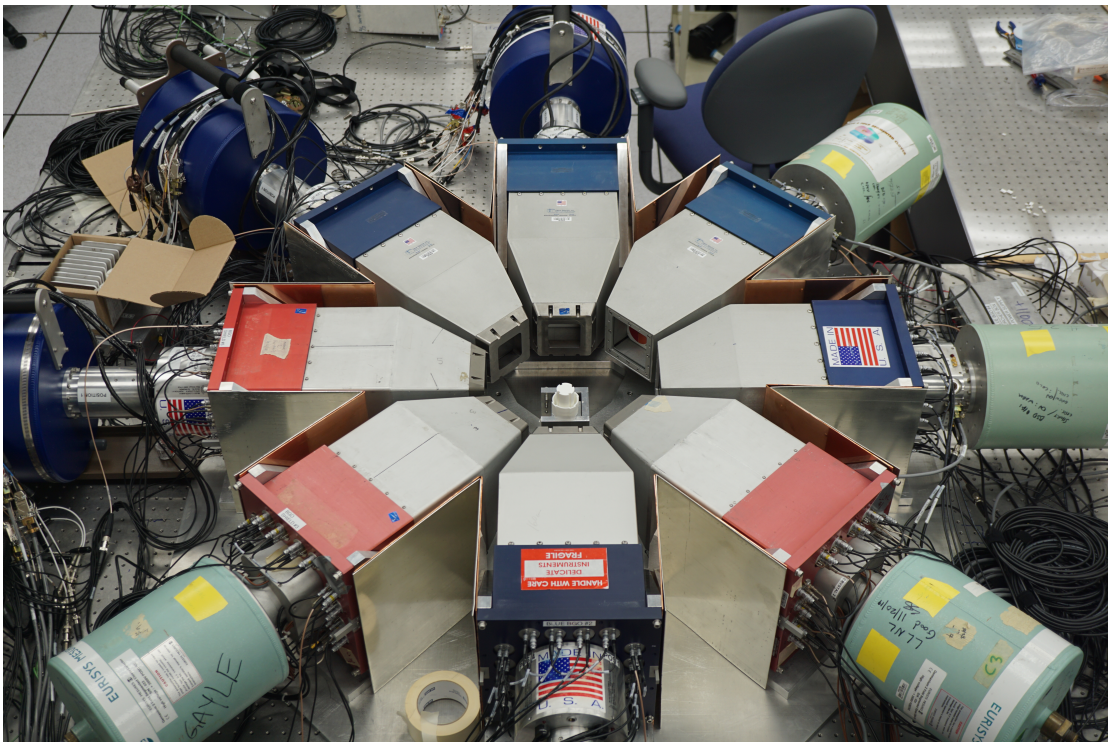

Figure 42: The Lāpaki array was initially assembled in the laboratory at LLNL to test the DAQ response to all eight clover detectors.

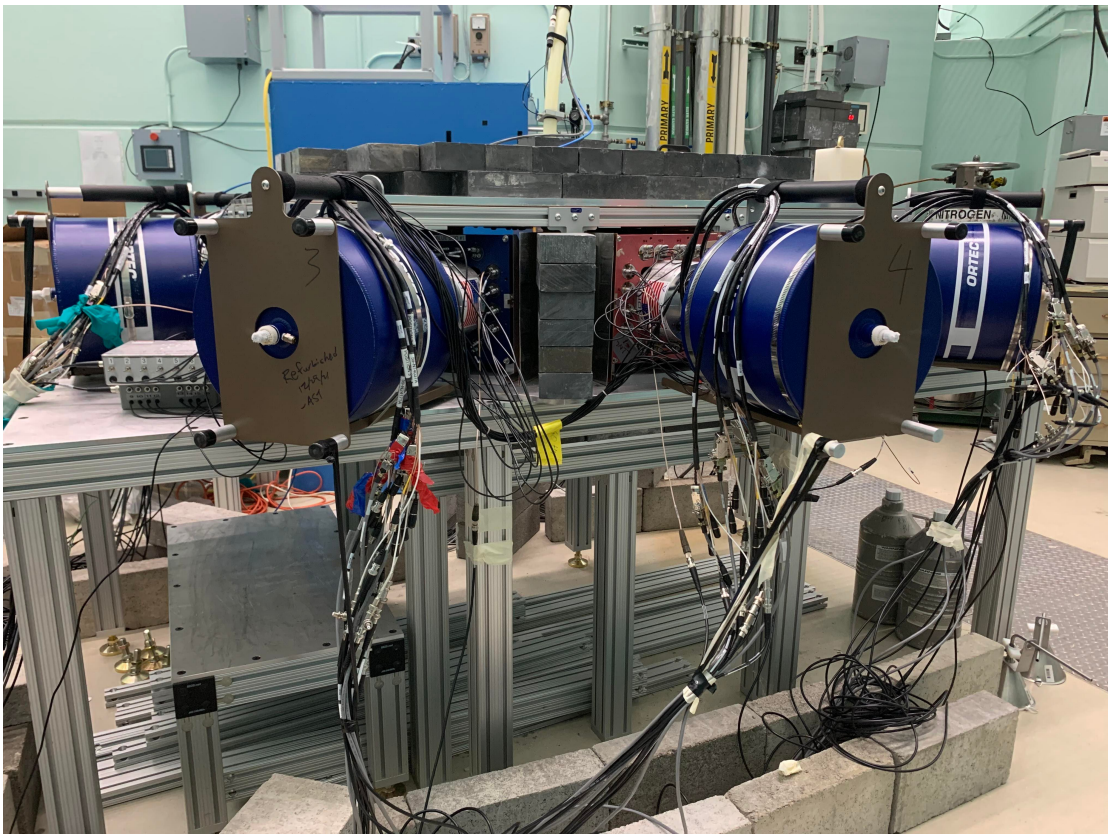

Figure 43: First experiment with the Lāpaki array performed at the OSU TRIGA reactor.

4.3.1 Lead-tin-copper castle

Surrounding the array is a graded shield comprised of lead, tin, and copper. The use of layered material attenuates secondary x-rays that may be produced from shielding background γ rays. In this case, copper is used to shield tin x-rays and tin is used to shield lead x-rays [118]. The 110 grade copper sheets were supplied by Ryerson with a thickness of 0.064 inches. The tin sheets were supplied by Ames Metal Products Co. with a thickness of 0.062 inches. Four inches of lead bricks were placed above and below the detection volume and a stack of lead bricks were placed in between each BGO detector. Figure 43 shows the Lāpaki array housed in the lead-tin-copper castle at the OSU TRIGA reactor.

4.3.2 Signal processing

The data acquisition (DAQ) system utilizes Mesytec's new digital DAQ [119]. Each BGO outputs a single signal from summing their sixteen PMT signals. At most, eight BGO signals are directly connected to a MDPP-16 QDC module [120]. Each clover has four output signals. At most, thirty-two clover signals are directly connected to two MDPP-16 SCP modules [121]. A third MDPP-16 SCP module is used to record the time signal from the optical sensors of the pneumatic transfer system. An external trigger logic is used with a 10 μs trigger inhibit to ensure that the DAQ is stable at high counting rates (see Figure 44). A CAEN V977 module [122] is used to send a common reset signal to the other VME modules and to accept a trigger out signal after the DAQ has started. A SIS3820 scaler [123] is used to count the trigger out (raw) signals and trigger in (live) signals. A Keysight 33600A waveform generator [124] is used to generate a 25 ns period clock signal with an uncertainty of 55 ps. The high voltage for the detectors is supplied by various modules in an ISEG MPOD crate. All the electronics mentioned are packed in two portable crates (see Figure 45).

The online acquisition is performed using mvme [125], an open source software from Mesytec. A C++/QT based software was developed to control the MPOD modules. The MVLC VME contoller, MPOD controller, and Keysight waveform generator are on a 1 Gigabit fiber optic network connected to a standalone Ubuntu system in a separate room from the detection system.

4.3.3 γ-ray efficiency

The efficiency curve was obtained by measuring a variety of γ sources and fitting each photopeak with a Gaussian and a linear background. The actual counts,

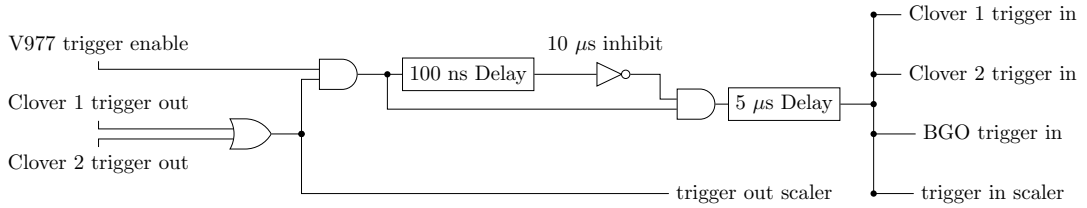

(a) External trigger logic for the trigger inhibit of the DAQ.

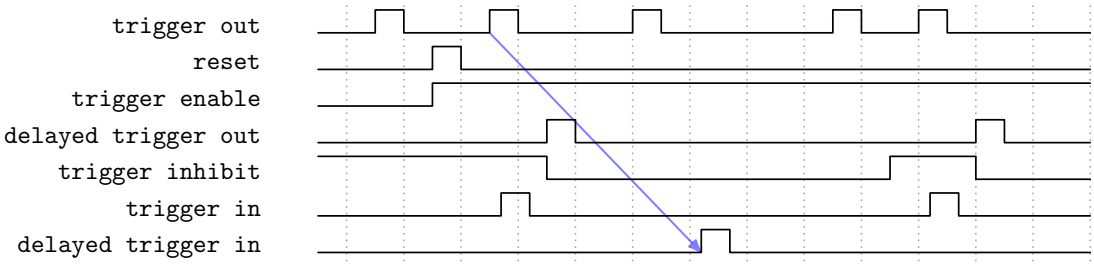

(b) Master trigger timing diagram. The arrow represents the resulting trigger-in signal from a trigger-out signal.

Figure 44: Trigger inhibit diagrams of the DAQ.

ΔC, were calculated by the following:

$$\Delta C = \frac{A_0}{\lambda R_\gamma} e^{-\lambda t_1} \left(1 - e^{-\lambda \Delta t}\right) \tag{18}$$

where R_γ is the γ-ray branching ratio, A_0 is the initial activity of the calibration source, λ is the decay constant of the source, t_1 is the time from calibration to time of measurement, and Δt is duration of measurement. The ratios of measured and actual counts are fitted with an efficiency curve:

$$\varepsilon(E) = p_0 E^{-p_1} + p_2 - p_3 e^{-p_4 E} \tag{19}$$

where p_i are parameters and E is energy in MeV [116]. The efficiency results with the fitted curve is shown in Figure 46. Six ORTEC® clovers were used to extrapolate the array efficiency of eight clover detectors. The array is up to 1,200% efficient relative to a 3"x3" NaI(Tl) detector 25 cm from a source at 1.33 MeV.

(a) The first row is the preamp power for the clover detectors. The second row is the MPOD crate which supplies the high voltage to the clover and BGO detectors.

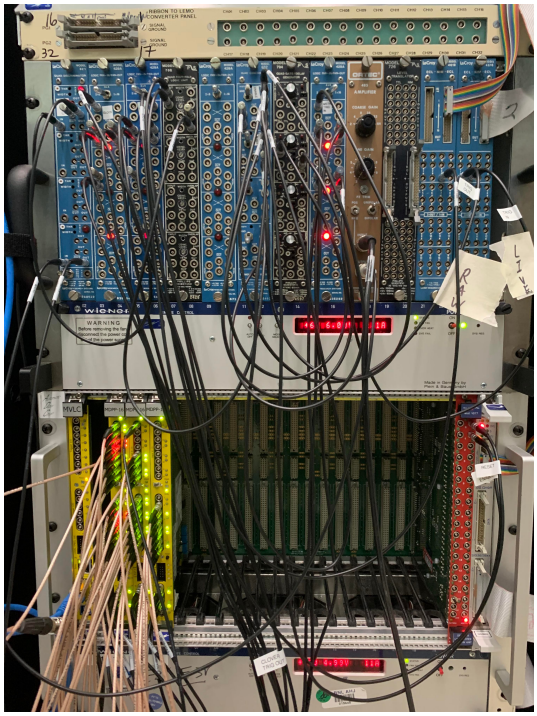

(b) The first row is the trigger inhibit and other NIM modules for the reset, clock, and scaler signals. The second row is the VME crate using a MVLC, MDPP-16 modules, CAEN V977, and SIS3820 modules.

Figure 45: Electronics crate used for the array.

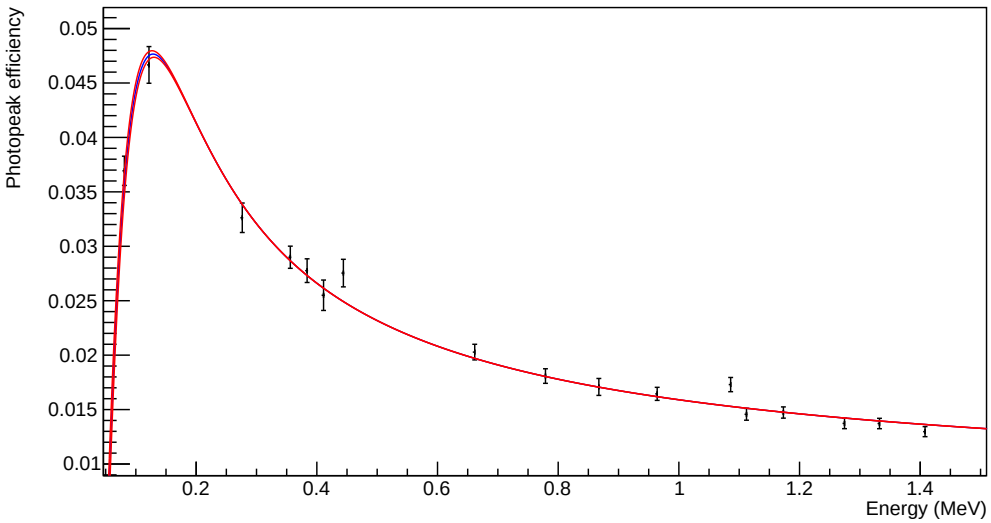

Figure 46: Measurements of different calibration sources (^{133}Ba, ^{137}Cs, ^{60}Co, ^{152}Eu, and ^{22}Na) were performed using the Lāpaki array with six clover detectors. Assuming that two more clover detectors would perform similarly like the first six, the efficiency of the Lāpaki array with was extrapolated to the curve shown above. The blue line is the efficiency curve and the red line is the upper and lower bounds of the uncertainty.

4.4 Pneumatic Transfer Tube

A pneumatic transfer tube is used to transport the sample within a carrier, known as a rabbit, to be irradiated and then transported back to the receiving end. The system uses a blower to produce negative pressure, causing a pressure differential to transport the rabbit. Figure 47 shows the diagram of a typical pneumatic transfer system used in a TRIGA reactor. The system uses titanium (in the reactor core), cross-linked polyethylene or PEX (in between the reactor core and receiver), and high density polyethylene (receiver). For the Lāpaki array, the receiving end is the terminus placed in the center of the array.

An optical sensor is placed near each end of the transfer tubes. The signals from both sensors assist in determining irradiation time and counting time. The time of the rabbit entering the lead-tin-copper castle is used to time align multiple measurements using the same irradiation time.

During an irradiation, there was neutron activated air (such as ^{41}Ar and ^{16}N) present within the rabbit and rabbit system. Loading a rabbit with a sample is normally performed in a clean hood and in open air. The air-filled rabbit and air surrounding the rabbit is then irradiated and there was neutron activated air within the rabbit and rabbit system. A new procedure to mitigate neutron activated air was developed for the rabbit and rabbit system. For the rabbit, a glove box filled with helium is used to load a sample in a rabbit. For the rabbit system, the system is purged with fresh air and followed by a rabbit irradiation.

4.5 High-purity polyethylene rabbit

The speed of the pneumatic transfer system allows for the measurement of short-lived isotopes. When measuring short-lived isotopes, there may be impurities

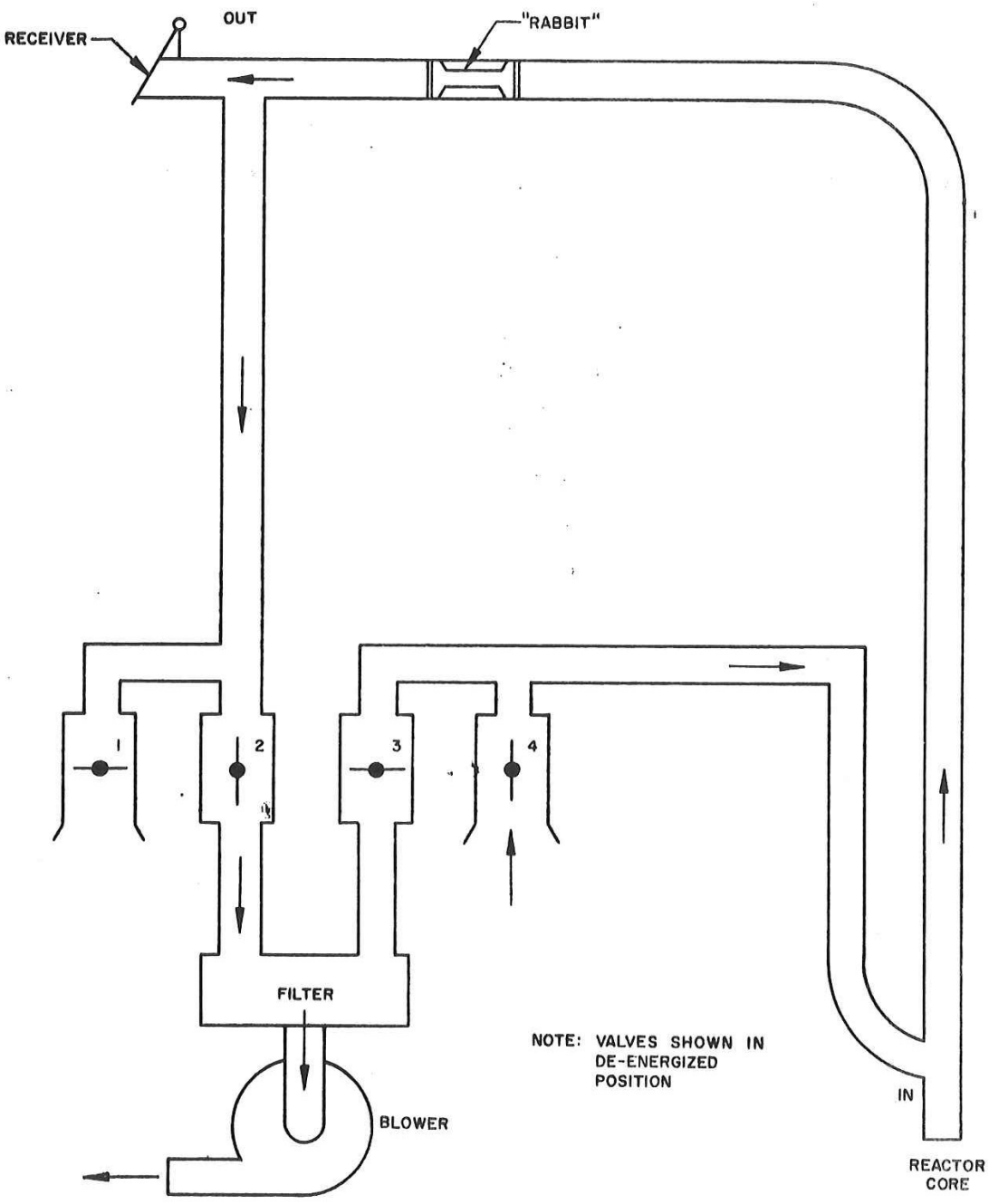

Figure 47: Typical diagram of a pneumatic transfer system in a TRIGA reactor [34].

present in the rabbit carrier interfering with the measurement. This may include a dominant γ ray from the activated rabbit causing a Compton continuum to hide low activity γ rays. To reduce γ rays from impurities in the current rabbit carrier at Oregon State University (OSU), a new polyethylene rabbit was designed with a purer polyethylene.

Traditionally, the rabbit was made of nylon [63], Lustroid [63], balsa wood [66], and aluminum [70]. Polyethylene rabbits were used since 1959, but the polyethylene had trace contaminants present [64]. The major impurity found in polyethylene is aluminum, which requires a waiting time after irradiation to the order of minutes, hindering the measurements of short-lived isotopes [64, 65, 68, 71, 72].

In 2019, a proof of principle study was conducted at OSU Training, Research, Isotopes, General Atomics (TRIGA) reactor rabbit facility [73]. This experiment was to show the feasibility in measuring fission product γ rays within seconds of irradiation. Initially, a quartz vial was used to contain ^{238}U. The vial was then placed inside a high density polyethylene (HDPE) rabbit and irradiated. A large dominant 1778 keV γ ray with a Compton continuum made it challenging to identify any of the short-lived fission product γ rays. It was determined that the 1778 keV γ ray originated from ^{28}Al which was produced by ^{28}Si(n,p)^{28}Al and ^{27}Al(n,γ)^{28}Al. The quartz vial contained silicon and the polyethylene rabbit carrier contained traces of aluminum. A second test was performed by placing ^{238}U in a low density polyethylene (LDPE) microcentrifuge vial encapsulated in a LAContainer NAA Polyvials™. Since the current rabbit carrier at OSU had impurities, the vial containing irradiated ^{238}U was removed from the rabbit and placed in front of a HPGe detector. The LAContainer NAA Polyvials™was very pure and allowed for short-lived fission product γ rays to be measured within 7

seconds of irradiation. This prompted the design of a new high purity polyethylene rabbit to perform like LAContainer NAA Polyvials™to study short-lived fission products within 3 seconds of irradiation. The next subsection describes the study process of different polyethylene samples to determine the purest one.

4.5.1 Polyethylene NAA study

Over the course of a year, three different pure polyethylene samples were irradiated in the OSU TRIGA rabbit facility. These samples were Chevron Phillips Chemical's Marlex® 9006 HDPE, Polymer Industries' Densetec® HDPE, and Westlake Chemical's EM800AA LDPE. The samples were placed in front of a γ detector after one minute of irradiation and counted for five minutes. The detector used for this measurement is an ORTEC® GEM p-type coaxial HPGe radiation detector. A DSPEC pro digital signal analyzer and GammaVision γ spectroscopy software were used to record the γ spectrum. The mass normalized γ-ray spectra obtained are shown in Figure 48.

A code written in C/C++/ROOT was used to identify the peaks in the spectrum and fit a Gaussian function with linear background to each of them. The net counts for a γ-ray peak is the integral of the Gaussian component of the fit function divided by the energy bin width. The uncertainty is calculated using error propagation. Division of the counts by the time of measurement yields the activity for that peak. A comparative value is the specific activity a (Bq/g) for each polyethylene sample (see Equation 20).

$$a = \frac{\gamma_{meas.}}{m_{poly}\Delta t_{meas.}} \tag{20}$$

$\gamma_{meas.}$ is the net counts for a γ-ray, m_{poly} is the polyethylene sample's mass, and

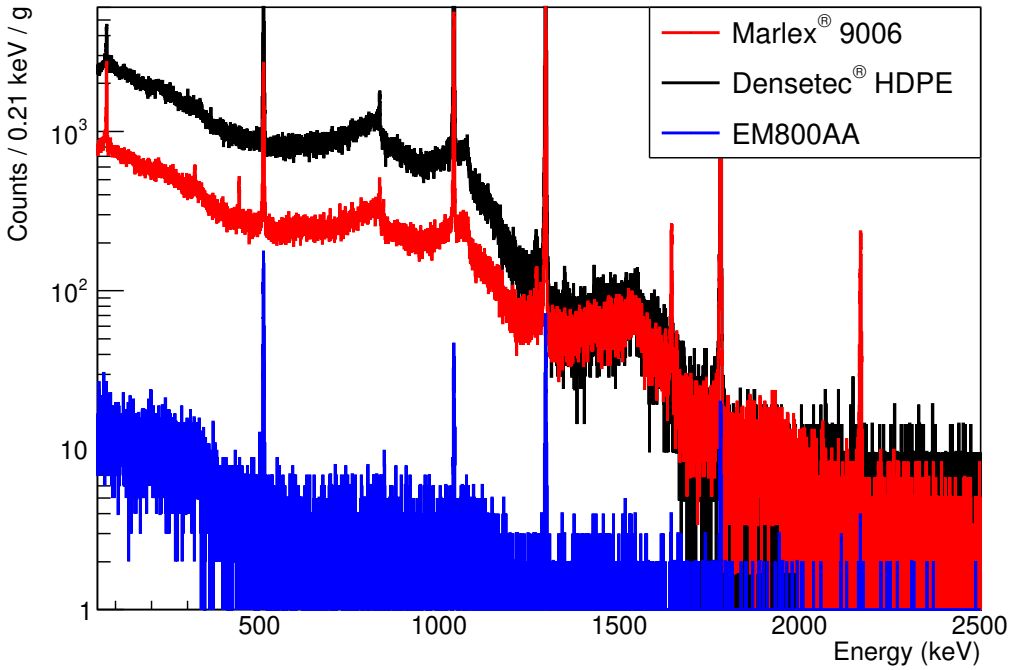

Figure 48: The γ-ray spectra of three polyethylene samples were measured within five seconds of irradiation in the OSU TRIGA reactor.

$\Delta t_{meas.}$ is the counting time. Specific activities of the polyethylene samples are listed in Table 28.

The Westlake Chemical EM800AA LDPE had the smallest amount of impurities based on specific activity. The new rabbits were injected molded by Xometry™using the EM800AA LDPE (see Figure 50). No release agents on the molds were used to prevent any additional impurities in the rabbit carrier. Figure 51 shows the difference between the current and the new rabbit mass normalized γ-ray spectrum. The current rabbit's mass is 8.35 grams and the new rabbit's mass is 9.87 grams. The mass multiplied by the specific activities are 595.61 Bq and 35.44 Bq for the current and new rabbits respectively. The new rabbits are essentially high-purity polyethylene rabbits.

The efficiency of the HPGe was calibrated by OSU. The function form of the efficiency curve is the following:

$$\ln(\epsilon_\gamma) = P_0 + (P_1 \ln(E_\gamma)) + (P_2 \ln(E_\gamma)^2) \tag{21}$$

where E_γ is γ-ray energy in keV and parameters P_i are listed in Table 29 (see Figure 49). This efficiency curve is for a sample placed 2 cm from the detector face. Each polyethylene samples were measured in this geometry.

The number of atoms produced from neutron activation can be calculated by the following:

$$N_{prod.} = \frac{a\Delta t_{meas.}}{R_\gamma \varepsilon_\gamma} \tag{22}$$

where a is specific activity from Equation 20, $\Delta t_{meas.}$ is measurement time, R_γ is γ-ray branching ratio, and ε_γ is detector efficiency.

Table 28: Neutron activation analysis of Marlex® 9006 HDPE, Densetec® HDPE, and Westlake EM800AA LDPE.

		Specific Activity (Bq/g)		
Production Mechanism	E_γ (keV)	Marlex® 9006	Densetec® HDPE	EM800AA
Pb $K_{\alpha 1}$ x-ray	75.5	76 ± 1	98 ± 2	–
$^{50}Ti(n,\gamma)^{51}Ti \xrightarrow{\beta^-} {}^{51}V$	320.28	8.9 ± 0.7	–	–
$^{68}Zn(n,\gamma)^{69m}Zn \xrightarrow{IT} {}^{69}Zn$	438.63	–	–	–
$^{127}I(n,\gamma)^{128}I \xrightarrow{\beta^-} {}^{128}Xe$	442.90	8.9 ± 0.6	–	–
$e^- + e^+$	511.0	150 ± 1	532 ± 2	8.7 ± 0.3
$^{65}Cu(n,\gamma)^{66}Cu \xrightarrow{\beta^-} {}^{66}Zn$	832.86	9.1 ± 0.7	36 ± 1	–
$^{26}Mg(n,\gamma)^{27}Mg \xrightarrow{\beta^-} {}^{27}Al$	843.8	–	–	–
$^{55}Mn(n,\gamma)^{56}Mn \xrightarrow{\beta^-} {}^{56}Fe$	846.76	–	–	–
$^{65}Cu(n,\gamma)^{66}Cu \xrightarrow{\beta^-} {}^{66}Zn$	1038.85	266 ± 2	1183 ± 3	1.7 ± 0.1
$^{30}Si(n,\gamma)^{31}Si \xrightarrow{\beta^-} {}^{31}P$	1267.9	3.0 ± 0.3	–	–
$^{41}Ar \xrightarrow{\beta^-} {}^{41}K$	1293.43	334 ± 2	1089 ± 3	3.0 ± 0.2
$^{63}Cu(n,\gamma)^{64}Cu \xrightarrow{\varepsilon} {}^{64}Ni$	1345.83	–	3.0 ± 0.3	–
$^{37}Cl(n,\gamma)^{38}Cl \xrightarrow{\beta^-} {}^{38}Ar$	1642.63	12.3 ± 0.4	1.6 ± 0.2	0.08 ± 0.03
$^{27}Al(n,\gamma)^{28}Al \xrightarrow{\beta^-} {}^{28}Si$	1778.80	100.0 ± 0.9	121 ± 1	0.91 ± 0.08
$^{55}Mn(n,\gamma)^{56}Mn \xrightarrow{\beta^-} {}^{56}Fe$	1810.73	–	–	–
3084.42 - 1022 keV	2062.42	0.48 ± 0.08	–	–
$^{55}Mn(n,\gamma)^{56}Mn \xrightarrow{\beta^-} {}^{56}Fe$	2113.09	–	–	–
$^{37}Cl(n,\gamma)^{38}Cl \xrightarrow{\beta^-} {}^{38}Ar$	2167.22	13.4 ± 0.3	1.1 ± 0.1	0.09 ± 0.03
3084.42 - 511 keV	2573.42	0.51 ± 0.09	–	–
$^{48}Ca(n,\gamma)^{49}Ca \xrightarrow{\beta^-} {}^{49}Sc$	3084.42	1.7 ± 0.1	–	–

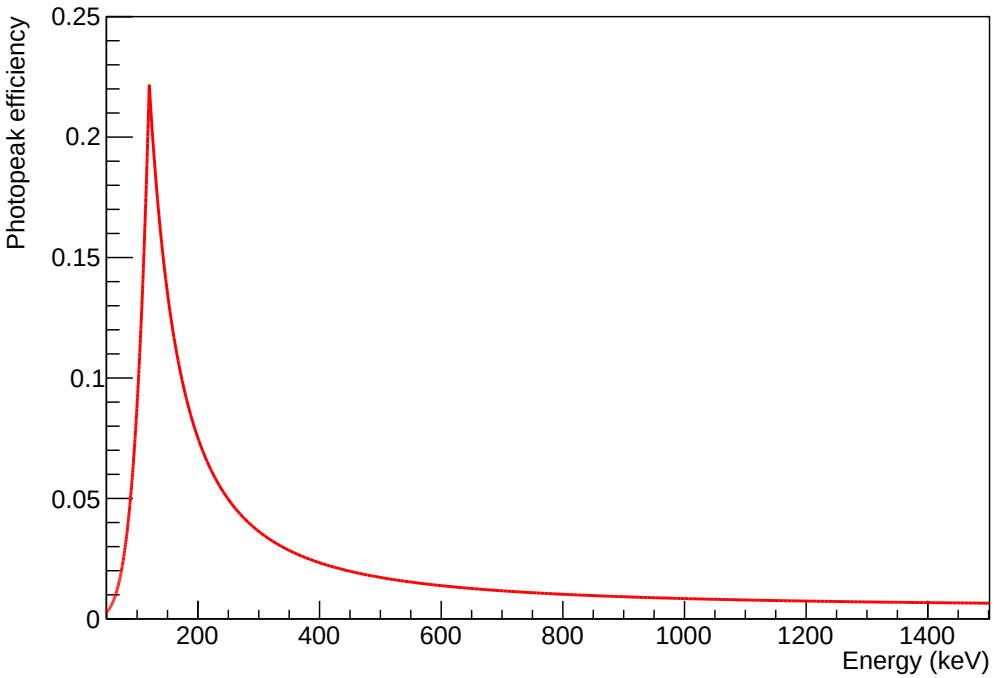

Figure 49: Efficiency curve provided by OSU using equation 21

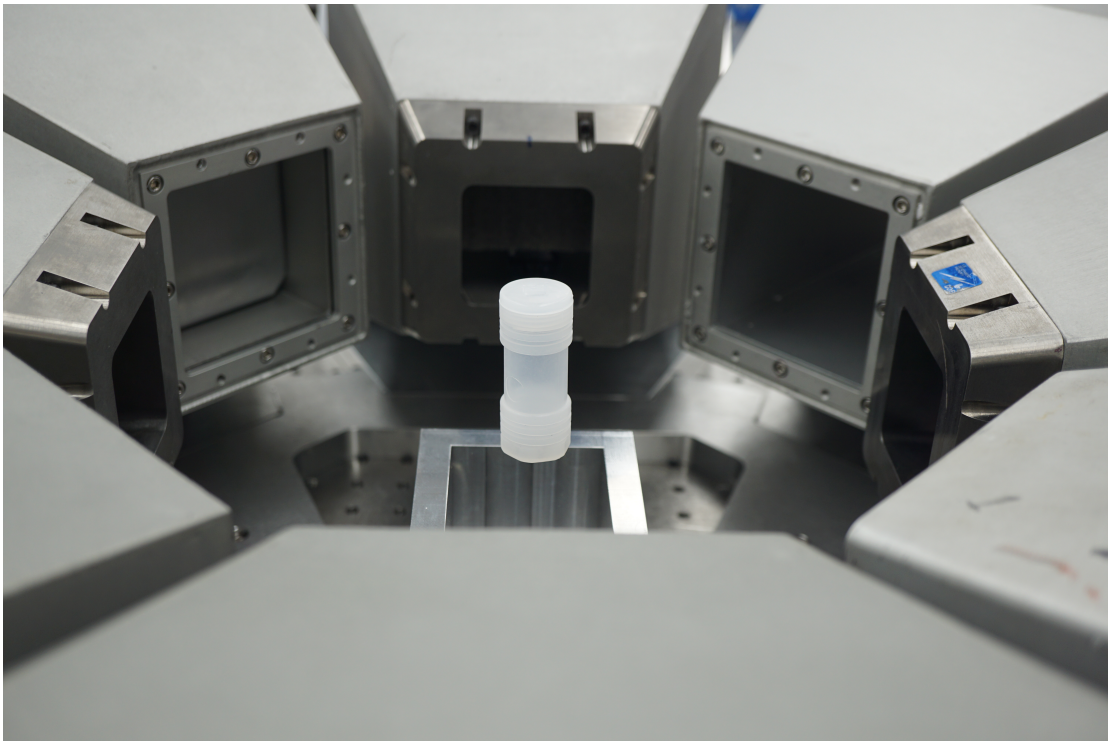

Figure 50: The new rabbit is 2.5 inches long and 1 inch in diameter.

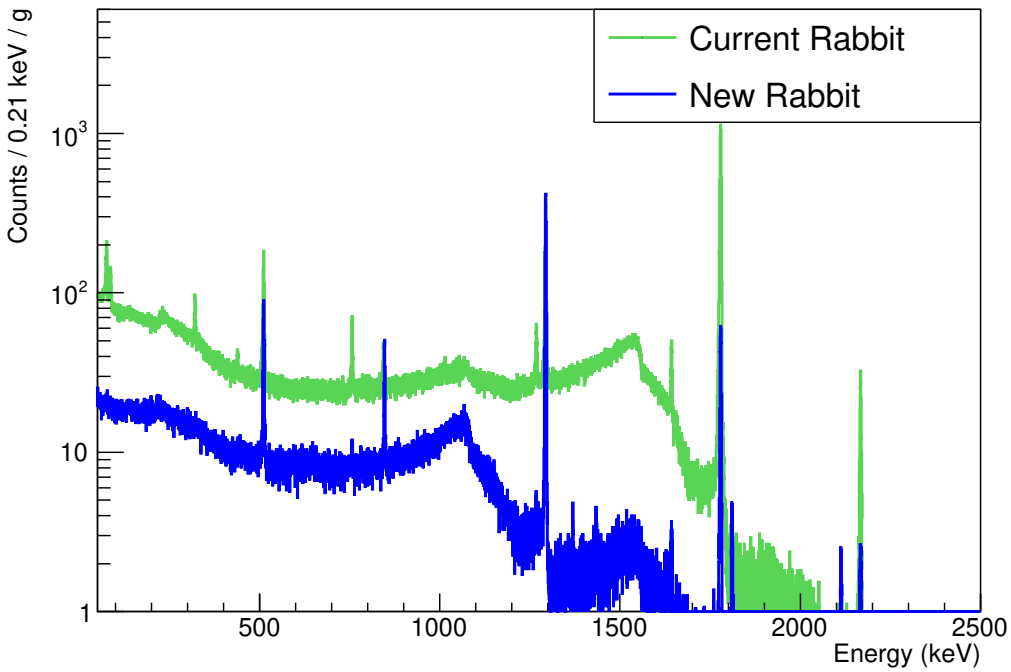

Figure 51: The current and new rabbits were measured within five seconds of irradiation in the OSU TRIGA reactor.

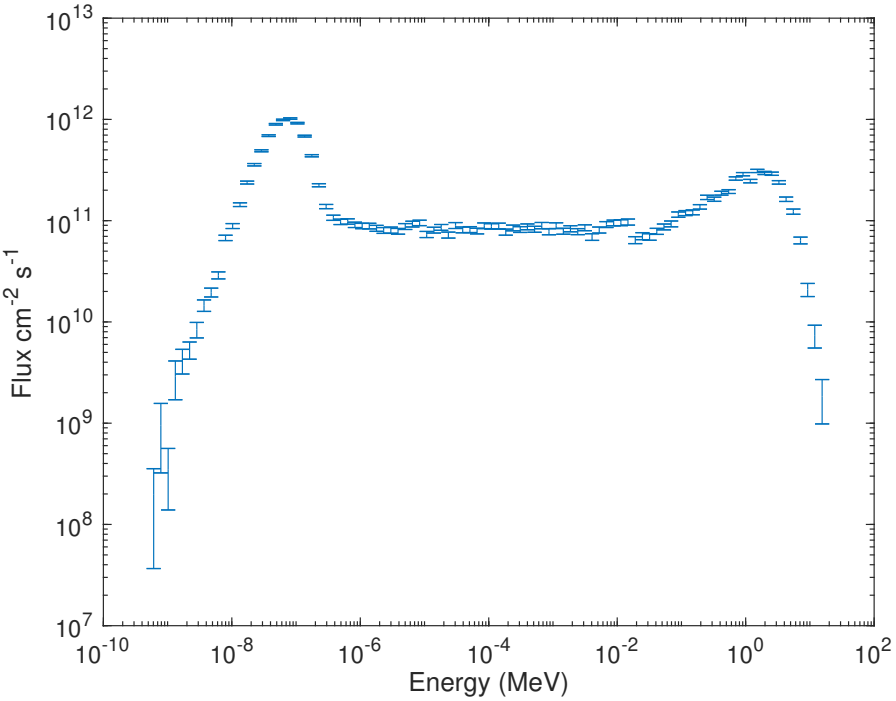

Figure 52: Simulated OSU TRIGA rabbit neutron flux profile $\phi(E)$ using MCNP and core configuration to date. The left peak is due to the large amounts of thermal neutrons (which have an energy of 0.025 eV or 2.5E-8 MeV) and the right peak is due to the fission neutron spectrum of the reactor fuel (19.75% enriched ^{235}U fuel or low enriched uranium (LEU) 30/20 fuel [35]).

Table 29: Efficiency curve parameters.

P_i	$E_\gamma \leq 120$ keV	$E_\gamma > 120$ keV
[0]	-25.47197	17.75908
[1]	5.006033	-5.744014
[2]	0.0	0.3592795

The number of impurity atoms $N_{imp.}$ are calculated by the following:

$$N_{imp.} = \frac{N_{prod.}}{\Delta t_{irrad.} \int \phi(E)\sigma(E)\, dE} = \frac{N_{prod.}}{n_{reac.}} \tag{23}$$

where $\phi(E)$ is neutron flux, $\sigma(E)$ is neutron cross subsection, and $\Delta t_{irradiation}$ is irradiation time. The neutron flux profile for the OSU TRIGA rabbit facility was simulated using MCNP (see Figure 52). The neutron cross subsection data were taken from ENDF/B-VIII.0 [126] and JEFF-3.3 [127]. The neutron cross subsection data were re-binned into the same energy bins as the neutron flux profile using an energy weighted average for each energy bin g (see Equation 24).

$$\sigma_g(E_g) = \frac{\int_{E_{g-1}}^{E_g} \sigma_\gamma(E)\, dE}{\int_{E_{g-1}}^{E_g} dE} \tag{24}$$

$\sigma_g(E_g)$ is the group cross subsection within energy bin E_{g-1} to E_g and $\sigma_\gamma(E)$ is the (n,γ) cross subsection data from the database. ENDF/B-VIII.0 cross subsection data was preferred, but uncertainties were only provided for ^{50}Ti, ^{127}I, ^{26}Mg, ^{55}Mn, ^{30}Si, and ^{27}Al. JEFF-3.3 provided cross subsection data with uncertainties for ^{68}Zn, ^{65}Cu, ^{63}Cu, and ^{48}Ca. No database provided cross subsection data with uncertainties for ^{37}Cl, so a 30% uncertainty in reaction rate was assumed. Integrating the re-binned neutron cross subsection data and neutron flux profile is the total reaction rate. Multiplication of the reaction rate by the irradiation time give the total number of reactions. Total reactions $n_{reac.}$ can be interpreted

Table 30: Neutron activation analysis of current rabbit, new rabbit, and LAContainer NAA Polyvials™. These are the different sample containers used for the rabbit facility.

		Specific Activity (Bq/g)		
Production Mechanism	E_γ (keV)	Current Rabbit	New Rabbit	LAContianer NAA Polyvials™
Pb $K_{\alpha 1}$ x-ray	75.5	6.8 ± 0.4	0.2 ± 0.2	0.20 ± 0.07
$^{50}\mathrm{Ti}(n,\gamma)^{51}\mathrm{Ti} \xrightarrow{\beta^-} {}^{51}\mathrm{V}$	320.28	1.8 ± 0.3	–	–
$^{68}\mathrm{Zn}(n,\gamma)^{69m}\mathrm{Zn} \xrightarrow{IT} {}^{69}\mathrm{Zn}$	438.63	0.5 ± 0.2	–	–
$^{127}\mathrm{I}(n,\gamma)^{128}\mathrm{I} \xrightarrow{\beta^-} {}^{128}\mathrm{Xe}$	442.90	8.9 ± 0.6	–	–
$e^- + e^+$	511.0	9.6 ± 0.4	4.6 ± 0.2	4.6 ± 0.2
$^{65}\mathrm{Cu}(n,\gamma)^{66}\mathrm{Cu} \xrightarrow{\beta^-} {}^{66}\mathrm{Zn}$	832.86	–	–	–
$^{26}\mathrm{Mg}(n,\gamma)^{27}\mathrm{Mg} \xrightarrow{\beta^-} {}^{27}\mathrm{Al}$	843.8	1.2 ± 0.2	–	–
$^{55}\mathrm{Mn}(n,\gamma)^{56}\mathrm{Mn} \xrightarrow{\beta^-} {}^{56}\mathrm{Fe}$	846.76	–	2.0 ± 0.2	0.2 ± 0.1
$^{65}\mathrm{Cu}(n,\gamma)^{66}\mathrm{Cu} \xrightarrow{\beta^-} {}^{66}\mathrm{Zn}$	1038.85	–	–	2.3 ± 0.2
$^{30}\mathrm{Si}(n,\gamma)^{31}\mathrm{Si} \xrightarrow{\beta^-} {}^{31}\mathrm{P}$	1267.9	2.2 ± 0.3	–	–
$^{41}\mathrm{Ar} \xrightarrow{\beta^-} {}^{41}\mathrm{K}$	1293.43	18.4 ± 0.5	21.7 ± 0.4	31.1 ± 0.5
$^{63}\mathrm{Cu}(n,\gamma)^{64}\mathrm{Cu} \xrightarrow{\varepsilon} {}^{64}\mathrm{Ni}$	1345.83	–	–	–
$^{37}\mathrm{Cl}(n,\gamma)^{38}\mathrm{Cl} \xrightarrow{\beta^-} {}^{38}\mathrm{Ar}$	1642.63	1.9 ± 0.2	0.14 ± 0.05	–
$^{27}\mathrm{Al}(n,\gamma)^{28}\mathrm{Al} \xrightarrow{\beta^-} {}^{28}\mathrm{Si}$	1778.80	71.3 ± 0.8	3.6 ± 0.2	0.98 ± 0.09
$^{55}\mathrm{Mn}(n,\gamma)^{56}\mathrm{Mn} \xrightarrow{\beta^-} {}^{56}\mathrm{Fe}$	1810.73	–	0.25 ± 0.05	–
3084.42 - 1022 keV	2062.34	–	–	–
$^{55}\mathrm{Mn}(n,\gamma)^{56}\mathrm{Mn} \xrightarrow{\beta^-} {}^{56}\mathrm{Fe}$	2113.09	–	0.12 ± 0.03	–
$^{37}\mathrm{Cl}(n,\gamma)^{38}\mathrm{Cl} \xrightarrow{\beta^-} {}^{38}\mathrm{Ar}$	2167.22	1.9 ± 0.1	0.14 ± 0.03	0.03 ± 0.01
3084.42 - 511 keV	2572.95	–	–	–
$^{48}\mathrm{Ca}(n,\gamma)^{49}\mathrm{Ca} \xrightarrow{\beta^-} {}^{49}\mathrm{Sc}$	3084.42	0.03 ± 0.02	0.02 ± 0.01	–

Table 31: Impurities identified and mass calculated based on the γ ray of the activated product.

		$m_{imp.}/m_{poly}$ (g/g)					
Trace Element	E_γ (keV)	Marlex® 9006 HDPE	Densetec® HDPE	Westlake EM800AA	Current Rabbit	New Rabbit	LAContainer NAA Polyvials™
^{50}Ti	320.2	1.5(1)E-8	–	–	3.1(4)E-9	–	–
^{68}Zn	438.6	–	–	–	2.0(7)E-12	–	–
^{127}I	442.9	9(4)E-12	–	–	9(4)E-12	–	–
^{65}Cu	833.0	2.6(2)E-6	1.03(4)E-5	–	–	–	–
^{26}Mg	843.7	–	–	–	1.4(3)E-8	–	–
^{55}Mn	846.7	–	–	–	–	6.1(6)E-12	7(3)E-13
^{65}Cu	1039.2	2.18(3)E-6	9.7(1)E-6	1.4(1)E-8	–	–	1.9(2)E-8
^{30}Si	1267.9	1.2(1)E-6	–	–	9(1)E-7	–	–
^{63}Cu	1345.8	–	1.9(2)E-9	–	–	–	–
^{37}Cl	1642.6	1.57(6)E-8	2.1(3)E-9	1.0(4)E-10	2.4(3)E-9	1.8(6)E-10	–
^{27}Al	1778.9	8.4(1)E-7	1.02(1)E-6	7.7(7)E-9	6.0(1)E-7	3.0(1)E-8	8.2(8)E-9
^{55}Mn	1810.7	–	–	–	–	4.6(9)E-12	–
^{55}Mn	2113.0	–	–	–	–	4(1)E-12	–
^{37}Cl	2167.2	1.40(5)E-8	1.1(1)E-9	9(3)E-11	2.0(1)E-9	1.5(3)E-10	3(1)E-11
^{48}Ca	3084.4	1.9(1)E-9	–	–	3(2)E-11	2(1)E-11	–

as the conversion factor from $N_{imp.}$ to $N_{prod.}$ in a neutron field.

The mass of impurity to mass of polyethylene, is the following:

$$\frac{m_{imp.}}{m_{poly}} = \underbrace{\left(\frac{M_{imp.}\Delta t_{meas.}}{N_{AV}}\right)}_{\text{constant}} \left(\frac{a}{R_\gamma \varepsilon_\gamma n_{reac.}}\right) \left(1 - e^{-\lambda_{prod.}\Delta t_{irrad}}\right) \tag{25}$$

where $\lambda_{prod.}$ is the product's decay constant, Δt_{irrad} is total irradiation time, N_{AV} is Avogadro's number, and $M_{imp.}$ is molar mass of the impurity. The uncertainty is calculated using error propagation. There were 11 trace impurities identified in the polyethylene samples. The calculated mass of impurity per mass of polyethylene is summarized in Table 31.

Marlex® 9006 HDPE had 7 impurities, Densetec® HDPE had 4 impurities, and Westlake EM800AA LDPE had 3 impurities. ^{65}Cu and ^{27}Al were the largest common impurities by mass. Of the three polyethylene samples, Westlake EM800AA LDPE had the smallest amount of ^{65}Cu and ^{27}Al by mass. The

new high-purity polyethylene rabbit is made out of Westlake EM800AA LDPE, but ^{65}Cu was not found as an impurity. Also, there are ^{55}Mn and ^{48}Ca found in the new rabbit carriers. The new rabbit carrier has 4 impurities and the current rabbit carrier has 8 impurities. ^{27}Al is the common impurity between the two rabbits. The new rabbit carrier has 73% less ^{27}Al than the current rabbit carrier. Overall, the new rabbit is an improvement to the current rabbit and is ready to be commissioned.

4.6 Conclusion

The goal of the Lāpaki array is to measure nuclear structure for short-lived fission products, fission product yields for various actinides, and NAA. A new procedure was developed to mitigate neutron activated air and a new high-purity polyethylene rabbit was constructed to reduce short-lived impurities in the current rabbit carrier. The array and DAQ were designed to be portable and were planned to be used in future experiments with OSU TRIGA rabbit facility, Godiva-IV critical assembly rabbit facility, and Maui D-T generator rabbit facility at LLNL.

Acknowledgements

This work was funded by the Office of Defense Nuclear Nonproliferation Research and Development within the U.S. DOE - NNSA. This work was performed under the auspices of the U.S. DOE by LLNL under Contract DE-AC52-07NA27344. This work was performed with the assistance of the Radiation Center at Oregon State University.

5 Conclusion

In this dissertation, ^{239}Pu and ^{237}Np fission product yields were measured and compared to evaluated values (ENDF/B-VIII.0 [37]). These results are part of a consistent set of experiments using Godiva IV (^{233,235,238}U, ^{239}Pu, and ^{237}Np). For the first time in history, these five actinides were measured using the same detectors and data acquisition system at Godiva IV. At the time of this thesis, Godiva IV is the only facility in the world to provide fission spectrum neutrons with a peak neutron flux of around 4×10^{18} neutrons/cm^2/sec during a prompt burst of around 24 μs FWHM [94]. Other facilities are not able to produce fission spectrum neutrons at this rate. This means that past measurements that required longer exposure time (e.g. hours, days, etc.) would need to account for neutron absorption of fission products being produced. The irradiation of actinides using Godiva IV produced very clean measurements of time-dependent γ-ray spectra. The use of time-dependent γ-ray spectra allows for the isotopes to be identified based on γ-ray energy and isotope half-life. This method of data analysis ensures the isotope analyzed is not being interfered by a neighboring γ ray, which would have been misinterpreted when analyzing a single γ-ray sum spectrum. The results from analyzing the fission product yields in this thesis (^{239}Pu and ^{237}Np) and past work (^{235}U and ^{238}U) showed their are variations between the measured fission product yield for different γ-ray energies compared to evaluated values.

Results from ^{239}Pu show there were improved uncertainties for ^{93}Y and ^{133}I from Pu3+Pu4 and ^{127}Sn, ^{128}Sn, and ^{130}Sb for Pu1. Measured values for ^{93}Y were within the error bars of the evaluated value of 3.817%, which had a relative uncertainty of 64%. The measured values were 3.5% and 3.0% with relative uncertainties of 11% and 15% respectively for two γ rays analyzed. Measured values

for ^{133}I were within the error bars of the evaluated value of 6.896%, which had a relative uncertainty of 64%. The measured values were 8.0%, 7.1%, 7.2%, and 7.3% with relative uncertainties of 5%, 5%, 6%, and 9% respectively for four γ rays analyzed. Measured values for ^{127}Sn were within the error bars of the evaluated value of 0.353%, which had a relative uncertainty of 64%. The measured values were 0.38% and 0.35% with relative uncertainties of 22% and 18% respectively for two γ rays analyzed. Measured value for ^{128}Sn was within the error bars of the evaluated value of 0.789%, which had a relative uncertainty of 64%. The measured value was 0.78% with relative uncertainty of 11% for one γ ray analyzed. Measured values for ^{130}Sb were within the error bars of the evaluated value of 0.953%, which had a relative uncertainty of 64%. The measured values were 0.91%, 0.93%, and 0.92% with relative uncertainties of 8%, 9%, and 9% respectively for three γ rays analyzed.

Results from ^{237}Np show there were improved uncertainties for ^{91}Sr , ^{93}Y and ^{133}I from Np1+Np3 and ^{105}Ru, ^{127}Sn, ^{128}Sn, and ^{130}Sb for Np2. Measured value for ^{91}Sr was within the error bars of the evaluated value of 3.925%, which had a relative uncertainty of 4%. The measured value was 4.0% with relative uncertainty of 3% for one γ ray analyzed. Measured values for ^{93}Y were within the error bars of the evaluated value of 5.116%, which had a relative uncertainty of 64%. The measured values were 4.7%, 5.0% and 4.2% with relative uncertainties of 10% for all three γ rays analyzed. Measured values for ^{133}I were within the error bars of the evaluated value of 6.460%, which had a relative uncertainty of 64%. The measured values were 6.8% and 7.3% with relative uncertainties of 3% for both γ rays analyzed. Measured values for ^{105}Ru were within the error bars of the evaluated value of 3.103%, which had a relative uncertainty of 6%. The measured values were 3.1%, 3.5% and 3.5% with relative uncertainties of 4% for

all three γ rays analyzed. Measured values for ^{127}Sn were within the error bars of the evaluated value of 0.258%, which had a relative uncertainty of 32%. The measured values were 0.24% and 0.30% with relative uncertainties of 21% and 15% respectively for two γ rays analyzed. Measured value for ^{128}Sn was within the error bars of the evaluated value of 0.635%, which had a relative uncertainty of 64%. The measured value was 0.62% with relative uncertainty of 8% for one γ ray analyzed. Measured values for ^{130}Sb were within the error bars of the evaluated value of 1.169%, which had a relative uncertainty of 64%. The measured values were 0.89% and 0.97% with relative uncertainties of 5% for both γ rays analyzed.

Other fission product yields not mentioned were not within evaluated values. Chapter 2 and 3 concluded that disagreement to evaluated values may be caused by discrepancies in γ-ray branching ratios. Even though there were measured fission product yields that improved uncertainties, γ-ray branching ratio is still an issue. This is shown in the variation of results from different γ rays analyzed for the same isotope. Each γ ray from the same isotope should result in the same fission product yield value. In order to improve fission product γ-ray branching ratio, a new detection setup called the Lāpaki γ-γ array was constructed. The array is comprised of up to eight HPGe clovers/BGO Compton suppression shield pairs. HPGe clover detectors were introduced in the 1990s, which makes these detectors the state-of-the-art HPGe detectors for γ-ray spectroscopy [128]. There are various arrays of clover detectors used for accelerator-based experiments, but this is the first time an array of clovers was designed to be used with a rabbit system and a neutron source. Lāpaki is coupled with a rabbit system to measured short-lived fission product yields within seconds of irradiation and perform γ-γ coincidence measurements. A new digital data acquisition system from Mesytec was put together for this experiment. The Lāpaki array and DAQ being portable

makes it possible to perform future experiments with this setup at any facilities.

Finally, a new high-purity polyethylene rabbit was designed and fabricated. Impurities in the polyethylene have been mentioned for past rabbit experiments since the 1950s, but a new high-purity polyethylene rabbit was constructed in the 2020s. Past measurements using the rabbit have required a period of time before γ counting to allow for neutron activated impurities to decay to a low enough activity. The reduction of impurities in polyethylene used for the rabbit decreased the background γ rays from neutron activated impurities. One prominent γ ray peak is at 1779 keV with a 2.25 minute half-life. This high energy γ ray produced a Compton background, reducing the signal to background ratio for any low activity γ ray below 1779 keV. This impurity is from trace amounts of aluminum found in polyethylene. The current rabbit had 600 ng of aluminum per gram of polyethylene and the new rabbit had 30 ng of aluminum per gram of polyethylene. A factor of 20 improvement for the 1779 keV γ ray in the new rabbit. Chapter 4 shows a comparison spectrum between the current and new rabbit. With the construction of a new detection setup and new rabbit, a series of ^{238}U samples were irradiated in the OSU TRIGA for approximately two seconds and γ rays were measured within three seconds after irradiation. Data collected form this measurement will be analyzed during the student's postdoctoral appointment.

Overall, the results from the campaign of measurements using Godiva IV will be a consistent set of data used for the applications mentioned in Chapter 1. Although, these results are limited to approximately 45 minutes after time of fission. The series of ^{238}U measurements at the OSU TRIGA rabbit facility will provide data within the time gap of the Godiva IV measurements. With a more complete understanding of fission product yields and from short time scales will improve time dependent isotopic abundance within nuclear fuel in reactors to

nucleosynthesis of stars in the universe.

5.1 Future Works

Lāpaki will be used with Maui (a new DT neutron generator and rabbit system at LLNL) for short-lived NAA and 14 MeV short-lived fission product yield measurements and cross section measurements. Also, a new rabbit system is being constructed with Godiva IV to measure fission spectrum short-lived fission product yields using Lāpaki.

All measurements from Godiva IV will be compiled onto a local server for further data analysis such as machine learning techniques. Efficiency of the detectors will be revisited calibrating at a higher energy around 2 MeV. This will resolve any discrepancies in the efficiency curve at higher energies.

The Lāpaki array was used to measure ^{238}U short-lived fission product yields within seconds of irradiation at the OSU TRIGA reactor. The data will be analyzed during the student's postdoctoral appointment for the following publications:

- *^{238}U Fission Product Yield Measurement Using The Oregon State TRIGA Reactor With The Lāpaki Array*
  A.S. Tamashiro et. al., Nuclear Data Sheets

- *^{238}U Fission Product γ-Ray Branching Ratio Measurement Using The Oregon State TRIGA Reactor With The Lāpaki Array*
  A.S. Tamashiro et. al., Physical Review C

References

[1] B. SINGH and J. CHEN, "Nuclear Data Sheets for A=85," *Nuclear Data Sheets*, **116**, 1–162 (2014).

[2] T. JOHNSON and W. KULP, "Nuclear Data Sheets for A = 87," *Nuclear Data Sheets*, **129**, 1–190 (2015).

[3] E. MCCUTCHAN and A. SONZOGNI, "Nuclear Data Sheets for A = 88," *Nuclear Data Sheets*, **115**, 135–304 (2014).

[4] B. SINGH, "Nuclear Data Sheets for A = 89," *Nuclear Data Sheets*, **114**, *1*, 1–208 (2013).

[5] C. M. BAGLIN, "Nuclear Data Sheets for A = 91," *Nuclear Data Sheets*, **114**, *10*, 1293–1495 (2013).

[6] C. M. BAGLIN, "Nuclear Data Sheets for A = 92," *Nuclear Data Sheets*, **113**, *10*, 2187–2389 (2012).

[7] C. M. BAGLIN, "Nuclear Data Sheets for A = 93," *Nuclear Data Sheets*, **112**, *5*, 1163–1389 (2011).

[8] S. BASU, G. MUKHERJEE, and A. SONZOGNI, "Nuclear Data Sheets for A = 95," *Nuclear Data Sheets*, **111**, *10*, 2555–2737 (2010).

[9] N. NICA, "Nuclear Data Sheets for A = 97," *Nuclear Data Sheets*, **111**, *3*, 525–716 (2010).

[10] E. BROWNE and J. TULI, "Nuclear Data Sheets for A=99," *Nuclear Data Sheets*, **145**, 25–340 (2017).

[11] D. DE FRENNE, "Nuclear Data Sheets for A = 103," *Nuclear Data Sheets*, **110**, *9*, 2081–2256 (2009).

[12] S. LALKOVSKI, J. TIMAR, and Z. ELEKES, "Nuclear Data Sheets for A=105," *Nuclear Data Sheets*, **161-162**, 1–353 (2019).

[13] A. HASHIZUME, "Nuclear Data Sheets for A = 127," *Nuclear Data Sheets*, **112**, *7*, 1647–1831 (2011).

[14] Z. ELEKES and J. TIMAR, "Nuclear Data Sheets for A = 128," *Nuclear Data Sheets*, **129**, 191–436 (2015).

[15] J. TIMAR, Z. ELEKES, and B. SINGH, "Nuclear Data Sheets for A = 129," *Nuclear Data Sheets*, **121**, 143–394 (2014).

[16] B. SINGH, "Nuclear Data Sheets for A = 130," *Nuclear Data Sheets*, **93**, *1*, 33–242 (2001).

[17] Y. KHAZOV, I. MITROPOLSKY, and A. RODIONOV, "Nuclear Data Sheets for A = 131," *Nuclear Data Sheets*, **107**, *11*, 2715–2930 (2006).

[18] Y. KHAZOV, A. RODIONOV, S. SAKHAROV, and B. SINGH, "Nuclear Data Sheets for A=132," *Nuclear Data Sheets*, **104**, *3*, 497–790 (2005).

[19] Y. KHAZOV, A. RODIONOV, and F. KONDEV, "Nuclear Data Sheets for A = 133," *Nuclear Data Sheets*, **112**, *4*, 855–1113 (2011).

[20] A. SONZOGNI, "Nuclear Data Sheets for A = 134," *Nuclear Data Sheets*, **103**, *1*, 1–182 (2004).

[21] B. SINGH, A. A. RODIONOV, and Y. L. KHAZOV, "Nuclear Data Sheets for A = 135," *Nuclear Data Sheets*, **109**, *3*, 517–698 (2008).

[22] J. CHEN, "Nuclear Data Sheets for A=138," *Nuclear Data Sheets*, **146**, 1–386 (2017).

[23] P. K. JOSHI, B. SINGH, S. SINGH, and A. K. JAIN, "Nuclear Data Sheets for A = 139," *Nuclear Data Sheets*, **138**, 1–292 (2016).

[24] N. NICA, "Nuclear Data Sheets for A=140," *Nuclear Data Sheets*, **154**, 1–403 (2018).

[25] N. NICA, "Nuclear Data Sheets for A = 141," *Nuclear Data Sheets*, **122**, 1–204 (2014).

[26] T. JOHNSON, D. SYMOCHKO, M. FADIL, and J. TULI, "Nuclear Data Sheets for A = 142," *Nuclear Data Sheets*, **112**, *8*, 1949–2127 (2011).

[27] E. BROWNE and J. TULI, "Nuclear Data Sheets for A = 143," *Nuclear Data Sheets*, **113**, *3*, 715–908 (2012).

[28] Y. KHAZOV, A. RODIONOV, and G. SHULYAK, "Nuclear Data Sheets for A = 146," *Nuclear Data Sheets*, **136**, 163–452 (2016).

[29] B. SINGH, "Nuclear Data Sheets for A=149," *Nuclear Data Sheets*, **102**, *1*, 1–291 (2004).

[30] B. SINGH, "Nuclear Data Sheets for A = 151," *Nuclear Data Sheets*, **110**, *1*, 1–264 (2009).

[31] J. DEUTCH, E. MONIZ, S. ANSOLABEHERE, M. DRISCOLL, P. GRAY, J. HOLDREN, P. JOSKOW, R. LESTER, and N. TODREAS, "The future of nuclear power," *an MIT Interdisciplinary Study, http://web. mit. edu/nuclearpower* (2003).

[32] V. A. NAUMOV and D. S. SHKIRMANOV, "Reactor Antineutrino Anomaly Reanalysis in Context of Inverse-Square Law Violation," *Universe*, **7**, *7* (2021).

[33] W. ZHU, Z. WANG, X. ZHU, N. SHU, and T. FAN, "A new evaluation of fission product yields for the neutron induced fission of U-233 and Th-232," *Fusion Engineering and Design*, **125**, 608 – 614 (2017).

[34] J. HUMPHRIES, J. BATCH, and R. PETERS, *TRIGA Mark II Pusling Reactor Mechanical Maintenance and Operating Manual for Oregon State University, Corvallis, Oregon* (1967).

[35] R. SCHICKLER, W. MARCUM, and S. REESE, "Comparison of HEU and LEU neutron spectra in irradiation facilities at the Oregon State TRIGA® Reactor," *Nuclear Engineering and Design*, **262**, 340–349 (2013).

[36] W. H. WALKER, "Status of fission product yield data for thermal reactors," Tech. rep., Canada (1974), aECL–4704.

[37] D. BROWN ET AL., "ENDF/B-VIII.0: The 8th Major Release of the Nuclear Reaction Data Library with CIELO-project Cross Sections, New Standards and Thermal Scattering Data," *Nuclear Data Sheets*, **148**, 1 – 142 (2018), special Issue on Nuclear Reaction Data.

[38] J. ENGLAND and B. RIDER, "ENDF/B-6 FPY: The ENDF/B-6 fission-product yield sub-libraries," Tech. rep., IAEA-NDS-106 (1995).

[39] R. BRUN and F. RADEMAKERS, "ROOT—an object oriented data analysis framework," *Nuclear Instruments and Methods in Physics Research Section A: Accelerators, Spectrometers, Detectors and Associated Equipment*, **389**, *1-2*, 81–86 (1997).

[40] N. R. COMMISSION ET AL., "SCALE: A modular code system for performing standardized computer analyses for licensing evaluation: Functional modules F1-F8," Tech. rep., Nuclear Regulatory Commission (1997).

[41] W. MAECK, "Fission product nuclear data requirements for the determination of nuclear fuel burnup: a review," Tech. rep., Allied Chemical Corp. (1974).

[42] J. DICKENS, "Review of new integral determinations of decay heat," Tech. rep., Oak Ridge National Lab. (1987).

[43] B. J. ADE and I. C. GAULD, "Decay heat calculations for pwr and bwr assemblies fueled with uranium and plutonium mixed oxide fuel using scale," *Oak Ridge National Laboratory, Oak Ridge, TN, Technical Report No. ORNL/TM-2011/290* (2011).

[44] M. FALLOT, "Getting to the Bottom of an Antineutrino Anomaly," *Physics*, **10**, 66 (2017).

[45] G. MENTION, M. FECHNER, T. LASSERRE, T. A. MUELLER, D. LHUILLIER, M. CRIBIER, and A. LETOURNEAU, "Reactor antineutrino anomaly," *Phys. Rev. D*, **83**, 073006 (Apr 2011).

[46] G. J. MATTHEWS, "Applications for fission product data to problems in stellar nucleosynthesis," NASA STI/Recon Technical Report N (Oct. 1983).

[47] P. HYPES, W. GEIST, and P. SANTI, "Chapter 20 - Analytical Techniques in Nuclear Safeguards," in M. F. L'ANNUNZIATA, editor, "Handbook of Radioactivity Analysis (Third Edition)," Academic Press, Amsterdam, pp. 1243 – 1280, third edition ed. (2012).

[48] I. A. E. AGENCY, *Fission Product Yield Data for the Transmutation of Minor Actinide Nuclear Waste: Non-serial Publications*, International Atomic Energy Agency (2008).

[49] C. WAGEMANS, *The Nuclear Fission Process*, CRC Press (1991).

[50] L. WILETS, *Theories of nuclear fission*, Clarendon Press (1964).

[51] E. K. HYDE, G. T. SEABORG, and I. PERLMAN, "The nuclear properties of the heavy elements," (1964).

[52] R. VANDENBOSCH and J. R. HUIZENGA, *Nuclear Fission*, Academic Press (1973).

[53] A. WAHL, "IAEA final report of a coordinated research project on "Compilation and evaluation of fissions yield nuclear data"," Tech. rep., IAEA (2000).

[54] H. O. DENSCHLAG ET AL., "Compilation and evaluation of fission yield nuclear data," Tech. rep., International Atomic Energy Agency (2000).

[55] O. R. FRISCH, "Physical evidence for the division of heavy nuclei under neutron bombardment," *Nature*, **143**, *3616*, 276–276 (1939).

[56] A. O. NIER ET AL., "Nuclear Fission of Separated Uranium Isotopes," *Physical Review*, **57**, 546–546 (1940).

[57] J. R. LAETER, "Mass spectrometry in nuclear science," *Mass Spectrometry Reviews*, **7**, 71–111 (1988).

[58] H. O. DENSCHLAG, "Independent Fission Yield Measurements," *Nuclear Science and Engineering*, **94**, 337–352 (1986).

[59] J. V. BOGGS, Ph.D. thesis (1966).

[60] J. K. DICKENS, R. W. PEELLE, and F. C. MAEINSCHEIN, *Experiment for Accurate Measurements of Fission Product Energy Release for Short Times After Thermal-Neutron Fission of 235U and 239Pu* (May 1975).

[61] J. K. DICKENS, J. F. EMERY, T. A. LOVE, J. W. MCCONNELL, K. J. NORTHCUTT, R. W. PEELLE, and H. WEAVER, *Fission-Product Energy Release for Times Following Thermal-Neutron Fission of 235U Between 2 and 14000 Seconds* (Oct 1977).

[62] J. BURKE, A. TAMASHIRO, B. ALAN, S. PADGETT, S. MENN, S. REESE, W. LOVELAND, L. MINC, C. PALMER, and K. ROBERTS, "Results from Oregon State University 1 MW TRIGA reactor irradiation of uranium-238," Tech. rep., Lawrence Livermore National Lab.(LLNL), Livermore, CA (United States) (2019).

[63] W. W. MEINKE, "Radiochemical separations and activation analysis: progress report 7, November 1957-October 1958," Tech. rep. (1958).

[64] R. S. MADDOCK and W. E. MEINKE, "ACTIVATION ANALYSIS NUCLEAR CHEMICAL RESEARCH RADIOCHEMICAL SEPARATIONS. Progress Report No. 8 for November 1958-October 1959," (11 1959).

[65] J. L. BROWNLEE, "Neutron activation analysis by means of short-lived isotopes: a dissertation... for the degree of Doctor of Philosophy in the University of Michigan," Tech. rep. (1960).

[66] A. O. PAAS and R. D. SULLIVAN, "Measurement of neutron activated short-lived nuclides using a pneumatic transfer system," Tech. rep., NAVAL POSTGRADUATE SCHOOL MONTEREY CA (1962).

[67] H. LUKENS, H. YULE, and V. GUINN, "Reactor pulsing in activation analysis," *Nuclear Instruments and Methods*, **33**, *2*, 273–276 (1965).

[68] J. R. DEVOE, *Activation Analysis: Cockcroft-Walton Generator Nuclear Reactor, LINAC, July 1966 Through June 1967*, vol. 13, US Government Printing Office (1967).

[69] D. E. ROBERTSON and R. CARPENTER, "Neutron activation techniques for the measurement of trace metals in environmental samples," (1 1974).

[70] D. W. SHEIBLEY, "Trace-element analysis of 1000 environmental samples per year using instrumental neutron activation analysis," (1974).

[71] "Elemental Analysis of Biological Materials," Tech. rep.

[72] J. KUČERA and L. SOUKAL, "Determination of trace element levels in polyethylene by instrumental neutron activation analysis," *Journal of Radioanalytical Chemistry*, **80**, *1*, 121–127 (Mar 1983).

[73] J. BURKE, A. TAMASHIRO, B. ALAN, S. PADGETT, S. MENN, S. REESE, W. LOVELAND, L. MINC, C. PALMER, and K. ROBERTS, "Results from Oregon State University 1 MW TRIGA reactor irradiation of uranium-238," Tech. rep., Lawrence Livermore National Lab.(LLNL), Livermore, CA (United States) (2019).

[74] B. D. PIERSON, A. M. PRINKE, L. R. GREENWOOD, S. C. STAVE, R. S. WITTMAN, J. G. BURCH, J. BURKE, S. W. PADGETT, J. J. RESSLER, G. SLAVIK, ET AL., "Improved cumulative fission yield measurements with fission spectrum neutrons on 235U," *Nuclear Data Sheets*, **155**, 86–97 (2019).

[75] B. PIERSON, L. GREENWOOD, S. STAVE, J. BURKE, S. PADGETT, A. PRINKE, J. GODA, J. BOUNDS, D. HAYES, A. TAMASHIRO, R. WITTMAN, G. SLAVIK, M. DION, J. BURCH, and T. PALMER, "Improved Cumulative Fission Yield Measurements with Fission Spectrum Neutrons on 238U," *Nuclear Data Sheets*, **163**, 249 – 260 (2020).

[76] J. GODA, C. BRAVO, T. CUTLER, T. GROVE, D. HAYES, J. HUTCHINSON, G. MCKENZIE, A. MCSPADEN, W. MYERS, R. SANCHEZ, and J. WALKER, "A New Era of Nuclear Criticality Experiments: The First 10 Years of Godiva IV Operations at NCERC," *Nuclear Science and Engineering*, **195**, *sup1*, S55–S79 (2021).

[77] T. ENGLAND and B. RIDER, "Evaluation and compilation of fission product yields 1993," Tech. rep., Los Alamos National Lab. (1995).

[78] R. P. LARSEN, N. D. DUDEY, C. E. CROUTHAMEL, A. D. TEVEBAUGH, and R. C. VOGEL, "CHEMICAL ENGINEERING DIVISION: BURNUP, CROSS SECTIONS, AND DOSIMETRY SEMIANNUAL REPORT, JULY–DECEMBER 1971." .

[79] L. D. NOBLE, G. KUSSMAUL, and S. L. DERBY, "EXPERIMENTAL PROGRAM RESULTS IN SEFOR CORE II." .

[80] L. D. NOBLE, G. KUSSMAUL, and S. L. DERBY, "EXPERIMENTAL PROGRAM RESULTS IN SEFOR CORE II." (1972), unpublished results for long-lived fission product yields.

[81] K. WOLFSBERG, "Estimated values of fractional yields from low-energy fission and a compilation of measured fractional yields," .

[82] N. D. DUDEY, R. J. POPEK, R. C. GREENWOOD, R. G. HELMER, J. W. ROGERS, L. S. KELLOG, and W. H. ZIMMER, "Fission-Product-Rate Measurements and Yields," *Nuclear Technology*, **25**, 294–304 (1975).

[83] A. N. GUDKOV, V. M. ZHIVUN, I. V. ZHUKOV, A. V. ZVONAREV, V. V. KOVALENKO, A. B. KOLDOBSKIJ, Y. KOLEGANOV, V. M. KOLOBASHKIN, M. KULAKOVSKIJ, and N. S. PIVEN', "Determination of 232Th, 233U, 235U, 238U, 239Pu fast neutron fission product yields," USSR (1977), Opredelenie vykhodov produktov deleniya toriya-232, urana-233, urana-235, urana-238, plutoniya-239 bystrymi nejtronami, pp. 192–196.

[84] L. . N. YUROVA, A. V. BUSHUEV, V. N. OZERKOV, V. V. CHACHIN, A. V. ZVONARYOV, Y. G. LIFOROV, Y. F. KOLEGANOV, V. V. MILLER, and O. V. GORBATYUK, "The Yield of Several Fragments During Fission of 235U, 238U, and 239Pu due to Neutrons of the Reactor BP-1 Spectrum," *Atomnaya Energiya*, **47**, 26–28 (1979).

[85] J. LAUREC, A. ADAM, T. DE BRUYNE, E. BAUGE, T. GRANIER, J. AUPIAIS, O. BERSILLON, G. L. PETIT, N. AUTHIER, and P. CASOLI, "Fission Product Yields of 233-U, 235-U, 238-U, and 239-Pu in Fields of Thermal Neutrons, Fission Neutrons, and 14.7-MeV Neutrons," *Centre d'Etudes Nucleaires* (1981).

[86] R. W. WALDO, R. A. KARAM, and R. A. MEYER, "Delayed neutron yields: Time dependent measurements and a predictive model," *Phys. Rev. C*, **23**, 1113–1127 (Mar 1981).

[87] T. GARLEA, C. MIRON, T. MUSAT, and C. ROTH, "Determination of Some Fission Yields in the Spectrum for the Reactions 235U (n,f), 239Pu (n,f), 238U (n,f)," *INDC(ROM)-014* (1982).

[88] J. BLACHOT, "Nuclear Data Sheets for A = 104," *Nuclear Data Sheets*, **108**, *10*, 2035–2172 (2007).

[89] D. DE FRENNE and A. NEGRET, "Nuclear Data Sheets for A = 106," *Nuclear Data Sheets*, **109**, *4*, 943–1102 (2008).

[90] E. BROWNE and J. TULI, "Nuclear Data Sheets for A = 137," *Nuclear Data Sheets*, **108**, *10*, 2173–2318 (2007).

[91] E. MCCUTCHAN, "Nuclear Data Sheets for A=136," *Nuclear Data Sheets*, **152**, 331–667 (2018).

[92] A. SONZOGNI, "Experimental data on ground- and excited-state properties for all nuclei with mass number A=144 have been compiled and evaluated. States populated in radioactive decay as well as in nuclear reactions have been considered. For these nuclei, level and decay schemes have been built, as well as tables of nuclear properties. This work supersedes the 1989 evaluation by J.K. Tuli (1989Tu02). Manuscripts published before December 2000 have been included in this work," *Nuclear Data Sheets*, **93**, *3*, 599–762 (2001).

[93] N. NICA, "Nuclear Data Sheets for A = 147," *Nuclear Data Sheets*, **110**, *4*, 749–997 (2009).

[94] R. E. MALENFANT, "Los Alamos Critical Assemblies Facility," (1981).

[95] L. R. GREENWOOD and C. D. JOHNSON, "User guide for the STAYSL PNNL suite of software tools," Tech. rep., Pacific Northwest National Lab.(PNNL), Richland, WA (United States) (2013).

[96] R. W. MILLS, *Fission Yield evaluation*, Ph.D. thesis, Ph. D. Thesis (1995).

[97] E. BROWNE and J. TULI, "Nuclear Data Sheets for A = 60," *Nuclear Data Sheets*, **114**, *12*, 1849–2022 (2013).

[98] M. S. BASUNIA, "Nuclear Data Sheets for A = 22," *Nuclear Data Sheets*, **127**, 69–190 (2015).

[99] Y. DONG and H. JUNDE, "Nuclear Data Sheets for A = 54," *Nuclear Data Sheets*, **121**, 1–142 (2014).

[100] M. BERGER, J. HUBBELL, S. SELTZER, J. CHANG, J. COURSEY, R. SUKUMAR, D. ZUCKER, and K. OLSEN, "*XCOM: Photon Cross Section Database* (version 1.5)," **[Online] Available: http://physics.nist.gov/xcom [2020, February 27]. National Institute of Standards and Technology, Gaithersburg, MD.**

[101] M. J. BERGER, J. COURSEY, M. ZUCKER, , J. CHANG, ET AL., *Stopping-power and range tables for electrons, protons, and helium ions*, NIST Physics Laboratory Gaithersburg, MD (1998).

[102] G. F. KNOLL, *Radiation Detection and Measurement*, Wiley (2010).

[103] A. S. TAMASHIRO, "Evaluation of ^{235}U and ^{238}U Fast Fission Product Yields from Godiva-IV Burst Irradiation via Gamma Detection," (Jan 2019).

[104] E. MICHELAKAKIS, W. D. HAMILTON, P. HUNGERFORD, G. JUNG, P. PFEIFFER, and S. M. SCOTT, "Levels and transitions

insup142,144/supCe populated following the decay ofsup142,144/supLa," *Journal of Physics G: Nuclear Physics*, **8**, *1*, 111–152 (jan 1982).

[105] K. DEBERTIN, "International intercomparison of gamma-ray emission-rate measurements by means of germanium spectrometers and 152Eu sources," *Nuclear Instruments and Methods*, **158**, 479–486 (1979).

[106] A. S. TAMASHIRO, J. T. HARKE, J. G. DUARTE, Y. MISHNAYOT, S. BURCHER, N. HARWARD, K. ROBERTS, S. MENN, T. M. STORY, S. REESE, S. SMITH, L. D. MINC, W. LOVELAND, V. L. ADRIATICO, B. A. KONSTANCZER, S. L. WEIDENBENNER, N. WILTBANK, M. BRANCO-KATCHER, C. KULAH, R. SCHICKLER, and C. J. PALMER, "The Lāpaki γ-γ Array," (2022), manuscript submitted.

[107] A. S. TAMASHIRO, J. T. HARKE, S. W. PADGETT, G. SLAVIK, S. BURCHER, N. HARWARD, N. GHARIBYAN, R. A. HENDERSON, L. R. GREENWOOD, B. D. PIERSON, J. M. GODA, J. A. BOUNDS, D. K. HAYES, and C. J. PALMER, "^{239}Pu Fission Spectrum Cumulative Fission Product Yield Measurement Using Godiva IV Critical Assembly," (2022), manuscript submitted.

[108] G. J. KIROUAC, H. M. EILAND, and C. J. SLAVIK, "Fast Neutron Flux Measurement," Tech. Rep. KAPL-P-4005, Knolls Atomic Power Laboratory (1973).

[109] N. D. DUDEY, R. J. POPEK, R. C. GREENWOOD, R. G. HELMER, J. W. ROGERS, L. S. KELLOG, and W. H. ZIMMER, "Fission-Product-Rate Measurements and Yields," *Nuclear Technology*, **25**, 294–304 (1975).

[110] L. S. KELLOGG, A. I. DAVIS, E. P. LIPPINCOTT, and J. M. RUGGLES, "EDB-II validated, key fission product yields for fast reactor application," Tech. rep., United States (1977), nUREG-CP–0004(Vol3).

[111] A. N. GUDKOV, V. M. ZHIVUN, A. V. ZVONAREV, A. F. ZOLOTOV, A. B. KOLDOBSKII, Y. F. KOLEGANOV, V. M. KOLOBASHKIN, S. V. KRIVASHEEV, and N. S. PIVEN', "Determination of the yield figures of the products resulting from the 237Np fission by fast neutrons with the aid of semiconductor spectrometry," *Soviet Atomic Energy* (Mar 1983).

[112] A. G. C. NÄIR, S. K. DAS, B. S. TOMAR, A. GOSWAMI, B. K. SRIVASTAVA, and S. PRAKASH, "Cumulative Yields of Short-Lived Ruthenium Isotopes in Thermal Neutron-Induced Fission of 241Pu," *Radiochimica Acta*, **42**, *1*, 7–8 (1987).

[113] A. RAMASWAMI, S. S. RATTAN, N. CHAKRAVARTY, R. J. SINGH, S. B. MANOHAR, S. PRAKASH, and V. RAMANIAH, "Charge Distribution Study in the Neutron Induced Fission of 237Np: Fractional Cumulative Yield of 134Te,135I and 138Xe," *Radiochimica Acta*, **41**, *1*, 9–10 (1987).

[114] "Hawaiian Dictionaries," .

[115] S. LESHER, L. PHAIR, L. BERNSTEIN, D. BLEUEL, J. BURKE, J. CHURCH, P. FALLON, J. GIBELIN, N. SCIELZO, and M. WIEDEKING, "STARS/LiBerACE: Segmented silicon and high-purity germanium detector arrays for low-energy nuclear reaction and structure studies," *Nuclear Instruments and Methods in Physics Research Section A: Accelerators, Spectrometers, Detectors and Associated Equipment*, **621**, *1*, 286–291 (2010).

[116] R. HUGHES, J. BURKE, R. CASPERSON, S. OTA, S. FISHER, J. PARKER, C. BEAUSANG, M. DAG, P. HUMBY, J. KOGLIN, E. MCCLESKEY, A. MCINTOSH, A. SAASTAMOINEN, A. TAMASHIRO, E. WILSON, and T. WU, "The hyperion particle- detector array," *Nuclear Instruments and Methods in Physics Research Section A: Accelerators, Spectrometers, Detectors and Associated Equipment*, **856**, 47 – 52 (2017).

[117] G. DUCHÊNE, F. BECK, P. TWIN, G. DE FRANCE, D. CURIEN, L. HAN, C. BEAUSANG, M. BENTLEY, P. NOLAN, and J. SIMPSON, "The Clover: a new generation of composite Ge detectors," *Nuclear Instruments and Methods in Physics Research Section A: Accelerators, Spectrometers, Detectors and Associated Equipment*, **432**, *1*, 90–110 (1999).

[118] J. E. MARTIN, *Physics for radiation protection: a handbook*, John Wiley & Sons (2006).

[119] A. RUBEN, P. C. BENDER, P. CHOWDHURY, P. L. KERR, F. LÜKE, G. MONTERMANN, A. M. ROGERS, and R. SCHNEIDER, "A new, versatile, high-performance digital pulse processor with application to neutron/gamma-ray pulse-shape discrimination in scintillator detectors," in "2018 Symposium on Radiation Measurements and Applications (SORMA XVII)," (2018).

[120] "MDPP-16 QDC," .

[121] "MDPP-16 SCP/RCP," .

[122] "V977 16 Channel Input/Output Register (Status A)," .

[123] "SIS3820 MULTI PURPOSE SCALER," .

[124] "33600A Series Trueform Waveform Generators," .

[125] "mvme - mesytec VME Data Acquisition," .

[126] D. BROWN, M. CHADWICK, R. CAPOTE, A. KAHLER, A. TRKOV, M. HERMAN, A. SONZOGNI, Y. DANON, A. CARLSON, M. DUNN, D. SMITH, G. HALE, G. ARBANAS, R. ARCILLA, C. BATES, B. BECK, B. BECKER, F. BROWN, R. CASPERSON, J. CONLIN, D. CULLEN, M.-A. DESCALLE, R. FIRESTONE, T. GAINES, K. GUBER, A. HAWARI, J. HOLMES, T. JOHNSON, T. KAWANO, B. KIEDROWSKI, A. KONING, S. KOPECKY, L. LEAL, J. LESTONE, C. LUBITZ, J. MÁRQUEZ DAMIÁN, C. MATTOON, E. MCCUTCHAN, S. MUGHABGHAB, P. NAVRATIL, D. NEUDECKER, G. NOBRE, G. NOGUERE, M. PARIS, M. PIGNI, A. PLOMPEN, B. PRITYCHENKO, V. PRONYAEV, D. ROUBTSOV, D. ROCHMAN, P. ROMANO, P. SCHILLEBEECKX, S. SIMAKOV, M. SIN, I. SIRAKOV, B. SLEAFORD, V. SOBES, E. SOUKHOVITSKII, I. STETCU, P. TALOU, I. THOMPSON, S. VAN DER MARCK, L. WELSER-SHERRILL, D. WIARDA, M. WHITE, J. WORMALD, R. WRIGHT, M. ZERKLE, G. ŽEROVNIK, and Y. ZHU, "ENDF/B-VIII.0: The 8th Major Release of the Nuclear Reaction Data Library with CIELO-project Cross Sections, New Standards and Thermal Scattering Data," *Nuclear Data Sheets*, **148**, 1–142 (2018), special Issue on Nuclear Reaction Data.

[127] A. J. M. PLOMPEN, O. CABELLOS, C. DE SAINT JEAN, M. FLEMING, A. ALGORA, M. ANGELONE, P. ARCHIER, E. BAUGE, O. BERSILLON, A. BLOKHIN, F. CANTARGI, A. CHEBBOUBI, C. DIEZ, H. DUARTE, E. DUPONT, J. DYRDA, B. ERASMUS, L. FIORITO,

U. FISCHER, D. FLAMMINI, D. FOLIGNO, M. R. GILBERT, J. R. GRANADA, W. HAECK, F.-J. HAMBSCH, P. HELGESSON, S. HILAIRE, I. HILL, M. HURSIN, R. ICHOU, R. JACQMIN, B. JANSKY, C. JOUANNE, M. A. KELLETT, D. H. KIM, H. I. KIM, I. KODELI, A. J. KONING, A. Y. KONOBEYEV, S. KOPECKY, B. KOS, A. KRÁSA, L. C. LEAL, N. LECLAIRE, P. LECONTE, Y. O. LEE, H. LEEB, O. LITAIZE, M. MAJERLE, J. I. MÁRQUEZ DAMIÁN, F. MICHEL-SENDIS, R. W. MILLS, B. MORILLON, G. NOGUÈRE, M. PECCHIA, S. PELLONI, P. PERESLAVTSEV, R. J. PERRY, D. ROCHMAN, A. RÖHRMOSER, P. ROMAIN, P. ROMOJARO, D. ROUBTSOV, P. SAUVAN, P. SCHILLEBEECKX, K. H. SCHMIDT, O. SEROT, S. SIMAKOV, I. SIRAKOV, H. SJÖSTRAND, A. STANKOVSKIY, J. C. SUBLET, P. TAMAGNO, A. TRKOV, S. VAN DER MARCK, F. ÁLVAREZ-VELARDE, R. VILLARI, T. C. WARE, K. YOKOYAMA, and G. ŽEROVNIK, "The joint evaluated fission and fusion nuclear data library, JEFF-3.3," *The European Physical Journal A*, **56**, *7*, 181 (Jul 2020).

[128] G. DUCHÊNE, F. BECK, P. TWIN, G. [DE FRANCE], D. CURIEN, L. HAN, C. BEAUSANG, M. BENTLEY, P. NOLAN, and J. SIMPSON, "The Clover: a new generation of composite Ge detectors," *Nuclear Instruments and Methods in Physics Research Section A: Accelerators, Spectrometers, Detectors and Associated Equipment*, **432**, *1*, 90 – 110 (1999).